

Occurrence and fate of micro- and nanoplastic in the terrestrial environment

Inaugural dissertation
of the Faculty of Science,
University of Bern

presented by

Alexandra Foetisch

from Cottens (VD)

Supervisor of the doctoral thesis:
Prof. Dr. Moritz Bigalke & Prof. Dr Adrien Mestrot

Geography Institute

Occurrence and fate of micro- and nanoplastic in the terrestrial environment

Inaugural dissertation
of the Faculty of Science,
University of Bern

presented by

Alexandra Foetisch

from Cottens (VD)

Supervisor of the doctoral thesis:
Prof. Dr. Moritz Bigalke & Prof. Dr Adrien Mestrot

Geography Institute

Accepted by the Faculty of Science.

Bern, 20. April 2023

The Dean
Prof. Dr. Marco Herwegh



This work is licensed under a Creative Commons Attribution 4.0 International License

<https://creativecommons.org/licenses/by/4.0/>

“Scientists have become the bearers of the torch of discovery in our quest for knowledge.”

-Stephen Hawking

Contents

LIST OF ABBREVIATIONS	III
SUMMARY	V
ACKNOWLEDGEMENTS	VII
CHAPTER 1 SUMMARIZING OVERVIEW	1
1.1 INTRODUCTION	2
1.2 MATERIAL AND METHODS	10
1.3 GENERAL RESULTS AND DISCUSSION	15
1.4 CONCLUSIONS	26
CHAPTER 2 ALL BLACK: A COLOUR-BASED IDENTIFICATION OF TIRE WEAR PARTICLES (TWP) FROM SOIL	31
2.1 INTRODUCTION	32
2.2 MATERIAL AND METHODS	35
2.3 RESULTS AND DISCUSSION	40
2.4 CONCLUSION	46
2.5 AUTHORS CONTRIBUTION	46
2.6 ACKNOWLEDGMENTS	46
CHAPTER 3 IDENTIFICATION AND CHARACTERISATION OF INDIVIDUAL NANOPLASTIC BY SCANNING	49
TRANSMISSION X-RAY MICROSCOPY (STXM)	49
3.1 INTRODUCTION	50
3.2 MATERIAL AND METHODS	51
3.3 RESULTS AND DISCUSSION	54
3.4 CONCLUSION	64
3.5 AUTHORS CONTRIBUTION	65
3.6 ACKNOWLEDGEMENTS	65
CHAPTER 4 AFTER THE SUN: A NANOSCALE INVESTIGATION OF THE SURFACE AGEING OF SOIL	67
WEATHERED PLASTICS	67
4.1 INTRODUCTION	68
4.2 MATERIAL AND METHODS	70
4.3 RESULTS & DISCUSSION	77
4.4 CONCLUSION	85
4.5 AUTHORS CONTRIBUTION	86
4.6 ACKNOWLEDGMENTS	86

Appendix A. Microplastics in agricultural drainage water: A link between terrestrial and aquatic microplastic pollution	87
Appendix B. Chapter 1	99
Appendix C. Chapter 2	103
Appendix D. Chapter 3	113
Appendix E. Chapter 4	125
LITERATURE CITED	133

List of abbreviations

AF4	Asymmetrical Flow Field-Flow Fractionation
AFM	Atomic Force Microscopy
ALS	Advanced Light Source
ATR-FTIR	Attenuated Total Reflectance Fourier Transformed Infrared
BE	Bern (canton)
BM	Bulk material
EDX	Energy Dispersive X-ray
EELS	Electron Energy Loss Spectroscopy
FTIR	Fourier Transformed Infrared
GR	Graubünden (canton)
HDTMS	Hexadecyltrimethoxysilane
HS-GC/MS	Headspace Gas Chromatography Mass Spectrometry
I	Transmitted light
I_0	Incident light
IR	Infrared
LC-MS	Liquid Chromatography Mass Spectrometry
LOD	Limit of Detection
LOESS	Locally weighted smoothing regression
LOQ	Limit of Quantification
MaP	Macroplastic
mF	Minimum Feret size
MNP	Micro- and nanoplastic
MP	Microplastic
MS	Mass Spectrometry
NaBr	Sodium Bromide
NaI	Sodium Iodide
NEXAFS	Near-Edge X-ray Absorption Fine Structure
NMR	Nuclear Magnetic Resonance
NOM	Natural Organic Matter
NP	Nanoplastic
OD_{norm}	Normalized Optical Density
$OD_{post-edge}$	Mean Optical Density value between 310 and 320 ev
$OD_{pre-edge}$	Mean Optical Density value between 280 and 283 ev
PA	Polyamide
PBAT	Poly(butylene-co-terephthalate)
PC	Polycarbonate
PE	Polyethylene
PEEM	Photo-Emission Electron Microscopy
PET	Polyethylene Terephthalate
PMMA	Polymethylmethacrylate
PP	Polypropylene
PS	Polystyrene

PSI	Paul Scherrer Institute
PUR	Polyurethane
PVC	Polyvinyl Chloride
Py-GC/MS	Pyrolysis Gas Chromatography Mass Spectrometry
SDS	Sodium Dodecyl Sulphate
SEM	Scanning Electron Microscopy
SIMS	Secondary Ion Mass Spectrometry
SINS	Synchrotron infrared Nanospectroscopy
SLS	Swiss Light Source
SOM	Soil Organic Matter
SPT	Sodium Polytungstate
STXM	Scanning Transmission X-ray Microscopy
TED-GC	Thermal Extraction Desorption Gas Chromatography
TEM	Transmission Electron Microscopy
TI	Ticino (canton)
TOC	Total Organic Carbon
TSPP	Tetrasodium Pyrophosphate
TWP	Tire Wear Particle
UV	Ultraviolet

Summary

The worldwide production of plastic has grown exponentially since the 1950's and revolutionized our daily life. Simultaneously, plastic pollution in the environment has become a global issue and micro- (MP) and nanoplastics (NP) have now been detected even in the most remote ecosystems. There is currently a data gap due to a lack of analytical methods on the occurrence and characterisation of two highly relevant categories of plastic in the soil environment: tire wear particles (TWP), which concentration in the environment is expected to be high and carry toxic additives, and NP, which toxicity has been demonstrated on soil organisms and is characterized by its ability to cross cell membranes. The effects of micro- and nanoplastic (MNP) on their surrounding environment are determined by their size, morphology, surface characteristics and chemical composition, which can be affected by soil residence time. As the soil is often considered as sink for MNP, it is crucial to investigate and understand the different weathering factors which might affect the MNP properties. To address these knowledge gaps, three main objectives were identified in the scope of this study: develop an extraction and single particle identification method for the quantification and characterisation of (i) TWP and (ii) NP in soil samples and (iii) characterise the physico-chemical properties at the surface of plastic debris occurring in the soil environment, as well as assess the effect of soil and UV weathering as single ageing factors.

In order to realise the first objective, a method of extraction and identification of TWP in soil samples based on their black colour was developed using optical microscopy. Cryo-grinded TWP down to a size of 35 μm could be detected with a >85% but the tests conducted with environmental TWP showed that the density used in this study was not efficient to separate the whole range of TWP occurring in different densities. Yet, TWP concentration in highway adjacent soil samples ranged between 8084 ± 1059 and 2562 ± 1160 TWP kg^{-1} dry soil and showed similar trends and magnitude order than previously reported concentrations. Thus, the developed protocol was estimated sufficiently accurate for TWP monitoring in soil samples.

Regarding the second objective, an extraction and identification method for NP in soil samples was developed using X-ray spectro-microscopy (STX-NEXAFS). The results demonstrated the suitability of the technique for the imaging and chemical characterisation of individual NP with a minimum dimension of ≈ 100 nm and its application to the analysis of pure NP and for NP present in environmental and food matrices. However, it was not possible to obtain quantitative data on the NP present in the samples, as the method was too time consuming to allow the measurement of a high number of particles.

For the last objective, STXM-NEXAFS was applied to the characterisation of the surface alterations of natural-soil weathered, soil-incubated and UV exposed polymers. A surface alteration on a depth varying between 150 and 1000 nm on could be observed and the analysis of the replicate's measurement acquired on the same plastic debris highlighted the heterogeneity of the processes affecting polymers surface. The comparison of UV weathered and natural-soil weathered samples showed that the two treatments led to different surface alterations and the absence of surface alteration after one-year soil incubation indicated slow aging of polymers in this medium. Moreover, the very first step of surface fragmentation was observed on a PS fragment, providing an insight on the factors and processes leading to the release of MP and NP in soils.

Overall, the present research contributed significantly to the development of innovative methods to characterise MNP in the soil environment. The results obtained helped to provide ground information on the characteristic of environmental MP and NP, which is of high importance to design ecotoxicological test using environmentally relevant material as well as validate predictive models to better understand the potential risk that MP and NP represent for the ecosystems.

Acknowledgements

This thesis was funded by the Swiss National Science Foundation (SNSF, 200021_182672/1) and carried out in the Soil Science group at the Institute of Geography of the University of Bern. The completion of this work could not have been possible without the help and support of people from my work environment who have accompanied me during this journey, and I wish to thank them.

Moritz Bigalke for the development of the project and having given me the opportunity to become a member of the “plastic” community, for his guidance, advices, valuable inputs and corrections, while always leaving room for my self-development as a scientist. I’d like to thank him also for his consideration and understanding of my well-being in the most critical times and for his legendary optimism. Adrien Mestrot for his efforts in building a diverse research team unit with the best atmosphere I ever had the chance to work in, and for our helpful discussions and brainstormings. Montserrat Filella for her presence and her help to “fish” during beamtimes, and our interesting discussions on science and future, as well as for her significant contributions and amazing efficiency in reviewing the papers we collaborated on. Benjamin Watts for the initiative of using STXM in plastic environmental monitoring, his company, support and special care he took of us during beamtimes, for his significant contributions to the papers we collaborated on and for all the culinary specialties he got us to discover. Katharina Witte and Simone Finizio for their help and emotional support during the different beamtimes at PolLux and/or ALS. Denise Mitrano for accepting to evaluate the present manuscript and for the organisation of workshops and conferences which gave me great opportunities to learn and extend my network. Adrian Grunder and Hannah Forsyth for joining the plastic team in Bern, teaching and helping me to conduct experiments, for their emotional support and for the nice discussions and great atmosphere in the office. Teresa González de Chávez for her creativity and amazing skills in organizing social events, for being present as a friend and a colleague, and whom, by being true to herself and the others, gave me the opportunity to discover and improve myself on a scientific and personal level. Sabnam Mahat, Maarika Bischoff and Tobias Stadler, for their refreshing energy and friendship, the crazy nights and their emotional support. Laure-Hélène Vinot, Maeva Bragoni, Milo Fieber, Gabi Witschi, Lina Horn, Benjamin Kunde, Yannick von Känel, Sarah Volken, Saskia Gianola and all the students who helped and contributed to the successful completion of this work during their studies. Jaime Caplette, Ursina Morgenthaler, Hang Guan, René Nussbaumer, Livia Vogel, Florian Christ, Anika Sidler, Daniela Fischer, Ladina Gaudy, Ariane Grimmer, Klaus Jarosch, Evelyn Vonwyl, Anna Müntwyler, Stephanie Pfister, Lucjia Stanistic, Andrea Sanchini, Lorenz Gfeller and Patrick Neuhaus for being present as colleagues and friends, providing an amazing emotional support, feeding me with delicious pastries during the difficult

times and creating a dynamic, rich and stimulating research unit. Isabella Geissbühler for all her hard work in creating a great work environment. Beat Haenni, Beatrice Frey and Agathe Martignier for their help and expertise with the different electronic microscopy techniques applied in this study. David Mennekes, Nicolas Beriot, Thibault Masset, Angélique Moraz, Guillaume Crosset-Perrotin and Narain Ashta for their friendship, support and encouragements during the different workshops and conferences we attended together.

Moreover, I would like to express my gratitude to the people who supported and encouraged me outside of the work environment. My mother, Michèle, and my brother and sister, Thomas and Emmanuelle, for their unconditional love, affection and support, which contributed to make this experience one of the best I ever had. My father, Christophe, whose presence I can still feel and I hope he is proud of this achievement. Vincent, for sharing my day-to-day life and giving me with your love and affection, for your patience and adaptability to my work schedule, for preparing so many meals for me to eat healthy, to drag me out from the lab/office to go climbing and for making my childhood dreams come true. Géraldine, for always picking up the phone no matter where she was around the world, for her advices, love, horse-riding as in the good old days and just being the wonderful person she is. Ylza, Adèle, Mathilde and Laetitia for the fun, friendship and support through all the different phases of the PhD. Finally, All the people I have been climbing with, for contributing to my work-life balance and allowing me to spend great time in an environment that I love.

Overall, I am grateful that I had the chance to live this thrilling experience. I was very fortunate to encounter and collaborate with people who made me grow on a scientific and personal level. The perspective of completing this PhD is bitter-sweet feeling as I am more than satisfied to have fulfilled this achievement but also know that I will often miss working at GIUB by closing this chapter of my life.

Chapter 1 Summarizing overview

1.1 Introduction

1.1.1 Plastic definitions in an environmental context

Plastic material was mostly developed in the XX^e century and has played an essential role in the advancement of technology. Due to its light weight, plastic role as a construction or packaging material significantly reduced fuel consumption during transportation. Additionally, plastic low-cost and versatility allowed for the development of completely new products, such as cell phones and computers, accessible to a large public (Brydson, 1999). Since its commercialisation in the 1950's, the global plastic production has grown exponentially and plastic has become omnipresent in our everyday life (PlasticsEurope, 2022). It has been estimated that, between 1950 and 2015, about 8300 million metric tons of plastic have been produced worldwide, 79% of which are accumulated in landfills or in the environment (Geyer et al., 2017). So, while this material revolutionized modern technology, plastic pollution omnipresence and its potential negative effects on the ecosystems also became a global issue despite early warnings from the scientific community (Carpenter and Smith, 1972). But what is plastic exactly? It is a wide class of materials, which consist at least partly in organic polymers and can be moulded into solid, non-soluble objects (Hartmann et al., 2019). An organic polymer is formed by a high number of repetitions of a single monomer containing carbon. The polymer type of plastic material is thus determined by the composition of its repeated monomers (Figure 1-1). In the present dissertation, the most commonly studied polymer types : polyethylene (PE), polypropylene (PP), polystyrene (PS), polyethylene terephthalate (PET), polyvinyl chloride (PVC), polycarbonate (PC), polymethyl-methacrylate (PMMA) polyamide (PA) and polyurethane (PU) (de Ruijter et al., 2020; Zhang et al., 2019) are grouped together under the term of "traditional" plastics, as suggested by (Goßmann et al., 2021). However, in an environmental context, the polymer type only is not sufficient to characterise the plastic material as several additional characteristics will determine its fate and impact in the environment. Indeed, plastic debris can contain a wide diversity of additives and can be found in a variety of sizes, morphologies and colours. In the context of plastic pollution, a nomenclature based on the plastic debris size has emerged but no consensus regarding the upper and lower size limits has yet been reached (Hartmann et al., 2019). In the present dissertation, macroplastics (MaP), microplastics (MP) and nanoplastics (NP) represent particles of a size range >2mm, 2mm-1µm and <1µm respectively. Microplastics and nanoplastics (MNP) can occur as primary, when they were manufactured in this size range for their initial purpose, or secondary if they result from the breakdown of a larger plastic debris (Cole et al., 2011). Thus, "plastic material" is a term which represents a vast category of material having a broad diversity of physical and chemical characteristics and being present in a large size range in the environment.

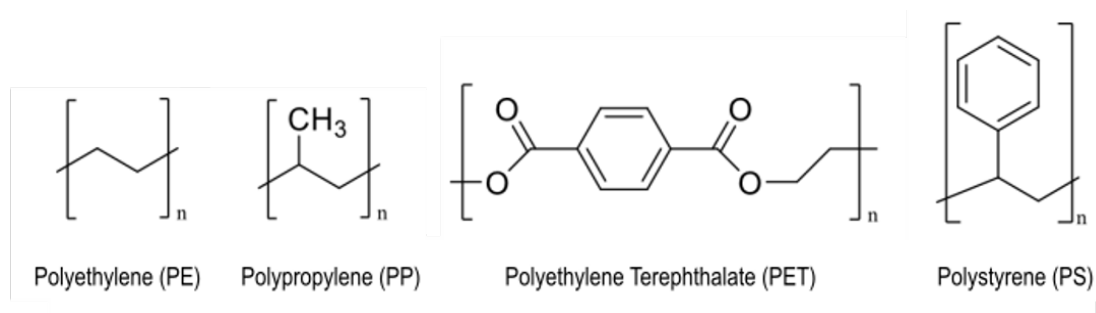


Figure 1-1: Chemical structure of the most commonly used polymers: Polyethylene (PE), Polypropylene (PP), Polyethylene Terephthalate (PET) and Polystyrene (PS).

1.1.2 Sources and impact of plastic in the terrestrial ecosystem

Plastic objects can enter the soil environment through several pathways, which are summarized in Figure 1-2. The road runoff plastic is mainly composed of tire wear particles (TWP) originating from the abrasion of vehicle's tires on the asphalt (Rogge et al., 1993). A modelling approach determined that TWP accounted for 93% of the plastic emitted per capita per year in Switzerland, which makes tire rubber the dominant source of plastic in the environment (Sieber et al., 2020). In agricultural systems, common practices will contribute significantly to the input of plastic in the soil. For example, it has been estimated that the total input of MP to soil through sewage sludge amendments lies between 63000 and 430000 tons per year in Europe (Nizzetto et al., 2016) and an accumulation of plastic following sequential sewage sludge applications was observed in field experiments (Corradini et al., 2019). Nonetheless, sewage sludge amendments, have been banned in several European countries and is forbidden in Switzerland since 2003. Composts from households and industry are also used as natural fertilizers but have been shown to contain MaP and MP in concentrations ranging from 20 to 146 particles kg⁻¹ dry weight (Weithmann et al., 2018). Coated fertilizers are widely used in golf courses and rice crops and allow to physically regulate the release of a fertilizer over time but are suspected to be a significant source of MP in those soils (Katsumi et al., 2020). Plastic mulches provide a wide range of benefits for the agriculture but is prone to UV degradation and its complete removal after use is difficult, leading to an accumulation of plastic fragments in the soil (Huang et al., 2020) and contributing up to 30% of the potential terrestrial sources of MP (Khalid et al., 2022). Finally, contaminated irrigation water (Pérez-Reverón et al., 2022), urban runoff that is not captured by the sewer systems (Hurley and Nizzetto, 2018), littering (Braun et al., 2023) and atmospheric deposition (Kernchen et al., 2022) are known sources of plastic in soils.

Once in the soil, plastic can affect the soil physico-chemical properties, such as the structure, porosity, bulk density, soil water, pH, organic matter and nutrients availability with negative, neutral or positive impact (Wang et al., 2022b). Several studies have already observed negative effects of MNP on soil organisms such as the microbiota and the functional diversity

of enzymes in soil (Awet et al., 2018), earthworms (Kwak and An, 2021; Zhu et al., 2018) or plants (Lozano et al., 2021). Regarding soil living organisms, determinant factors to predict MNP toxicity are the polymer type, the particles size and surface charges, their concentration and their shape (Wang et al., 2022a). For example, concentration was a key factor to assess the effect of PS MP on earthworms growth and fitness (Cao et al., 2017) and (Sun et al., 2020) showed that positively and negatively charged PS nanobeads were both impacting the phenotype of the plant *Arabidopsis thaliana* but with different toxicity mechanisms. Thus, a full characterisation of the plastic occurring in the environment is crucial to correctly assess the risk that MNP represent for the organisms.

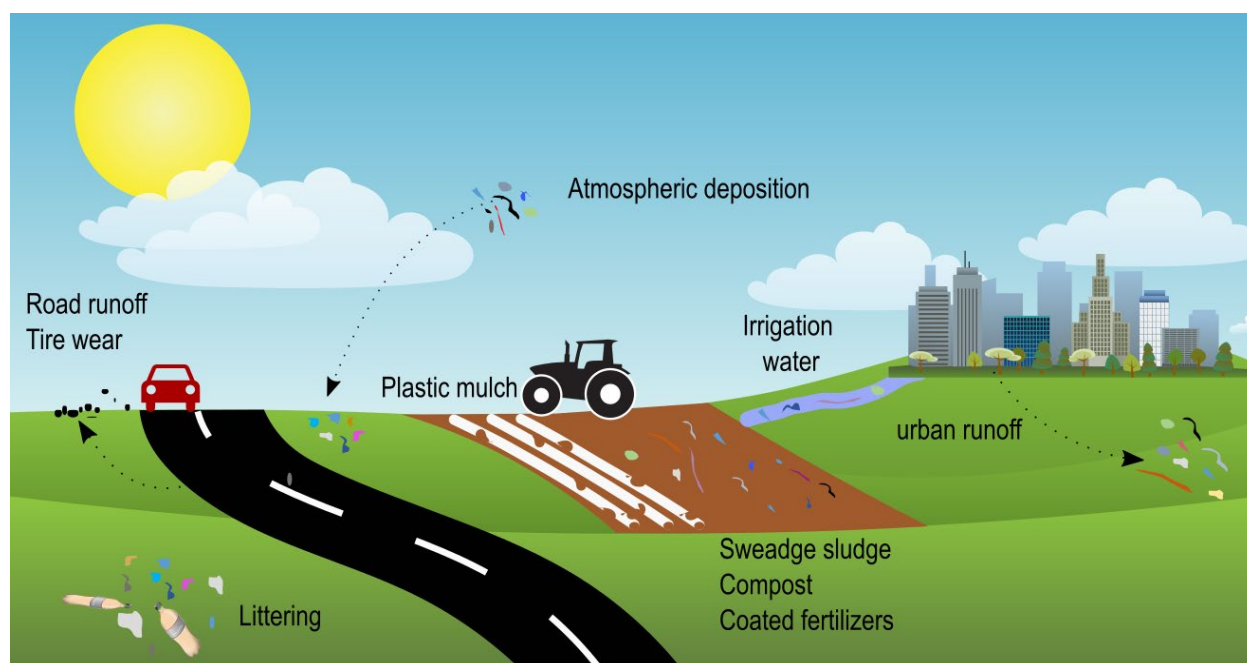


Figure 1-2: Main sources of Macro-, micro- and nanoplastic in soil.

1.1.3 Assessing plastic concentration in the soil environment

To quantify and characterise the plastic present in soil samples, MaP, MP and NP are most often separated from the soil matrix and identified by their polymer type. However, no agreed standard method is yet available (Junhao et al., 2021). The challenge in developing a standardized method arise from the diversity of plastic particle sizes and density occurring in the environment, as well as the heterogeneity in the constituent and their proportions of the soil matrix. MP extraction generally consists in a density separation to allow the elimination of the soil mineral fraction, followed by a reduction of the soil organic matter (SOM). The most common techniques applied for traditional MP identification in environmental samples are light microscopy, Fourier-transform infra-red spectroscopy (FTIR), attenuated total reflectance FTIR (ATR FTIR), Raman spectroscopy and pyrolysis gas chromatography mass spectrometry (Py-GC/MS). The great asset of FTIR and Raman spectroscopy is to provide a

full characterisation of the particles by providing the polymer type, size and shape characteristics of the plastic occurring in the environment. Py-GC/MS does not allow for single particle analysis but has a high sensitivity allowing for a low limit of detection (Möller et al., 2020). With the help of these techniques, traditional MP concentrations in the range of <1 to 12760 items kg⁻¹ dry soil were observed in terms of particles count and between 0 to 55.5 mg kg⁻¹ dry soil in term of mass. Soils with a sewage sludge amendment had an average MP concentration of 1998 items kg⁻¹ or 2.2 mg kg⁻¹ dry soil and was equivalent to soils prone to receive road dust or littering but was one order of magnitude higher than soil where plastic mulch was used. Additionally, a positive relationship between population density and MP concentration in soil was observed, as concentration in industrial areas > suburban areas > rural areas (Büks and Kaupenjohann, 2020).

However, most of the studies focusing on the occurrence of MP in the soil do not include TWP, as the most common identification techniques used for traditional MP are not suitable for TWP detection. Yet, TWP represent an important category of MP, as their environmental concentrations are expected to be high and several studies have already shown TWP toxic effects on soil organisms, mainly due to leaching of chemicals (Kim et al., 2022, 2021; Selonen et al., 2021; Sheng et al., 2021). Most of the available data on TWP in soil are based on prediction models and the measurement data are scarce (Mennekes and Nowack, 2022). Tires are generally composed of about 50% natural or synthetic (styrene-butadiene) rubber, 45% softening and hardening materials and 5% of other additives. Their final composition can vary widely, depending on the application of the final product (Verschoor, A. et al., 2016). Despite the fact that they only partly consist of artificial polymers, TWP are still considered as MP (Committee for Risk Assessment (RAC), 2020). FTIR and Raman spectroscopy cannot be used to detect TWP because they are typically opaque to IR light, due to black carbon total absorbance, and do not deliver specific Raman spectra (Müller et al., 2022; Wagner et al., 2018). ATR-FTIR can be used to identify TWP but this method is limited by the size of particles it can measure ($\geq 500\mu\text{m}$) (Leads and Weinstein, 2019). Mass spectrometry techniques target analytical markers, which can be organic, polymeric, or elemental, to infer TRWP bulk mass in environmental samples. Molecular markers are organic additives which can be traced using chromatography techniques coupled with mass spectrometry (MS) (Knight et al., 2020). If they are considered specific to trace TWP, organic markers are prone to leaching and degradation (Unice et al., 2015) thus increasing significantly the uncertainty of the results. Polymeric markers are representative of the polymeric fraction of the tires and are potentially more consistent than molecular markers. (Rødland et al., 2022) used Py-GC-MS to assess the suitability of different polymeric markers as well as markers combinations to quantify the amount of TWP in environmental samples. They obtained an accuracy range of 85-151 %,

reflecting how inferring the concentration of TWP from an indirect measure is hindered by the high variability of tires initial composition and marker stability. Therefore, the currently available techniques either fail to positively identify the TWP (FTIR, Raman) or to provide TWP size and shape distribution (mass spectrometry). Nevertheless, mass spectrometry techniques provided the first TWP mass estimations in soil lying between 155 and 64000 mg kg⁻¹ dry soil and showed a positive correlation between the TWP concentrations, the proximity from the road, the traffic density and the break and acceleration frequency (Klößner et al., 2021a; Müller et al., 2022; Panko et al., 2012; Thomas et al., 2023; Unice et al., 2015). These mass concentrations agree well with the prediction that TWP are much more abundant in the environment than traditional MP. To the best of our knowledge, only one study reported TWP concentration in soil in particle number. They analysed road runoff water and found concentrations ranging from 0.66 to 65 TWP/mL (Knight et al., 2020) but did not provide systematic information on particle size and morphology. Thus, most of the data reporting TWP in soil are mass-based and no information on TWP shape and size distribution are yet available, due to the lack of identification methods for environmental TWP allowing single particle characterisation.

The number of studies which successfully quantified and characterized NP in soil are much lower compared to MP. Particles of a size <1 µm typically behave as colloids (Gigault et al., 2018) and thus cannot be extracted with the same methods developed for MP. For example, sodium bromide (NaBr) saturated solutions are often used for the density separation of MP, but in the case of NP, the ionic strength of the solution induces a strong aggregation of the NP, which hinders an efficient separation from the soil matrix. Moreover, the identification of NP from environmental matrices cannot be achieved using infrared or Raman spectroscopy as they have a spatial resolution limited to 20 and 1 µm respectively (Cerasa et al., 2021). NP of PE, PS and PVC could be recently detected and quantified in a size range of 20-150 nm in a soil amended with plastic debris using a combination of asymmetric field flow fractionation (AF4) and Py-GC/MS (Wahl et al., 2021). This work was the first to show evidence of the presence of NP in soil samples, but the techniques applied could not deliver single particle information (size, morphology) which are needed to fully characterise environmental NP. To achieve single particle analysis at the nm scale, the detection technique must be able to provide high resolution images and to collect single particle signal but currently, to our knowledge, no such method is available.

1.1.4 Plastic fate and impact in the soil

Once emitted in to the environment, MNP can be further transported vertically and horizontally by a combination of abiotic (water flow, ploughing) and biotic (earthworms, roots growth) factors (Helmberger et al., 2020). They can eventually exit the soil and enter the aquatic

system by reaching the groundwater (Re, 2019) and the marine environment is generally accepted to be the ultimate sink of plastic particles (Villarrubia-Gómez et al., 2018). However, the retention time of plastic in soil can vary on large time scales and be influenced by the plastic debris properties (size, zeta potential) and soil properties (Hurley and Nizzetto, 2018; Lehmann et al., 2019). In the terrestrial system, several mechanisms can lead to plastic partial or total degradation. These mechanisms include abiotic processes, such as thermal degradation (Pielichowski and Njurguna, 2005), photo-degradation (Cai et al., 2018; Luo et al., 2020b) and mechanical breakdown (He et al., 2018), as well as biotic processes such as bio-fragmentation (Cadée, 2002; Dawson et al., 2018) and biodegradation (Danso et al., 2019; Sander et al., 2019; Zumstein et al., 2018). The efficiency of these mechanisms to degrade plastic will depend on the physico-chemical properties of the polymer, such as the particle size (Luo et al., 2020a; Wang et al., 2020), its chemical structure (Gewert et al., 2015) and its crystallinity (Julienne et al., 2019), and environmental conditions, such as the oxygen concentration and humidity (Wang et al., 2020), temperature (Chen et al., 2020) and organic matter concentration (Cai et al., 2018; Liu et al., 2020). So far, most of the research concerning plastic weathering was conducted in aquatic or air media but only little is known about plastic aging in soils (Büks and Kaupenjohann, 2022; Duan et al., 2021). Among the diversity of weathering factors, the most studied is UV radiation. It has been showed that UV-induced photo-oxidation can lead to surface morphology alterations (cracks, fragmentation) and a deterioration of mechanical properties (Ainali et al., 2021; Cai et al., 2018; Meides et al., 2022). Photo-oxidation generally results in an cleavage in the polymeric chain and oxygen present in the atmosphere binds to the formed radical, increasing the proportion of hydroxyl (O-H) and carbonyl (C=O) groups in the material (Rånby, 1989).

Before being buried in soil, plastic fragments can lie in sunlight for an undetermined period of time and be exposed to UV radiation. Once buried in the soil, plastic is no longer exposed to UV but to soil microorganisms and roots in a mostly humid environment where expected aging factors include secreted enzymes, organic and inorganic acids, bioturbation, frequent leaching and freeze-thaw cycles. However, the effect and importance of these weathering factors are yet unknown (Büks and Kaupenjohann, 2022). Previous work used a biodegradable ¹³C-labelled poly(butylene-co-terephthalate) (PBAT) to show for the first time the biodegradation of a polymer in agricultural soil (Zumstein et al., 2018) and many different enzymes and/or bacterial stains have been tested for their efficiency of polymer biodegradation (Amobonye et al., 2021). However, the consequent polymer surface modifications are still unknown, yet important to assess the particles fate and impact in the soil.

1.1.5 Objectives and structure of this study

Given the potential threat that MNP represent for the soil living organisms and their possible effects on the soil properties, there is an urgent need to quantify and characterize the MNP pollution in soil. Currently, methodological gaps are hindering the quantification and characterisation of two highly relevant categories of environmental plastic. First, the TWP which were estimated to represent more than 90% of the plastic emitted per capita in Switzerland and which concentration in the environment is expected to be high. Secondly, the NP which toxicity has been demonstrated on soil organisms and is characterized by its ability to cross cell membranes. Moreover, the effects of MNP on their surrounding environment are determined by their size, morphology, surface characteristics and chemical composition, which can be affected by soil residence time. As the soil is often considered long-term reservoir for MNP, it is crucial to investigate and understand the different weathering factors which might affect the MNP properties. Therefore, the aim of this PhD thesis was to contribute to the development of new extraction and identification protocols for MNP present in soil as well as characterise the surface physico-chemical properties of the plastic being retained in the soil for long periods of time. The general structure of this dissertation is represented in Figure 1-3. The **Chapter 1** presents an overview of the different optimisation steps and methods tested to achieve the three following objectives:

- Develop an easy-to-use single particle based method to quantify and characterise TWP in the soil (**Chapter 2**)
- Develop an extraction protocol and single particle identification method to characterise NP in the soil (**Chapter 3**)
- Investigate the physico-chemical ageing of plastic surfaces exposed to UV and soil (**Chapter 4**)

The purpose of these objectives is to address the current methodological gaps for the extraction and identification of two highly relevant categories of plastic (TWP and NP) and to provide a first characterisation of sizes and shapes distribution, as well as surface chemical characteristics, for plastic occurring in the soil environment.

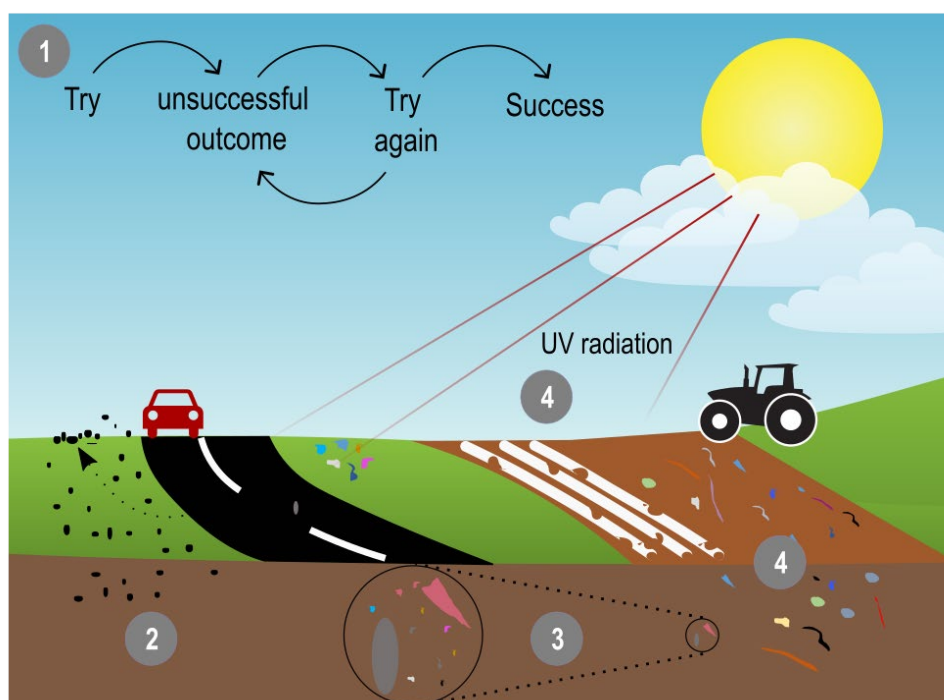


Figure 1-3: Schematic representation of the chapter structure and objectives of the thesis.

The **Chapter 3** has been published in the *Journal of Hazardous Material* in 2022 and the **Chapter 2** and **4** will soon be submitted in peer-reviewed journals. As these chapters are meant to be understood independently, repetitions between the 1st chapter and the following ones are possible but necessary to provide an overview of the thesis.

Along with the primary objectives outlined above, I also lectured twice in the Soil Biogeochemistry course and co-supervised Bachelor (Benjamin Guggisberg, Sarah Volken, Saskia Gianola) and Master (Gaby Witschi, Milo Fieber, Tobias Stadler, Laure-Hélène Vinot, Maeva Bragoni, Yannick von Känel, Michelle Dür) students on plastic-related themes. I co-authored one of the Master's project that dealt with MP in drainage water and was published in the journal *Science of the Total Environment* in 2022 (Appendix A). I instructed two PhD students (Adrian Grunder and Hannah Forsyth) on the lab techniques relating to MNP and trained external students, lab technicians and professors to the method of MP extraction from soil. I implemented a R script to automatize the comparison of our MP FTIR spectra to our own reference measurement and the OpenSpecy database (Cowger et al., 2021) simultaneously. I worked together with Tobias Stadler and Adrian Grunder on the extraction and identification protocol for traditional MP in soil which will soon be published in a peer-reviewed journal and of which I'll be a co-author. I was involved in four successful beamtime applications at the Swiss Light Source facility (Institute Paul Scherrer, Switzerland) and a fifth one at the Advanced Light Source facility (Berkeley Lab, USA). Finally, I had the opportunity to present my research in national (Swiss Geoscience Meeting 2019, MP-CH meeting 2022 &

2023) and international conferences (German and Swiss Soil Science Society meeting 2019, Eurosoil 2020, Society of Environmental Toxicology and Chemistry 2022 and Microplastics 2022).

1.2 Material and methods

The purpose of this section is to provide an overview of the many optimization procedures carried out prior to arriving at the final protocols, which are covered in more details in the appropriate chapters.

1.2.1 TWP extraction and identification in soil samples

The protocol for traditional MP and TWP extraction applied in **Chapter 2** was adapted from earlier work (Olsen et al., 2020; Scheurer and Bigalke, 2018) and optimised for our detection method. Preliminary tests showed that, when the final extracts were filtered down a filter for further FTIR analysis, three main factors were slowing down or hindering a proper identification of the TWP present in the sample: (i) a high quantity of fine particles on the final filter formed a dark background and was challenging the particles automatic detection by lowering the contrast between the particles and the background, (ii) the remaining NOM after Fenton reaction alone could cover significant areas on the final filter and potentially hide underlying TWP and (iii) the accumulation of precipitated iron oxides from the Fenton reaction on the final filter was significantly affecting particles colour and could even form a layer thick enough to cover and hide TWP.

To decrease the quantity of fine particles on the final filter, we examined the impact of a larger filter pore size in the first filtration phase by substituting the initial 0.45 μm PC filters by 10 μm stainless steel filters. In this aim, a density separation was applied to soil sample replicates and filtered through both filters. The improvement was then assessed by visual comparison. To reduce the amount of NOM, a new step, which was previously applied to MP extraction in the marine environment (Olsen et al., 2020), was implemented before the Fenton reaction. This step consists in immersing the sample in 25 mL NaUT (6% urea, 8% thiourea, 8% NaOH) solution before freezing it for 40 min at $-20\text{ }^{\circ}\text{C}$ to initiate a crystallisation process. The crystals formation causes the NOM structure to weaken and makes its later mineralisation easier. The effect of this new step was assessed by measuring the area covered by the particles on the filters after the Fenton reaction on soil sample replicates. Finally, a treatment of 2M H_2SO_4 was tested to remove the iron oxide precipitates on the final filter by adding sequences of 3 x 50 μL H_2SO_4 + 15 mL MilliQ water until full dissolution of the iron oxides.

Next, the efficiency of optical microscopy together with a machine learning algorithm to detect TWP based on their black colour was evaluated and the minimum particle size detected was determined. The extraction and identification procedure recovery and the method limit of

detection (LOD) and quantification (LOQ) were assessed using cryo-grinded TWP and tunnel dust samples. Additionally, as a similar black colour-based identification was previously applied to detect charcoal particles in sediments samples (Mooney and Tinner, 2011), we investigated charcoal possible interferences in the TWP identification process. The newly developed method of extraction and identification was finally applied to highway adjacent soil samples and the observed concentrations were compared to previously reported TWP quantification data. The identification protocol and the experimental design applied to TWP in soil is presented in detail in **Chapter 2**.

1.2.2 NP extraction and identification in soil samples

In **Chapter 3**, we aimed to develop an extraction protocol and an identification method allowing for the full characterisation of NP in soil. First, a magnetic extraction developed previously for MP and involving coated Fe nanoparticles to magnetize the plastic was tested. For this, Fe nanoparticles were modified with hexadecyltrimethoxysilane (HDTMS), forming Fe nanoparticles with hydrophobic tails which preferentially bind to the plastic in environmental samples (Grbic et al., 2019) and allow to extract the plastic with a magnet. To test the efficiency of this method to selectively bind to the plastic, a spike soil extract was prepared: soil samples were suspended in a sodium pyrophosphate tetrabasic (TSPP) solution, homogenised and let settle for 18 h. Then, 5 mL of the top solution were collected and spiked with 2 mL of 100 nm, 250 nm, 500 nm and 1 μm PS nanobeads mix. The spiked soil solution was then incubated for 12 h with the modified Fe nanoparticles. A magnet was used to retain the Fe nanoparticles and the material they had bound to at the bottom of the vials while the liquid phase was discarded. Finally, the extract was re-suspended into 3 mL of MiliQ water and a 2 μL drop of the solution was deposited on a silicon wafer and imaged using scanning electron microscopy (SEM) and energy dispersive x-ray (EDX). Next, extraction steps from protocols applied to metallic nanoparticles (Schwertfeger et al., 2017) and MP from soil (Scheurer and Bigalke, 2018) were adapted to NP: (i) the elimination of the soil mineral fraction by centrifugation assisted density separation at a speed of 22 000 rpm (acceleration of approx. 109.500 g) for 2 h was tested on PS 100 nm beads with a NaBr ($\rho = 1.5 \text{ g/cm}^3$) and a sucrose ($\rho = 1.3 \text{ g/cm}^3$) cushion and (ii) the reduction of total organic carbon (TOC, Vario TOC cube, Elementar®) as proxy for SOM oxidation was tested with a 24-h 5% H_2O_2 treatment with a unique or sequential H_2O_2 additions and the potential effects of the treatments were investigated on PS nanobeads by SEM imaging.

Preliminary tests of NP deposition on a substrate for further analysis using pure PS nanobeads centrifuge-deposited on a SiN substrate revealed a very low recovery rate. The suitability of a 1 μL drop deposition and 4 hours at 2780 x g force centrifugation in glass tubes for the deposition of NP on various substrate compositions (SiN and MgO) was therefore examined

by SEM imaging using a PS beads size mixture of 100, 250 and 500 nm and homemade PC NP (see Appendix D.1 for detailed preparation of the NP) suspended in pure ethanol. The particles were automatically counted on the SEM images using the Fiji open-source software (Schindelin et al., 2012).

For the subsequent NP identification, three synchrotron based analytical techniques were tested for their suitability to image and identify NP in environmental matrices. In a synchrotron, electrons are accelerated to a speed almost equal to the speed of light and their trajectory is bended by dipole magnets for their path to form a round-cornered polygon. The redirection of the accelerated electrons generates a beam of light (beamline) which is characterised by a high brilliance, c.a. a high concentration of photons (Boscherini et al., 2015). This characteristic of the beam makes it very powerful for the investigation of nanosized objects, as it allows to collect a strong signal on a high spatial resolution.

We first tested synchrotron infrared nanospectroscopy (SINS) coupled with atomic force microscopy (AFM) for the identification and imaging of the particles at the 5.4.1 beamline of the Advanced Light Source (ALS) in the Berkeley Lab (California, USA). It allows to acquire FTIR spectra in the 400-11000 cm^{-1} frequency range with a 20 nm spot size (Figure 1-4, A). SINS-AFM main advantage is that the identification of the particles relies on IR spectroscopy, for which consequent polymer databases and libraries are already available (Cowger et al., 2021; Primpke et al., 2020). For this technique, samples must be AFM compatible (e.g. objects present on the substrate should have a height < 1 μm) and be deposited on a highly reflective surface to maximise the detection of the scattered IR. PS nanobeads of 100, 250 and 500 nm as well as homemade NP of PP, PC PET, PVC, polyurethane (PUR) and polyamide (PA) suspensions were prepared in 100% and 50 % ethanol to test SINS capacity to identify the polymer type of single NP. The 50% ethanol solutions were prepared to allow sample transportation by plane and allow new NP deposition directly at the Berkeley Lab. The suspensions in 100% ethanol were deposited on silver-coated SiN substrates by a 4 h centrifugation at 2780 x g in glass vials and 1 μL of the 50% ethanol suspensions was drop deposited on gold substrates. Additionally, spiked and unspiked water and soil samples were extracted and deposited onto silver-coated SiN substrate to assess the capability of SINS to distinguish the different polymers from NOM.

The second analytical technique we tested was photo-emission electron microscopy (PEEM) at the Surfaces/Interfaces Microscopy (SIM) beamline of the Swiss Light Source (SLS) of the Institute Paul Scherrer (PSI, Switzerland) (Figure 1-4, B). The PEEM has a spatial resolution down to 100 nm and provides near-edge absorption fine structure (NEXAFS) spectra of the investigated material by varying the energy of incident X-rays between 280 and 350 eV, just

above the carbon 1s absorption edge, and collecting the scattered electrons. Its main advantages are its capacity of acquiring spectra over a $15 \times 15 \mu\text{m}^2$ area at once, allowing for the simultaneous measurement of several particles, and that PEEM only analyses first 5 nm at the surface of the material and is thus not limited by the thickness of the NP for signal acquisition. To test the ability of PEEM-NEXAFS to identify NP polymer type, pure suspensions of 250 nm PS beads and homemade PC NP as well as a mixture of PET, PA, PMMA were prepared in 100% ethanol and were deposited by a 4 h centrifugation at $2780 \times g$ in glass vials onto SiN substrates carrying a MgO stripe in their middle. NEXAFS spectra were acquired on a $15 \times 15 \mu\text{m}$ field of view with a 3 s dwell time.

The last method tested was scanning transmission x-ray microscopy (STXM) coupled with NEXAFS spectroscopy at the PoLux beamline at SLS of PSI and is described in detail in **Chapter 3**. With the STXM, a sample can be scanned using monochromated x-rays with photon energies just above carbon 1s absorption edge and render an image of all the objects containing carbon in the sample with a spatial resolution of 30 nm (Figure 1-4, C). As for PEEM, the photon energy can be varied in the C1s absorption energy range (280-320 eV) to acquire NEXAFS spectra. At first, NEXAFS spectra of NP were acquired on manufactured PS nanobeads and homemade NP to assess the suitability of STXM-NEXAFS to identify NP polymer types and determine the lower size limit of the method. The combination of the extraction and identification method was then tested by extracting spiked water and soil samples. Finally, the optimised method was applied on unspiked samples of tea preparation and soil samples to assess its suitability to differentiate NP from food and environmental matrices.

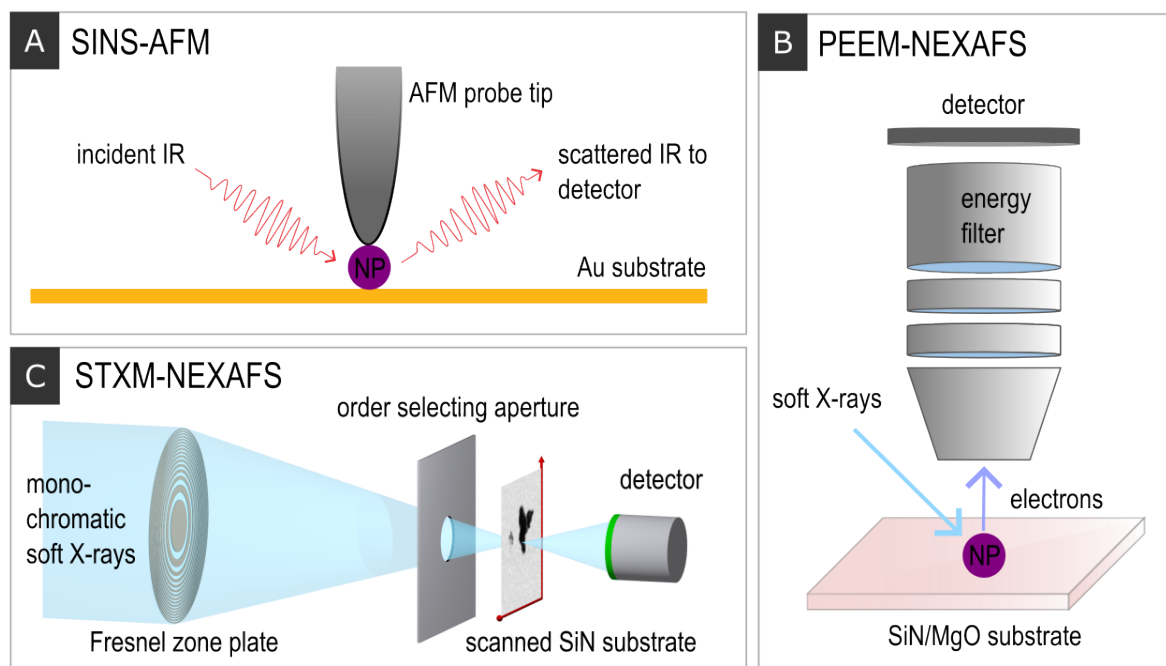


Figure 1-4: Schematic representation of the three synchrotron-based techniques tested in this study for the identification of NP in environmental matrices (figure credits: Alexandra Foetisch and Benjamin Watts).

1.2.3 Physico-chemical ageing of plastic surfaces

In **Chapter 4**, the knowledge acquired on the STXM-NEXAFS technique, during the development of the identification of NP in soil (**Chapter 3**), was transposed to a new application in order to study the surface chemical alteration of plastic debris occurring in the soil environment. For this purpose, NEXAFS spectra were acquired on the surface – bulk material (BM) gradient of plastic debris collected from agricultural and roadside soil samples, providing polymer chemical information with a spatial resolution of 30 nm. To perform this analysis, polymers needed to be cut in ~200 nm thick sections by ultramicrotomy and deposited onto a SiN substrate (Figure 4-1). Preliminary tests showed that, depending on the type of plastic object and the type of polymer, the sections were not always sharp or even in thickness. Indeed, fabric, foam and film lacked sufficient rigidity and PA and PE were too soft to provide high-quality sections. Thus, fabric, foam, and film were imbedded into an epoxy resin before the cutting, and cryo-ultramicrotomy was tested on a PE fragment in the aim to retrieve useful sections.

Additionally, the single weathering factors were tested in controlled experiments: (i) the effect of soil burial was tested by incubating five different polymers in two different soils for a three-month and one-year duration and (ii) the effects of UV radiation were investigated by exposing polymers to UV in an accelerated weathering experiment. Potential changes in surface morphology due to soil weathering were investigated using SEM on soil incubated polymers. Finally, the characteristics of the chemical surface alteration were investigated the same ways

as for the environmental plastic debris and the results were compared. As no optimized software was available for the treatment and analysis of the data generated with this specific application of the STXM, a semi-automated data processing script was written on the open-source platform Rstudio (RStudio Team, 2020).

1.3 General results and discussion

1.3.1 Easy-to-use single particle based method to quantify and characterise TWP in soil

One of the main challenges arising when studying MP in the soil environment is to efficiently isolate the plastic from the soil mineral and organic constituents. The development, optimisation and validation of the extraction method which was performed in collaboration with Adrian Grunder, Tobias Stadler and Benjamin Kunde and will be published shortly. For this reason, only the optimisation and validation steps relevant to TWP are discussed in this thesis. The Figure 1-5 shows a simplified representation of the different extraction steps applied to TWP in soil in **Chapter 2** and the pictures illustrate the effects of the different optimised steps.

The visual comparison of the soil extract replicates filtered on the 0.45 µm PC filter and the 10 µm stainless steel filter (Figure 1-5, A) showed a clear difference. Reduced particles filter coverage results from the fine size fraction particles that are retained on the 0.45 µm pore size filter passing through the 10 µm pore size filter. As a 35 µm minimum size threshold was determined for optical identification of TWP (see section 2.3.1), a potential loss of TWP under that size threshold would not affect the results in our case. The introduction of the NaUT treatment before the Fenton reaction allowed to significantly reduce the amount of unwanted remaining NOM on the final filter (Figure 1-5, B). The mean reduction of the filter area covered by NOM was 33.2% but varied between 9.6 to 75.9 % depending on the soil tested (data not shown). Regarding the significant improvement brought by this step, we decided to include it into the extraction protocol. However, (Olsen et al., 2020) tested the effect of the NaUT treatment coupled with a 30% H₂O₂ + 1% NaOH oxidation step on PE, PS, PP, PET and PA and observed structural changes for PA (embrittlement) and weight loss for PET and PA. Thus, it would still be important to assess the effect of the NaUT treatment combined with the Fenton reaction to ensure a proper recovery of all MP polymers, including TWP. Finally, the implementation of an acidic treatment to dissolve the iron oxide present at the surface of the filter after the last filtration allowed to remove almost completely the orange layer impacting the colour of the particles presents (Figure 1-5, C). As the acidic treatment was not as strong as previously applied (Bigalke et al., 2022), we assumed it would not degrade the plastic present on the filter.

In brief, the optimised extraction method consists in the following steps. After sampling, the soil is dried and sieved to 2 mm. The soil aggregates are broken by ultrasonication and the mineral fraction of the soil is eliminated by density separation using a sodium bromide (NaBr) salt solution of a density 1.5 g/cm³. After centrifugation, the supernatant is filtered through a metallic filter (10 µm pore size). The retentate, containing mainly the plastic and the natural organic matter, are resuspended in the NaUT solution and kept at -20°C for 40 min, until crystals appear into the solution. The NaUT solution is then washed away and the SOM is oxidized by Fenton reaction which uses hydrogen peroxide as oxidizing agent and Fe as catalyst. The samples are washed afterwards on a metallic filter (10 µm pore size) and a second density separation (NaBr, 1.5 g/cm³) is applied to remove residual minerals. The resulting supernatant is finally filtered onto an Anodisc filter and the 2M H₂SO₄ acidic treatment is applied to remove the iron oxide from the Anodisc filter.

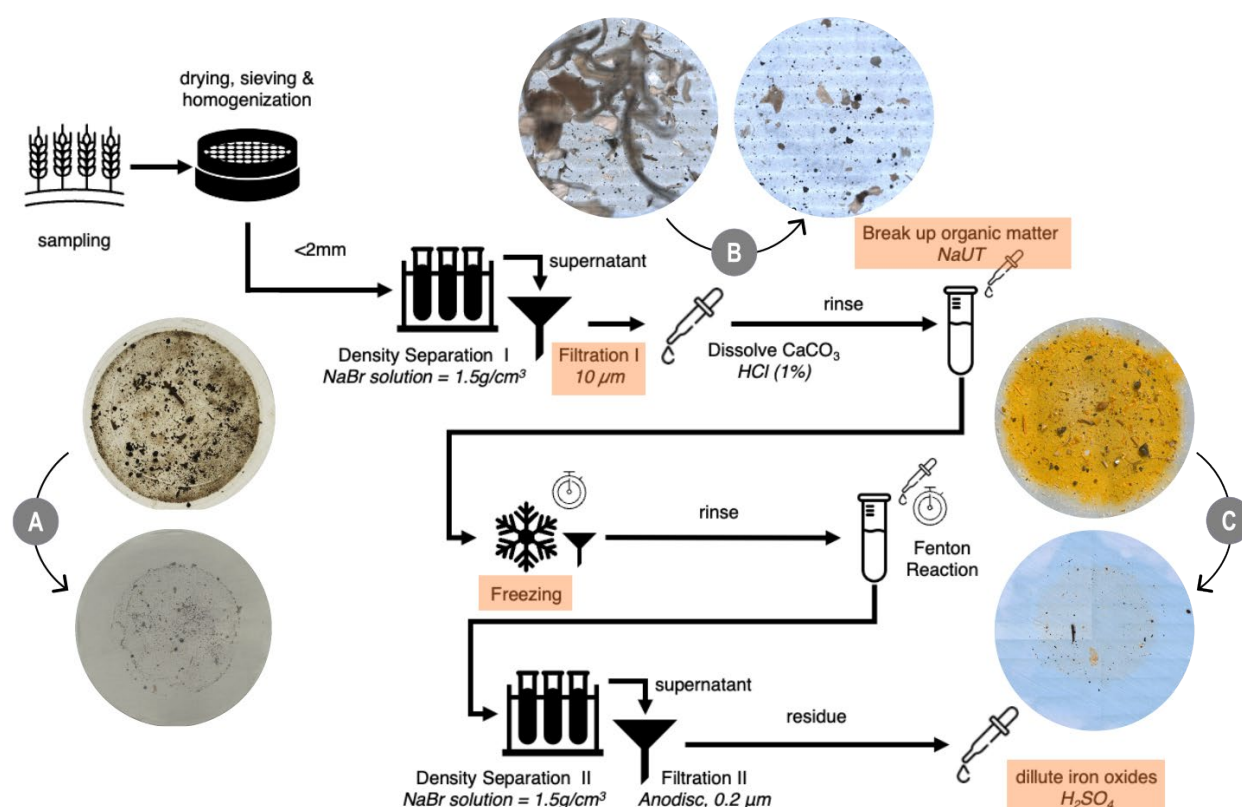


Figure 1-5: Schematic representation of the different steps for the extraction of MP from soil samples. The optimized steps are highlighted in orange and optical pictures illustrate the improved steps effects. (A) Fine particles reduction, (B) NOM reduction, (C) iron oxides dissolution. (Figure credit: Adrian Grunder, Tobias Stadler, Alexandra Foetisch).

In **Chapter 2**, the above presented method was applied to extract TWP from soil and they were identified on optical microscopy images by a machine learning segmentation model. An 85.4 % recovery rate was achieved using cryo-grinded TWP for particle sizes > 35 µm with a LOD and LOQ calculated at 1 particle. The density of traditional MP typically varies between

0.9 and 1.45 g/cm³ (He et al., 2020) and saturated salt solution of 1.2 to 1.5 g/cm³ are commonly used in MP research (Bläsing and Amelung, 2018; Nabi et al., 2022; Perez et al., 2022). However, the density of TWP can vary widely between 1.2 and 2.2 g/cm³ (Klößner et al., 2021b, 2019) depending on the amount and type of mineral encrustment that is carried on their surface (Kovochich et al., 2021). A density separation performed on a tunnel dust sample showed that the 1.5 g/cm³ density of the NaBr solution was not high enough to isolate the whole TWP fraction present in environmental samples (Appendix C.4). The ultrasonication applied during the extraction could induce a partial loss of the encrusted mineral particles and thus change the range of densities in which environmental TWP are present. It is thus not possible to infer the recovery rate of our method on environmental TWP. Recent work has shown that the majority of the TWP in highway tunnel dust were present in the <1.7 g/cm fraction (Klößner et al., 2021b) and density solution of 1.8-2.2 g/cm³ using sodium iodide (NaI) or sodium polytungstate (SPT) were suggested for the extraction of TWP from environmental samples. Although these solutions allow to obtain higher recovery rates, they are harmful for the environment and their use should be minimized. The analysis of the highway soil showed a general decrease of the TWP concentrations with 8080 ± 1059 , 9106 ± 3234 , 4091 ± 623 and 2562 ± 1160 particles kg⁻¹ dry soil for a distance of 1, 2, 5 and 10 m from the road, as observed in previous studies (Baensch-Baltruschat et al., 2021; Fauser et al., 2002; Knight et al., 2020; Müller et al., 2022; Panko et al., 2012). This indicates that, even if the totality of TWP cannot be extracted, the method already allows to detect general patterns in their occurrence. However, future research should focus on studying the effect of ultrasonication on the TWP mineral encrustment stability to allow a better estimation of environmental TWP concentration.

TWP have been very well characterized in previous work for TWP generated on a road simulator (Kovochich et al., 2021) and detected in air born samples (Rausch et al., 2022) using SEM-EDX. They are most of the time described as “having an elongated shape and a mineral encrustment” (Kreider et al., 2010). However, our results showed that, in the 2mm - 35µm size range, TWP circularity was well distributed between 0.25 and 0.75 (Figure 2-4) , indicating there was a smooth distribution of the elongated and almost spherical particles in that size range, which, to our knowledge, was never reported before. The experimental design presented in **Chapter 2** did not allow to assess if the particles having a broader shape distribution resulted from their formation processes being different compared to other study sites or from an ageing of the particles in the environment. Yet, the application of the colour-based identification method would be suitable to answer this specific question and future research should investigate the effect of the different factors affecting TWP formation (road type, vehicle speed, tire initial composition, frequency of breaks and acceleration) on the

shape and sizes of the TWP present in soil. Moreover, the TWP mass concentration can be inferred from the measured dimensions of each particle (Tanoiri et al., 2021) and compared to results obtained with different MS analytical techniques such as.

1.3.2 Single particle based method to quantify and characterise NP in soil

In the specific case of NP, the same extraction protocol as for MP or TWP could not be applied. Due to their size range, NP can behave differently in similar conditions (Gigault et al., 2018). The attempt to use a magnetic extraction on PS nanobeads led to the formation of massive NP aggregates (Figure 1-6). The sizes of the spheres observed in the samples were always larger than expected. The EDX analysis (Appendix B.1) revealed that all the spheres were covered by Fe, suggesting the change of size was due to the presence of an iron outer layer. In addition to the spheres, irregularly shaped particles in a wide size range were also observed. Because of the iron covering them, it was not possible to determine their elemental composition with EDX but they could be composed of Fe alone or Fe-covered SOM. Such aggregates hinder single-particle analysis as the particles are not physically isolated. Moreover, the iron covering the particles might interfere with the detection signal to identify the polymers. Thus, a further separation of the NP from the iron would be required. However, the modified Fe hydrophobic tails form S-O bonds (bond energy of 452 kJ/mol) with the plastic surface, which are stronger than C-C bonds (bond energy of 345.6 kJ/mol) (Grbic et al., 2019), allows for efficient separation without affecting the polymer unlikely. As a result, due to the probably low selectivity of the modified Fe nanoparticles to bond to plastic and the difficulty represented by the isolation of the NP from the Fe, this method was not further considered.

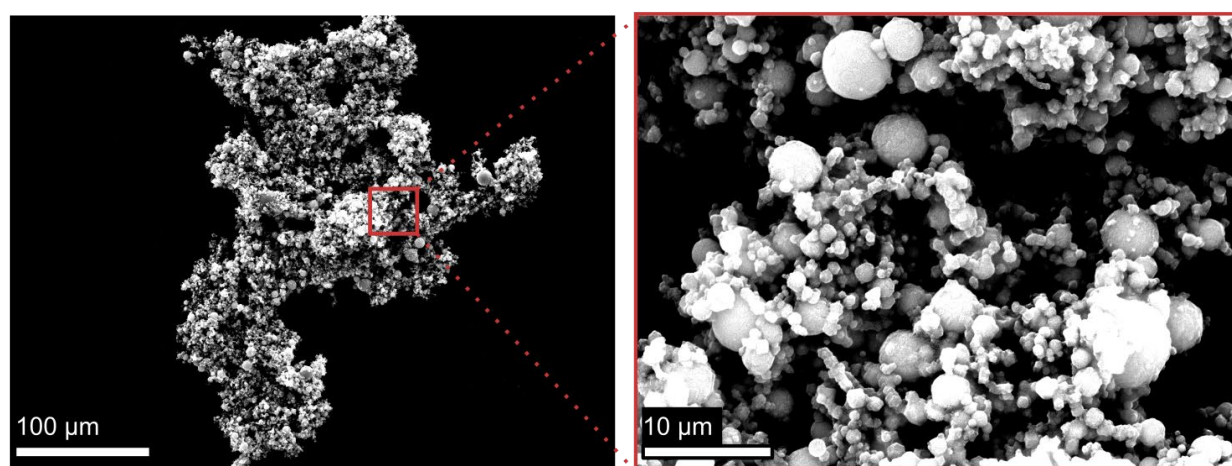


Figure 1-6: SEM back scattering images of a PS nanobeads aggregate formed during NP magnetic extraction.

Nevertheless, more promising results could be obtained by adapting and combining steps applied for the extraction of metallic nanoparticles and MP. While the elimination of the mineral

fraction by density using NaBr ($\rho = 1.5 \text{ g/cm}^3$) induced a strong aggregation of the PS beads in the suspension (Figure 1-7, A), the sucrose allowed to concentrate the nanobeads at the surface of the cushion in a homogenous cloud (Figure 1-7, B) and was thus selected for this application in **Chapter 3**. Yet, it was not possible to reach a density $>1.3 \text{ g/cm}^3$ and it is likely that denser polymers, such as PET or PVC ($\sim 1.45 \text{ g/cm}^3$) could be lost during this step. Thus, more effort should be dedicated in finding a suitable solution with a higher density or different conditions to ensure the recovery of most traditional polymers.

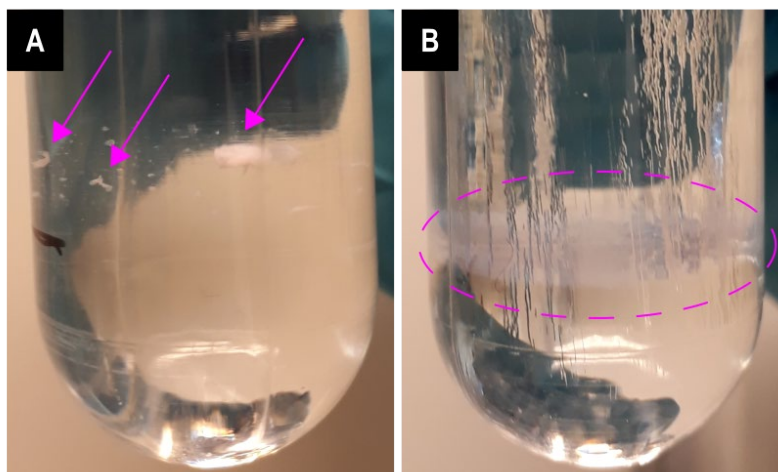


Figure 1-7: Effect of density separation using NaBr (A) and sucrose (B) cushions on the behaviour of PS 100 nm beads in solution.

The results of the SOM oxidation optimisation are presented in detail in Section 3.2 and Appendix D.3. The sequential addition of H_2O_2 every 2 h to maintain a $\sim 5\%$ H_2O_2 concentration showed a continuous reduction of the TOC in the samples while the effect of a single H_2O_2 addition stopped after 2 h incubation. The SEM imaging of the 100 nm PS spheres after 24 h of sequential additions showed that the solution still contained a concentration of sucrose high enough for it to crystallise on the substrate and nanobeads surface (Figure 1-8). Thus, it was not possible to infer possible surface modifications induced by the treatment. Still, the beads were spherical and had a diameter corresponding to the expected 100 nm spheres, indicating that this treatment did not induce a size reduction or shape alteration. PS beads are often used for method validations as they are commercially available, and their spherical shape allows to recognise them in a sample without the help of a spectroscopic method. Nonetheless, MP research showed that not all the polymers have the same sensitivity to the same treatment (Monteiro and Pinto da Costa, 2022). The availability of nanospheres made of other polymers than PS at a reasonable price would help to assess the effects of the different treatments on a wider range of nano polymers.

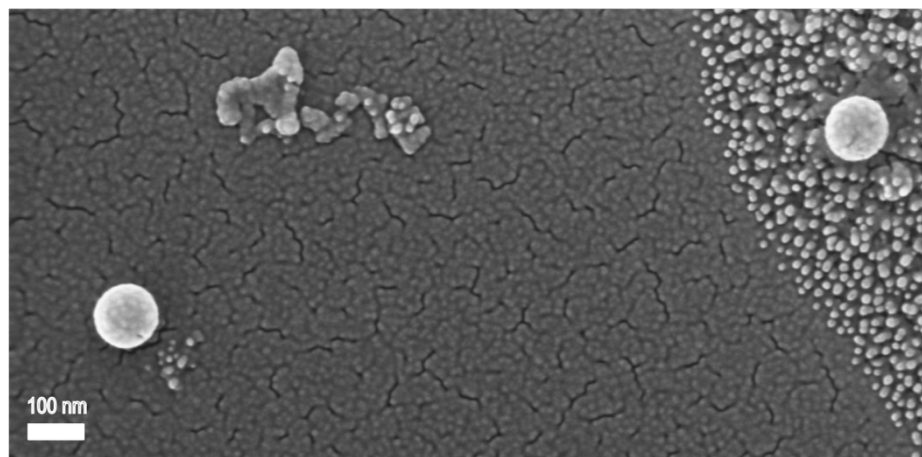


Figure 1-8: SEM InLens images of PS 100 nm beads after 24 h of H_2O_2 sequential addition. (Image credit: Laure-Hélène Vinot)

The **Chapter 3** describes in detail the final extraction protocol. In summary, it consists in a first homogenisation of the soil sample into a dispersant solution and a settlement to separate particles according to their sizes (Stokes, 1851). The smaller particle fraction is collected and centrifuged on top of a sucrose cushion, to separate the mineral from the organic fraction. The remaining SOM is oxidized with 5% hydrogen peroxide (H_2O_2) and the sample is filtrated and concentrated by pressure assisted filtration until reaching a final volume of 10 mL.

After their extraction, single NP identification requires particles to be deposited on a substrate on which every particle can be localised and measured, or areas of the substrate can entirely be scanned. The NP extracted from any environmental matrix needs then to be deposited on the smallest area to minimise the surface which need to be scanned. Depending on the amount of material to be measured (e.g. remaining OM, actual NP), the characterisation of all particles would still be too time consuming. In that case, it is conventionally accepted to measure random areas of the substrates and to extrapolate the results for the whole sample. However, this extrapolation method assumes that particles are homogeneously distributed. Thus, an ideal NP extraction method would allow to maximise the concentration of NP in the final extract, which should then be distributed homogeneously on a substrate. In the field of metallic nanoparticles, an homogeneous deposition is most often achieved by centrifuging the particle down on a substrate (Markelonis et al., 2015). As preliminary test showed a poor recovery of PS beads on a SiN wafer, we tested the effect of the substrate composition on the recovery by centrifuging PS and homemade PC NP suspensions down SiN and MgO substrates. The recovery of PS nanobeads was ~ 16 x higher on a MgO than a SiN substrate (Figure 1-9, A and B) and the recovery of PC, on the contrary, was ~ 3 x higher on a SiN than a MgO substrate (Appendix B.2). These results show that the material of the substrate, the polymer type and/or the conditions of NP production will affect NP their recovery when being

deposited by centrifugation, resulting most likely from the interaction of the charges present at the surface of each material. This also suggests that the recovery of environmental NP after their extraction will depend on their surface properties, which can vary according to the polymer types and the conditions in which they were released into the environment. In light of these results, drop deposition of PS suspensions was also tested in the aim to ensure the whole NP fraction deposition on the final substrate. Drop deposition only allowed to deposit a very small fraction (μL) of the NP suspension, while centrifugation can deposit a much bigger volume (mL) on the substrate. Additionally, a coffee ring effect where particles aggregate in concentric circles (Hu and Larson, 2002; Mampallil and Eral, 2018) was systematically observed, leading to a highly heterogeneous distribution of the particles (Figure 1-9, C).

Despite a recovery fluctuating with the different polymer and substrate test materials, centrifugation was preferred over drop deposition as NP homogenous distribution was more favourable for single particle analysis. Thus, even if the method developed in **Chapter 3** allowed to detect NP from soil samples, work effort should focus on ways to maximise NP concentration in the final extract solution and homogeneously distribute NP on a substrate with an equivalent recovery rate for all polymer types to allow quantitative analysis of NP in soil (and other matrices) samples.

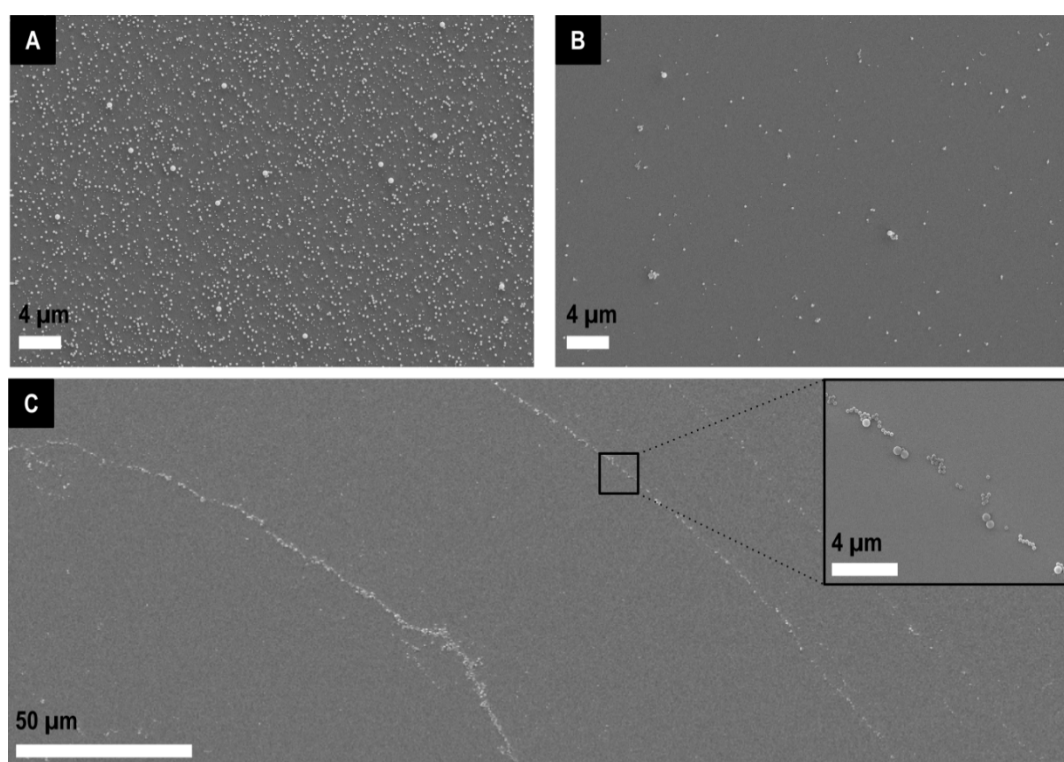


Figure 1-9: SEM secondary electron images illustrating the challenge of NP concentration and of their homogenous distribution on a substrate. (A) PS nanobeads suspension deposited by centrifugation on a magnesium oxide (MgO) substrate. (B) Same PS nanobeads suspension as shown in (A) deposited by centrifugation on a silica (Si) substrate. (c) Coffee ring effect after drop deposition and evaporation of a PS nanobeads suspension. The zoom in show that's the visible circle segments are nanobeads aggregations.

After NP extraction, SINS-AFM was tested for NP identification. Despite our expectations, several reasons led us to conclude that this technique could not be applied in NP monitoring. Indeed, even after a sample preparation fitting the AFM requirements, the golden cantilever tip broke several times. The replacement of the probe implied the realignment of the setup, which could take up to 4 h. The sample scanning with AFM was slow and the absence of motorized stage hindered the possibility of targeting an area previously localized by SEM or optical microscopy. Additionally, despite AFM having a high spatial resolution for imaging and allowing almost a three-dimensional representations of the particles, some particles could be missed out when they do not adhere strongly to the substrate by dragging them along the scanned area. No NP polymer could be positively identified because of a weak signal to noise ratio and apparent AFM instability. Indeed, the closer the AFM tip is to the reflective surface, the stronger the signal is. It could thus be possible that the weak signal to noise ratio observed in our measurements was induced by the particles being too thick and hence the tip being too far from the reflective surface. A PC measurement example is provided in Figure 1-10 A and the resulting absorption spectrum is displayed together with PC reference measured by ATR-FTIR. While some features could be observed in the 1300-800 cm^{-1} region, they did not match the ATR-FTIR spectrum of the corresponding material, and no signal was detected above 1300 cm^{-1} . Indeed, in addition to being influenced by the sample's composition, the near-field effect of the tip-sample region can also impact the scattered light and, consequently, the resulting nanoFTIR spectrum. A direct comparison between far-field (e.g. ATR-FTIR) and near-field (nanoFTIR) spectrum is thus not always possible, challenging the polymer chemical identification (Nan et al., 2021). Finally, the instability of the AFM affected more than 60% of all acquired spectra by inducing sinusoidal waves in the signal and rendering unreliable spectra (Appendix B.3). With these first results, no additional beamtime was requested at the ALS 5.4.1 beamline. However, nanoFTIR should not be disregarded as a potential method for identifying NP polymers. The MIRIAM beamline B22 at Diamond Light Source (Oxford, UK) offers near-field FTIR microscopy in photo-thermal mode. This means that, instead of measuring the scattered IR light, the expansion of the material is tracked by the AFM tip while being exposed to IR. The variation in the material expansion when exposed to a 4000-400 cm^{-1} IR range can then be converted into a FTIR spectrum. This technique has already allowed to identify 700 nm PMMA beads embedded into a protein film (Cinque et al., 2016) and further tests could be conducted to determine the lower particle size threshold this technique can achieve. Unfortunately, we did not have the opportunity to test this technique, as the last call for beamtime application was in 2018 and has not been renewed since.

The tests conducted to assess PEEM suitability to identify NP ruled out this option. The different steps to introduce a sample into the chamber, focusing the beam and start measuring

could take up to several hours, preventing an acceptable sample throughput. As we were working with solutions containing only NP, we expected to obtain a signal specific to every polymer type, similar to NEXAFS previously measured on different polymers (Appendix D.7). Replicate measurements acquired on a pure 250 nm PS beads sample (Figure 1-10, B) or a pure PC sample showed all the same spectrum which was not corresponding to the PS or PC NEXAFS reference. When measuring the mix of NP, all particles < 1 μ m analysed rendered the same spectrum as observed for the PS beads (data not shown). Nevertheless, we were able to recognise some typical features of PA and PMMA on several particles > 2 μ m (Appendix B.4), indicating a probable effect of the particle size on PEEM ability to identify the polymer type. The other polymers present in the mix (PET, PP) were not detected at all. It is likely that the three dimensional state of the particles in the system impacted the images and spectrum acquisition due to localized charging occurring with non-conductive material (Gilbert et al., 2000) and hindering the identification of NP with this technique. Therefore, the use of PEEM for NP identification was not carried on further.

Finally, STXM appeared to be a good candidate for the NP identification task. The detailed protocol for NP identification with STXM-NEXAFS is presented in **Chapter 3**. It allowed to positively identify NP and determine their polymer type in food and environmental matrices. An example of a PA nanoparticle measurement from a tea infusion prepared with PA teabags is presented in Figure 1-10, C. The technique allowed to detect and characterize the size and shape NP extracted from agricultural soil samples for the first time and led to a publication in the *Journal of Hazardous Material* in 2022. The STXM has a spatial resolution of 30 nm but the minimum NP size which can be positively identified is limited by its thickness. Indeed, the investigated material needs a minimum thickness of around 100 nm to absorb a sufficient amount of photons and render spectrum with an acceptable signal to noise ratio (Appendix D.8). However, to our best knowledge, no single particle analysis technique achieved yet to provide chemical information on environmental NP <100 nm and effort should be made to lower this threshold.

Even if NP could be detected with this technique, no quantitative data could be acquired due to the time needed for a measurement and the challenge of NP concentration and recovery with the applied centrifugation deposition. Thus, the combination of STXM-NEXAFS with a thermal analytical technique such as Py-GC/MS could provide complementary information on the total mass per polymer and the particles size and shapes in the > 100 nm range.

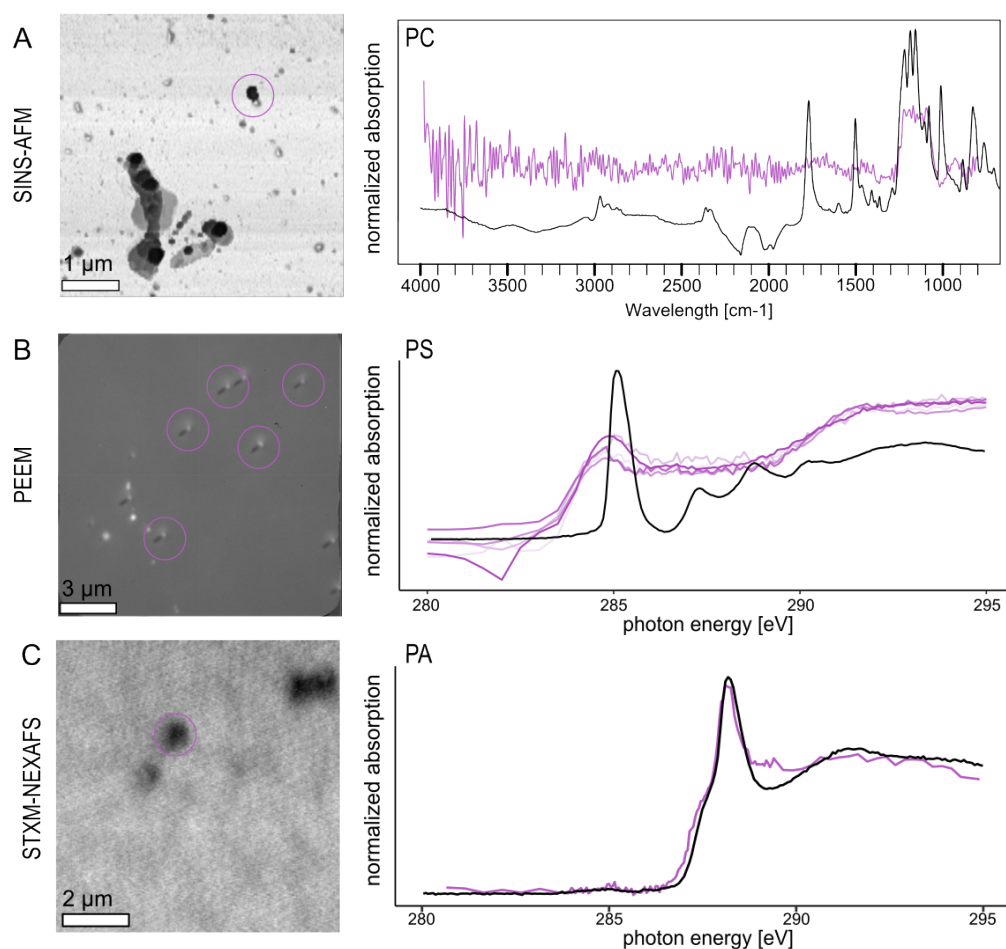


Figure 1-10: Examples of images and spectra acquisition for (A) a homemade PC nanoparticle with SINS-AFM, (B) PS nanobeads with PEEM and (C) a PA formed by the fragmentation of a tea bag with STXM-NEXAFS. The black line corresponds to a reference spectrum and the purple line to our measurements. The position of the measured NP is indicated by a circle on the images.

1.3.3 Surface physico-chemical properties of plastic occurring in soil

While numerous studies have described the effect of UV radiation on polymers (Ainali et al., 2021; Cai et al., 2018; Fachine et al., 2002; Kamweru et al., 2011; Mylläri et al., 2015; Ramani and Ranganathaiah, 2000; Turton and White, 2001), (Büks and Kaupenjohann, 2022) recently highlighted the lack of knowledge on the effect of biogeochemical aging factors occurring in the soil (secreted enzymes, organic and inorganic acids, bioturbation, frequent leaching and freeze-thaw cycles). The exposition of plastic particles to the soil is susceptible to change its surface properties and thus to play an important role in determining their fate and impact in the soil environment. Most of these biogeochemical factors, as opposition to UV irradiation, cannot be accelerated while maintaining environmentally relevant conditions and the processes affecting the polymers surface are expected to be slow. Consequently, an analytical tool allowing to detect changes in polymer chemical composition on a nanoscale was needed. The knowledge on the STXM-NEXAFS technique acquired when developing the **Chapter 3**

gave the opportunity to extend its application and the **Chapter 4** consist in a pioneer work in characterising traditional plastic surface composition with a spatial resolution of 30 nm.

The preparation of polymer thin sections for this type of analysis worked well for hard polymer fragments such as PET (Figure 1-11, A), PS, PC and PP but PA and PE fragments (Figure 1-11, B, D) were too flexible to produce high quality sections. As an alternative, it is possible to embed plastic into an epoxy resin to form a hard and easy to cut shell. However, only areas of the section which are detached from the epoxy resin during the cutting process can further be analysed by STXM, significantly decreasing the suitable areas for the chemical analysis. The epoxy embedment still allowed to obtain good quality sections for a PET fabric despite the initial flexibility of the object (Figure 1-11, F), but did not improve the section quality of PA fragments (Figure 1-11, B), PE films (not shown) or PU foam (Figure 1-11, C). Cryo-microtomy was tested on a PE fragment and allowed to produce sections of a much better quality (Figure 1-11, E). Yet the deposition of the section onto the SiN substrate was challenging and we did not manage to lay the sections flat during the allocated time. Thus, more time dedicated to the development of an efficient deposition method for cryo-microtomed sections could allow to expand the range of polymers that can be analysed for surface chemical composition. The efficiency of the combination of embedment with cryo-microtomy should also be tested.

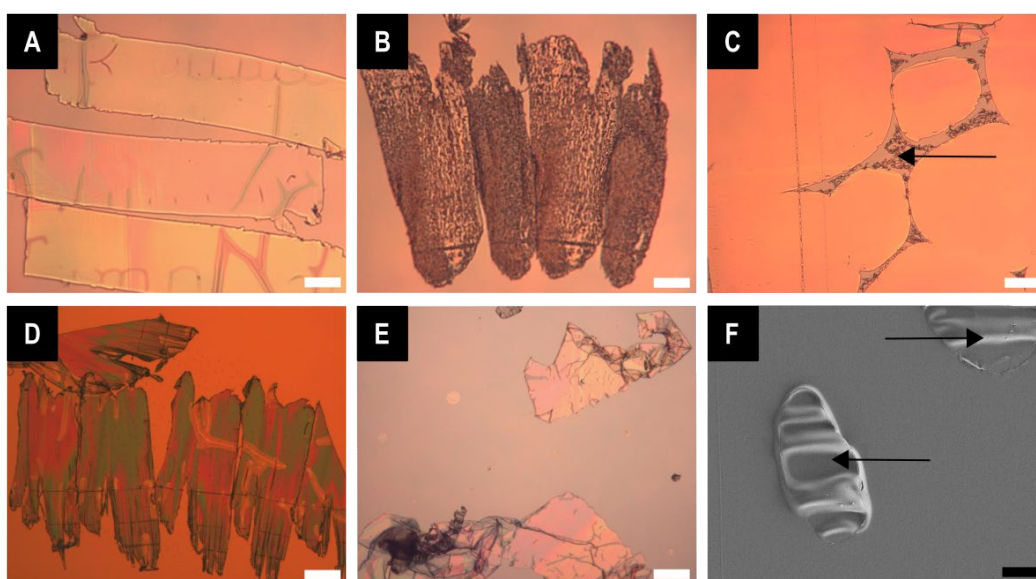


Figure 1-11: Microtomy sections optical microscopy images of (A) PET, (B) PE, (C) PU embedded into epoxy, (D) PA, and (E) cryo-microtomed PE. The white scale bars represent 100 μm . (F) Microtomy section SEM secondary electron image of a PET fabric embedded into epoxy. The black scale bar represents 5 μm . The position of the polymer is indicated with black arrows when embedded into epoxy.

Our results showed that, indeed, plastic fragments recovered from soil samples could have a modified surface and that the surface alteration, when present, was different compared to polymers only exposed to UV radiation, supporting the hypothesis of (Büks and

Kaupenjohann, 2022). However, no surface chemical (Figure 4-4) or morphology (Appendix B.5) alteration after one year of controlled soil incubation could be detected. Therefore, further experiments including long term field incubation need to be conducted. This would allow to investigate the effect of the weathering factors in a more dynamic environment than a bottle in an incubator and to estimate a timescale for the weathering processes occurring in the soil.

The observation of surface fragmentation initiation on a weathered PS debris gave an insight of the most probable chemical signature of a future secondary NP (Figure 4-3). The predicted chemical signature of the particle would then be different from the initial polymer composition. This rises again the question of the ability of the detection techniques in the nanoscale range to positively identify this particle as plastic and to still be able to retrieve its polymer type. These possible surface alterations and particles formation processes should be taken in account when choosing the adequate test material for ecotoxicological studies or investigating the behaviour and interaction of the plastic in the environment. In that sense, (Alimi et al., 2022) highlighted the need of harmonized weathering protocol in effects studies to allow the comparability of the results. Thus, the mechanisms and the effects of the biogeochemical factors occurring in the soil need to be further investigated to produce testing material which is environmentally relevant. Nonetheless, one should keep in mind that a harmonized protocol allows for reproducibility but in the case of a heterogeneous matrix such as the soil, a unique method might fail to be representative for the whole diversity of soil occurring in the terrestrial environment.

1.4 Conclusions

The work presented in this thesis aimed to contribute to close the methodological gaps to quantify and characterize two highly relevant categories of plastic debris occurring in the soil environment as well as investigate the effect of soil weathering on polymer surface chemical composition to better understand and predict MNP interaction within the soil. The different analytical techniques tested and developed in this thesis are summarized in Table 1-1. In the following paragraphs, the main objectives are repeated with respective conclusions, followed by a general conclusion.

Develop an easy-to-use single particle based method to quantify and characterise TWP in the soil

As stressed by the UN Plastics Treaty adopted in May 2022, there is an urgent need of a standardized protocol for monitoring TWP in the environment to assess their potential risk, as well as evaluate the effect of future mitigation measures (UNEP, 2022). Indeed, the majority of the data currently accessible were estimated using prediction models, and almost no validation data backs up these estimates (Mennekes and Nowack, 2022). The TWP extraction

and identification method developed in **Chapter 2** showed to be efficient to characterise environmental TWP not only in terms of concentration, but also in providing qualitative information on the particle size and shape distributions. The colour-based detection of TWP has a real advantage over mass-spectrometry techniques because it is common for all TWP regardless of their initial composition and is not prone to change by an exposition to environmental weathering factors.

To the best of our knowledge, this is the first time such data on TWP in soil have been reported. The application of the developed method to environmental soil samples could thus provide monitoring data to validate or adjust the prediction models. It could also be applied in research focusing on TWP transport dynamic in the soil or on the effect of driving conditions on the particle size and shape of TWP released in the environment, for example. This knowledge would make it possible to characterize environmental TWP more accurately in terms of their size and shape, which are key elements in determining their potential toxicity and providing the basis for the development of environmentally relevant test material.

Develop an extraction protocol and single particle identification method to characterise NP in the soil

The method developed in **Chapter 3** allowed to detect the presence of NP in agricultural soils for the first time, but challenges in sample preparation and STXM low sample throughput did not allow to collect quantitative information. The real advantage of STXM-NEXAFS lies in its ability to efficiently differentiate polymers from NOM in a nanoscale and is thus powerful to validate the presence of NP in a well characterized sample. The presence of NP in agricultural soil suggests a potential plant uptake and transfer to livestock and humans through crop consumption. Currently, NP ecotoxicology tests are using elevated NP concentrations and commercially available testing material in order to detect an effect on organisms and to characterise the toxicity mechanisms. However, to determine the risk that NP can represent for the environment, organisms' exposure to NP in the soil needs to be assessed. Combining STXM-NEXAFS with a thermal analytical method like Py-GC/MS could provide further details on the total mass per polymer and give the most complete NP characterisation in soil to date. This information would allow to design more realistic ecotoxicology tests to assess not only the toxicity but also the risk that NP represent in the soil environment. Though, both STXM-NEXAFS and Py-GC/MS rely on the chemical composition of the polymer to identify the plastic in a sample, but the chemical structure of soil environmental NP is unknown. Indeed, the factors inducing a release of NP and NP exposition to environmental conditions can affect their chemical fingerprint, and the ability of the different techniques applied for weathered NP detection has not yet been assessed. It is thus critical to understand better the processes

leading to NP release in the soil and the NP chemical characteristics, as well as determine the ability of the two techniques to positively identify them.

Investigate the physico-chemical ageing of plastic surfaces exposed to UV and soil

The application of STXM-NEXAFS allowed polymer surface characterisation on a depth gradient at a resolution which was never achieved before. Such a resolution enables the identification of very thin altered layers at the polymer surface and can be used to investigate the physicochemical processes induced by a wide range of environmental weathering factors. It is particularly interesting in the case of soil weathering, as the soil biogeochemical processes are expected to be slow and can hardly be accelerated while maintaining environmentally relevant conditions. The soil incubation performed in **Chapter 4** did not induce any detectable surface alteration on the tested polymers but longer incubations in more dynamic conditions (field experiments) could be conducted to provide a time estimation for the weathering processes to occur in soil. The comparison of UV and naturally-soil weathered plastic agreed well with (Büks and Kaupenjohann, 2022) assumptions that soil biogeochemical factors are affecting polymers surface and that artificial aging of test material using UV radiation might fail to produce soil representative MNP. Thus, the effect of individual soil weathering factors could be compared with environmental plastics surface to determine which factors lead to which alteration and to propose a procedure for the fabrication of environmentally relevant artificially aged polymers. As plastic surface features govern their distribution, transport, and interaction within the soil ecosystems, soil plastic surface characterisation could be useful in improving prediction of these phenomena. To broaden the range of polymers that can be investigated with this technique, efforts should be dedicated to optimise the sample preparation using cryo-microtomy to section the more flexible polymers such as PE, PA and PU.

General conclusion

Both the scientific community and the public became alarmed by the possible damage that plastic might represent for the environment as plastic pollution became more and more obvious. If it is generally accepted that plastic in the environment significantly degrades landscape natural beauty, the risks it represents for the environment has not fully been assessed yet. The aim of plastic monitoring is to provide a comprehensive understanding of the distribution, behaviour and impact of plastic in the environment. The main aim of this PhD thesis was to address the methodological and data gaps for the characterisation of MNP in soil samples. The development and use of the techniques introduced in the present thesis can considerably advance our understanding of the sources, interactions, and behaviour of plastics in soil as well as their shape and physico-chemical properties. Yet, these analytical techniques continue to have limitations that hinder the characterisation of the whole plastic

diversity occurring in the soil environment. Therefore, more research is required, in particular to enhance quantitative estimations and decrease the minimum size examined. The results obtained with these techniques brought attention to the fact that MNP characteristics varied depending on the environmental compartment they were occurring in. This emphasizes how crucial it is to monitor MNP in soil because its characteristics cannot always be expected to be identical to those of other mediums, such as air or water. A full characterisation of MNP in soil is of high importance for plastic risk assessment, as its toxicity is determined by these characteristics. Risk assessment studies, can then be able to provide the ground information for policies and management strategies, which aim to reduce the negative impact of plastic on environment and human health. The participation of this research in the process of risk mitigation is highlighted in Figure 1-12.

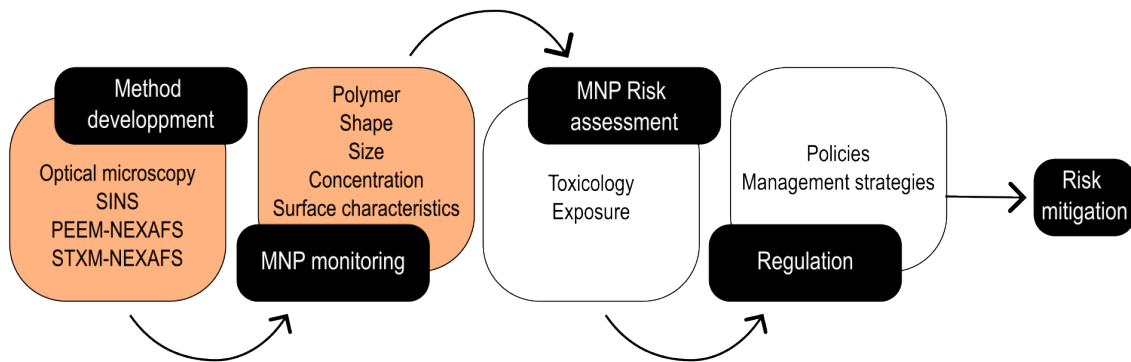


Figure 1-12: Process of plastic risk mitigation

Table 1-1: Possible applications of the analytical methods tested in this study.

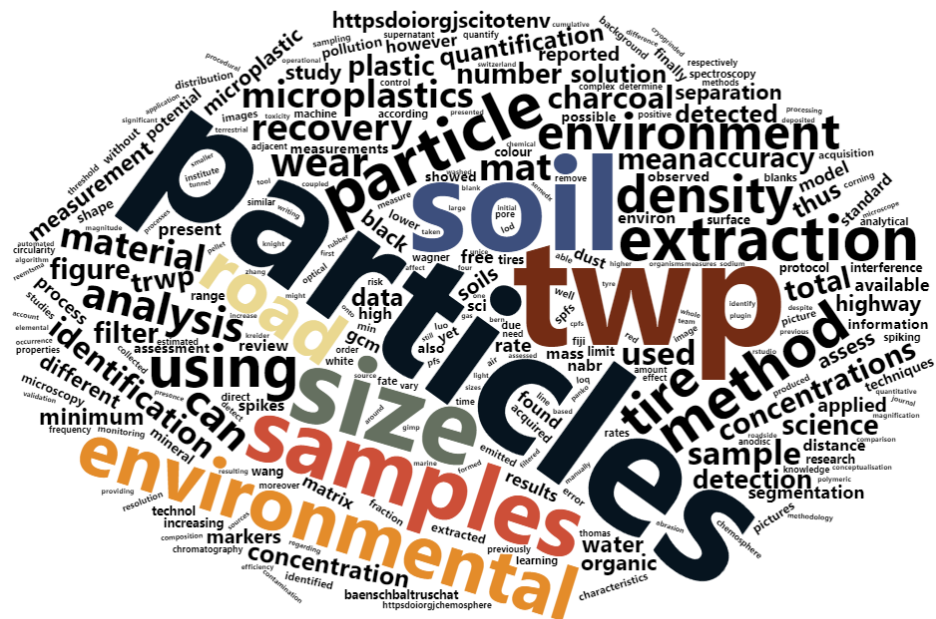
	Optical microscopy	SINS-AFM	PEEM	STXM-NEXAFS
Instrument used in this study	Leica M205C microscope equipped with a LED300 RL ring illuminator and a DMC5400 camera	5.4.1 beamline of the Advanced Light Source (ALS) in the Berkeley Lab (California, USA)	Surfaces/Interfaces Microscopy (SIM) beamline of the Swiss Light Source (SLS) of the Institute Paul Scherrer (PSI, Switzerland)	PolLux beamline of the Swiss Light Source (SLS) of the Institute Paul Scherrer (PSI, Switzerland)
Spatial resolution	1.5 μm	<20 nm	100 nm	30 nm
Single particle	MP	Yes	No	?
	NP	No	Yes	Yes
Particle imaging	Yes	Yes	Yes	Yes
Chemical information	No	Too weak for NP	Not possible for NP	Yes
Quantitative	Yes	No	No	No
Measurement time	4 h/sample	2-4 h/sample mounting 15 min/particle	2 h /sample mounting 15 min/particles	30 min/sample mounting 15 min/particles
Accessibility	Basic lab equipment	Through beamtime application proposal	Through beamtime application proposal	Through beamtime application proposal
Cost	Inexpensive as it requires only common lab equipment	The analysis and scientific/technical assistance is covered by the synchrotron facility. The costs include travel and accommodation for ~four people to cover the 24h shifts. For STXM, yet, remote experiments are possible once the users are trained on the machine.		
Application in this study	TWP	NP	NP	NP, weathering

Chapter 2 All black: a colour-based identification of tire wear particles (TWP) from soil

Alexandra Foetisch^a, Adrian Grunder^a, Benjamin Kunde^a, Moritz Bigalke^{b*}

^a Institute of Geography, University of Bern, Hallerstrasse 12, 3012 Bern, Switzerland, ^b Institute of Applied Geoscience, Technical University of Darmstadt, Schnittspahnstrasse 9, 64287 Darmstadt, Germany

*correspondence to: bigalke@geo.tu-darmstadt.de



This is a preprint version of the manuscript to be submitted for publication

Abstract

Despite tire wear particles (TWP) have been estimated to represent up to more than 90% of the total microplastic (MP) emitted in European countries and may have environmental health effects, only few measurements data are available today. The lack of data is due to the fact that no standardized, cost efficient or accessible method is available yet so most of the times, TWP detection in environmental matrices requires highly trained scientific staff and state of the art instruments and implies too much effort to analyse a relevant number of samples. Here, we present a method using only a conventional optical microscope to identify TWP in soil by their colour. Our method showed a mean recovery of 85% in the 35-2000 μm particles size range with a limit of detection of 1 particle, corresponding to the operational resolution. We applied the method to a highway adjacent soil at 1 m, 2 m, 5 m, and 10 m and detected TWP in all samples with a tendency to higher concentrations at 1 and 2m than 5 and 10 m from the road. The observed TWP concentrations varied between 2562 and 9106 TWP/kg and were in the same order of magnitude than what was previously observed in highway adjacent soil. These results demonstrate the method potential to provide quantitative data on the occurrence and characteristics of TWP in the environment. Since the method can be easily implemented in many labs, we suggest it as a protocol for large scale TWP monitoring in soil, to address our knowledge gap regarding TWP in soils.

2.1 Introduction

Microplastics (MP) are distributed globally and have negative consequences on a variety of organisms (Luo et al., 2021; Wagner et al., 2018). MP in the terrestrial environment have been increasingly studied for more than a decade and it is estimated that a significant part of all the MP emitted are tire wear particles (TWP) (An et al., 2020; Baensch-Baltruschat et al., 2020; Sieber et al., 2020; Siegfried et al., 2017; Sommer et al., 2018; Wang et al., 2019), originating from the abrasion of vehicle's tires on the road (Rogge et al., 1993). Because of its estimated high contribution to the overall MP pollution and its toxic additives (Cao et al., 2022; Tian et al., 2022), there is a urgent need to assess TWP environmental concentrations in soils. However, while there are first data about the concentrations characteristics of traditional MP (such as e.g. PE, PP or PET)(Büks and Kaupenjohann, 2020), only model generated predictions of the amount of TWP emitted in soil are yet available (Baensch-Baltruschat et al., 2021, 2020; Luo et al., 2021). In Switzerland, a rubber input of 0.96 ± 0.35 kg/capita into the natural environment, 4% of which ended up the soil compartment, was estimated for 2018 (Sieber et al., 2020). (Kole et al., 2017) predicted the amount of tire material emitted per capita in 13 countries and found a range of 0.23-4.5 kg /year with an average at 0.81 kg/year. They found a value of 1.1 kg/year for Germany, which was confirmed by (Juergen Bertling et al., 2018), who predicted 1.22 kg/year. However, measurement data to validates these

estimations are scarce (Mennekes and Nowack, 2022) and the TWP characteristics in soil, such as size and shape, are yet unknown.

Tires are generally composed of about 50% natural or synthetic (styrene-butadiene) rubber, 45% softening and hardening materials and 5% of other additives. However, the composition can vary widely, depending on the application of the final product (Verschoor, A. et al., 2016). Despite the fact that they only partly consist of artificial polymers, TWP are still considered as MP (Committee for Risk Assessment (RAC), 2020). TWP are formed from the abrasion of the tire tread on the asphalt typically results in TWP encrusted with mineral from the road. The amount and characteristics of TWP emitted depend on a variety of factors ranging from which initial material the tire and the road are made of, to the habits of the driver (Luo et al., 2021). Observed TWP produced in simulators had a minimum size of around 40 nm (Gustafsson et al., 2008) and a maximum size of around 400 μm (Kreider et al., 2010). Once formed, TWP can be deposited on the road and be washed out with the road runoff or emitted in the air and transported to other environmental compartments (Baensch-Baltruschat et al., 2020). Regarding road sided soil, TWP can be transported further away than the directly adjacent zone of the road due to air turbulence induced by high speed vehicles, wind and spray water (Baensch-Baltruschat et al., 2020; Folkesson et al., 2009). When reaching the soil, TWP are suspected to affect soil properties, such as bulk density and water holding capacity, and leach chemical substances, both affecting soil organisms (Kim et al., 2022).

Most of protocols applied to extract traditional MP from soil include a density separation (Nabi et al., 2022) in order to remove the soil mineral fraction. The mineral incrustation at the surface of TWP can extend particles density from 1.2 g/cm^3 to 1.5-2.2 g/cm^3 depending on their size (Kayhanian et al., 2012). Thus, density solution of a density lower than 2.2 might not be able to isolate the whole TWP fraction (Goßmann et al., 2021) and can lead to an underestimation of environmental TWP concentrations. Yet, the stability of the incrustated mineral at the surface of the TRWP has not been studied and it is unclear how different extraction processes might affect their stability (Klößner et al., 2021b), thus modifying TWP density.

The most common identification techniques used for traditional MP are not suitable for TWP detection. FTIR and Raman spectroscopy cannot be applied as TWP are typically opaque to IR light, due to black carbon total absorbance, and do not deliver specific Raman spectra (Müller et al., 2022; Wagner et al., 2018). ATR-FTIR can be used to identify TWP but this method is limited by the size of particles it can measure ($\geq 500\mu\text{m}$) (Leads and Weinstein, 2019) and is time consuming as single particle measurements are acquired manually. Previous studies have reported TRWP concentrations in soil ranging from 155 to 64 000 mg/kg using Pyrolysis Gas Chromatography mass spectrometry (Py-GC/MS) (Panko et al., 2012),

Liquid Chromatography (LC-MS)(Klößner et al., 2021a; Unice et al., 2015), thermal extraction desorption gas chromatography (TED-GC)(Müller et al., 2022) and Headspace Gas chromatography (HS-GC/MS)(Thomas et al., 2023) and observed a positive correlation between TRWP concentration and the proximity to the road, the traffic density and the break and acceleration frequency.

However, mass spectrometry techniques target analytical markers, which can be organic, polymeric or elemental, to assess TRWP presence and abundance in environmental samples. Molecular markers are organic additives which can be traced using chromatography techniques coupled with mass spectrometry (MS)(Knight et al., 2020). If they are considered specific to trace TWP, organic markers are prone to leaching and degradation (Unice et al., 2015) thus increasing significantly the uncertainty of the results. Polymeric markers are representative of the polymeric fraction of the tires and are potentially more consistent than molecular markers. (Rødland et al., 2022) used Py-GC-MS to assess the suitability of different polymeric markers as well as markers combinations to quantify the amount of TWP in environmental samples. They obtained an accuracy range of 85-151 %, reflecting how inferring the concentration of TWP from an indirect measure is hindered by the high variability of tires initial composition and marker stability. Moreover, none of the techniques cited above has been broadly established as they all require specialized and high cost equipment and expert knowledge. Furthermore, beside the total concentration, the size and shape of MP are very important to understand their possible toxicity and consequences in soils (Colpaert et al., 2022; de Souza Machado et al., 2019; Rillig, 2012) but mass based techniques are not able to deliver information about the particle size and shape distribution.

(Rausch et al., 2022) applied scanning electron microscopy coupled with energy dispersive x-ray spectroscopy (SEM-EDX) with a machine learning algorithm using morpho-textural and elemental information to automatically quantify and characterise TRWP in air born samples. However, for soil, the TRWP would first need to be extracted to avoid soil organic matter (SOM) interferences and the TWP elemental signature could be affected by the extraction, complicating the process. Additionally, SEM-EDX is comparably expensive to MS techniques.

Based on our information,(Knight et al., 2020) are the only one so far to have performed a direct single particle analysis of TWP in soil. They used optical microscopy to quantify TWP down to a 50 µm size and identified them by their colour, their elasticity and their resistance to stress cracking. Despite their size limitation due to manual particles handling, they could report concentrations between 0.6 ± 0.33 and 65 ± 7.36 TRWP/mL in roadside drains but did not describe TWP size and shape distributions. Thus, there is an urgent need for an extraction and identification protocol allowing a direct and precise quantification of TWP in different soils

and providing morphological information that are crucial to better understand their formation processes, fate and potential effect on organisms.

In the present study, we aimed to develop a method of extraction and identification of TWP in soil samples based on their characteristic black colour, providing information on the particles number, size and shape with optical microscopy, which is commonly available in many laboratories worldwide. To do so, we (i) evaluated the efficiency of optical microscopy together with a machine learning algorithm to detect TWP based on their black colour and determined the minimum particle size detected (ii) Assessed the extraction and identification procedure recovery, as well as the method limit of detection (LOD) and quantification (LOQ), (iii) investigate possible interferences in the TWP identification process from SOM and charcoal and (iv) apply the extraction and identification method to highway adjacent soil samples and compare our results to previously reported TWP concentrations.

2.2 Material and methods

2.2.1 Sample materials

Plastic free soil sample from a high mountain area (study site n°29 from (Scheurer and Bigalke, 2018)) was used for validation purpose and four soil samples for method application were collected at increasing distances from a highway in Mattstetten (47°01'30N 7°31'03O), Switzerland, during the summer of 2019. The road has a traffic density of 55000 cars/day (SARTC, Swiss Automatic Road Traffic Counts). The soils were taken at 1m (MAT1), 2m (MAT2), 5m (MAT5) and 10m (MAT10) away from the road and consist of 3 subsamples collected in 0-5 cm depth on a 10x10 cm² area and 5 meters apart from each other on a straight line parallel to the road. Detail of sampling plan and soil characterisation are provided in Appendix C.1. The sampling was conducted wearing non-black cotton cloths and using a small steel spade, which was cleaned with distilled water after each sampling to avoid cross-contamination. The soils were packed in aluminium trays, dried at 50°C for 24h in a drying oven, sieved at 2 mm using a metallic sieve (Retsch, stainless steel, 2mm) and stored at room temperature. The reported concentrations in the present study take only in account the size fraction <2mm.

To assess a potential TWP loss during the density separation using NaBr, environmental TWP from a highway tunnel dust were collected in the Büttenberg tunnel (Switzerland, BE). The dust next to the road was sampled into corning tubes using a clean white toothbrush. In a second time, 9.9 mg of the collected dust was suspended into 35 mL of sodium bromide (NaBr) solution, vortexed for 30 s, shaken for 30 min and centrifuged at 2500*g for 30 min. The particles in the supernatant were separated from the pellet as described in (Grunder et al, in prep) using a decanting aid and deposited down polycarbonate filters (Whatman Nucleopore,

47 mm, 0.8µm pore size, WHA111109) by vacuum assisted filtration. The pellet material was resuspended into MiliQ and deposited on a filter in the same way. The particles were then transferred onto a carbon conductive tab fixed on a SEM holder. The morphology and elemental composition of the particles TWP present in the supernatant were analysed by SEM (GeminiSEM 450, Zeiss) and EDX spectroscopy and compared to the particles in the pellet material. Measurements were acquired in backscattering mode with a working distance of 8.5 mm and 12 kV.

2.2.2 Spiking material

We choose to use self-made cryo-grinded TWP as spiking material, as no reference material exists yet for TWP and that TRWP produced from road simulator are not commercially available. Moreover, we needed a spiking material containing only TWP without road material to correctly quantify the particles number in the spikes before the extraction process. Thus also road site dust was no option because it still contains a larger portion of not TWP material (Gunawardana et al., 2012).

Tire chips were produced from 4 different tires (Bridgestone Potenza S001 225/45R1895Y MO, Continental WinterContact TS860 195/65R15 91T M.S, Kleber Viaxer 155/65 R13 and Falken Azenis FR510 255/35 ZR20 97Y) using a planer plough. The chips were then milled with liquid nitrogen using a ultracentrifugal mill (ZM200, Restch, Germany) and sieved to < 0.3 mm.

For quality control of the extraction and identification method, spikes were prepared by suspending 0.1046 g of the resulting TWP powder into 20 mL of ethanol ($\geq 99.8\%$, Prod.-No 51976, Sigma Aldrich, USA). The suspension was sonicated for 10 minutes and stirred in a magnetic plate for 30 minutes. To spike the individual samples, 15 µL of the suspension were collected from the stock solution while being stirred and deposited onto an Anodisc filter (Whatmann® Anodisc inorganic filter, AIO, pore size = 0.2 µm, diameter = 13 mm) placed into a vacuum filtration apparatus. The solution was vacuum filtered and the filter was photographed under the microscope (see section 0). After picture acquisition, the spiking material was flushed into 50 mL corning tubes using 35mL of a 0.2 µm filtered (Whatman® membranes, 47 mm, 0.8 µm pore size) sodium bromide (NaBr) density solution. In total, 9 spikes were prepared; 3 of them were directly redeposited on a new Anodisc filter to assess the potential loss of particles in the transfer process (S0), 3 were used as positive control to assess the extraction and identification recovery (S) and 5 g of the plastic free soil was added to the last 3 spikes (SPFS) before proceeding to their extraction to assess the recovery rate in a complex matrix. Charcoal from a fireplace located in Bern surroundings (46.956987, 7.422781) was sampled in three positions according to the centre of the last fire made there

(Appendix C.2), to obtain charcoal formed at different temperatures. The sampling was done with a stainless steel spatula, which was washed with ethanol in between sample position, and the charcoal material was transferred into glass vials. To determine a possible interference of the charcoal with the TWP during the identification process, 3 charcoal spikes with (CPFS) and without plastic free soil (C) were prepared by hand picking fragments of each charcoal sampling position and depositing them onto an Anodisc filter. After picture acquisition, the charcoal material was flushed into a corning tube using 35 mL of the NaBr density solution.

2.2.3 Extraction

All extraction steps were conducted under a clean hood wearing white cotton lab coat and blue nitrile gloves. The extraction was done according to Grunder et al. (in prep.) The mineral fraction of the soil was eliminated by density separation using a sodium bromide (NaBr) salt solution of a density 1.5 g/cm³. As a first step, the samples were mixed with the density solution into a 50 mL PP transparent corning tube with orange cap, vortexed for 30 secs, ultrasonicated for 10 min, shaken for 30 min and centrifuged for 30 min at 2500xg. After centrifugation, the supernatant was filtered through a metallic filter (10 µm pore size) and the retentate, containing the plastic and the natural organic matter mainly, were resuspended in a NaUT (6% urea, 8% thiourea, 8% NaOH) solution and kept at -20°C for 40 min, until crystal appeared into the solution (Olsen et al., 2020). The NaUT solution was then washed away and the SOM was oxidized by Fenton reaction, which uses hydrogen peroxide as oxidizing agent and Fe as catalyst. The samples were washed afterwards on a metallic filter (10 µm pore size) to remove iron oxides from the Fenton reaction and a second density separation (NaBr, 1.5 g/cm³) was applied to remove residual minerals. The resulting supernatant was finally filtered onto an Anodisc filter and the filter was stored in plastic boxes covered with aluminium foil. To assess a possible contamination of the samples during the extraction process, blanks (B) were also extracted. The detailed extraction protocol has been described in a previous publication. All samples were processed in triplicates and summary of each sample purpose can be found in Table 2-1.

Table 2-1: Sample overview and description. The name corresponds to the samples abbreviations used in the present publication. The type of sample

NAME	TYPE OF SAMPLE	SAMPLE DESCRIPTION
B	Procedural blank	Only extraction solution; to assess the possible contamination of the samples during extraction
S0	Positive control	Spike redeposited on filter without going through the extraction process; to assess the potential particles loss during transfer.

S	Positive control	Only TW particles; to assess the effect of the extraction method on the particles as well as the method recovery rate for TW.
C	Interference	Only charcoal; to determine it can be a source of interference with TW particles during the identification method.
PFS	Matrix blank	Only plastic free soil; allows to determine the background signal from the soil only
SPFS	Positive control in soil	Plastic free soil and TW; allows to determine the recovery rate of the tire into a complex matrix
CPFS	Interference in soil	Plastic free soil and charcoal; to determine its possible interference with TW identification in a complex matrix.
MAT1	Environmental	1 m distance from highway; environmental sample
MAT2	Environmental	2 m distance from highway; environmental sample
MAT5	Environmental	5 m distance from highway; environmental sample
MAT10	Environmental	10 m distance from highway; environmental sample

2.2.4 Images acquisition, particles identification and quantification

Images of spikes and extracted samples were acquired using a Leica M205C microscope equipped with LED300 RL ring illuminator and mounted with a DMC5400 Leica camera at a magnification of 50x. The light intensity was set at 100% and the exposure was 180 ms. Four high resolution images per filter of 1.5 $\mu\text{m}/\text{pixel}$ were acquired with the Leica software LASX. The plugin Live Image Builder XY was used to record each of the four pictures, as it was not possible to record the whole filter with the plugin because of file size limitations. The four recorded images were then manually assembled using GIMP2.0 (The GIMP Development Team, 2019), rendering a 1.8 GB file. Filters pictures were then individually screened and all material corresponding to insect, seeds, roots and leaf fragments were manually covered in white. The automated picture post-processing using the open source platform Fiji (Schindelin et al., 2012, <https://fiji.sc/>) implied an increase of the exposure and of the black levels to remove the filter blueish colour and enhance the contrast between TRWP and the background. The particles were finally identified by classifying each pixel of the filter final pictures into a TWP or background category using the Weka Segmentation (Arganda-Carreras et al., 2017) plugin in Fiji. Sub-regions of the pictures acquired for blanks, TWP spikes, charcoal spikes and plastic free soil were used to train machine learning models by marking black particles as potential TWP and other coloured particles as background. The results of the segmentation render a red (TWP)/green (background) binary image. In Fiji, the images were converted into 8 bits and the automatic threshold was applied for the TWP to be black and the background

to be white. A watershed function is applied to separate particles which touch each other. For this, the Fiji Adjustable Watershed plugin was used with a watershed tolerance of 3. Finally, the “Analyze particles” tool of Fiji was used, including particles size of 0 to infinity, to obtain the number and measures of all TWP present on a filter. The minimum Feret diameter (mF) was then used as the particles size estimation in the data analysis. Thus, all mention of size in the following text refers to the mF diameter. A detailed example of the image processing is available in Appendix C.3. All measurements for individual particles are available in the supplementary files.

2.2.5 Data analysis and statistics

All data processing, analysis and plots were performed using RStudio (RStudio Team, 2020). The efficiency of the whole procedure was assessed by computing the particles number recovery rate in different sizes classes of sample S0, S and SPFS. The effect of the distance from the road on the mean particle number found after extraction was tested by running a non-parametric independent Kruskal-Wallis rank sum test and significant difference were assessed using a Dunn posthoc test using the FSA R package. Finally, an estimation of TWP soil contamination was extrapolated from measurements data in particles number Kg^{-1} dry soil by multiplying the mean particles number of each sample by the initial subsample weight.

To investigate the size measurement accuracy of the microscopic setup and particle recognition, the mF was manually measured on 101 random particles across all the S samples before extraction. The accuracy was calculated by dividing the mF of the particle as identified by the classification model by the manual mF measurement and multiply it by 100. A locally weighted smoothing (LOESS) regression implemented in the R package “ggplot2” was used to help visualize the relation between the particles mF and the measurement accuracy. Finally, a segmented linear model was fit to the data, to identify from which mF value the accuracy starts to stabilize, using the *n/sLM* function of the “minpack.lm” (Elzhov et al., 2022) R package.

The operational resolution of the method corresponds to a minimum of 1 particle in the processed subsample. Procedural blanks (B) were used to calculate the method limit of detection (LOD) and limit of quantification (LOQ) for soil samples according to a recent study (Horton et al., 2021) where:

$$\text{LOD} = \text{mean}_{\text{blank}} + 3 * \text{standard deviation}_{\text{blank}} \quad \text{Eq. (1)}$$

$$\text{LOQ} = \text{mean}_{\text{blank}} + 10 * \text{standard deviation}_{\text{blank}} \quad \text{Eq. (2)}$$

2.3 Results and discussion

2.3.1 Particle detection and recovery

The analysis of the image segmentation showed that the detection of particles, as well as the accuracy of their measurements, were size dependant (Figure 2-1). As the segmentation model was trained to identify black pixels, it was not able to detect the objects where the light diffraction rendered only blue, yellow and red pixels, without having black pixels in the particle centre (Figure 2-1, a). From around 15 μm size, the particles were detected but the error in the size measurement was important, as most of the particle surface is still diffracting the light (Figure 2-1, b). The relation between the measurement accuracy and the detected particle size is shown in (Figure 2-1 ,right). The change of point detection function (red line) indicates that the accuracy stabilises around 90% for particles bigger than 25 μm . Hence, the experimental set up used in this study allowed to detect and measure particles size accurately down to a size of 25 μm . For smaller sizes, the measurement accuracy dropped drastically and the size estimation was not reliable anymore. To lower this detection limit, pictures of a higher magnification could be acquired. However, this would imply dedicating more time for pictures acquisition, processing and segmentation for each sample in our instrumental setup, resulting in a lower sample throughput. Additionally, increasing the magnification will increase the depth of focus and might render sharp images for small objects but blurry for the biggest ones, thus affecting the reliability of the particles size measurements. Time could be save if (1) pictures were acquired using a motorized xyz microscope stage, which would automatically optimise the focus for each picture and drastically improve the efficiency of picture acquisition and if (2) the segmentation model was run on an analysis cluster having more than 32 RAM. With this equipment, increasing the picture magnification and thus lowering the particles minimum size which is detected is feasible. Nonetheless, we consider a minimum detection size of 25 μm acceptable as it is similar to μFTIR where particles $<20 \mu\text{m}$ are not consistently detected (Käppler et al., 2016).

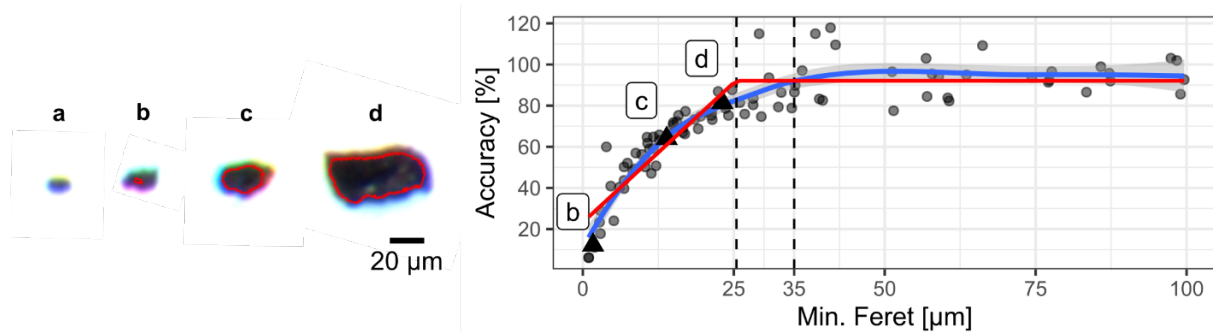


Figure 2-1: Particle minimum size detected by the segmentation model. Left: examples of TWP of increasing sizes (a-d) with the red outline showing how their detected perimeter by the segmentation model. Right: Accuracy of the measurement according to the particle size. The particles showed on the right are highlighted by triangles in the graph. A LOESS regression is displayed (blue line) to show the general trend of the data. A segmented linear model (red line) shows from which size value the accuracy of the measurement stabilises. The dashed lines indicate the position of the minimum particle size from which a mean of 90% size accuracy is obtained (25 µm) and the particle size threshold in this study (35 µm).

The mean recoveries of the different types of spiked samples, according to the minimum particle size taken in account, are shown in Figure 2-2. Regardless of the minimum particle size, the mean recovery rates of the S0 and S samples were generally lower than for the SPFS samples. Indeed, during sample processing and extraction, we observed that the cryo-grinded TWP were adhering on the PP corning tube walls when they were processed without soil. In presence of soil (SPFS), however, no abnormal particle adhesion was observed. It is most likely that the mechanical forces induced by the shaking steps in presence of soil, together with the chemical interaction of the TWP with the soil constituents have prevented their adhesion. If a few studies have reported losing particles in their extraction process because of them sticking to their vial's walls (Hidalgo-Ruz et al., 2012; Imhof et al., 2012) this difference in particle's behaviour with and without soil matrix has, to our knowledge, not been reported yet. We hypothesized that the adherence was due to a modification of particles surface charges induced by the cryo-grinding and/or sieving processes. In this regards, the S0 and S samples were considered as non-representative of the method efficiency in soils and only the SPFS replicates were used to assess the method recovery rates for soil samples. The mean recovery rates of the SPFS samples tended to increase when excluding small particles sizes from the analysis (Figure 2-2), as it was already observed in previous studies (Colson and Michel, 2021; Huang et al., 2021; Kotar et al., 2022). This can be due to the fact that smaller particles takes longer to migrate in the upper layers of the density separation solution (Wang et al., 2018). In the literature, mean recovery rates for MP extracted from soil samples can vary between 71% for high density polymers and 93% for low density polymers (Way et al., 2022). To minimize the error in the reported particles concentration values, we chose 80% as a threshold for an acceptable mean recovery rate, setting the minimum particle size taken in account in this study to 35 µm (recovery rate = 85.4 % \pm 9.54% standard error) (Figure 2-2). This particle size threshold is also conservative regarding the accuracy of the automated size

measurement, as it is above the estimated minimum particle size detected with a 90% size measurement accuracy (Figure 2-1, dashed lines).

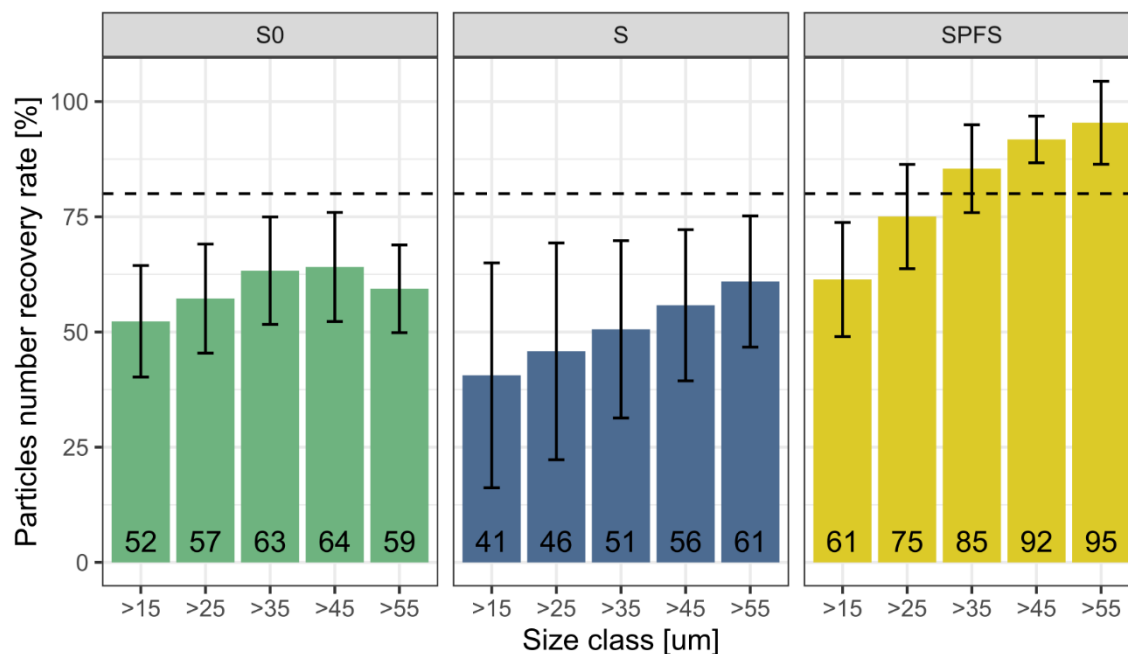


Figure 2-2: Mean recovery rates with their standard deviation of the TWP spikes samples according to the different minimum particle size taken in account. **S0**: spike redeposited on filter without going through the extraction process. **S**: extraction of TWP alone. **SPFS**: extraction of plastic free soil spiked with TWP. The horizontal dashed line highlights the threshold of an 80% recovery rate.

This recovery rate, however, was obtained by testing the method using cryo-grinded TWP. This kind of spiking material can have different properties than TWP produced from road simulator and environmental TWP, especially in its density. TWP produced from road abrasion are typically incrustated with mineral road material, which can result in particles densities up to 2.3 g/cm^3 (Klößner et al., 2021b, 2019; Rausch et al., 2022). The results of the SEM-EDX analysis on the particles present in the supernatant and in the pellets after the sonication and density separation of the tunnel dust showed that TWP were still present in the pellet (Appendix C.4). This indicate that the sonication applied in the extraction protocol do not allow to remove completely the mineral encrustments at the surface of the TWP. Thus, a density $>1.5 \text{ g/cm}^3$ is needed to isolate the whole diversity of environmental TWP. As a maximum of TWP was previously found in the $1.3\text{-}1.7 \text{ g/cm}^3$ density fraction (Klößner et al., 2021b), this issue can be overcome by replacing NaBr by another salt, such as zinc chloride (ZnCl_2) or sodium iodide (NaI), which have densities of 1.7 and 1.8 g/cm^3 respectively but are less environmental friendly and more expensive than NaBr.

2.3.2 Blanks and interferences

In the procedural blanks without (B) and with soil (PFS), no particles in the size range 35-2000 μm could be detected (Figure 2-3). This shows that the measures applied to avoid contamination were sufficient and that the chosen plastic free soil matrix did not cause any interference in the results. Regarding those information, the LOQ and LOD were fixed at the same level than the operational resolution, thus 1 particle per subsample and no blank correction was applied to the environmental samples (MAT1-10). Moreover, as a similar detection technique was used for quantifying charcoal in sediments (Mooney and Tinner, 2011), the reduction of charcoal content by the extraction process was assessed. The charcoal was not completely reduced by the extraction process and a mean of 1.33 ± 1.53 and 1.33 ± 2.31 particles were identified in the C and CPFS samples respectively after extraction. Thus, the extraction procedure led to a mean reduction of 92.25 % of the detected particles number. Despite this strong reduction, an elevated concentration of charcoal and the conditions (temperature, original organic material) in which it is formed present in the soil can interfere with the TWP detection and lead to overestimations.

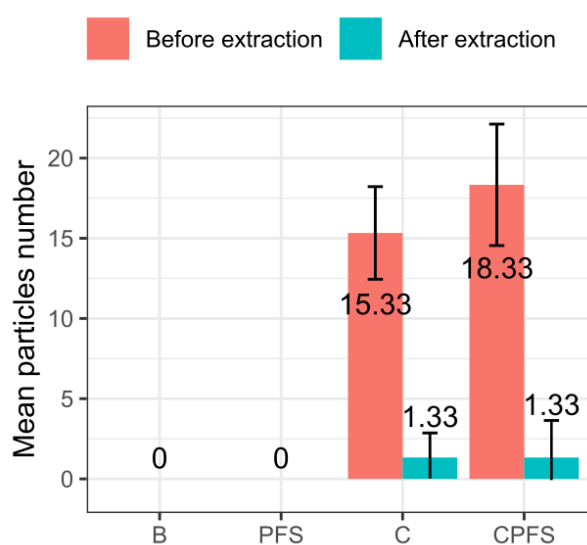


Figure 2-3: Mean particles number detected in procedural blanks (B, PFS) and interference testing samples (C, CPFS) before and after extraction in the size range 35-2000 μm .

2.3.3 Environmental samples

To compare the results of the extraction and identification method to previously reported TWP concentrations, soil samples of increasing distances from a highway were extracted and analysed. The extrapolated (Appendix C.5) mean particles number were 8080.4 ± 1059.8 , 9106.6 ± 3234.8 , 4091.15 ± 623.8 and 2562.8 ± 1160.3 particles kg^{-1} dry soil for MAT1, MAT2, MAT5 and MAT10 respectively (Figure 2-4). (Yu and Flury, 2021) demonstrated that the accuracy of an extrapolated concentration is strongly dependant on the contaminant actual

concentration, its spatial distribution in the studied matrix and the volume of matrix extracted. As road sided soils are expected to be highly contaminated and to have a uniform TRWP distribution, it can be expected that the error of these estimations would lie between 5 and 10%. This assumption is also supported by the low standard error in between replicates. There was no significant difference in the particles count at a distance of 1, 2 and 5 m from the road but the particle count at 10 m was significantly lower than the samples closer to the road. To our knowledge, only one study so far reported TRWP concentrations in soil samples as particle count (Knight et al., 2020) but had a particle size limit of 50 μm and did not report their concentrations in particles/kg, which hamper direct concentration comparison. However, they extracted a similar sample amount and had particles concentrations in the same order of magnitude, which shows our concentration are consistent with previous findings. Moreover, the mean particles number tended to decrease with increasing distances from the road, as it was already observed before (Baensch-Baltruschat et al., 2021; Fauser et al., 2002; Knight et al., 2020; Müller et al., 2022; Panko et al., 2012). A rough estimate of the total TWP mass content in each sample was calculated using the model developed by (Tanoiri et al., 2021) (Appendix C.6), giving concentration of 1.32, 1.94, 0.205 and 0.261 mg/kg for MAT1, MAT2, MAT5 and MAT10 respectively. These mass estimations are one order of magnitude lower than the ones reported from soil samples using styrene-butadiene rubber as a marker (Müller et al., 2022). The difference most likely arise from using a density of 1.5 g/cm³ to isolate the TWP from the soil. Figure 2-4 B and C show the cumulative frequency of the particles size and circularity, respectively, for each environmental sample triplicate. MAT5 and MAT10 tend to have a higher proportion of smaller particles than MAT1 and MAT2, which agree with the assumption that bigger particles will be transported on a shorter distance than smaller particles. With a particles upper size limit of 2000 μm , most of the TRWP identified in all environmental samples had a mF in the 35-150 μm size range and only 1 particle of 300 μm was found in MAT2. Finally, the distance from the road did not seem to have an effect the circularity of the particles (Figure 2-4 C) and there was a continuum of particles circularity cumulative frequency, meaning that their shape were well distributed between elongated and round particles. No correlation between the particle size and circularity was found (Appendix C.7).

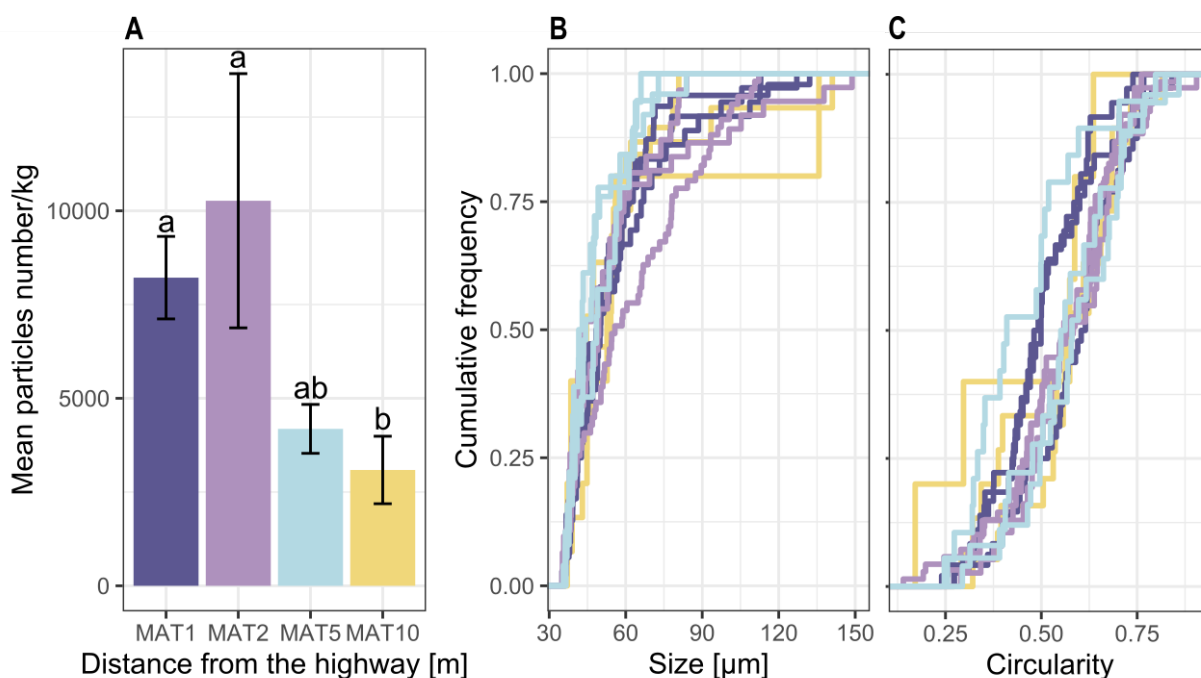


Figure 2-4: TRWP found in environmental samples. (A) Mean particles number kg^{-1} with standard error. Different letters indicate significant differences between mean particles number (Dunn test, p -value < 0.05) (B) Cumulative frequency of the particles size for each environmental sample's triplicate. (C) Cumulative frequency of the particles circularity determined by the image analysis for each environmental sample's triplicate.

2.3.4 Addressing the TWP data gap

A stressed by the UN Plastics Treaty adopted in May 2022, there is an urgent need of a standardized protocol for monitoring TWP in the environment to assess their potential risk, as well as evaluate the effect of future mitigation measures (UNEP, 2022). In another context, California, within the Safe Drinking Water Act, was the first state to agree on MP standard operating procedures (Frond et al., 2022) to monitor plastic in California's drinking water, allowing a large scale understanding of MP distribution. Such an agreement need also to be reached for TWP. Having a simple method facilitate its application on a large scale, as it maximises the number of laboratories and scientific staff taking part in the monitoring effort. The method presented in this study required basic lab and IT equipment (Appendix C.8) and can be easily trained to scientific staff. Here, 16 samples required 7 days of technical work for samples and blank extractions and image acquisition and 2 additional days of automated analysis for TWP identification. The samples throughput is thus the main limitation of the method. If the presence of non TWP black particles was not detected in the matrix blank, this is prone to vary with the origin of soil analysed, as their organic constituent may vary broadly. Additionally, a high content of charcoal might also interfere in the analysis. Despite its limitations, the results presented above showed that this method was able to detect similar patterns identified by GC-MS and PyGC-MS (Müller et al., 2022; Thomas et al., 2022). Direct concentration comparison with literature was not yet possible, as the 3 studies on TRWP in soil available had different particles size range and/or reported their concentrations in mg/kg

(Knight et al., 2020; Müller et al., 2022; Thomas et al., 2022). Single-particle analysis is a direct measure and gives information on particles number and size and shape distribution, which are not available from MS techniques but are crucial for risk assessment. Furthermore, the direct particle identification by colour is an advantage, compared to the detection through analytical markers in the case of TWP: all tyres are black, while the proportion of the target markers can vary broadly in the initial composition of the tires, resulting in large errors in recovery rates. Moreover, the concentration of the targeted analytical marker can also change with time when the TWP undergo weathering processes (Mattonai et al., 2022), complicating even more the analysis of environmental TWP, while, to our knowledge, no study showed that weathering factors could affect TWP colour.

2.4 Conclusion

The study presented here showed that optical microscopy coupled with a machine learning classification algorithm was able to accurately detect and measure black particles on white filters down to a mF size of 35µm, making it a powerful tool for TWP detection in environmental samples. A method recovery of >85% was achieved using cryo-grinded TWP, with an LOD and LOQ corresponding to the operational resolution of 1 particle. The recovery rate, however, is most likely lower for environmental TWP as they are characterised by a surface mineral encrustment, which can increase the particles density above the used NaBr (1.5 g/cm³) density solution. The extract recovery rate of environmental TWP from soil is thus unknown and this issue could be addressed by using a salt of a higher density, such as ZCl or NaI. While no particles were detected in the B or in the PFS, pieces of charcoal remained after the extraction, indicating it could interfere with the TWP detection if present in high concentration. Finally, the analysis of TWP concentration in highway adjacent soil samples showed similar trend and magnitude order than previously reported concentrations. Thus, we believe this operation protocol is sufficiently accurate and easily implementable in many laboratories, as only basic lab and IT equipment are required, to allow a large-scale monitoring of TRWP in soil samples.

2.5 Authors contribution

Alexandra Foetisch: Conceptualisation, Methodology, Software, Investigation, Validation, Formal analysis, Data curation, writing – original draft, visualisation. **Benjamin Kunde:** Conceptualisation, writing – review and editing **Adrian Grunder:** Methodology, writing – review and editing **Moritz Bigalke:** Conceptualisation, Methodology, resources, writing – review and editing, project administration, funding acquisition, supervision.

2.6 Acknowledgments

This study was funded by the Swiss National Science Foundation (SNSF, 200021_182672/1). We would like to acknowledge members of the Institute of Geography at the University of

Bern: Yannick von Känel, Sarah Volken, Saskia Gianola, and Benjamin Guggisberg for their considerable and precious contribution to the method validation via their master or bachelor thesis. We also would like to thank Tobias Stadler who developed and improved the extraction protocol, for their valuable work, Michael Scheurer for providing the plastic free soil. Daniela Fischer, Maarika Bischoff and René Nussbaumer for their general support in the lab. Elmar Scheiwiller for making organizing the tunnel dust sampling. Finally, we are grateful to Stehle Bernhard, Dominika Kudel, Andreas Fliessbach and Andrea Wiget from the Research Institute of Organic Agriculture FiBL for providing the spiking material.

Abstract

Nanoplastics (NP) are of environmental and human health concern. We tested a novel NP extraction method and scanning transmission X-ray spectro-microscopy (STXM) in combination with near-edge X-ray absorption fine-structure spectroscopy (NEXAFS) to image and identify individual NP in environmental and food matrices. We 1) discussed the potential of STXM compared to other methods potentially suitable for NP analysis, 2) applied the method on NP suspensions of eight of the most common polymers, 3) analyzed environmental water and soil samples spiked with NP and 4) characterized NP in tea water infused in plastic teabags and unspiked soil samples. Here we show that STXM has methodological advantages and that polymers give characteristic spectra, which allows NP identification in environmental and food matrices. For soils we deliver a visual and spectroscopic characterization of NP, proving their presence and highlighting their diversity. Thus, STXM, can be used for the detection and characterisation of NP in different types of matrices.

3.1 Introduction

Since 1950, about 8300 million metric tons of plastic have been produced worldwide, 79% of which are accumulated in landfills or in the environment (Geyer et al., 2017). Among the diversity of plastic waste generated, nanoplastics (NP), plastics of a size $< 1 \mu\text{m}$, are of environmental importance. They can be either released directly from manufactured products or produced by the physical, chemical or mechanical degradation of larger polymer objects. As several studies on microplastics (MP) have shown that the particle size distribution found in the environment is heavily skewed towards the smallest detectable particles (Enders et al., 2015; Fok et al., 2017; Scheurer and Bigalke, 2018), one can expect NP to be present in high numbers. However, research on NP occurrence in the environment is in its infancy and limited monitoring data are available (Jiang et al., 2020). Indeed, infrared (IR) and Raman spectroscopy as commonly used in MP research have a resolution limited to the $>10 \mu\text{m}$ and $>1 \mu\text{m}$ size range, respectively (Schwaferts et al., 2019). Chromatographic analysis of pyrolysis products or extracted polymers allow for the identification of polymers but do not provide any information on the size or shape of the particles analysed (Duemichen et al., 2019; Ter Halle et al., 2017). Yet, all these characteristics are critical to assess any potential NP environmental effect. Until now, the behavior and fate of NP in the environment have mostly been studied using artificial NP labeled with metals, fluorescent dyes or enriched stable isotopes (Li et al., 2020; Mitrano et al., 2019; Sander et al., 2019).

Here, we demonstrate how scanning transmission X-ray spectro-microscopy (STXM) can be effectively applied for imaging and identifying NP in different environmental matrices. For this purpose, we 1) discuss analytical techniques potentially suitable for NP analysis and introduce

STXM, 2) purchased or produced NP of polypropylene (PP), polyethylene (PE), polyvinyl chloride (PVC), polyethylene terephthalate (PET), polystyrene (PS), polyamide (PA), polycarbonate (PC) and polymethylmetacrylate (PMMA) and acquired STXM images and NEXAFS spectra of individual NP to confirm the suitability of this technique to identify and characterize plastics in the nano size range, 3) developed an extraction protocol, combined it with STXM and tested it for NP extraction from spiked water and soil samples and 4) analyzed unspiked samples like tea from plastic tea bags and natural soil samples to test the application of the method on environmental and food matrices.

3.2 Material and methods

3.2.1 Nanoplastic materials

We purchased or produced nanoparticles suspension of eight common polymers. Pellets of PA Radilon, PC Makrolon, LDPE Lupolen, HDPE Hostalen, PMMA Altuglas, and PP Moplen and PVC lab bottles were provided by Semadeni Plastics group, Switzerland. NP preparation was performed by adapting previously published methods (Astner et al., 2019). In a first cryo-grinding step, 60 – 80 g of the initial material was grinded twice for 10 s with a Pulverisette 11 (Fritsch, Germany) in liquid nitrogen. The resulting powder was then sieved and the fractions <250 µm or <63 µm (depending on the available mass) were collected and milled in a cryo-grinding jar with 15 mm or 3 mm stainless steel beads. The jar was sealed, frozen into liquid nitrogen and shaken at a frequency of 28 Hz for 5 min with a mixer mill (MM 400, Retsch GmbH, Haan, Germany). The freezing and grinding steps were repeated ca. 40 times to maintain the brittleness of the material while grinding. A portion of the resulting powder was suspended in 600 µL ethanol (≥99.8%, Prod.-No 51976, Sigma Aldrich, USA) and allowed to settle for 5 min before collecting the nanoparticle-containing supernatant. Protocols specific to each polymer are available in the supplementary material (Appendix D.1). Nanoparticles of PET were produced from a regular transparent PET water bottle (M-Budget still water, Switzerland) by adapting an existing method (Rodríguez-Hernández et al., 2019)(Appendix 0). Fluorescent PS nanobeads of 100 nm (micromer®-redF, plain, 30-00-102) and 250 nm (micromer®-greenF, plain, 29-00-252) were purchased from Micromod, Germany. White, non-fluorescent 500 nm PS beads (95585-5ML-F) were purchased from Sigma-Aldrich (USA).

3.2.2 Natural water and soil samples

A water sample was collected in Lake Luzern (47°02'31.5"N 8°19'52.9"E, Switzerland) in November 2020 with a 3 m pole and a glass bottle from a pontoon at the outflow of the lake. The water sample had a conductivity of 210 µS cm⁻¹ and was kept refrigerated until spiking it with a mix of approximately 0.07 g PC, 0.3 g PMMA and 3 g PP powders resulting from the cryo-grinding and 10 mL of suspended PET particles to 1 L of the lake water sample. Soil

samples were collected in the mountains in Laax (GR, Switzerland) at a site which did not contain any MP (Scheurer and Bigalke, 2018). This clean soil was spiked with approximately 1 g of PA powder or 41 μL of 250 nm PS beads in 50 g of soil to test the extraction analysis. Further soil was sampled at two agricultural fields in Sant'Antonino (SAN; TI, Switzerland) and Gampelen (GAM; BE, Switzerland) with a history of mulch foil application and irrigation and two roadside soils in Belpberg Dufti (DUF; BE, Switzerland; 8 m wide rural street, 2 m from the road) and Wohlen bei Bern, Breitacher (BRA; BE, Switzerland; 6 m wide rural street, 10 m from the road), respectively. These soils were not spiked but analyzed to observe the NP composition of their respective localities. Green and peppermint tea in plastic teabags were purchased from a local grocery store.

Water and soil samples extraction

All equipment used for the extraction of NP was cleaned first with a brush, soap and water, ultrasonicated for 10 minutes, rinsed with ethanol, rinsed with MilliQ water and finally dried under a laminar flow clean bench (FMS SuSi, Spetec, Erding, D). All work except the ultracentrifugation was done on the clean bench with HEPA (H14) filtered air and all-cotton lab coats were worn.

Soil samples (50 g) were suspended in 1 L of 2.5 mM ultrafiltrated (<10 KDa, Amicon Stirred Cell, Merck Millipore, Sigma Aldrich, USA) tetrasodium pyrophosphate (TSPP, $\text{Na}_4\text{P}_2\text{O}_7$, $>95\%$, Sigma Aldrich, USA), shaken for 30 min at 100 rpm, ultrasonicated for 2 min with a Labsonic L (B. Braun, Switzerland) at a frequency of 20 kHz and a power of 100 W, and then allowed to settle for 18 h (Schwertfeger et al., 2017). Then, 30 mL of solution were collected from the surface with a glass volumetric pipette and transferred into a new glass vial. A 5 mL aliquot of sucrose solution ($\geq 99\%$, Sigma Aldrich, USA) of a density 1.37 g mL^{-1} (1220 g L^{-1} MilliQ water) was deposited at the bottom of 38.5 mL polyclear tubes (25-30-70, Hemotec, Switzerland) while carefully avoiding to deposit any drops on the tube wall. 30 mL of the solution collected after settlement was then gently deposited on the top of the sucrose solution and the tubes were centrifuged at 22 000 rpm (acceleration of approx. 109.500 g) for 2 h (Ultracentrifuge CP100NX, HITACHI, Japan) for the mineral particles (density $>1.37 \text{ g mL}^{-1}$) to migrate through the sucrose to the bottom of the centrifuge tube. After centrifugation, the upper solution and the upper 5 cm ($\sim 2 \text{ mL}$) of the sucrose were collected with a pipette and transferred to a new glass vial. Then, the walls of the tubes were rinsed with ethanol, which was also collected with a pipette and added to the first supernatant. In order to oxidize the remaining natural organic matter (NOM) and sucrose from solution, hydrogen peroxide (H_2O_2 , 30%, Sigma Aldrich, USA) solution was added to the samples to reach a concentration of a 5% (v/v). The addition was repeated every 2 h for 22 h. This treatment was chosen to avoid

high H₂O₂ concentrations in the samples which could oxidize NP. The dissolved C in the sample was analyzed with a DOC analyzer (DIMATOC 2000, Dimatec, Essen, D), by combustion of the sample and detection of the released CO₂. After every 2 h the 5% H₂O₂ are consumed by the oxidation of the sucrose and OM in the sample, so that the H₂O₂ concentration never exceeds 5%. After about 11 additions, the concentration of dissolved C in the sample showed only a slow decrease, so that no further H₂O₂ was added (Appendix D.3). After this treatment, samples were washed and concentrated using an ultrafiltration cell (Amicon Stirred Cell, Merck Millipore, Sigma Aldrich, USA) with a <10 kDa polyethersulfone membrane (Biomax Ultrafiltration Discs, Sigma Aldrich, USA). The samples were transferred into the ultrafiltration cell and the cell volume was completed (200 mL) with MilliQ water. The sample was then filtrated until approx. 10 mL of solution remained. The last two steps were repeated three times to further wash dissolved compounds (TSP, sucrose, salts, etc.) from the sample. The 10 mL of sample remaining in the cell at the end of the procedure was transferred into a clean glass vial and the ultrafiltration membrane was rinsed with 10 mL of ethanol (99.8%, Sigma-Aldrich; ref 51976-500ML-F). Our final soil extract was thus a suspension in a 50:50 ethanol/water solution.

Spiked water and soil samples extraction

NP in tea were produced following the procedure described in a previous study (Hernandez et al., 2019) except that in our experiment the tea was kept in the tea bag during preparation to have a realistic matrix for the analysis of food samples. A single tea bag of each tea was soaked in 12 mL 95°C MilliQ water for 5 minutes. The spiked water and the tea samples were treated with the same procedure than the soil samples except without the first extraction step with the TSP, which was not necessary for liquid samples. So spiked water and tea samples were treated with a density separation step, an oxidation of organic matter step, a washing step in the ultrafiltration cell and finally deposited on the membrane for analysis.

3.2.3 STXM sample preparation

Standard (SiRN-5.0-200-1.0-100) and finder (with gold finder grid; SiRN-5.0-200-1.0-100+G1Au20) membranes (1x1 mm, 100 nm thick Si₃N₄ windows) were purchased from Silson, U.K. Nanoplastic particles were placed on the membranes either by drop deposition (particles from pure plastic suspensions; the membrane was tilted to reduce the coffee ring effect) or by sedimenting the particles out of the 50:50 water:ethanol solution onto the membrane fixed to the bottom (via an aluminium holder) of a 15 mL glass centrifuge tube for 3.5 h at 3400 g (for particles which were extracted from soil, tea and water samples). Some membranes with finder grid were analyzed by SEM (Gemini 450, Zeiss; JSM7001F, JEOL) prior to or after STXM measurements with the aim of either localising particles more quickly

on the membrane during the STXM measurement or of acquiring a high-resolution picture of NP. A voltage of 15 and 10 kV was used with secondary-electron in-lens detector and membranes were coated with a c.a. 5 nm gold layer. After recognizing the serious radiation damage caused by SEM analysis prior to STXM (Appendix D.4), samples were only imaged by SEM after the STXM analysis.

3.2.4 Data acquisition and processing

The STXM measurements were performed at the PoILux beamline of the Swiss Light Source (SLS) synchrotron at the Paul Scherrer Institute in Villigen, Switzerland. The detailed beamline layout has been described before (Raabe et al., 2008). A 25 nm zone plate was used to focus the monochromated soft X-ray beam (spot size of ~30 nm) on the membrane and particles were imaged by raster scanning an area of the membrane at 350 eV. Once a particle was found, a zoomed-in and focused picture was taken. NEXAFS spectra were then acquired by line or stack measurement in the energy range between 280 and 350 eV corresponding to the C K-edge. We analyzed a variety of sizes of NP for each polymer to test for which size range STXM is suitable. The acquired NEXAFS spectra were extracted with aXis2000 (<http://unicorn.mcmaster.ca/aXis2000.html>) and normalized and plotted with RStudio (RStudio Team, 2020) to allow comparison of the characteristic peaks for the individual NP with published reference spectra (Dhez et al., 2003). As no reference could be found for PVC, we measured our own reference on a microtomed sample. Particle size was measured on SEM and/or STXM pictures using ImageJ. The given size on this study corresponds to the longest distance between any two points along the selection boundary (Merkus, 2009; Appendix D.5). The thickness is estimated by multiplying the optical density value at 320 eV by the attenuation length. The attenuation length depends mostly on the material chemical structure and density (Appendix D.6).

3.3 Results and discussion

3.3.1 Relating STXM to other analytical methods for NP analysis

Identifying NP in environmental matrices requires the ability to interrogate individual nanoparticles, coupled with a spectroscopic tool with natural contrast (i.e. is not reliant on labelling) that is capable of providing information about molecular structure such that polymers can be distinguished from the natural organic matter that is abundant in all ecosystems. The examination of individual particles typically requires nanoscale focusing, both to isolate the signal of a single particle and to obtain sufficient signal strength. For many analytical probes, this is restricted by the Abbe diffraction limit (Abbe, 1873), which says that the probe beam cannot be focused to less than about half of its wavelength. While there exist many super-resolution strategies to circumvent this limit, they each introduce their own restrictions that

may preclude their application to label-free spectroscopy. For example, super-resolution techniques based on sub-pixel localisation or the manipulation of sample fluorescence are generally unhelpful for spectroscopic applications (Chapman et al., 2020; Wöll and Flors, 2017). Further, super-resolution techniques based on near-field effects can have severely limited application to nanoparticles larger than the evanescent wave, thus excluding the majority of the nano-scale size range.

The list of analytical techniques capable of differentiating organic materials is limited by the specific need to probe the molecular structure, which is what defines the identity of an organic substance (Favre and Powell, 2014). Other physical properties such as the density, or constituent elements of an organic substance are not indicative of the molecular structure and therefore do not make a significant contribution toward material identification. Vibrational spectroscopies, such as IR and Raman spectroscopy indicate the characteristic oscillations of functional groups within the sample, and so provide an excellent probe for differentiating organic materials (Hashimoto et al., 2019). While the visible wavelengths used for Raman allow sub-micron focusing and optical trapping of nanoparticles (Gillibert et al., 2019; Penders et al., 2018), the signal is typically very weak and easily overwhelmed by fluorescence effects. Recently, Raman spectroscopy was coupled with scanning electron microscopy (Zhang et al., 2020) to spectroscopically identify sub-micron particles and PVC NP. While technically fulfilling the requirements for nanoscale imaging and spectroscopy, this characterization strategy may not be generally applicable to all NP characterizations. Firstly, the Raman signal to noise ratio is expected to deteriorate rapidly as the particle size decreases below the spatial resolution of the visible laser probe. Secondly, it is our experience that some polymer types are very sensitive to electron beams (Figure S1) such that particle spectra are modified beyond recognition after SEM imaging. Applications of IR spectroscopy to nanoparticles require a super-resolution technique (Nan et al., 2020). Nuclear magnetic resonance (NMR) can be used to identify molecular structures and, although super-resolution techniques are routinely applied to exceed the Abbe diffraction limit of the radio-frequency excitation pulses, sub-micron resolution is difficult to attain (Glover and Mansfield, 2002). However, nanoscale NMR measurement has been demonstrated by exploiting the extreme sensitivity of near-surface nitrogen-vacancy defects in diamond (Mamin et al., 2013). Mass spectrometry techniques such as secondary ion mass spectrometry (SIMS) measure the mass of molecular fragments blasted from the sample, the distribution of which indicate the elements and molecular groups comprising the sample material (Wien, 1997). While these probes can be focused to nanoscale resolution, the limited volume of individual nanoparticles severely restricts the statistical significance of measurements on small nanoparticles (Liang et al., 2015) unless a post-ionisation scheme is used to enhance the secondary ion yield (Popczun et al., 2017).

Pyrolysis gas chromatography mass spectrometry is analogous to SIMS and while a nano-focused heat source could be implemented, the material volume provided by an individual nanoparticle is unlikely to produce convincing pyrogram statistics. The method can be applied to samples which are prior fractionated to a defined size by filtration or other separation techniques (Ter Halle et al., 2017; Wahl et al., 2021), and thus confirm the association of polymers with particles in the nano-size range. However, it cannot measure the characteristics (size, shape, molecular structure) of the individual NP. Wahl et al. (2021) used asymmetric flow-field flow fractionation to separate nanoparticles from plastic-contaminated soil extract and identified molecular species indicative of common polymers via pyrolysis gas chromatography mass spectrometry. While this method establishes the presence of nanoparticles in the soil and their association with polymer materials (or their breakdown products), it lacks evidence that any individual nanoparticles are chiefly composed of polymer. For example, inorganic nanoparticles associated or coated with polymer are also consistent with the observations by Wahl et al. (Wahl et al., 2021) but are not consistent with the common understanding that NP should consist of the same material throughout its thickness.

Finally, spectroscopies involving electronic excitations of the core shell of carbon atoms can identify the bonding schemes present in an organic material and are routinely probed by beams of electrons (electron energy loss spectroscopy; EELS) or soft X-rays (near-edge X-ray absorption fine-structure spectroscopy; NEXAFS) with nanoscale resolution (Hitchcock et al., 2008). Scanning and transmission electron microscopy (SEM/TEM) can provide excellent spatial resolution for EELS, but causes a high rate of radiation damage in organic samples (Hitchcock et al., 2008). While this radiation damage tends to not significantly alter the size and shape of the organic nanoparticles, the molecular structure, and hence the absorption spectrum, is significantly altered (Appendix D.4). Note that energy dispersive X-ray spectroscopy (EDX), which is commonly performed in electron microscopes, only provides elemental composition and is unable to discern polymers from natural organic matter commonly found in the environment (Egerton, 2009). NEXAFS spectroscopy has been successful in positively identifying polymer materials (Dhez et al., 2003; Watts et al., 2011) by measuring spectra at the carbon K-edge (near 300 eV, or about 4 nm wavelength) (Ade and Hitchcock, 2008; Watts and Ade, 2012). Soft X-rays in this spectral range can also be focused by a Fresnel zone plate for the nanoscale imaging of structures composed of polymer, biological and other organic materials (Raabe et al., 2008). Soft X-ray microscopy can be implemented in full-field, scanning and ptychographic designs, however, STXM has strong advantages for performing nano-spectroscopy of organic materials due to the ease of keeping focus while acquiring spectra and excellent radiation dose efficiency (Jacobsen, 2019). As a non-destructive technique, STXM can also be combined with complementary techniques for

further analysis of NP. Thus, e.g. SEM images can be acquired after the sample analysis by STXM to observe the particles with high spatial resolution (Appendix D.5) or EDX can be used to investigate metal additives within NP. To find back the particles analysed by STXM with other techniques finder membranes with a 100x100 μm gold grid can be used.

STXM raster-scans a sample region across a nano-focused X-ray beam to form X-ray transmission images with spatial resolution down to 7 nm (Raabe et al., 2008) (, a). Varying the photon energy of the incident X-ray beam allows STXM to perform X-ray spectroscopy on nanoscale objects and to use spectroscopic effects to generate quantitative contrast mechanisms based on physical and chemical properties such as elemental composition, oxidation state, molecular structure, molecular orientation and local magnetization (Ade and Stoll, 2009). The minimal optical design of STXM maximizes the radiation dose-efficiency and positioning precision, both laterally (for high spatial resolution) and along the optical axis for easy focusing, which is important for performing spectroscopy with the dispersive Fresnel zone plates required for soft X-ray nano-focusing. As a synchrotron-based method, STXM is not easily available for routine measurement in one's own lab, but can be accessed (free of charge for academic use) by any researcher after a successful application to one of the many facilities worldwide (e.g. CA, CH, CN, DE, FR, GB, JP, UK, US) (<https://lightsources.org>; <https://wayforlight.eu>).

NEXAFS spectroscopy at the carbon K-edge (X-ray photon energy near 300 eV) involves resonance peaks that correspond to photo-excited transitions from the C 1s orbital to unoccupied molecular orbitals corresponding to anti-bonding states. The peaks will thus indicate the presence and the proportion of particular bonding types, characterising the molecular structure surrounding the absorbing C atoms. This means that C K-edge NEXAFS spectra can function as highly specific fingerprints of organic materials and there is no need for labelling or staining in order to positively identify a material. The influence of other factors such as physical state and intermolecular interactions are very small and a C K-edge NEXAFS spectrum is typically well represented simply by the sum of the spectra of its component structures (Stöhr, 1992). Moreover, in the case of C-based polymers, a given set of bonds is usually repeated many times and, thus, the corresponding C K-edge NEXAFS spectra tend to consist of strong, clearly defined resonance peaks that make them straightforward to identify (Dhez et al., 2003) (Figure 3-1, c and Figure 3-2, a-h; Appendix D.7). On the contrary, natural organic matter is normally a mixture of a broad variety of bonding types and gives nonspecific spectra (Figure 3-2, i-j).

In practice, a spectro-microscopy analysis of nanoparticles deposited onto an X-ray transparent substrate can be performed in a number of ways. First, organic particles can be

separated from any mineral and salt particles remaining from the sample preparation by comparing images measured with photon energies below (280 eV) and above (350 eV) the C K-edge. Materials with a high carbon content will show a strong difference in X-ray absorption between these two energies, while other materials will show little contrast. Once located, the spectrum of a particle is measured by recording the X-ray transmission through the particle location while scanning the photon energy across the C K-edge.

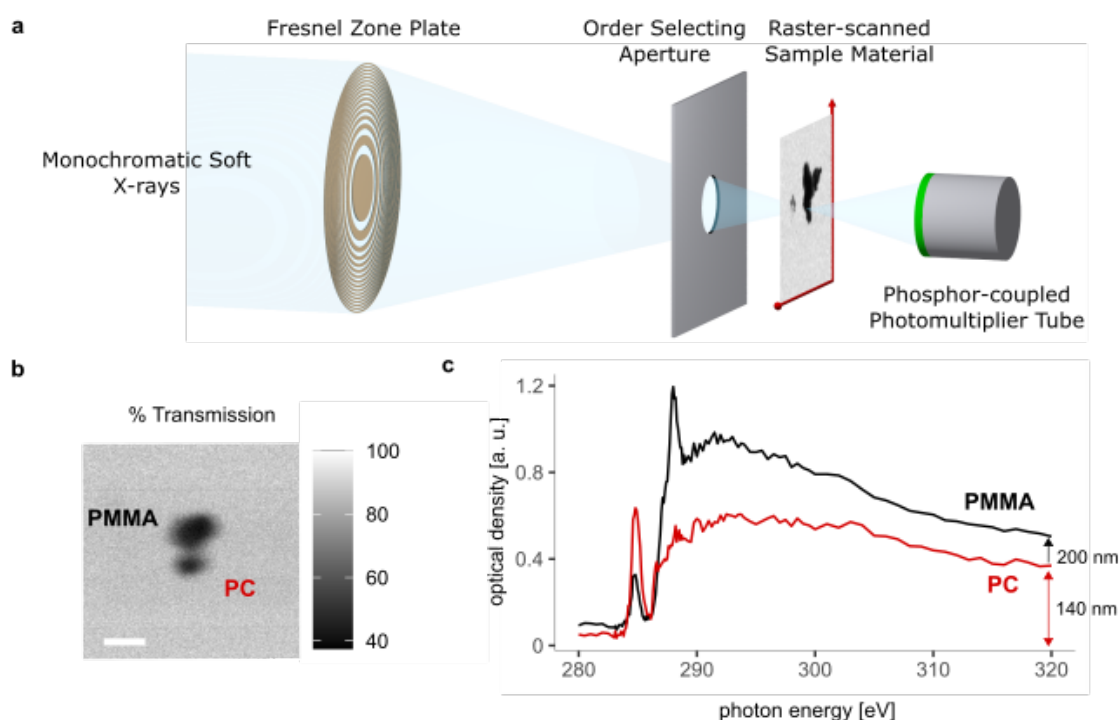


Figure 3-1: Illustration of STXM principle and NEXAFS acquisition for PMMA and PC polymers. (a) Schematic illustration of the setup of a STXM instrument, (b) STXM image taken at 350 eV photon energy of a pair of particles. The white scale bar is 500 nm. (c) NEXAFS spectra of the particles in (b) and identified as PMMA and PC. The particles thicknesses are estimates from the post-edge absorbance to be 200 nm and 140 nm respectively.

3.3.2 Nanoplastic identification

The spectra of nanoparticles composed of eight common polymers were matched with reference spectra (Dhez et al., 2003). STXM, as a transmission technique, is mostly limited by the thickness (Z dimension) of a particle and not by its size appearance in a 2D image (X and Y dimension). Particles were observed and identified down to a particle thickness of about 100 nm (Figure 3-2), at which point the statistical efficiency of the technique is rapidly decreasing (Appendix D.8). Note that the STXM measurements were performed on a bend-magnet beamline and an undulator-based instrument would provide about 100 times more X-ray flux and hence a commensurate improvement in either spectral quality or acquisition rate. In some cases, we used self-produced NP, with varying lower size limits. In line with the theoretical considerations, we observed that the spectral quality remained unchanged with

respect to the lateral size of the particle but decreased with decreasing thickness of the particle, causing noisy spectra at particle thicknesses <100 nm e.g. for the thinnest particles of PP, PVC, PS and PMMA (Figure 3-2, a, c, e, h). Depending on polymer properties, mechanical grinding and chemical precipitation can lead to nanoparticles with varying shapes. The thinner a particle is, the more photons will be required to obtain a spectrum of the same quality. As particles tend to deposit with a preference to lay flat against the substrate, the shortest dimension of a particle is the one limiting its analysis.

The spectra can be attributed to specific polymers by comparing the exact position and relative intensity of the main peaks to those of reference spectra of polymers or of molecules with shared bonding structures (Dhez et al., 2003). Some of the polymers studied showed differences in the spectra compared to the references, the most common being a decrease of the main peak intensity, often accompanied by the appearance of a new peak at 285 eV (Figure 3-2). These differences between experimental (Figure 3-2, a-h black lines) and reference, (Figure 3-2, a-h blue lines) spectra indicate radiation damage induced by the X-ray beam during the STXM analysis. Similar differences between the nanoparticle measurements and reference materials can be observed in Figure 3-3. The estimated radiation dose (Appendix D.9) in many cases are above the critical doses for the alteration of carbonyl, phenyl and C-H groups in polymers, which are quite sensitive to ionizing radiation and have been systematically studied (Coffey et al., 2002; Wang et al., 2009). The most significant radiation damage effect observed in common polymers is a decrease in the $C1s \rightarrow \pi^*_{C=O}$ resonance near 287 eV, often accompanied by an increase in the $C1s \rightarrow \pi^*_{C=C}$ resonance near 285 eV, that is caused by the reduction of carbonyl groups (which produces vinyl C=C bonds). Such radiation damage is clearly seen in the spectra in Figure 3-2 and Figure 3-3, especially for PA and PMMA for which carbonyls dominate the molecular structure, but also for PET and PC (note that the $C1s \rightarrow \pi^*_{C=O}$ resonance for PC is shifted to 291 eV), which also contain carbonyl groups. The radiation dose could be further reduced by careful attention to the spatial scanning parameters in order to evenly spread the dose across the entirety of the limited nanoparticle volume, and by limiting the spectral quality (in terms of energy points measured and counting time) to the minimum required for identification. While the deposition of a carbonaceous layer is a common issue during STXM analysis, it appears unlikely in this case as none of our spectra show an increase at 288.5 and 293 eV, which would be typical for a carbon layer deposition (Leontowich and Hitchcock, 2012).

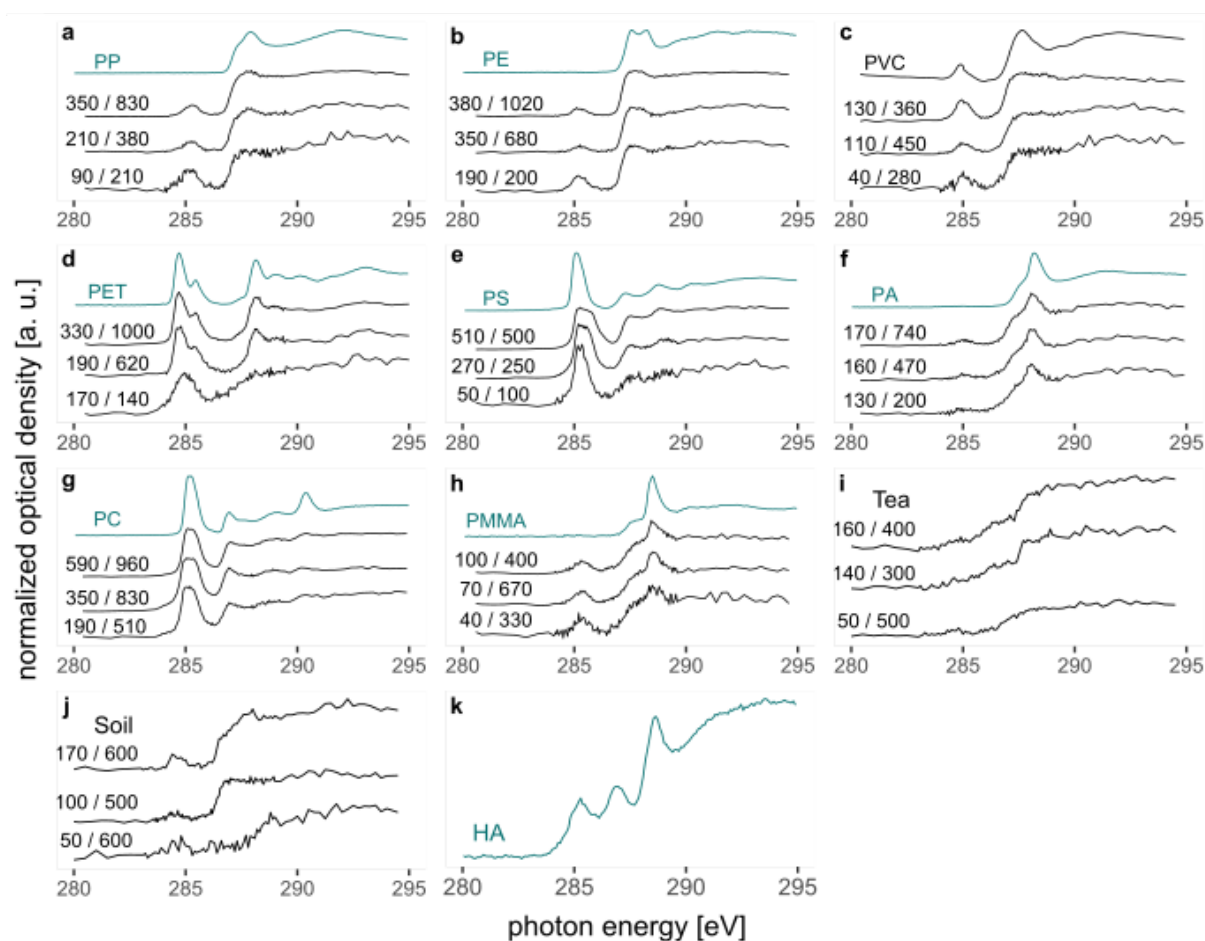


Figure 3-2: Differentiation of polymers by C K-edge NEXAFS spectroscopy. (a-h) Comparison of NP spectra from eight polymers (black spectra) compared with a reference spectrum (blue) (Dhez et al., 2003). All spectra have been normalized to fit the scale. The energy position was corrected for the first peak of PS to match the reference: (a) polypropylene, (b) polyethylene high and low density, (c) polyvinyl chloride, (d) polyethylene terephthalate, (e) polystyrene, (f) polyamide, (g) polycarbonate, (h) polymethylmethacrylate. The thickness [nm] / Feret diameter [nm] of the particle corresponding to the spectrum is written on the left hand-side of each NEXAFS spectrum. As no PVC reference spectrum was available in the literature, we measured the NEXAFS spectrum of a microtomed PVC sample. (i-j) NEXAFS spectra of common natural organic matter occurring in tea and soil, respectively. (k) Humic acid (pH = 6) reference spectrum (Christl and Kretzschmar, 2007).

Finding NP in spiked environmental matrices

In environmental samples, a wide variety of particles exist simultaneously in the media and can interfere with the identification and characterisation of NP, making it difficult to find NPs simply by being present in much higher numbers. A method to extract NP from soil and water samples (Figure 3-3, a; Figure 3-4, a) was developed, based on methods for the extraction of metallic nanoparticles (Schwertfeger et al., 2017) and for the purification of MP (Hurley et al., 2018; Liu et al., 2019), with some adaption to NP specific characteristics (e.g., higher sensitivity to oxidation and aggregation) (Schwaferts et al., 2019). With this aim, the density separation was modified to use sucrose to prevent aggregation of NP in concentrated salt solutions like $ZnCl_2$ or NaBr that are often used in MP research (Bläsing and Amelung, 2018; Liu et al., 2019). A gentle oxidation step using low concentration hydrogen peroxide to remove

natural organic matter but prevent oxidation of NP and a final ultrafiltration step (Ter Halle et al., 2017) were added to the procedure to clean the samples and preconcentrate the NP prior to their deposition on a silicon nitride membrane by centrifugation. The method was tested on PA NP and was found to have no influence on the NEXAFS spectra of the particles (Appendix D.10).

A lake water sample from Lake Lucerne (Switzerland) and a soil sample from a remote mountain soil (Laax, Switzerland) were spiked with NP and then subjected to the above described extraction and analysis procedures. The water sample was spiked with PMMA, PC, PET and PP, and the soil sample, which had proven to be clean from MP and larger plastics (Scheurer and Bigalke, 2018), with PA (Figure 3-3, a). In the water sample, NP of PMMA, PC and PET were found (Figure 3-3, b blue lines) but not of PP, possibly because too few PP particles spiked were in the NP range (< 1000 nm). In the spiked soil sample, we retrieved the PA NPs (Figure 3-3, b, brown line).

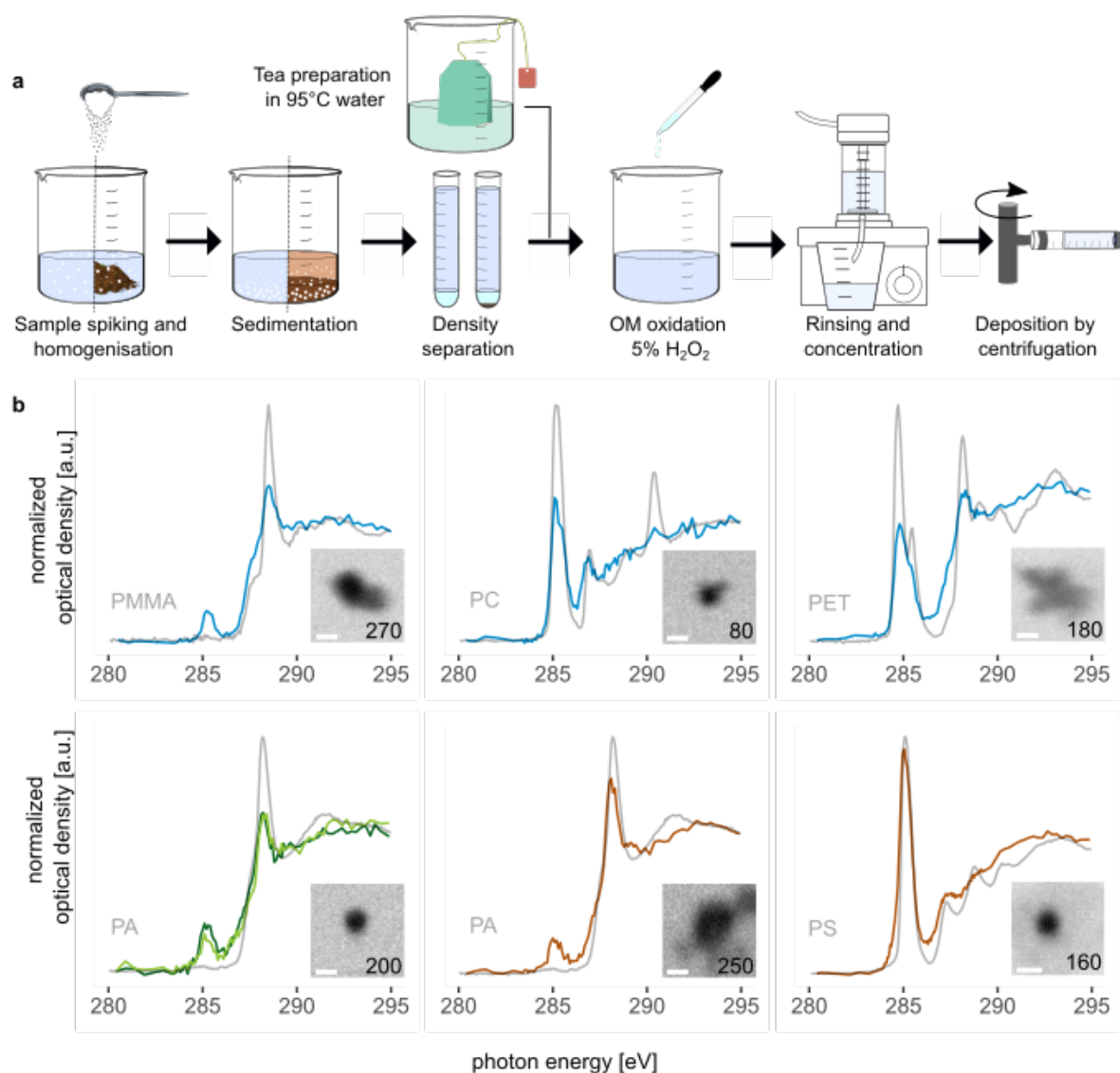


Figure 3-3: Identification of NP in spiked water, brewed tea water and spiked soil samples. (a) Schematic representation of the spiking and extraction protocol for water and soil matrices. The water sample was spiked with powder of PMMA, PC, PET and PP. The tea bags were made out of PA. A soil sample was spiked with a powder of PA and another soil sample with 250 nm PS beads. (b) NEXAFS spectra together with a normalized reference spectrum (grey lines, (Dhez et al., 2003)) and STXM image of the corresponding particle found in the water spiked sample (blue lines), the peppermint and green tea (dark green, light green) and the soils (brown lines). The measured spectra and the corresponding reference were normalized at the pre (280 eV) and post edge (295 eV) energy to fit the scale. The images were acquired at 350 eV and the white scale bar is 250 nm. The number in the image refers to the particle thickness (nm). The small peak at 285 eV, which is not visible in the reference spectra of PMMA and PA but in the spectra from the NP, as well as the differences between the reference and the measure spectra in the 287-293 eV region for PC and PET are most probably due to radiation damage.

Characterising NP in environmental and food samples

To assess the suitability of the method to find NP in unspiked food samples, we first analyzed green and peppermint tea prepared from PA teabags (Figure 3-3, a). In spite of the high organic matrix of the tea, we were able to differentiate PA from the tea matrix and find PA NP in both tea samples, confirming the previous report of teabags releasing NP in tea infused water (Hernandez et al., 2019) (Figure 3-3, b green lines).

For the soils, samples SAN and GAM were collected at agricultural sites, where mulching foil had been applied, while samples DUF and BRA were from pasture sites close to roads. In the road site soils we did not check for tire wear particles but for other plastic waste usually found close to roads due to plastic waste thrown out of cars. We found NP of three different polymers (PA, PP, PS) in a size range of 250-900 nm and mostly irregularly shaped (Figure 3-4). The presence of PA in the roadside soil can be attributed to NP formation from packing material waste, while the NP in the arable soils most probably originate from mulch foil, nets and nonwoven covers (PP), strings to fix foil tunnels (PA) and other agricultural applications (PS) (Scarascia-Mugnozza et al., 2011). The fact that no PE (the most commonly used polymer for mulch films) was found, even at the sites with mulching film application, might be either due to PE being a polymer not very susceptible to NP formation (either slow formation or short lifetime) or due to the spectrum of aged PE being very similar to natural organic matter and thus, difficult to differentiate.

NP formation has been reported recently in a heavily plastic contaminated soil by AF4 and py-GC-MS (Wahl et al., 2021) and in marine waters (Ter Halle et al., 2017). Our results show the occurrence as well as the characteristics of individual NP in common agricultural soils at common plastic concentrations. The finding of NP in the studied soils show that NP form from larger plastic items in the soils. This NP formation will be favored by physical stress applied to plastic waste occurring in soil such as cutting the grass at roadside soils that will also cut the plastic waste and ploughing at arable soils might also that grind larger plastic items to NP. Beside the physical stress, UV radiation will age plastics as long as they occur at the soil surface and microbial attack might cause disintegration of certain polymers after the plastics are buried into the soil (Krueger et al., 2015; Otake et al., 1995). Beside providing useful insights on NP formation in soils, our results also have implications for the design of ecotoxicological and environmental fate (e.g. transport) studies. While in most such studies, spherical PS/PE NP are used (Thomas et al., 2021) – due to its easy availability and defined shape – our data clearly show that NP from different polymers occur and that their shape is mostly not spherical but rather what is referred as a fragment. Work on engineered nanoparticles has shown that nanoparticle shape has implications for its toxicity (Demir, 2020; Pikula et al., 2020) and transport in porous media (Wang et al., 2016). NP extracted from the marine environment have also been reported to have different toxicities from artificial spherical NP (Baudrimont et al., 2020).

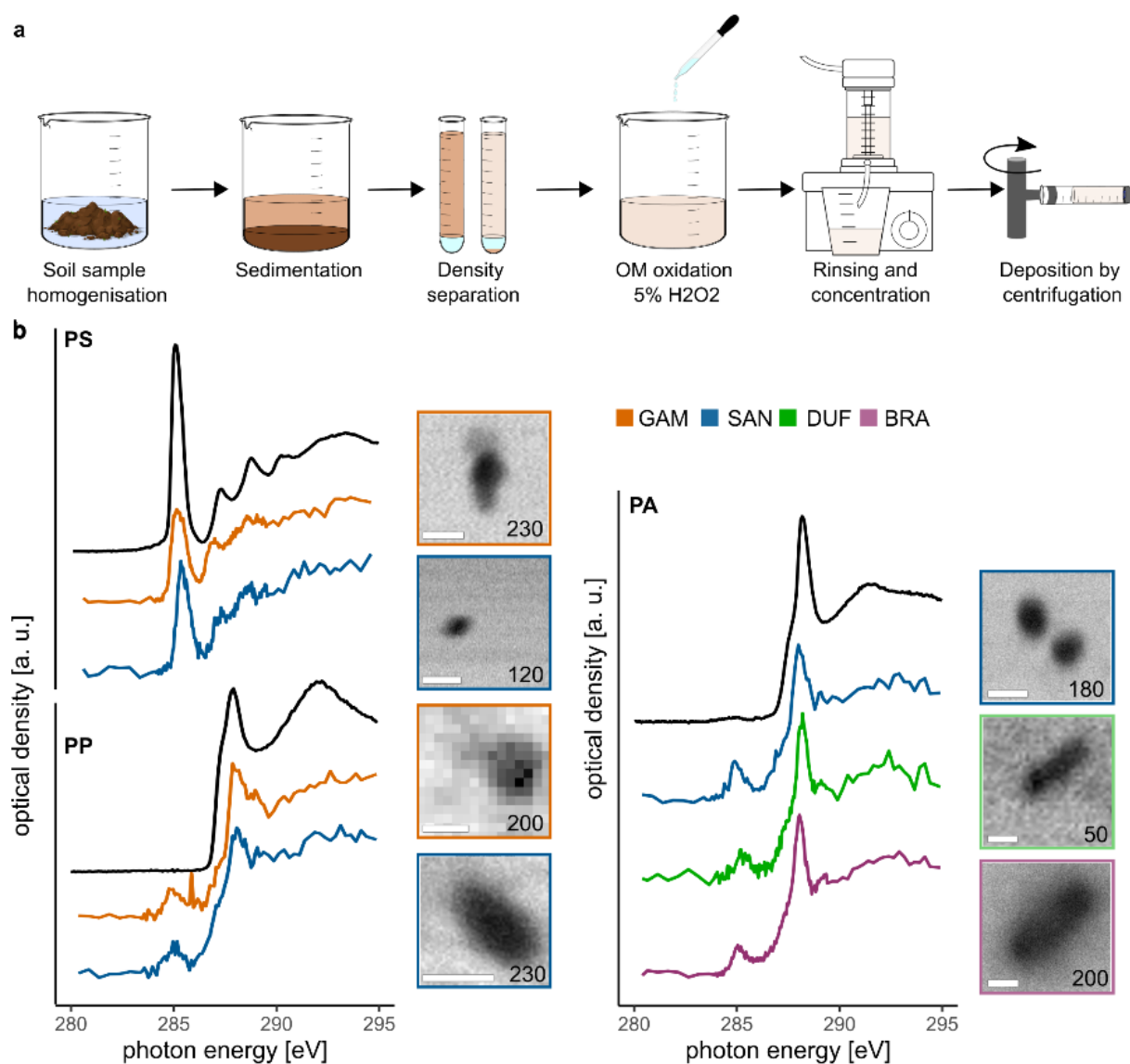


Figure 3-4: Identification of NP in 4 natural soil samples. (a) Schematic representation of NP extraction from soil matrices. (b) NEXAFS spectra together with a normalized reference spectrum (grey lines) (Dhez et al., 2003) and STXM image of the corresponding particle found in Sant' Antonino (SAN, brown lines), Gampelen (GAM, blue lines), Belpberg Dufti (DUF orange line), and Wohlen b.B Breitacher (BRA, yellow line). The images were acquired at 350 eV. The small peak at 285 eV, which is not visible in the reference spectra of PP and PA but in the spectra from the NP, is most probably due to radiation damage. The white scale bar is 500 nm. The number on in the image refers to the thickness [nm].

3.4 Conclusion

We have demonstrated the use of STXM for the imaging and chemical characterisation of individual NP with a minimum dimension down to about 100 nm. We show that it can be applied to the analysis of pure NP and for NP present in environmental and food matrices. While STXM cannot provide statistically significant information on particle numbers, its strength is the high-resolution imaging and spectral investigation of individual particles or complex particle mixtures. For the soil samples analyzed here, three different polymers with different shapes and sizes were found. These results indicate the formation of NP in normal

agricultural soils and have implications for future studies on soil nanoparticles and nanoparticle ecotoxicology.

Among the analytical techniques available to analyze the molecular structure of particles, STXM is probably one of the most suitable for the analysis of NP characteristics, because of its high spatial and spectral resolution and the ability to limit radiation damage to the sample. However, STXM analysis of complex samples requires the use of extraction techniques that concentrate NP and eliminate most of the other materials from the sample matrix. Because of the considerable time needed to image particles by raster scanning (1-10 minutes/image depending on the resolution) and for spectral analysis (10-30 minutes depending on the dwell time), it is impractical to analyze enough particles to obtain a statistically significant quantification of the NP concentration in a sample. The strength of STXM is instead the differentiation of natural environmental particles (e.g. clay particles, natural organic matter) from NP and to combine imaging with spectroscopy to deliver a full chemical, size and shape characterization of the NP. Due to its high lateral resolution, STXM can trace chemical changes in individual NP or can analyze complex particle aggregates. STXM can be accessed (free of charge for academic use) by any researcher after a successful application to one of the many facilities worldwide (<https://lightsources.org>; <https://wayforlight.eu>).

3.5 Authors contribution

Alexandra Foetisch: Conceptualisation, Methodology, Software, Validation, Formal analysis, Investigation, Data Curation, Writing – Original Draft, Writing – Review & Editing, Visualization

Montserrat Filella: Conceptualisation, Methodology, Investigation, Writing – Review & Editing

Benjamin Watts: Conceptualisation, Methodology, Software, Investigation, Resources, Data Curation, Writing – Review & Editing, Visualization **Laure-Hélène Vinot:** Methodology, Validation, Investigation **Moritz Bigalke:** Conceptualisation, Methodology, Investigation, Resources, Writing – Review & Editing, Supervision, Project administration, Funding acquisition.

3.6 Acknowledgements

This study was funded by the Swiss National Science Foundation (SNSF, 200021_182672/1). We acknowledge the Paul Scherrer Institute, Villigen, Switzerland for provision of synchrotron radiation beamtime at beamline PoLLux of the SLS and would like to thank Katharina Witte and Simone Finizio for their assistance. We also thank Beatrice Frey from the Department of Chemistry, Biochemistry and Pharmacology of the University of Bern and Agathe Martignier from the Department of Earth Sciences of the University of Geneva, Reto Zanoni from the Veterinary Institute of the University of Bern and Jaime Caplette, Milo Fieber, Daniela Fischer, Adrien Mestrot, Anna Muntwyler, Lucija Stanisic, Gaby Witschi and Evelyn Vonwyl from the

Institute of Geography of the University of Bern for helpful suggestions and help in the lab and/or during beamtimes.

Abstract

Once emitted into the environment, macro- (MaP), micro- (MP) and nanoplastics (NP) are exposed to environmental weathering. Yet, the effects of biogeochemical weathering factors occurring in the soil environment are unknown. As the transport, fate, and toxicity of MP and NP depend directly on their surface properties, it is crucial to characterize their transformation in soils to better predict their impact and interactions in this environment. Here, we used scanning transmission x-ray micro spectroscopy to characterize depth profiles of the surface alteration of environmental plastic debris retrieved from soil samples. Controlled weathering experiments in soil and with UV radiation were also performed to investigate the individual effect of these weathering factors on polymer surface alteration. The results revealed a weathered surface on a depth varying between 1 μm and 100 nm in PS, PET and PP environmental plastic fragments naturally weathered in soil. Moreover, the initial step of surface fragmentation was observed on a PS fragment, providing an insight on the factors and processes leading to the release of MP and NP in soils. The comparison of environmental, soil incubated (for 1 year) and UV weathered samples showed that the treatments led to different surface chemical modifications. While the environmental samples showed evidence of alteration involving oxidation processes, the UV weathered samples did not reveal oxidation signs at the surface but only decrease in peak intensities (indicating decrease of the number of chemical C bonds). After a one-year incubation of samples in soil no clear aging effects were observed, indicating that the aging of polymers can be slow in soils.

4.1 Introduction

The total amount of plastic accumulated in landfills and the environment between 1950 and 2016 was estimated to be 4900 Mt (Geyer et al., 2017) and was projected to become approx. 12000 Mt in 2050 (Geyer 2020). Much of the plastic ends up in soils and can affect its physicochemical properties, and the health of soil organisms and plants growing in the soil (; Ren et al., 2021a; Rodriguez-Sejjo et al., 2017). The main sources of plastic in soil are littering (Braun et al., 2023; Ledieu et al., 2022; Pietz et al., 2021), road runoff (Knight et al., 2020; Sommer et al., 2018), and atmospheric deposition (Kernchen et al., 2022; Wright et al., 2020). In agriculture, practices such as sewage sludge (Corradini et al., 2019), compost (Weithmann et al., 2018) amendments, the use of plastic mulches (Khalid et al., 2022) and coated fertilizers (Katsumi et al., 2020), contribute significantly to the plastic input in soils (Hurley and Nizzetto, 2018). Once in the soil, plastics can fragment, forming micro- (MP, 0.001-5 mm) and nanoplastics (NP, <0.001 mm). To understand the impact, fate and accumulation of plastic in soil, it is important to assess how they change over time and to determine the factors causing such changes. In the environment, plastic debris will be exposed to several weathering factors, which can lead to changes in their morphology, chemistry, and physical properties. The

possible mechanisms of environmental plastic degradation include abiotic processes, such as thermal degradation (Pielichowski and Njurguna, 2005), photo-degradation (Cai et al., 2018; Luo et al., 2020b) and mechanical breakdown (He et al., 2018), as well as biotic processes such as bio-fragmentation (Cadée, 2002; Dawson et al., 2018) and biodegradation (Danso et al., 2019; Zumstein et al., 2018). In turn, the efficiency of the different mechanisms to degrade plastic will depend on the particle size (Luo et al., 2020a; Wang et al., 2020) and physico-chemical properties of the polymer, such as its chemical structure (Gewert et al., 2015) and crystallinity (Julienne et al., 2019), and environmental conditions, such as the oxygen concentration, humidity (Wang et al., 2020), temperature (Chen et al., 2020), and organic matter concentration (Cai et al., 2018; Liu et al., 2020). So far, most of the research concerning plastic weathering has been conducted in aquatic or air media but only little is known about plastic aging in soils (Duan et al., 2021). Before being buried in soil, plastic fragments can lie in sunlight for some period of time. Previous work has investigated the effect of UV on polymer chemistry and morphology using mostly attenuated total reflectance Fourier transformed infrared spectroscopy (ATR-FTIR) and scanning electron microscopy (SEM). The most common reported effects of UV on polymers are the formation of hydroxyl (OH) and carbonyl (C=O) groups (Ainali et al., 2021; Cai et al., 2018; Fernández-González et al., 2021). In the soil, plastic is no longer exposed to UV but instead to soil microorganisms and roots in a mostly humid environment where the expected aging factors include extracellular enzymes and organic and inorganic acids, as well as mechanical effects, e.g. by bioturbation, soil compaction, or freeze-thaw cycles. However, the effect and importance of these weathering factors are yet unknown (Büks and Kaupenjohann, 2022). Previous work used a biodegradable ¹³C-labelled poly(butylene-co-terephthalate) (PBAT) to show for the first time the biodegradation of a biodegradable polymer in agricultural soil (Zumstein et al., 2018). Many different enzymes and/or bacterial strains have been tested for their efficiency to biodegrade conventional and biodegradable polymers (Amobonye et al., 2021). However, the consequent polymer surface modifications of conventional polymers are still unknown, despite their importance in assessing the particles' fate and impact in the soil.

The study of plastic biodegradation in soil is challenging, as the processes cannot be accelerated while maintaining environmentally relevant conditions. ATR-FTIR usually has a penetration depth varying between 0.2 and 5 µm, and will therefore not detect changes on polymer surface if the depth of alteration is outside this scale range. A high resolution analytical technique providing chemical information on a nanoscale is therefore required. Such a technique would allow to investigate the potential effects of soils on polymer surface chemical properties. Scanning transmission x-ray microscopy (STXM) coupled with near-edge x-ray absorption fine structure (NEXAFS) spectroscopy. The STXM technique uses X-rays

generated by a synchrotron with a photon energy that covers the 1s K- carbon edge and provides information on the type and proportion of carbon bonds in the material under study. It was previously used to identify NP in environmental matrices (Foetisch et al., 2022) and can provide chemical information with a 30 nm resolution (Raabe et al., 2008).

In this study, we applied for the first time STXM-NEXAFS spectroscopy to access the depth and chemical changes of plastic fragments aged under different conditions in order to better understand the mechanisms and temporal development of environmental plastic ageing. The objectives were: a) to access the depth of surface chemical alteration of environmental plastic fragments found in soils, b) to compare it with the surface chemical alteration of plastics incubated in soil under controlled laboratory conditions for one year, and c) to reveal the depth of surface chemical alteration aged under UV exposure (300-400 nm wavelength). For this purpose, we characterised the surface alterations along a depth profile from the surface to the bulk material (BM) of the plastic fragments aged under the different conditions.

4.2 Material and methods

4.2.1 Environmental samples

Environmental plastic fragments weathered in natural conditions (history unknown) of polystyrene (PS), polyethylene terephthalate (PET) and polypropylene (PP) were retrieved from agricultural and roadside soil samples collected between 0-20 cm depth in Switzerland in 2018 and 2021. The samples labelled GUR were collected from an agricultural soil in Gurzelen (BE, 46°46'45.94" N, 7°32'15.57" E) where compost had been applied. The samples labelled SAN were collected from an agricultural field in Sant'Antonino (TI, 46° 9' 42.45"N, 8°57'41.43"E) where plastic mulch had been applied. Finally, samples labelled ES were collected from a roadside soil in Bern's surroundings (BE, 46°57'31.59"N, 7°23'19.99"E) where littering was apparent. The soil samples were sieved and macroplastics with a size of 5-100 mm collected, washed (see section 4.2.2), and analysed by ATR-FTIR (ATR-FTIR, LUMOS II, Bruker Cooperation, Billerica, Massachusetts) to assess their polymer composition.

4.2.2 Soil incubation

Soil was collected from a pasture near Geneva, Switzerland (Avully, 46°10'10.21"N, 6°0'5.51"E). The soil had a clay, lime, and sand content of 17, 32 and 52% [w/w], respectively, a total nitrogen and carbon content of 0.12 and 1.12% [w/w], respectively, and a pH of 5.4. The moist soil was sieved to 10 mm on the day of sampling and homogenized by a repetition of soil division and re-homogenisation until reaching portions of around 110 g. Each soil portion was then transferred into brown glass vials (11x5 cm) for the incubation.

Fragments of approx. 500 µm diameter of PA Radilon, PC Makrolon and PEHD Hostalene (Semadeni Plastic Group, Switzerland) were selected after cryo-grinding initial pellets with a Pulverisette11. Fragments of approx. 1 mm of PET and PU were produced by cutting a water bottle and a foam stopper, respectively, with a blade on a glass slide. The polymers were chosen to represent the plastic most often found in the soil (Büks and Kaupenjohann, 2020) as well as a diversity of hydrolysable and non-hydrolysable polymers (Amaral-Zettler et al., 2020). The plastic fragments were then distributed evenly in brown glass vials containing the soil at 2.5 cm under the surface using a tweezer. Fragments were incubated in the soil at 30°C and 60% humidity. The soil water content was adjusted to 60% of the water holding capacity twice a week (Appendix E.2), by adjusting the weight of the soil with water. After one year of incubation, fragments were visually sorted from soil by spreading it in water on a glass petri dish under a magnification lamp. Negative control of PA, PET, PE, PP, PS, PC and PU underwent the same treatment to reproduce the handling and matrix conditions but were incubated only for 24 h. For each polymer, 9 fragments were incubated to ensure at least 3 replicates for SEM imaging and 3 replicates for STXM-NEXAFS spectroscopy. Fragments retrieved from the soil treatment and environmental soil samples were shaken in water with tweezer and placed into petri dishes with 2% sodium dodecyl sulphate (SDS). They were gently agitated for 5 min on a shaking plate. Finally, the SDS was discarded and replaced by MiliQ water at 50°C and the fragment were agitated again for 5 min on a shaking plate. This washing procedure was chosen in order to remove soil being present on the fragment while not affecting the surface of the polymer (adapted from Montazer et al., 2018). The polymer fragments were individually wrapped into aluminium foil and kept at room temperature until further analysis.

4.2.3 UV treatment

PS Total ®, polycarbonate (PC) Makrolon ®, PP Total ® (Semadeni Plastic Group, Switzerland) and PET from a water bottle (Aproz®) were exposed to UV irradiation. Pellets of PS, PC and PP were sectioned by microtomy (UC6, Leica Microsystems, Vienna, Austria) to create a flat and fresh surface which was not exposed to UV radiation before. PET did not need such a preparation, as the fragments were already flat. For this experiment the samples could not be produced by cryomilling (as for the soil incubation) as bigger particles were needed for the two sectioning steps. Fragments were placed into a glass Petri dish and covered with a thin plastic foil (Migros, Tangan N°11) to prevent fragments from moving under the air flow of the UV chamber. UV treatment was performed in an Atlas Suntest CPS+ chamber (Atlas Material Technology LLC, Chicago, USA) equipped with a Xenon lamp (1500 W) and a Daylight filter. The irradiation, between 300 and 400 nm, had an intensity of 65 W/m² and the chamber was cooled by a continuous air flow. The Petri dish was placed into the UV

aging chamber and fragments were removed after 160 hours of exposure, corresponding to approximately 63 days of exposure in central Europe (calculation according to Gewert et al., 2018, Section SI 1) The fragments were aged only on one side. The non-exposed side was marked using a metallic pen (Edding 780, gold colored), which can be detected by optical microscopy to avoid confusing the exposed and not exposed sides.

4.2.4 *Sample preparation for STXM*

For further STXM-NEXAFS investigation of the aging processes occurring on a gradient from the surface to the bulk material (BM) of the different polymers, the fragments were cut in thin sections by ultramicrotomy (UC6, Leica Microsystems, Vienna, Austria). Initially, the examined fragments from uncontrolled soil weathering were embedded into an epoxy resin to facilitate the sectioning. However, the contact between the epoxy resin and the polymer increased the difficulty of locating the surface of the polymer in the STXM. Thus, this procedure was not applied in the following samples. Instead, the remaining fragments from the different treatments were glued on a microtomy block and cut into 200 nm thick slices (Figure 4-1, a). This procedure allows to have particle surfaces free from epoxy resin. Between two and four slices of our own initial macro particle were deposited on a SiN₂ membrane (SiRN-5.0-200-1.0-100, Silson, United Kingdom) for STXM analysis and dichlorethane was applied on the slices to flatten them (Figure 4-1, b). As mentioned above, we chose PA, PC, PE, PET and PU polymers that were likely to be found in soil and that covered the range of potential degradability in soil, according to their chemical composition (whether or not they have heteroatoms in their backbone). However, after finishing the soil incubation, when we tried to produce the microtomy sections we found that we could not use PA, PE and PU, because they were too soft to be cut by microtomy. So, we replaced PA, PE and PU by PP and PS for the UV aging experiment. Finally, we were able to cut thin sections of PC, PET, PP and PS. However, due to the experimental sequence, we only have soil incubations for PC and PET. PA, PE and PU were too flexible and soft and all sections produced showed uneven thickness and/or ripped edges. Therefore, PA, PE and PU could not be further analyzed with STXM-NEXAFS and are not present in the results and discussion section. PA, PE and PU were too flexible and soft and all the sections produced showed an uneven thickness and/or ripped edges. Therefore, PA, PE and PU could not be further analysed with STXM-NEXAFS and are not present in the Results and Discussion section. This method of sample preparation is thus suitable only for the less-elastic polymers and for fragment sizes which allows them to be handled manually. Future work could overcome this problem by using cryo-microtomy to produce the polymer sections.

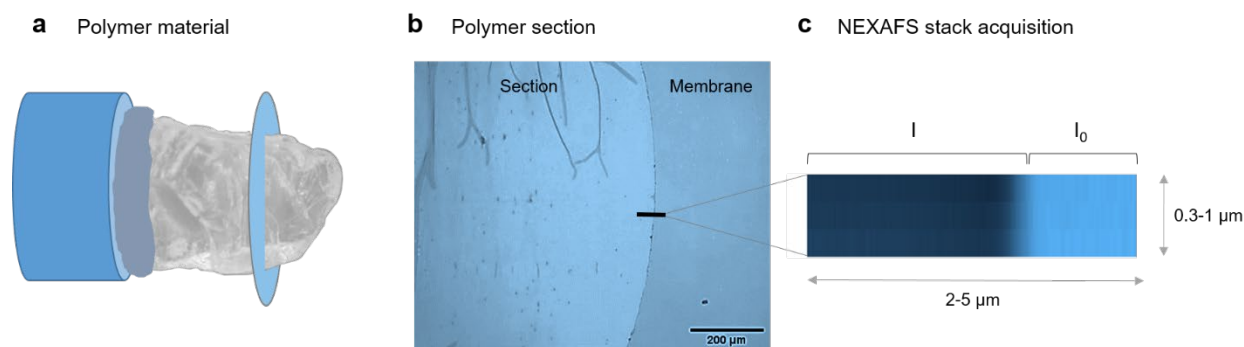


Figure 4-1: Sample preparation for STXM-NEXAFS analysis. (a) The polymer was glued on a block and microtomed in thin sections. (b) The sections were deposited on SiN membranes for STXM analysis. (c) NEXAFS stacks were acquired on the edge of the section. The light blue part corresponds to the area outside the thin section, while the dark blue part corresponds to the edge of the thin section.

4.2.5 STXM data acquisition

The STXM measurements were performed at the PoLLux beamline of the Swiss Light Source (SLS) synchrotron at the Paul Scherrer Institute in Villigen, Switzerland. The detailed beamline layout has been described before (Raabe et al., 2008). A nickel Fresnel zone plate with an outermost zone width of 25 nm was used to focus the monochromated X-ray beam (spot size of ~30 nm) on the membrane and the transmitted X-rays were detected by a photomultiplier tube coupled with a phosphor screen. Sections were imaged in STXM by raster scanning an area of the membrane at 350 eV to locate their edges. Once an edge was located, NEXAFS stack measurements along a set of $0.3\text{-}1\text{ }\mu\text{m}$ lines of $2\text{-}5\text{ }\mu\text{m}$ in length were acquired in the energy range between 280 and 320 eV corresponding to the C K-edge (energy resolution: $283\text{-}283\text{ eV} = 0.5$, $283\text{-}289\text{ eV} = 0.1$, $289\text{-}294\text{ eV} = 0.25$, $294\text{-}300\text{ eV} = 0.5$ and $300\text{-}320\text{ eV} = 1$) and a dwell time of 60 ms. The spatial resolution of the NEXAFS acquisition in the surface- BM direction was of 30 nm. Each stack included a portion of empty membrane (for I_0 normalization), the edge of the section and a portion of the BM (I) (Figure 4-1, c). The estimated energy dose of each measurement is available in Appendix E.3. A minimum of three stacks were acquired at random places around the section for each fragment analysed. A summary of data available for the different polymers and different sample treatment types (field weathering, UV, soil incubation and control) is provided in Table 2. No PC fragment could be found in the environmental field samples and, for logistic reasons, a control for PP was not measured. Finally, since the different experiments were run in parallel and not sequentially, PS and PP were not included in the initial soil incubation experiments.

Table 2: Summary of the samples for the four polymers and four treatments used in this study. Fragment refers to the name of the sample while n indicates the number of replicate measurements acquired on the same fragment.

Polymer	Field weathering		UV 160h		Soil incubation		Control	
	Fragment	n	Fragment	n	Fragment	n	Fragment	n
PS	GUR3b	11	PS3	3	NA	NA	PS_ctrl	5
	GUR3	11						
	ES6	4						
	ES9	4						
	ES15	4						
PET	SAN1a	4	PET3	3	PET_A_S	4	PET_ctrl	4
	ES2	5						
PC	NA	NA	PC3	3	PC_A_S	3	PC_trl	3
PP	SAN2b	4	PP3	4	NA	NA	NA	NA
	ES10	3						

4.2.6 Data processing

All I_0 were manually extracted using aXis2000 (["http://unicorn.mcmaster.ca/aXis2000.html,"](http://unicorn.mcmaster.ca/aXis2000.html) n.d.) and data were further processed with RStudio software (RStudio Team, 2020). The whole stack measurement was extracted from the HDF5 data file and converted in a dataframe using the *rhdf5* library (Fischer et al., 2020). The stack (I) was normalized to I_0 following the Beer-Lambert Law:

$$OD = -\log(I/I_0) \quad \leftarrow \text{Raw data} \quad (2)$$

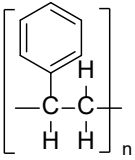
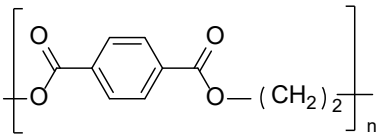
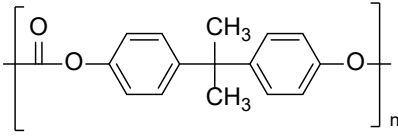
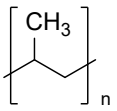
where OD is the optical density, I is the intensity of the measured spectra in the thin section and I_0 the intensity of the background spectra outside the thin section. Data were then normalized using the pre- and post-edge absorption intensities to mask the effect of the section thickness on spectra intensity:

$$OD_{\text{norm}} = (OD - OD_{\text{pre-edge}}) / (OD_{\text{post-edge}} - OD_{\text{pre-edge}}) \quad \leftarrow \text{Normalized data} \quad (3)$$

where $OD_{\text{pre-edge}}$ is the mean OD value between 280 and 283 eV and $OD_{\text{post-edge}}$ is the mean OD value between 310 and 320 eV. The thickness of the section along the stack is then approximated by multiplying the $OD_{\text{post-edge}}$ by each polymer attenuation length (Appendix E.4). All spectra acquired on a thickness < 40 nm are marked as background and not considered in the next processing steps. The 40 nm cut off value was chosen according to the minimum particle thickness measured in previous work (Foetisch et al., 2022) where the noise to signal

ratio still allowed peak identification. A non-ideal (e.g. not sudden) sample thickness onset at the edge of the material could be caused by a combination of the sample particles surface not being parallel to the normal of the section plane and image blurring by the finitesiz of the X-rays beam focus. The energy calibration offset of the STXM at PolLux was estimated at -0.4 eV by comparing the bulk PS C 1s (C–H) $\rightarrow 1 \pi_{C=C}^*$ peak energy in our measurements to the values provided by (Dhez et al., 2003). To detect the presence of chemically distinct layers in the particle from the surface to the BM, the spectra of one stack measurement was divided in three groups using a complete linkage hierarchical clustering (*hclust* function from stats package) (RStudio Team, 2020). This method allows the identification of clusters of similar spectra. All spectra from a given group were averaged and the average of each group of a stack plotted together. The number of groups was chosen to summarize the data while still allowing the observation of a potential evolution of the spectral features along the depth gradient. Additionally, the intensity of spectral features for each polymer was displayed along the surface – BM gradient to track their evolution. The energies corresponding to the different electronic transitions for PS, PET, PC and PP as identified by (Smith et al., 2001), (Dhez et al., 2003) and (Klein et al., 2008) are given in Table 3. Source code for all RStudio scripts is available on the Zenodo platform ([10.5281/zenodo.8037412](https://zenodo.org/doi/10.5281/zenodo.8037412)).

Table 3: Molecular structure of PS, PET, PC and PP and the photon energy [eV] of the NEXAFS peak corresponding to the different electronic transitions for each non-weathered polymer as identified by (Smith et al., 2001), (Dhez et al., 2003), (Klein et al., 2008) and this study.

Polymer	Electronic Transition	Energy [eV]			
		(Smith et al., 2001)	(Dhez et al., 2003)	Klein et al. (2008)	This study
PS 	C 1s (C-H) \rightarrow 1 $\pi_{C=C}^*$	285.3	285.18	285.3	285.1
	C 1s (C-H) \rightarrow σ_{C-H}^* In CH ₂	287.7	287.29	287.5	287.4
	C 1s (C-H) \rightarrow 2 $\pi_{C=C}^*$	288.8	288.86	288.9	288.9
	C 1s (C-H) \rightarrow $\sigma_{C=C}^*$	294	293.1	293.7	293.15
PET 	C 1s (C-H) \rightarrow $\pi_{C=C}^*$ and C 1s (C-R) \rightarrow $\pi_{C=C}^*$	284.8, 285.6	284.8, 285.61		284.9, 285.3
	C 1s (C=O) \rightarrow $\pi_{C=O}^*$	288.2, 290.1	288.2, 290.1		288.1, 290.15
	C 1s (C-R) \rightarrow $\pi_{C=C/C=O}^*$		287.5		287.5
	C 1s (C-H) \rightarrow $\pi_{C=C/C=O}^*$		289.2		289.1
PC 	C 1s (C-H) \rightarrow $\pi_{C=C}^*$ and C 1s (C-R) \rightarrow $\pi_{C=C}^*$	287.0	285.25, 286.98		285.0, 286.9
	C 1s (C-R) \rightarrow $\pi_{C=C/C=O}^*$		289.1		~288.9
	C 1s (C=O) \rightarrow $\pi_{C=O}^*$	290.4	290.44		290.4
PP 	C 1s (C-H) \rightarrow σ_{C-H}^* (In CH ₃)		287.24		Not visible
	C 1s (C-H) \rightarrow σ_{C-H}^* (In CH ₂)		287.93		287.7
	C 1s (C-C) \rightarrow σ_{C-C}^*		292		291.9

4.3 Results & discussion

4.3.1 Surface alteration of polymer naturally weathered in soil

Buried plastic fragments recovered from agricultural and road side soils were analysed to investigate and characterise the surface alteration of polymers naturally weathered in soil. In total, 5 PS, 2 PET and 2 PP fragments were analysed; an example of each of them is given in Figure 4-2. The spectrum hierarchical clustering of a single measurement on a PS fragment (Figure 4-2, PS-A) showed that the chemical composition of the fragment was different at the surface compared to the BM. At the surface, the intensity of the $C1s(C-H) \rightarrow 1 \pi_{C=C}^*$ peak at 285.1 eV (black arrow) is approximately a sixth of its intensity in the BM. Additionally, two new peaks at 286.7 and 288.5 eV are present at the surface but absent in the BM. The variation of the intensity of these three peaks along the surface-bulk gradient showed that these surface changes extended to a depth of around 750 nm. The transition layer between the surface and the BM shows a smooth change of the chemical composition from the surface to the bulk (Figure 4-2, PS-B). The stack replicates acquired on this fragment ($n = 10$) (Figure 4-2, PS-C) showed all the same pattern but the thickness of the surface layer varied between 250 and 1000 nm in the fragment, indicating a spatial heterogeneity of the alteration depth. These results agree well with what was previously observed by (Klein et al., 2008) after exposing PS films to increasing doses of UV together with ozone. They attributed those changes in the spectra to the UV induced breakage of the C=C bonds of the phenyl rings ($C1s(C-H) \rightarrow 1 \pi_{C=C}^*$ decrease at 285.1 eV) coupled with an ozone reaction with the C=C broken bonds to forms C=O bonds (increase at 286.7 eV) and a removal of the C-H bonds from the phenyl ring ($C1s(C-H) \rightarrow \sigma_{C-H}^*$ decrease at 287.4 eV).

A similar pattern was observed at the surface of a PET fragment (Figure 4-2, PET-A,B), where the intensity of the peak $C1s(C-H) \rightarrow \pi_{C=C}^*$ at 284.9 eV is also a sixth of the peak in the BM, a new peak appeared at 286.7 eV and the intensity of the $C1s(C=O) \rightarrow \pi_{C=O}^*$ peak at 288.1 eV increased. The layer with a different chemical composition had a depth of only 200 nm and the transition layer was thin, indicating an abrupt change in composition between the surface and the BM. The replicates acquired on this PET fragment ($n=4$) (Figure 4-2, PET-C) showed three measurements with the same pattern as the given example and a fourth one where no change was observed between the surface and the BM. No studies using NEXAFS to investigate PET degradation are available, but ATR-FTIR showed that one can expect similar results as for PS, as both have phenyl rings in their structure and cleaving the phenyl ring requires less energy than the C-C bond of the backbone (Saito et al., 1981). Moreover, PET weathered in marine conditions analysed by ATR-FTIR showed an increasing C=O index with

increasing exposure time (Fernández-González et al., 2021), which correspond to our observations, meaning the surface of this fragment was oxidized.

The analysis of the PP field fragment did not show any new peak appearing in the PP spectrum along the surface – BM gradient, only a variation of the relative proportion of the $C1s(C-H) \rightarrow \sigma_{C-H}^*$ at 287.7 eV and $C1s(C-C) \rightarrow \sigma_{C-C}^*$ at 291.9 eV (Figure 4-2, PP-A, B). These results are very similar to the ones described by (Zhou et al., 2008), where they studied the effect of x-ray radiation damages on the PP NEXAFS spectrum. X-rays and UV are both ionising radiations and thus, their effects/damage on the polymer can be expected to be similar. Unfortunately, they did not report the energy dose applied in their different treatments. However, as the exposure time (0.6 s) of the material to the x-ray beam was shorter in our experiment than (Zhou et al., 2008) minimum exposure time (20 s), it is more likely that the alteration observed is not resulting from beam damages but an actual environmental weathering.

These results show that changes in the chemical composition of the polymer can be detected by the combination of STXM and NEXAFS with a pixel resolution of 15 nm. The heterogeneity of the alteration depth and/or co-occurrence of presence and absence of alteration on the same fragment analysed highlights the spatial heterogeneity of the weathering processes occurring at the surface of the polymers at our measurement scale (60000 nm²). In the environment, plastic can be half-buried, have other particles attached to it or carry a biofilm, that might protect sections of the polymer when exposed to UV radiations (Weinstein et al., 2016). For polymers buried in soil, observed spatial heterogeneity will also include the effect of the heterogeneous composition of the soil itself, where parts of the plastic surface could be in contact with water, air, natural organic matter, mineral particles or soil organisms. Thus, different processes might occur at the different contact sites and different aging will occur at different spots of their surface. In our case, out of the five PS fragment analysed, three showed a surface alteration pattern similar to the example given in Figure 4-2 (GUR3b, GUR3 and ES15), and the remaining two showed no clear differences in chemical composition between the surface and the BM (ES6, ES9). For PET and PP, the second fragments analysed had no clear alteration of their surface (Appendix E.5). As the history of these samples (initial product, exposure to UV, burial date, etc.) is unknown, the absence of detected effects can be explained either by the absence of surface alteration due to short exposure times or specific exposure conditions.

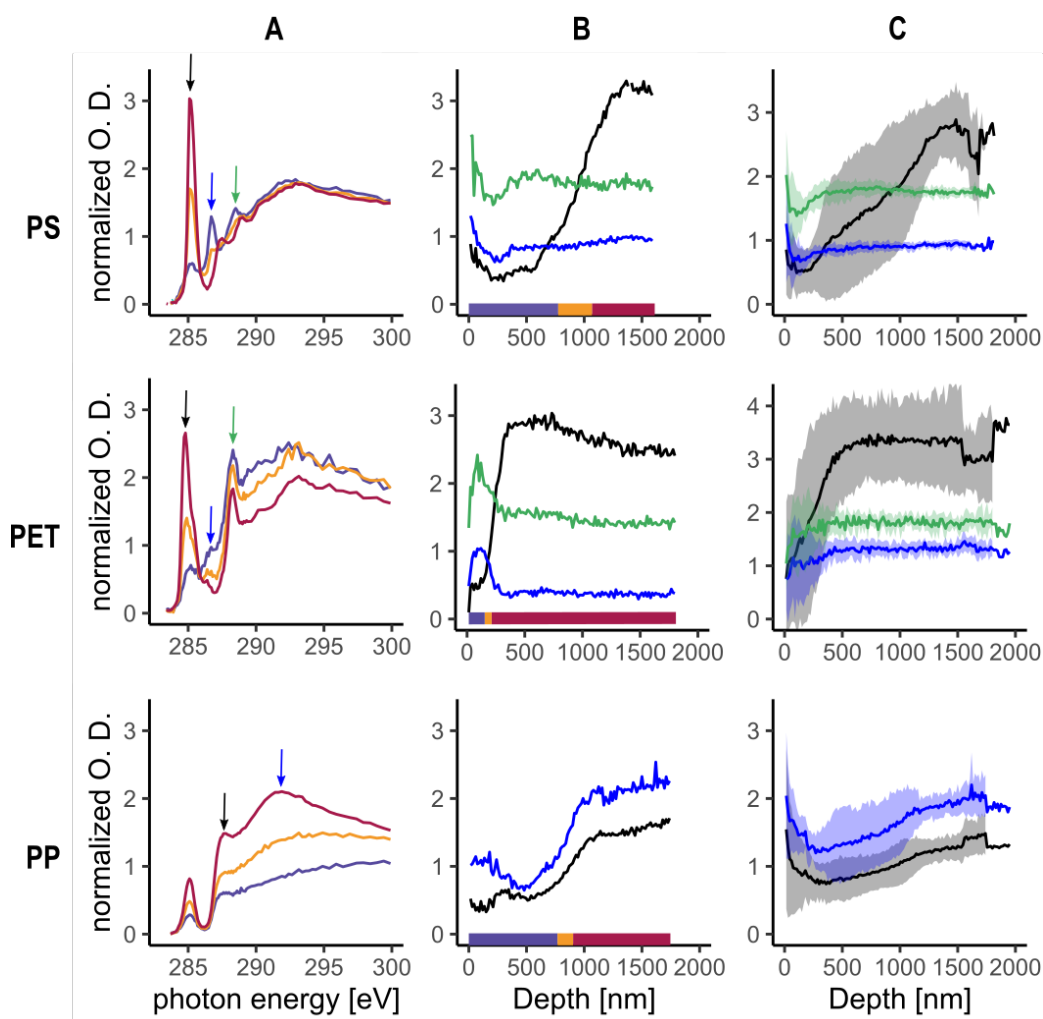


Figure 4-2: NEXAFS spectra of PS, PET and PP fragments retrieved from agricultural and road-sided soil, all NEXAFS data were normalized to pre- and post-edge to remove the effect of the sample thickness on the optical density. (A) Average spectra of each group determined by hierarchical clustering for a single stack measurement acquired on one fragment. The coloured arrow indicates the position of the peaks presented in B. (B) Intensity of the peaks highlighted by the arrow in A along the surface – BM gradient of the same stack measurement on the fragment shown in A. The coloured bar shows the position of the cluster group showed in the surface – BM gradient. (C) Average intensity of the peaks highlighted by the arrow in A along the surface – BM for all replicate stack measurements acquired on the same plastic fragment. The coloured ribbon indicates the standard deviation around the mean for each peak intensity

Additionally, in one measurement acquired on a PS fragment retrieved from soil, a bilateral alteration was observed at the surface. The change of the chemical composition was similar to the one presented for PS in Figure 4-2 but the distribution of the altered layer was different. Indeed, there was a layer in the 800-1100 nm depth where spectra were more similar to the one observed at the surface (Figure 4-3, A and B). The measurement position is clearly visible on the SEM image of the area investigated due to carbon deposition from the STXM chamber atmosphere (Boller et al., 1983; Watts et al., 2018) (Figure 4-3, C). The position of this change of peak intensity coincides with a visible depression in the material, which suggests a future detachment point of a smaller particle. It is known that micro cracks can form at the surface following the exposition of the polymer to weathering conditions (Deng et al., 2022; Naebe et

al., 2016) and the formation of $< 1 \mu\text{m}$ fragments was already observed after PS exposition to 2400 h of UV radiation (Meides et al., 2021). In our sample, it is not possible to resolve the full size of the particle potentially detaching from the surface but it would have at least a thickness of $1 \mu\text{m}$ (Figure 4-3, B dashed line). Additionally, the identification of this particle in an environmental matrix using STXM-NEXAFS could be challenging, as the predicted spectrum would integrate the information collected on the whole particle and will be an average of the purple and yellow lines of Figure 4-3, A. This result shows how important it is to understand the different weathering processes occurring in the environment to better predict the polymer structural composition of secondary MP.

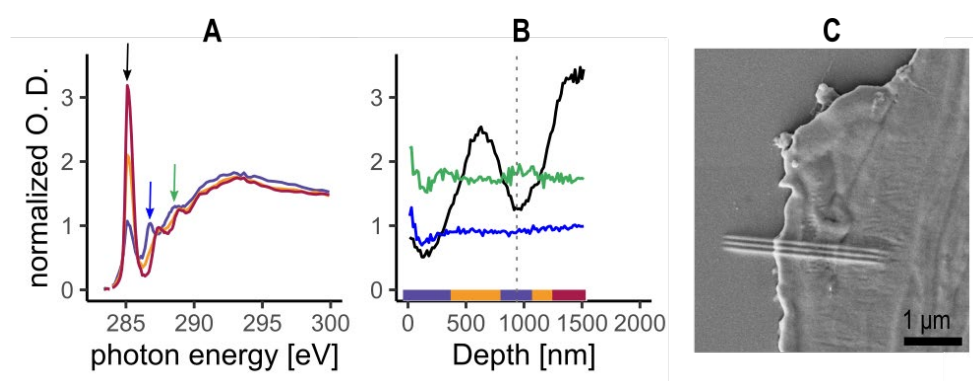


Figure 4-3: STXM-NEXAFS analysis of PS fragment retrieved from agricultural soil showing possible particle detachment, NEXAFS data were normalized to pre- and post-edge to remove the effect of the sample thickness on the optical density. (A) Average spectra of each group determined by hierarchical clustering for a single measurement. The coloured arrow indicate the position of the peaks presented in B. (B) Intensity of the peaks highlighted by the arrow in A along the surface – BM gradient of the same measurement shown in A. The coloured bar shows the position of the cluster group in the surface – BM gradient. (C) SEM image of the PS section. The position of the measurement presented in A and B is highlighted by the three horizontal lines, resulting from the carbon deposition from the STXM chamber during the measurement.

4.3.2 Controlled weathering experiments

Virgin polymers

To investigate the effect of well-defined weathering factors on the surface of polymers on the nanoscale range, virgin polymers were compared to polymers weathered in controlled conditions by UV radiation and/or incubated in soil for one year (Figure 4-4, control). First, the virgin polymers were examined as control particles. The control PS had all the peaks clearly defined from the surface to the particle interior. The only change in relative intensity was observed for the $\text{C}1\text{s}(\text{C}-\text{H}) \rightarrow 1 \pi_{\text{C}=\text{C}}^*$ peak at 285.1 eV, which was reduced at the surface was $2/3$ of the bulk polymer value. The measurements acquired on the control PET fragment showed a surface altered up to $1 \mu\text{m}$ depth where the $\text{C}1\text{s}(\text{C}-\text{H}) \rightarrow 1 \pi_{\text{C}=\text{C}}^*$ peak at 284.9 eV and the $\text{C}1\text{s}(\text{C}-\text{R}) \rightarrow \pi_{\text{C}=\text{C}/\text{C}=\text{O}}^*$ peak at 287.5 eV gradually increased from the surface to the BM, the $\text{C}1\text{s}(\text{C}-\text{H}) \rightarrow 1 \pi_{\text{C}=\text{C}}^*$ having a stronger relative change in its intensity. The control fragment

of PC showed a general reduction of the optical density in the 100 first nanometres. Between 100 and 400 nm below the surface, there was a simultaneous decrease of the $C1s(C=O) \rightarrow \pi_{C=O}^*$ peak at 290.4 eV and an increase of the $C1s(C-H) \rightarrow \pi_{C=C}^*$ at 285.0 eV and of the $C1s(C-R) \rightarrow \pi_{C=C}^*$ at 286.9 eV, suggesting that the surface was oxidized at these depths. The variations of the relative peak intensity observed for the control samples of PS, PET and PC indicate that the fragments used in this study had already a slightly different chemical composition at the surface compared to the BM, with variations similar to the UV exposed corresponding fragments (Figure 4-4, UV). However, while fragments exposed to UV were cut to provide a flat surface allowing the UV to homogeneously reach the fragment, no newly exposed surface was created for the control and soil incubated fragments. This means that control and soil incubated fragments can be compared directly, while the results obtained from the UV weathering samples can only be qualitatively compared to the samples weathered in the environment.

Soil weathered polymers

No clear effect of the soil incubation on the surface of PET and PC could be detected (Figure 4-4, control -> soil incubation). In the case of PET, the control fragment had a stronger and deeper surface alteration than the soil incubated one. In order for our sample to be representative of a PET fragment formed from littering, the PET initial material was obtained from a commercial water bottle. However, once microtomed, it was not possible to recognize anymore which side of the fragment had been exposed to air or to water. It is thus possible that the two sides of the fragment had weathered differently before the experiment, as they were exposed to different conditions (UV/water). The result is that it is not possible to evaluate the different controlled treatments of PET.

PET and PC were initially chosen for containing heteroatoms in their backbone and thus being more susceptible to enzymatic degradation than polymers containing a carbon backbone only (Amaral-Zettler et al., 2020). The absence of detected surface alteration indicates that a one-year soil incubation in our experimental conditions did not induce aging, even at the very high spatial resolution of STXM. So, even allowing for the fact that effects might differ depending on the conditions in soil, our results indicate that plastic weathering in soil is a rather slow process. The incubation performed in this study did not include plants or soil macro fauna, and thus relied on the microbial community present in the soil as aging factor. In real soils a more complex biological community and environmental conditions (soil management, freeze thaw cycles etc.) occur. Thus, further experiments including incubation in different soils for extended periods of times are needed to better assess the effect on polymer surfaces of aging in soil.

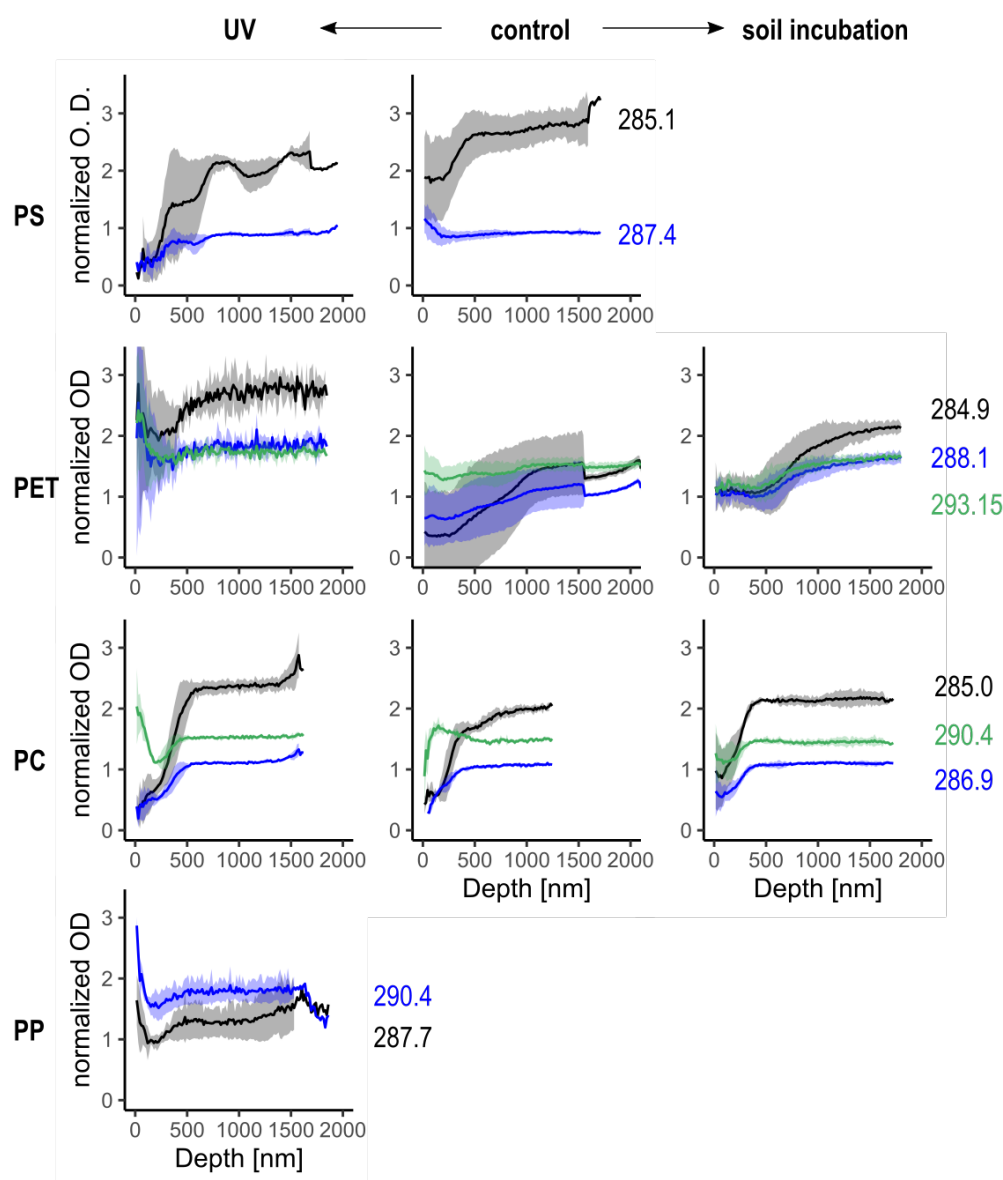


Figure 4-4: NEXAFS spectra of the control, UV and soil weathered fragments of PS, PET, PC and PP. All NEXAFS data were normalized to pre- and post-edge to remove the effect of the sample thickness on the optical density. Average intensity of the polymers typical peaks along the surface – BM for all replicate stack measurements acquired on the same plastic fragment. The energy [eV] of each peak intensity followed by polymer is given on the right side of the graphs. The coloured ribbon indicates the standard deviation around the mean for each peak intensity.

UV weathered polymers

An example of the effect of UV irradiation for each polymer type is given in Figure 4-5. When exposed to UV radiation, PS showed an altered surface up to a depth of approx. 250 nm where the $C1s(C-H) \rightarrow 1 \pi_{C=C}^*$ peak at 285.1 eV decreased to a tenth of its initial value and the $C1s(C-H) \rightarrow \sigma_{C-H}^*$ peak at 287.4 eV was also reduced to a fifth compared to the BM, suggesting that the C=C bonds from the phenyl rings are being broken by the UV at the surface of the polymer, as already observed by (Klein et al., 2008). However, contrary to the fragment

retrieved from a field sample, no new peak appeared at 286.7 eV in the surface layer indicating an absence of oxidation processes taking place under this study experimental conditions for PS. Additionally, a drop in the $C1s(C-H) \rightarrow 1 \pi_{C=C}^*$ peak at 285.1 eV occurred at a depth of approx. 1 μm , similarly to the field fragment presented in Figure 4-3. This suggests that this in-depth alteration could be induced by UV radiation and that the very first reaction towards surface embrittlement consists on the rupture of the C=C bonds from the phenyl rings.

For PET, a general reduction of the peak intensity was observed after UV exposure, but only on a depth of approx. 500 nm and the relative decrease of the $C1s(C-H) \rightarrow \pi_{C=C}^*$ at 284.9 eV at the surface was never as strong as in the control (Figure 4-4). As for PS, no newly formed peak at 286.7 eV and no increase of the intensity of the $C1s(C-R) \rightarrow \pi_{C=C}^* / C=O$ peak at 287.6 eV was observed after UV exposure. This absence of effect caused by UV at the surface of the polymer can be explained by the usual presence of additives used to stabilize the PET to UV radiation and to ensure a longer lifetime of the water bottle (Fechine et al., 2002).

When exposed to UV, the surface of the PC fragment had a higher intensity of the $C1s(C=O) \rightarrow \pi_{C=O}^*$ peak at 290.4 at the surface than in the BM but the $C1s(C-H) \rightarrow \pi_{C=C}^*$ and the $C1s(C-R) \rightarrow \pi_{C=C}^*$ have a similar evolution in the surface- BM gradient compared to the control fragment. Additionally, there is a slight increase of the absorption at 289.2 eV, corresponding to the $C1s(CH_2) \rightarrow \sigma_{C-OH}^*$ in the surface layer. The composition of the surface is similar between the control, UV and soil incubation PC fragments and these results agree well with the occurrence of a photo-fries rearrangement at the surface of the polymer, where the O of the backbone change its position to the aromatic ring to form a stronger bond (Ramani and Ranganathaiah, 2000). As a photo-fries reaction in polycarbonate induces the production of photostabilizers (Clark and Munro, 1983; Torikai et al., 1984), it is likely that the bulk polymer is then protected by the surface layer against UV radiation.

The fragment of PP exposed to UV had a 30 nm layer at the surface in which the $C1s(C-H) \rightarrow \sigma_{C-H}^*$ peak at 287.7 eV has a reduced intensity compared to the BM and the transition layer is very similar to the one of the BM. None of the acquired measurements on these samples showed signs of radiation damage, as discussed in section 4.3.1 A previous study showed that PP irradiated at 280 nm with 500 W/m² led to the formation of carbonyl species in the material only after 45 days of exposure (Ainali et al., 2021). It is thus likely that the UV treatment applied to this fragment was not long or intense enough to initiate any photo-oxidation processes.

UV treatment affected the surface of PS, PC and PP but the surface of PET did not seem to be altered. The alteration observed after UV exposure was different from the one of fragments

recovered from agricultural fields for PS, PET and PE, suggesting that the processes and the resulting surface modifications occurring in the two environments are different. Indeed, while naturally soil-weathered and UV exposed fragments of PS and PET had a common decrease in the C 1s(C-H) \rightarrow 1 $\pi_{C=C}^*$ peak, indicating a breakage of the C=C bonds of their aromatic rings, only the naturally soil-weathered fragments of these two polymers showed signs of surface oxidation with the apparition of new peaks indicating the presence of new C-O or C=O bonds. The fact that these two new peaks were not observed on the soil incubated fragments can be explained by the processes taking more than a year to occur and/or that the controlled conditions were not representative enough of the environmental conditions. As previously highlighted by (Büks and Kaupenjohann, 2022), these findings strengthen the importance of better understanding the effect of the different weathering factors occurring in the soil to predict the surface characteristics of the plastic. Indeed, plastic surface characteristics, including chemical composition, charge and morphology, will impact their fate in the environment (Lwanga et al., 2022).

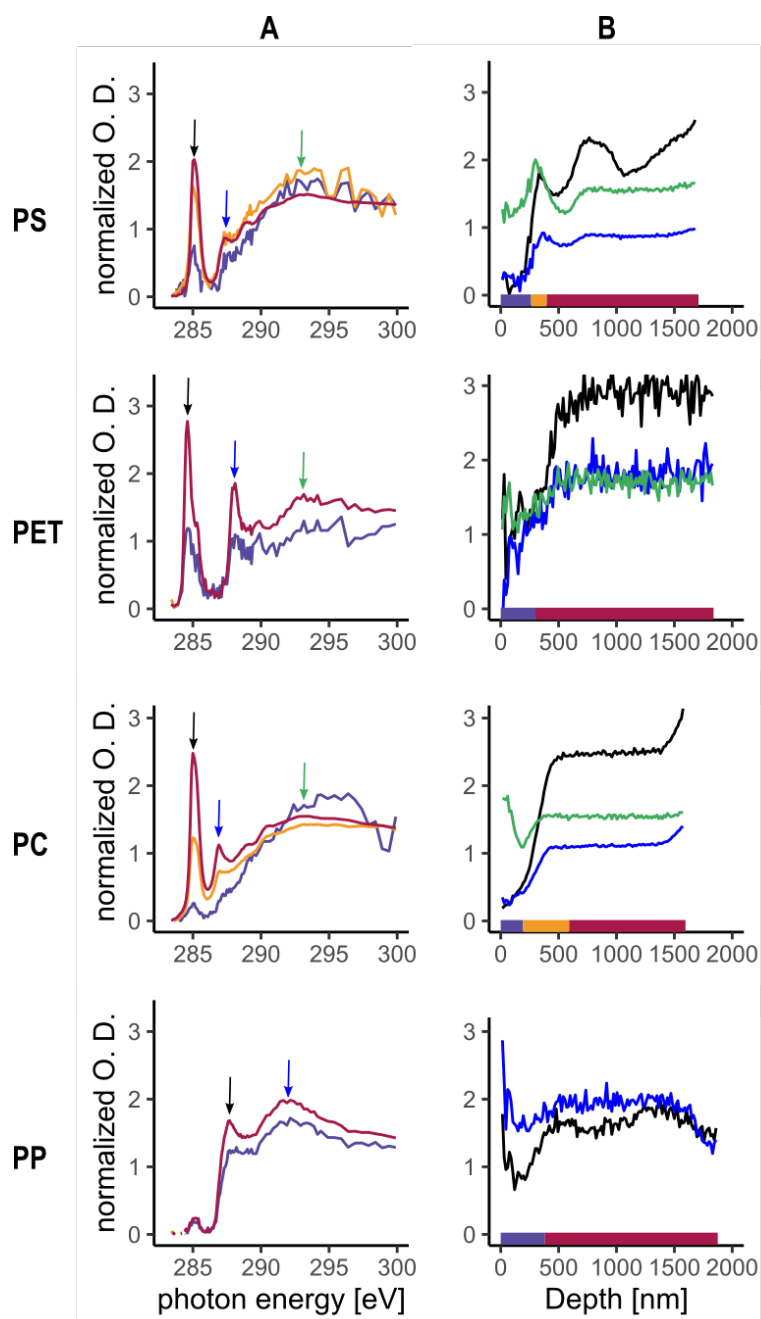


Figure 4-5: Detailed NEXAFS analysis of the UV weathered polymer, all NEXAFS data were normalized to pre- and post-edge to remove the effect of the sample thickness on the optical density. (A) Average spectra of each group determined by hierarchical clustering for a single stack measurement acquired on one fragment. The coloured arrow indicates the position of the peaks presented in B. (B) Intensity of the peaks highlighted by the arrow in A along the surface – BM gradient of the same stack measurement on the fragment shown in A. The coloured bar shows the position of the cluster group in the surface – BM gradient.

4.4 Conclusion

STXM coupled with NEXAFS is a technique allowing to track changes in polymer chemical composition with a spatial resolution of 30 nm. Our method for sample preparation, based on microtomy, and analysis worked well for PS, PET and PC and we were able to reveal surface alteration on a depth varying between 250 and 100 nm in plastic fragments naturally weathered in soil. Interestingly, different replicates acquired on different positions in each

polymer fragment highlighted the heterogeneity of the surface chemical composition and the need to be extremely cautious to avoid overinterpretation of changes observed in a limited number of analysis. Interestingly, the very first step of surface fragmentation was observed on a PS fragment, providing an insight on the factors and processes leading to the release of MP and NP in soils. Comparison of the surface chemical composition of UV weathered and natural soil-weathered samples showed that the two treatments led to different surface alterations. While the natural soil-weathered samples showed evidence of alteration involving oxidation processes, the UV weathered samples did not reveal oxidation signs at the surface but only evidence of C=C bond breakage. No clear effect of aging of PET and PC in soils was found after a one-year soil incubation, indicating slow aging of polymers in this medium. Future work should include in situ weathering for extended periods of time for the aging to occur under more realistic environmental conditions and the use of cryo-microtomy to section more flexible polymers such as PE, PA and PU.

4.5 Authors contribution

Alexandra Foetisch: Conceptualisation, Methodology, Software, Validation, Formal analysis, Investigation, Data Curation, Writing – Original Draft, Visualisation. **Montserrat Filella:** Investigation, Writing – Review and Editing. **Maeva Bragoni:** Investigation, Writing – Review and Editing. **Benjamin Watts:** Software, Investigation, Writing – Review and Editing. **Moritz Bigalke:** Conceptualisation, Investigation, Resources, Writing – Review and Editing, Supervision, Project Administration, Funding acquisition.

4.6 Acknowledgments

This study was funded by the Swiss National Science Foundation (SNSF, 200021_182672/1). We acknowledge the Paul Scherrer Institute, Villigen, Switzerland for provision of synchrotron radiation beamtime at beamline PoLLux of the SLS and would like to thank Hannah Forsyth and Simone Finizio for their help and support during our beamtimes. We are grateful to Ralf Kaegi and Brian Sinnet from Eawag for providing us the SUNTEST chamber and helping us setting the experiment and to Andreas Gubler from Agroscope for providing the soil for the soil incubation experiment. From the Institute of Geography of the University of Bern, we would like to thank Gaby Witschi, Adrian Grunder and Maarika for their help in sample collection and/or lab work, Teresa González de Chávez for her help with Chemdraw. Beatrice Frey from the Department of Chemistry, Biochemistry and Pharmacology of the University of Bern for the SEM images and, finally, Beat Haenni, from the Institute of Anatomy of the University of Bern, for his creativity and reactivity to prepare the polymers microtomy sections.

Appendix A. Microplastics in agricultural drainage water: A link between terrestrial and aquatic microplastic pollution

Moritz Bigalke^{a*}, Milo Fieber^a, Alexandra Foetisch^a, Julien Reynes^b, Peter Tollan^b

^aInstitute of Geography, University of Bern, Hallerstrasse 12, 3012 Bern, Switzerland

^bInstitute of Geology, University of Bern, Baltzerstrasse 3, 3012 Bern, Switzerland

*corresponding author: moritz.bigalke@giub.unibe.ch

This paper was published in the journal Science of the Total Environment (Bigalke et al., 2022) and has undergone minor modifications for consistency with this dissertation

Abstract

Microplastic (MP) contamination has been reported to be higher in terrestrial compared to aquatic environments. This is probably due to the fact that plastic items are mostly produced and used in terrestrial environments and have a longer residence time. However, there are several links between the terrestrial and aquatic environments. We analyzed drainage water samples from agricultural soils in the Seeland, a heavily drained agriculturally intensive area in Switzerland for its MP (>100µm) concentration and composition. We found MP in relevant numbers (mean $10.5 \pm 9.5 \text{ N L}^{-1}$). The polymers were mainly PA and PE, and the size distribution showed an exponential increase with decreasing particle size. The results show considerable MP concentrations in drainage water and imply a transport of MP in soils down to the drainage pipes. Given the large areas drained both in Switzerland and globally, it is proposed that MP leaching from soil can be a significant source of MP to aquatic ecosystems. Such a contribution should be considered when dealing with MP cycling on a local to global scale.

Introduction

Since 1950, about 8300 million metric tons of plastic have been produced worldwide, 79% of which are accumulated either in landfills or in the environment (Geyer et al. 2017). Soils are the main reservoirs of waste plastics, having 4-23x higher plastic concentrations compared to aquatic systems (Horton et al. 2017). However, as the environmental compartments are linked, microplastics (MP) can readily exchange between terrestrial to aquatic systems and vice versa (Horton et al. 2017). On the one hand, plastic particles can be transferred from

aquatic to soil systems e.g. by flooding or irrigation (Scheurer and Bigalke 2018; Blasing und Amelung 2018). On the other hand, terrestrial MP can be transferred to aquatic systems by erosion and runoff (Rezaei et al. 2019; Tagg und Labrenz 2018; Horton et al. 2017) or with drainage water from drained soils. While water erosion might be more significant in areas with elevated topography, drainage water is more important in flat areas and former wetlands (e.g. Germany, USA; Schultz et al. 2005). Initial studies only considered erosion and runoff when modelling soil to water fluxes of MP, neglecting the contributions from drainage water (Tagg und Labrenz 2018; Horton et al. 2017; Nizzetto et al. 2016; Hurley and Nizzetto 2018).

Drained areas are generally under intense human use (otherwise they would not be drained) and host settlements, infrastructure or agriculture. In all these land use systems, plastics are likely to be broadly dispersed, e.g., due to littering and plastic use in agriculture (Blasing und Amelung 2018; Kawecki und Nowack 2019). In settlements, soils are mostly sealed and drainage water is treated in sewage systems before release back into the environment. However, in agriculture, drainage water is mostly released to aquatic systems without any treatment. While subsurface drainage is the most common drainage system in temperate zones, surface drainage is more common in the arid and semi-humid areas of the world. In total, open drains and surface drainage make up about 55% of the drained area, while subsurface drainage and vertical drainage cover 38% and 7% respectively (Schultz et al. 2007). Due to the transport of MP in soils (Maass et al. 2017; Rillig et al. 2017; Zubris and Richards 2005; Wanner 2021) the plastics dispersed at the soil surface can reach deeper soil sections and eventually the shallow groundwater table. These transport pathways enable MP to be transported to the subsurface drainage system and be directly drained to adjacent surface waters (Wanner, 2020).

Currently, however, there is no information about MP leaching to, and MP concentrations in, drainage water, making it impossible to assess its impact on MP concentration in surface waters. To address this significant gap in knowledge, we analysed drainage water samples from 11 different subsurface drainage sites at the Swiss Seeland to answer the following questions:

- 1) Are the MP present in agricultural soils transported sufficiently in order to reach the drainage water system?
- 2) Does drainage water contribute to increased MP concentrations in surface waters?

Material and Methods

Eleven study sites were selected in the Swiss Seeland (Figure A A.1). The Seeland is an intense agricultural area with a high proportion of intense vegetable production and a high use of mulch foil, mulch tunnels and other plastic items. From the eleven sites, eight were equipped with a drainage systems where the water is either constantly passively released through an open system or first collected in a collection basin and then passively released (Figure A A.1). The other three sites were equipped with a newer type of drainage system where the water is collected in a collection basin and then automatically pumped to surface waters, when the water level in the basin reach a certain level. In the latter system, surface water which has not been transported through the soils can also contribute to the water in the basin. Five of the sites were sampled at two different times (31.01.2020 and 03.05.2020) to test the temporal variability. Both sampling dates were set at times with considerable precipitation. The sum of precipitation of the 7 and 3 days before sampling were 31.6 mm and 16 mm at January 31, and 43.1 mm and 12.7 mm at May 03, respectively. In total we analyzed 19 samples from 11 sites.

At the study sites with flowing water (F1-F8), the water was sampled directly into a 3L glass container. When the samples were taken from a collection basin (S1-S3), they were sampled with a pre-cleaned metal bucket and then transferred to a 3L glass container (Figure A A.1). When taking a sample with a bucket, the light MP (e.g. PE, PA) floating on the surface of the collection basin might be favored compared to heavy MP (e.g. PET, SBR) which will sink to the bottom of the basin.

The glass container was pre-cleaned three times with Milli-Q® water and three times with the drainage water directly at the site. The samples were further processed following the protocol of Cabernard et al. (2016). The samples were filtered through a membrane filter with a pore diameter of 8 µm (Whatman®, Cellulose Nitrate). The filtered material was recovered by placing the filter upside down, backwashing with 15 ml of 60% H₂SO₄ (density 1.5 g cm⁻³) and collecting the rinsing solution. After exposure to the acid (30 min) to oxidize organic material, the samples were centrifuged (3000 RPM, 30 min, 20 °C) to separate the MP from the inorganic material by density separation. The supernatant containing the MP was filtered through an Anodisc filter (Whatman®, 0.2 µm), which was subsequently washed with MilliQ water and dried before Fourier transform infrared spectroscopy (FTIR) analysis for chemical characterization and identification. The Anodisc filter is suitable for FTIR analysis in the mid-IR for wavenumbers > 1200 cm⁻¹ (Loder et al 2015).

Each filter was measured with a Bruker Tensor II FTIR coupled to a Hyperion 3000 microscope (Bruker Cooperation, Billerica, MA). Single measurements were acquired with a square

aperture ($\sim 100 \times 100 \mu\text{m}$) using a 15x cassegrain objective and a liquid nitrogen-cooled mercury cadmium telluride (MCT) detector in transmission mode over the wavenumber range $600\text{--}4000 \text{ cm}^{-1}$. Background measurements were done on clean Anodisc filter with 32 scans and sample measurements with 32 scans and using a resolution of 4 cm^{-1} . The spectra were cut in the range $1300\text{--}3300 \text{ cm}^{-1}$ and baseline corrected (10 iterations, concave rubberband algorithm from OPUS® software).

Chemical identification was achieved by comparing four distinct wavenumber regions ($2980\text{--}2780$, $1800\text{--}1740$, $1760\text{--}1670$, $1480\text{--}1400 \text{ cm}^{-1}$) with the database and protocol from Löder et al. (2015), using the spectrum search tool from OPUS®. Particles were classified as MP if hit qualities were >700 . Only particles $>100 \mu\text{m}$ in diameter were analyzed. We tested the effect of the method on polyethylene (PE), polypropylene (PP) and polyvinylchloride (PVC) MP (about 1 mm in diameter) and found no visual change (under the microscope) of the particles following the acid treatment, consistent with the results of Cabernard et al. (2016). To prevent contamination of the samples, most preparation steps were done under a laminar flow clean hood with HEPA (H14) filtered air and all lab equipment was rinsed with Milli-Q® water and ethanol before use. To test for possible contamination, blanks (2.5 L Milli-Q® water) were processed together with the samples and gave a mean count of 0.8 particles L^{-1} . The detection limit of our method ($\text{mean}_{\text{blank}} \pm 3\text{SD}$) was calculated to be 2.2 particles L^{-1} . To determine the particle recovery rate of the method, 10 MP particles (diameter $1\text{--}2 \text{ mm}$) each of PE, PP and PVC were dispersed in water and prepared like the normal samples. Following this, all of the particles were successfully recovered. One sample was sampled and analyzed in triplicate and one in duplicate. The mean RSD was 54%, probably due to the high heterogeneity of the water samples.

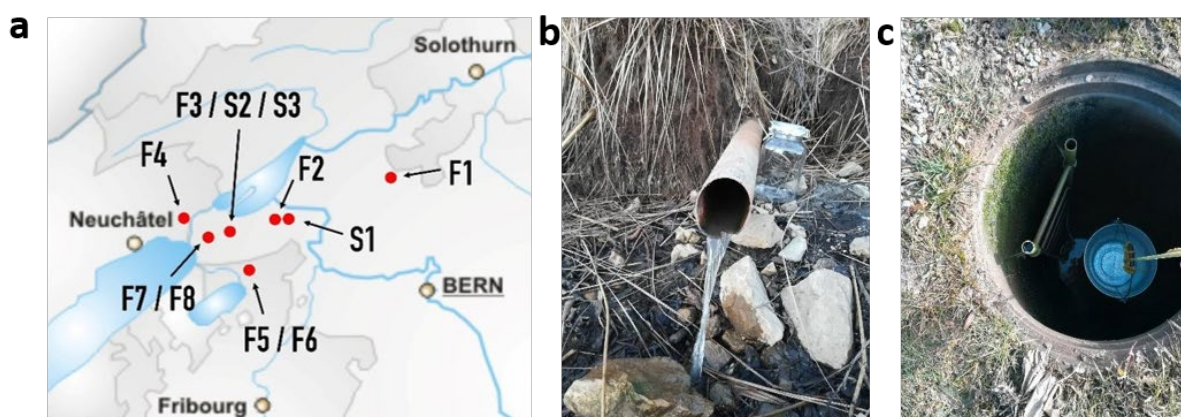


Figure A A.1: Sampling sites, a) Location of the sampling sites in Switzerland. F_x corresponds to sampling site where the water flow is passive and constant. S_x corresponds to sampling sites where the drainage water is collected into a basin before being released into surface waters. b) Example for constant drainage at F7 and c) drainage water collection at S3 (while sampling with the metal bucket).

Results

The number (N) of MP L⁻¹ in the drainage water shows considerable variation, with MP numbers being below detection limit in some samples while in other samples reaching up to 34.6 N L⁻¹ (Figure A A.2). The mean of the MP number is 10.5 N L⁻¹. The mean relative standard deviation (RSD) of samples sampled two times at the same sampling site but at different times was 72% (range 38-106%), indicating high variability. Polyamide (PA) and PE are the most common polymers in the drainage water (Figure A A.2, b). The size distribution of the MP showed a strong increase with increasing particle size, with PA being the most abundant polymer in the smallest size range (100-150 μm) and PE being the most abundant in the size range 150-300 μm (Figure A A.2, c)

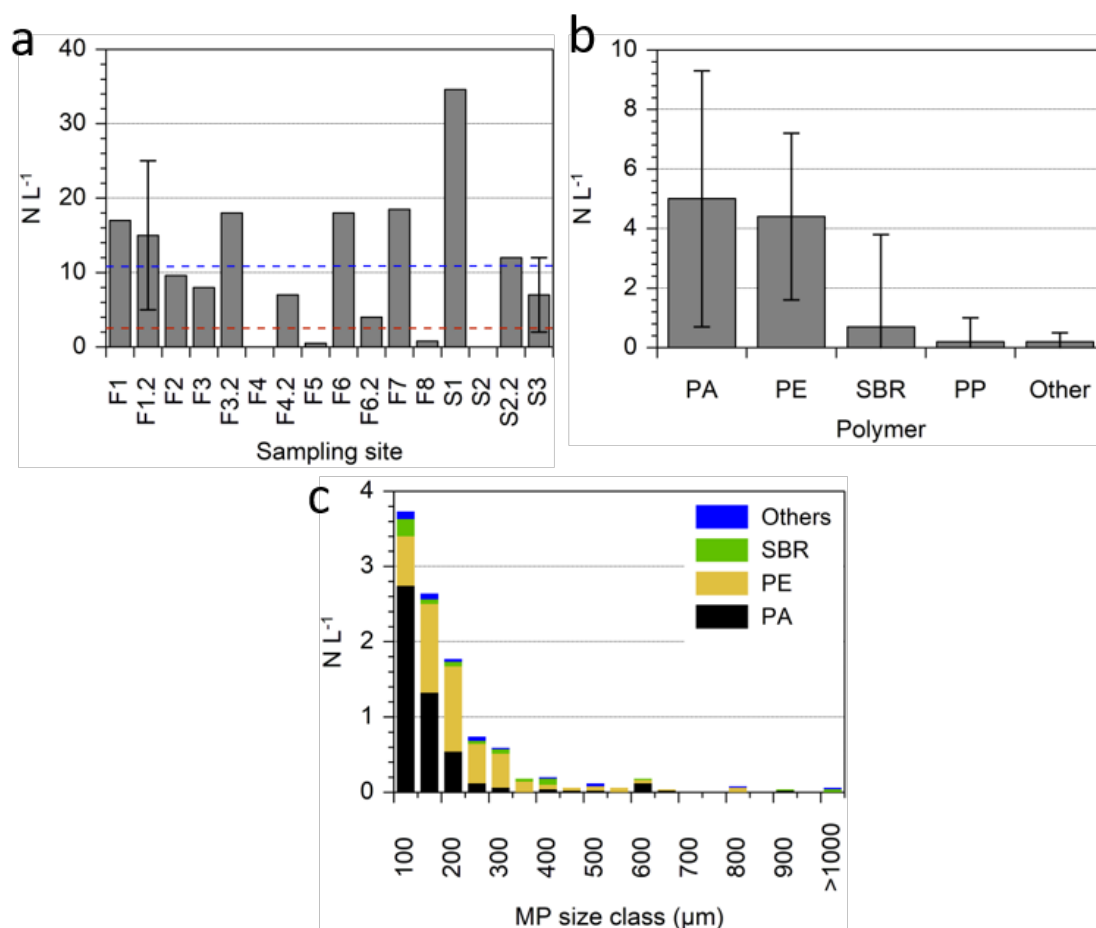


Figure A A.2: a) MP numbers in the individual samples. Samples labeled with .2 in the name were taken at the second sampling date. Error bars show the standard deviation of replicate samples taken at the same time. The red line shows the method limit of detection, the blue line shows the mean value b) Mean particle numbers of the individual polymers in the drainage water samples. Error bars refer to standard deviation between all sites. c) The size dependent MP numbers and polymer composition.

Discussion

The leaching of MP in soils

The occurrence of MP in the drainage water sheds light on the transport of MP in soils. Depth transport has been reported along preferential flow path (Zubris und Richards 2005) but was also reported in unsaturated column experiments, without preferential flow (Mitropoulou et al. 2013; Hoggan et al. 2016). Column experiments with spherical shaped microplastic particles illustrated that the transport is size dependent, that aggregation and deposition of the particles is the major removal mechanism from soil, that these processes depend on the ionic strength of the solution and that a lower pore water saturation resulted in increased retention (Hoggan et al. 2016; Mitropoulou et al. 2013; Wanner 2021). More advanced studies with differently shaped particles and columns with natural soils or complex fillings illustrated the co-transport of MP with mobile organic particles and the effect of particle shapes (spheres being more mobile than fibers). Furthermore, they demonstrated that biotic factors like earthworm activity can also have a considerable effect on the transport of MP (Lwanga et al. 2017; Maass et al. 2017; Rillig et al. 2017).

Based on those findings plastic transport to groundwater has been assumed (Wanner 2021). Our data show that this transport occurs under normal environmental conditions under a central European climate and moderate precipitation and that MP can reach drainage pipes and therefore also the shallow groundwater. Furthermore, the size distribution of the MP in the water samples shows that smaller particles (<350 µm) are much more mobile and reach drainage water while bigger particles are rarely present. From the literature about plastic leaching (Wanner 2021) it can be assumed that particles <100 µm, which were not analyzed in this study, will be even more mobile in the soils and will occur in much higher concentrations. Our samples show a considerable variability at sampling at the same time point, which we assume to be due to the small water volume analyzed and the high heterogeneity of MP leaching. The variability between the different sampling dates is even more pronounced and probably due to the difference in precipitation events and water flow in the soils at the different times.

The PE found in the drainage water is consistent with the heavy use of PE for mulch-, greenhouse- and tunnel foils on soils but also the fact that modern drainage pipes are often made of PE (Scarascia-Mugnozza et al. 2011). The PA has no common use in agriculture but is mostly used for textile and packaging production. The most probable sources for this polymer are past sewage sludge applications (Mahon et al. 2017) and littering. Styrene butadiyl rubber (SBR) is a common polymer in tires and probably indicates the presence of tire wear in the water samples, while PP is used for similar applications as PE, just in a lower quantity.

As plastic use in agriculture still persists and plastic has a very long residence time in soils, we assume that plastic leaching to drainage waters will continue. Furthermore, the plastic disintegration to MP as well as its transport in soils takes time (Zubris and Richards 2005; Krueger et al. 2015) so that the MP we find in the drainage water today were probably released to the soil years ago. This means that even if plastic emission to soils is strongly reduced and agriculture change to biodegradable mulch films, a decrease of plastic leaching from soil will only occur after a prolonged transition period.

Implications of MP leaching from soils to surface waters

The MP concentrations reported in the literature are strongly dependent on the MP sizes analyzed. In some studies Manta nets with a mesh size of 300 μm are used to sample the MP. This kind of sampling normally generates low MP counts, because only bigger MP are sampled. The number of MP reported increase strongly when other methods are used that consider smaller MP. The different sampling and analytical techniques used make the data of different studies hardly comparable (Triebkorn et al. 2019). The MP concentrations we find in the drainage water samples ($10.5 \pm 9.5 \text{ N L}^{-1}$) are considerable, and tend to be higher than the concentrations in Swiss surface waters ($7 \pm 5 \text{ N L}^{-1}$, Cabernard et al. 2016; 0.007 N L^{-1} , Faure und Alencastro 2014) and comparable or higher than most surface water systems (Triebkorn et al. 2019). With these numbers, our data indicate that MP in drainage water might have a considerable influence on surface water concentrations. However, more studies with a wider geographical spread about the MP concentrations in surface and drainage water are needed to get a better and more general idea on the impact of MP release through drainage water channels.

Depending on the MP concentrations drainage water might contribute considerable to MP release. Taking Switzerland as an example, about 18% ($1,9 \cdot 10^5 \text{ ha}$) of the agricultural area are drained, mainly with subsurface drainage. At these sites, 58-86% of the precipitation goes into the drainage systems, which contributes about $8,9 \cdot 10^8 \text{ m}^3$ or 2% to the total runoff in Switzerland (Gramlich et al. 2018; Kobierska et al. 2020; Hürdler et al. 2015). With a rough estimation based on our MP concentrations, this would mean about $9,3 \cdot 10^{12}$ MP particles released from agricultural drainage in Switzerland each year. Worldwide about $1,9 \cdot 10^8 \text{ ha}$ of agricultural land are drained, which represents about 13% of the total arable land (Schultz et al. 2005). If we roughly assess the water from drainage systems with a mean global precipitation of about 1000 mm m^{-2} (Adler et al. 2017) and assume a drainage of only about 50% we can assess that about $9,5 \cdot 10^{11} \text{ m}^3$ water are going through drainage systems every year. This is of course only a very rough estimate but illustrates that MP in this water constitutes a considerable flux.

Most of the drainage systems are surface drainage (Schultz et al. 2007) and cannot be directly compared to our data. However, we assume that surface drainage might also have an effect on plastic transport as plastic is not filtered in the soils, but rather directly washed away to surface waters. Most of the drained area is in developed countries with intensive agriculture involving plastic use (Schultz et al. 2007; Schultz et al. 2005). Thus, the MP load might be significant not only for the directly affected rivers and lakes, but also for the global aquatic plastic budget.

Conclusions

Our results show a considerable presence of MP in drainage water and imply that MP are leached through the soils to drainage water systems. Given the drained area worldwide, MP from drainage water might contribute to increased MP concentrations in surface waters. Thus, drainage water should be considered when assessing MP fluxes to surface waters. Future research is needed to confirm our findings with a higher number of samples from different locations worldwide.

Acknowledgements

This study was funded by the Swiss National Science Foundation (SNSF, 200021_182672/1). We acknowledge Prof. Jörg Herrmann from the Institute of Geoscience of the University of Bern for access to the FTIR, Ramona Sieber and Edith Durisch-Kaiser from the Office for Waste, Water, Energy and Air of the canton of Zürich for the introduction in the extraction method, Daniela Fischer, Patrick Neuhaus, Adrien Mestrot from the Institute of Geography of the University of Bern for their general help and support.

References

- Adler, Robert F.; Gu, Guojun; Sapiano, Matthew; Wang, Jian-Jian; Huffman, George J. (2017): Global Precipitation: Means, Variations and Trends During the Satellite Era (1979–2014). In: *Surv Geophys* 38 (4), S. 679–699. DOI: 10.1007/s10712-017-9416-4.
- Blasing, M.; Amelung, W. (2018): Plastics in soil. Analytical methods and possible sources. In: *Sci Total Environ* 612, S. 422–435. DOI: 10.1016/j.scitotenv.2017.08.086.
- Cabernard, L.; Durisch-Kaiser, E.; Vogel, JC.; Rensch, D.; Niederhauser, P. (2016): Mikroplastik in Abwasser und Gewässern. In: *Aqua und Gas* 2016 (7/8), S. 78–85.
- Faure, F.; Alencastro, F. (2014): Evaluation de la pollution par les plastiques dans les eaux de surface en Suisse. École Polytechnique Fédérale de Lausanne. Lausanne.

- Geyer, Roland; Jambeck, Jenna R.; Law, Kara Lavender (2017): Production, use, and fate of all plastics ever made. In: *SCIENCE ADVANCES* 3 (7), e1700782. DOI: 10.1126/sciadv.1700782.
- Gramlich, Anja; Stoll, Sebastian; Aldrich, Annete; Stamm, Christian; Walter, Thomas; Prasuhn, Volker (2018): Einflüsse landwirtschaftlicher Drainage auf den Wasserhaushalt, auf Nährstoffflüsse und Schadstoffaustrag. Eine Literaturstudie. Zürich: Agroscope (Agroscope science Umwelt, Nr. 73 (November 2018)). Online verfügbar unter <https://www.agroscope.admin.ch/agroscope/de/home/publikationen/suchen/agroscope-science.html>.
- Hoggan, James L.; Sabatini, David A.; Kibbey, Tohren C. G. (2016): Transport and retention of TiO₂ and polystyrene nanoparticles during drainage from tall heterogeneous layered columns. In: *J Contam Hydrol* 194, S. 30–35. DOI: 10.1016/j.jconhyd.2016.10.003.
- Horton, Alice A.; Walton, Alexander; Spurgeon, David J.; Lahive, Elma; Svendsen, Claus (2017): Microplastics in freshwater and terrestrial environments: Evaluating the current understanding to identify the knowledge gaps and future research priorities. In: *Sci Total Environ* 586, S. 127–141. DOI: 10.1016/j.scitotenv.2017.01.190.
- Hürdler, J.; Prasuhn, V.; Spiess, E. (2015): Abschätzung diffuser Stickstoff- und Phosphoreinträge in die Gewässer der Schweiz. MODIFFUS 3.0. In: Agroscope.
- Hurley, R., R.; Nizzetto, L. (2018): Fate and occurrence of micro(nano)plastics in soils. Knowledge gaps and possible risks. In: *Current Opinion in Environmental Science & Health* 1 (6-11).
- Kawecki, Delphine; Nowack, Bernd (2019): Polymer-Specific Modeling of the Environmental Emissions of Seven Commodity Plastics As Macro- and Microplastics. In: *Environ Sci Technol* 53 (16), S. 9664–9676. DOI: 10.1021/acs.est.9b02900.
- Kobierska, Florian; Koch, Ulrike; Kasteel, Roy; Stamm, Christian; Prasuhn, Volker (2020): Plant protection product losses via tile drainage: A conceptual model and mitigation measures.
- Krueger, M. C.; Harms, H.; Schlosser, D. (2015): Prospects for microbiological solutions to environmental pollution with plastics. In: *Appl Microbiol Biot* 99 (21), S. 8857–8874. DOI: 10.1007/s00253-015-6879-4.
- Löder, Martin Günter Joachim; Kuczera, Mirco; Mintenig, Svenja; Lorenz, Claudia; Gerdts, Gunnar (2015): Focal plane array detector-based micro-Fourier-transform infrared

- imaging for the analysis of microplastics in environmental samples. In: *Environ Chem* 12 (5), S. 563. DOI: 10.1071/EN14205.
- Lwanga, E. H.; Gertsen, H.; Gooren, H.; Peters, P.; Salanki, T.; van der Ploeg, M. et al. (2017): Incorporation of microplastics from litter into burrows of *Lumbricus terrestris*. In: *Environ Pollut* 220, S. 523–531. DOI: 10.1016/j.envpol.2016.09.096
- Maass, S.; Daphi, D.; Lehmann, A.; Rillig, M. C. (2017): Transport of microplastics by two collembolan species. In: *Environ Pollut* 225, S. 456–459. DOI: 10.1016/j.envpol.2017.03.009.
- Mahon, A. M.; O'Connell, B.; Healy, M. G.; O'Connor, I.; Officer, R.; Nash, R.; Morrison, L. (2017): Microplastics in Sewage Sludge: Effects of Treatment. In: *Environ Sci Technol* 51 (2), S. 810–818. DOI: 10.1021/acs.est.6b04048.
- Mitropoulou, Polyxeni N.; Syngouna, Vasiliki I.; Chrysikopoulos, Constantinos V. (2013): Transport of colloids in unsaturated packed columns: Role of ionic strength and sand grain size. In: *Chemical Engineering Journal* 232, S. 237–248. DOI: 10.1016/j.cej.2013.07.093.
- Nizzetto, L.; Bussi, G.; Futter, M. N.; Butterfield, D.; Whitehead, P. G. (2016): A theoretical assessment of microplastic transport in river catchments and their retention by soils and river sediments. In: *Environ Sci-Proc Imp* 18 (8), S. 1050–1059. DOI: 10.1039/c6em00206d.
- Rezaei, Mahrooz; Riksen, Michel J. P. M.; Sirjani, Elham; Sameni, Abdolmajid; Geissen, Violette (2019): Wind erosion as a driver for transport of light density microplastics. In: *Sci Total Environ* 669, S. 273–281. DOI: 10.1016/j.scitotenv.2019.02.382.
- Rillig, M. C.; Ziersch, L.; Hempel, S. (2017): Microplastic transport in soils by earthworms. In: *Sci Rep-Uk* 7:1362, S. 1–6.
- Scarascia-Mugnozza, Giacomo; Sica, Carmela; Russo, Giovanni (2011): PLASTIC MATERIALS IN EUROPEAN AGRICULTURE: ACTUAL USE AND PERSPECTIVES. In: *J Agricult Engineer* 42 (3), S. 15. DOI: 10.4081/jae.2011.3.15.
- Scheurer, M.; Bigalke, M. (2018): Microplastics in Swiss Floodplain Soils. In: *Environmental Science and Technology* 52, S. 3591–3598. DOI: 10.1021/acs.est.7b06003.
- Schultz, Bart; Thatte, C. D.; Labhsetwar, V. K. (2005): Irrigation and drainage. Main contributors to global food production. In: *Irrig. and Drain.* 54 (3), S. 263–278. DOI: 10.1002/ird.170.

- Schultz, Bart; Zimmer, Daniel; Vlotman, Willem F. (2007): Drainage under increasing and changing requirements. In: *Irrig. and Drain.* 56 (S1), S3-S22. DOI: 10.1002/ird.372.
- Tagg, Alexander S.; Labrenz, Matthias (2018): Closing Microplastic Pathways Before They Open: A Model Approach. In: *Environ Sci Technol* 52 (6), S. 3340–3341. DOI: 10.1021/acs.est.8b00961.
- Triebkorn, Rita; Braunbeck, Thomas; Grummt, Tamara; Hanslik, Lisa; Huppertsberg, Sven; Jekel, Martin et al. (2019): Relevance of nano- and microplastics for freshwater ecosystems: A critical review. In: *Trac-Trend Anal Chem* 110, S. 375–392. DOI: 10.1016/j.trac.2018.11.023.
- Wanner, Philipp (2021): Plastic in agricultural soils - A global risk for groundwater systems and drinking water supplies? - A review. In: *Chemosphere* 264 (Pt 1), S. 128453. DOI: 10.1016/j.chemosphere.2020.128453.
- Zubris, K. A. V.; Richards, B. K. (2005): Synthetic fibers as an indicator of land application of sludge. In: *Environ Pollut* 138 (2), S. 201–211.

Appendix B. Chapter 1

B.1. Magnetic extraction of PS nanobeads

EDX spectrum of a PS nanobeads acquired on a Jeol2300 in backscattering mode at 15 kV.

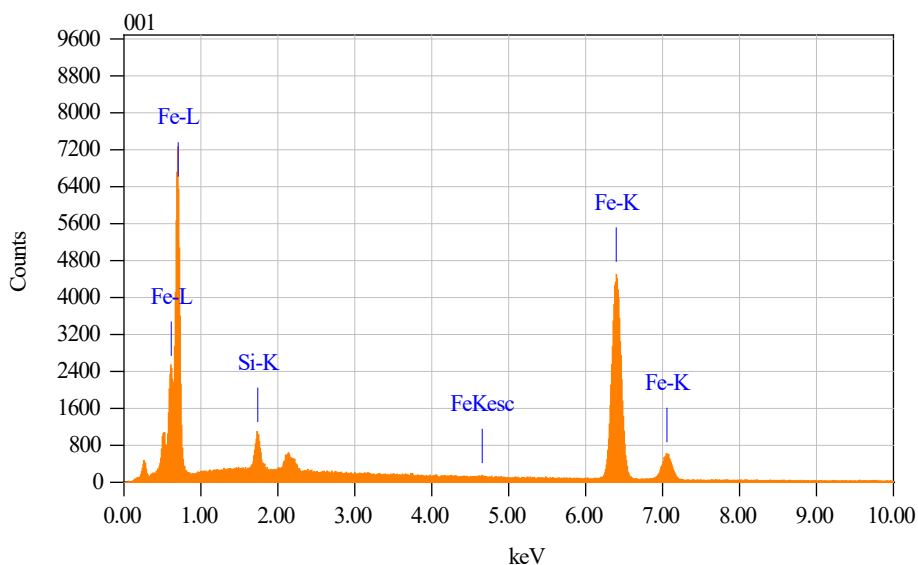


Figure A B.1: EDX spectrum acquired on the PS nanobeads extracted using modified Fe nanoparticles.

B.2. NP deposition by centrifugation

Five random areas of the SiN and MgO wafers carrying PC and PS NP were imaged by SEM at a 2000 X magnification. The particles count was automatically obtained using the Fiji open source software.

Table A B-1: Mean particle obtained from Fiji Analyze particles tool for PS and PC deposited on MgO and SiN wafers.

Polymer	Substrate	Mean p. number	Standard deviation
PS	MgO	4199	98
PS	SiN	266	56.8
PC	MgO	537	47.5
PC	SiN	1582	125

B.3. AFM instability effect on nanoFTIR spectrum

The Figure A B.2 illustrates the sinusoidal effect appearing in the nanoFTIR spectrum caused by AFM instability.

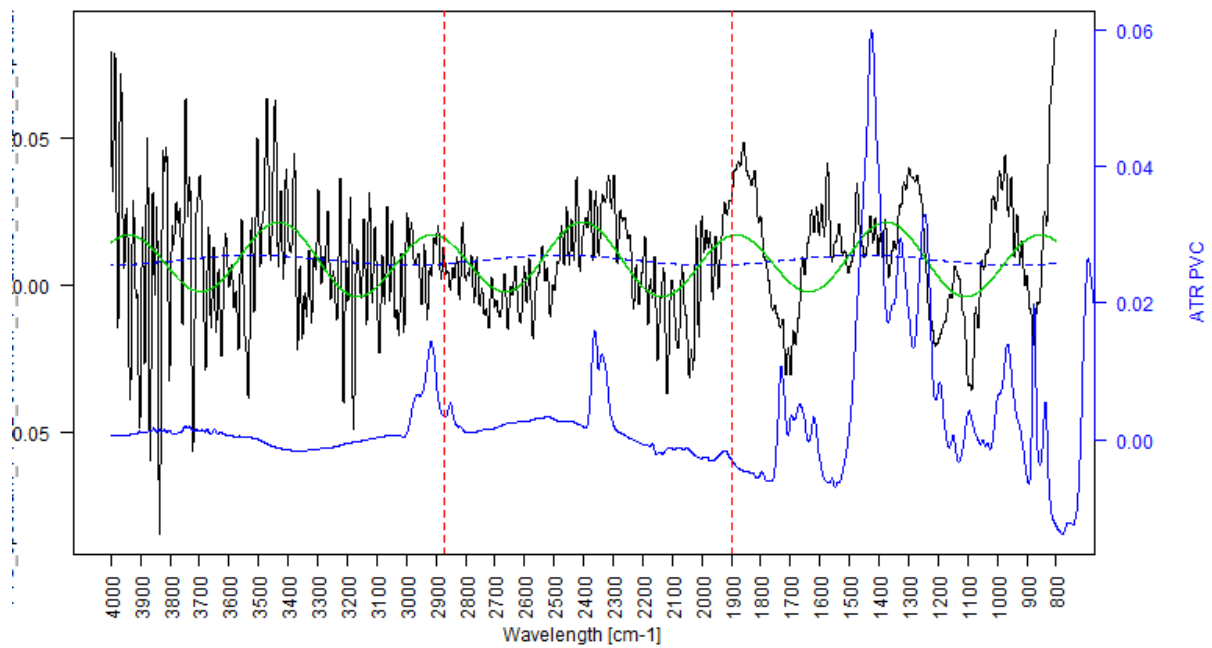


Figure A B.2: NanotFTIR spectrum of a PVC nanoparticle. The black line corresponds to our measurement and the blue line correspond to an ATR PVC reference spectrum. The green line highlights the sinusoidal nature of the detected signal.

B.4. PA and PMMA PEEM-NEXAFS spectra

NEXAFS were acquired from a mixed NP sample containing PA, PMMA, PET, PC and PP NP. Spectral features corresponding to PA and PMMA could be detected on particles $> 2\mu\text{m}$ (Figure A B.3).

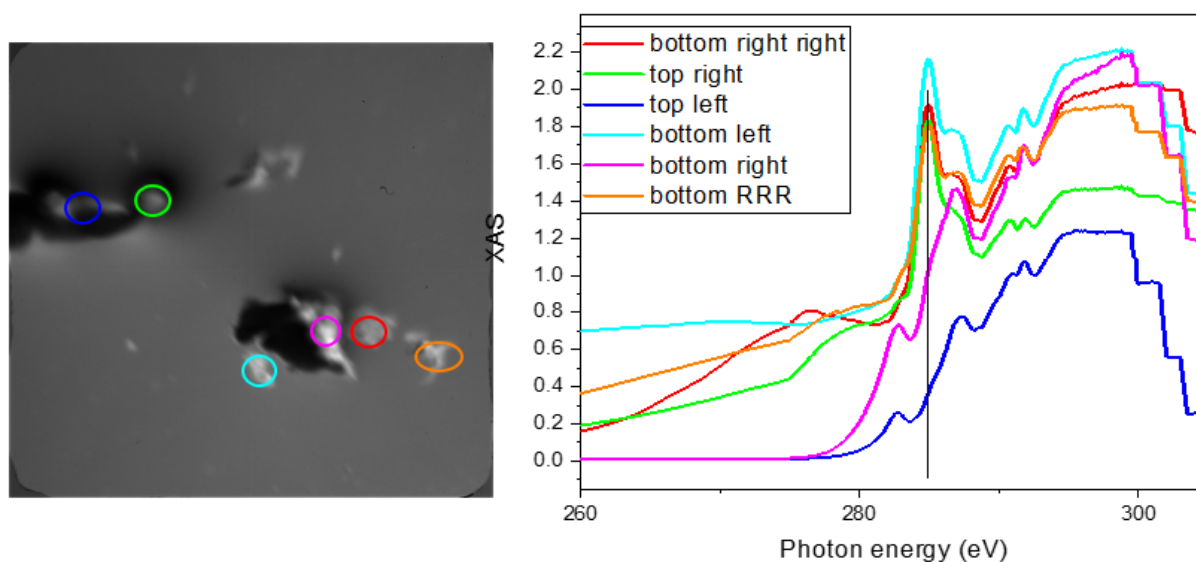


Figure A B.3: Left: PEEM image of particles observed in the mix NP sample. The field of view is $15 \times 15 \mu\text{m}$. Right: NEXAFS spectra acquired on PA (light blue, orange, red and green) and PMMA (pink, dark blue) particles. The area integrated for to obtain each spectrum is highlighted by a circle of the corresponding colour on the left side image.

B.5. Effect of soil incubation of polymer surface morphology

Possible polymer surface modifications induced by soil incubation were investigated by comparing SEM images of polymers surface before and after one-year soil incubation (Figure A B.4). Pictures were acquired with a secondary electron detector at 100 and 5000 X, 10 kV and a working distance between 7.5 and 8.9 mm. The picture comparison did not allow to observe any clear effect of the soil incubation and the slight increase of particles at the surface of polymers was most probably soil remaining event after the washing procedure. The effect could not be determined on PA, as no PA fragments could be found in the soil after one-year incubation.

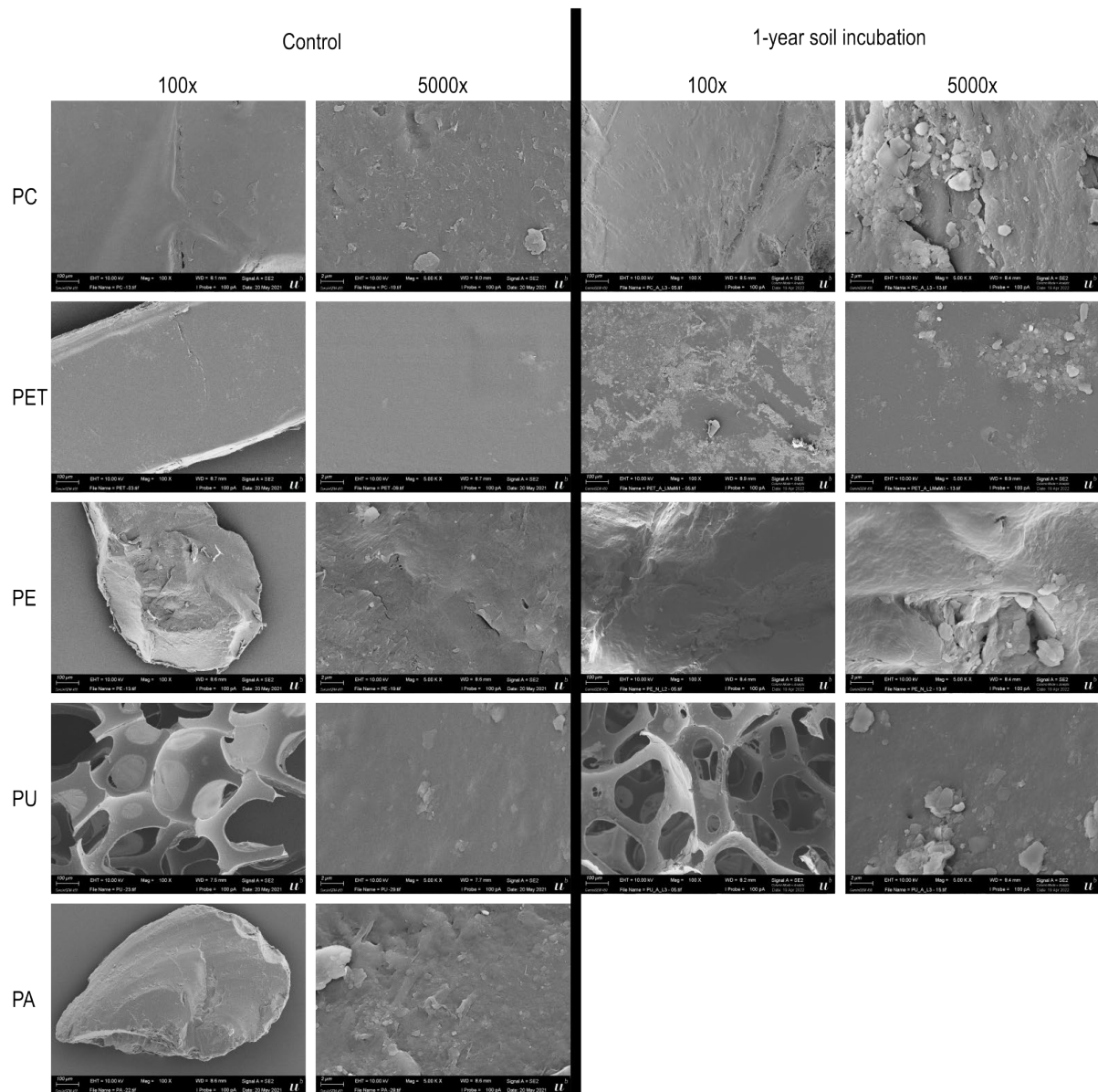


Figure A B.4: SEM images of the

Appendix C. Chapter 2

C.1. MAT sampling plan and soil characteristics

The Figure A C.1 illustrate the sampling strategy for the environmental samples located close to a highway in Mattstetten. The 5 g extracted in the study were taken from the pooled samples.

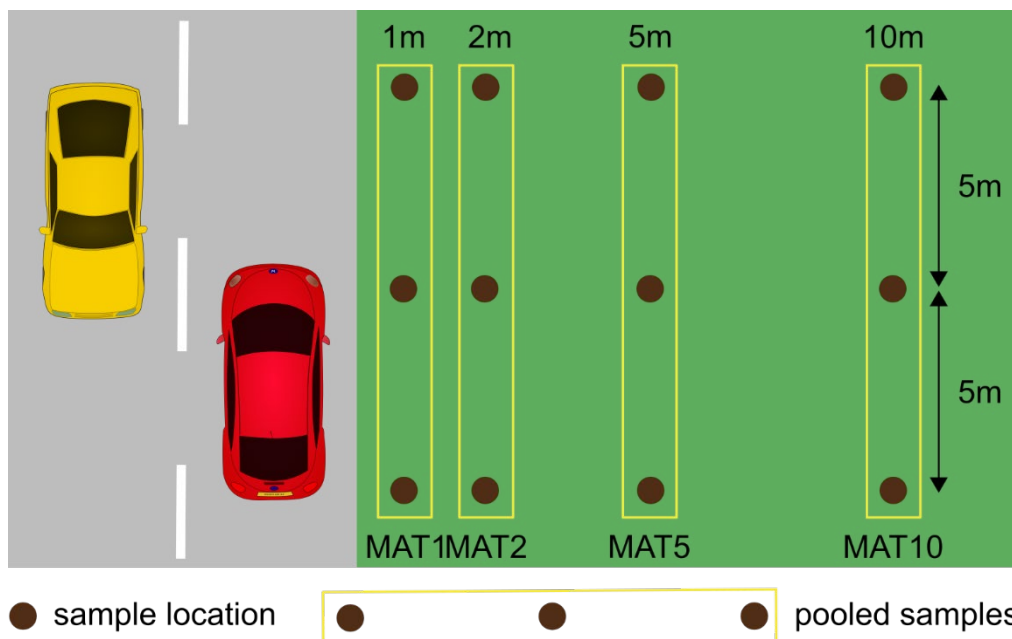


Figure A C.1: Sampling plan for soil expected to be contaminated with tire wear particles. The image is not to scale.

In, the proportion of clay, silt sand and C_{org} are given for the plastic free (PFS) soil and highway soil used in this study.

Table A C-1: Sampling plan for soil expected to be contaminated with tire wear particles. The image is not to scale.

	Clay [%]	Silt [%]	Sand [%]	C_{org} [%]	Soil type	localisation	GPS coordinates
PFS	7.53	49.62	42.84	UP	alluvial	Scuol	46°47'23.6"N 10°16'22.9" E
MAT	UP	UP	UP	UP	grassland	Mattstetten	47°01'31.4"N 7°31'07.4"E

C.2. Charcoal sampling positions

To test the interference of charcoal in the TRWP identification process, charcoal pieces were collected from a fire place in Bern's surroundings. The Figure A C.2 shows the 3 positions on which charcoal was collected in a fire place.



Figure A C.2: Sampling spots of charcoal material from a fireplace in Bern's surroundings. The charcoal is sampled in 3 areas from the centre (1) of the last fire, to it's very border (3).

C.3. Image processing example

The following steps were applied in order to acquire particles count and measurements for each sample described in the linked publication. An example illustrate each step in Figure A C.3.

1. Four automatically stitched pictures were acquired using the Leica LASX Lime image builder xy. The intensity of the light was intentionally kept low to see filter structure and correctly image empty white areas of the filters.
2. The four images are then manually assembled using GIMP2.0 to form a single picture per sample.
3. The picture is cropped to remove the black and blue background originating from the microscope settings.
4. zoomed in from picture showed in 3 (yellow rectangle) is shown to allow a better visualisation of the processing effects
5. Obvious non-TRWP are manually covered in white
6. The black levels and the exposure are increased in the whole picture (The following macro commands were used to automate the processing of all pictures:

```
run("Window/Level...");
```

```
setMinAndMax(19, 133);
```

7. The segmentation of the model is then applied to the whole picture. As this analysis requires a lot of computation power, a high RAM memory is needed to process a picture

at once. However, this issue could be overcome by a script allowing to split the picture in tiles, which are then classified one after the other, and merging each tile classification to form the entire result. The output of the Weka segmentation plugin is a green/red binary image.

8. The image is converted to 8bit and the threshold automatically adjusted. A watershed function is applied using the Adjustable Watershed plugin in Fiji setting the tolerance to 3.
9. The “analyse particles” Fiji tool is finally applied to quantify and measure all particles identified by the model.

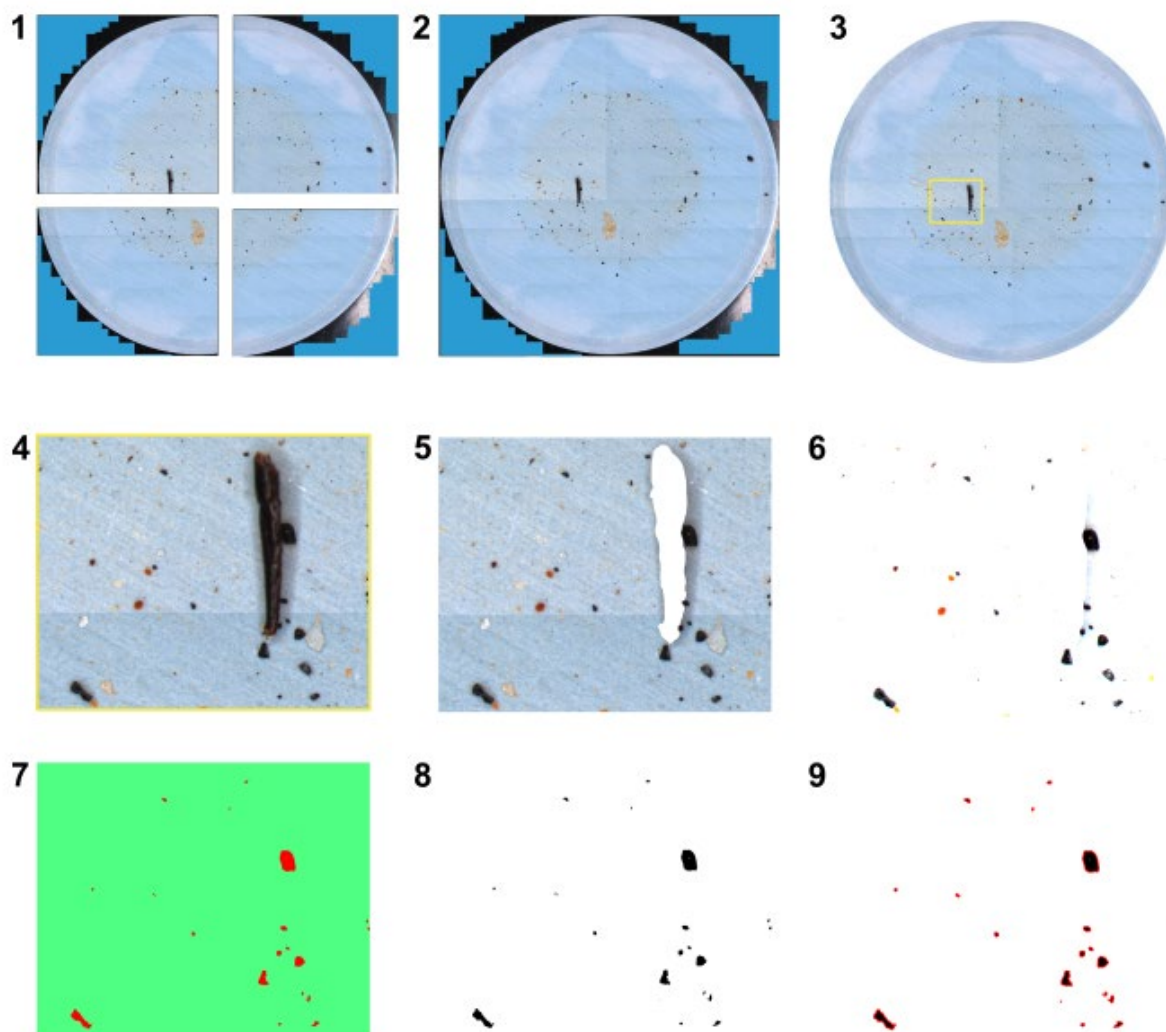


Figure A C.3: Illustration of the picture acquisition and processing steps. The numbers correspond to the numbered items in the text.

C.4. SEM-EDX analysis of highway tunnel dust

Images and EDX spectra acquired on the tunnel dust after density separation with sodium bromide in the supernatant showed the expected presence of TWP, with a typical elemental composition of C, O, Fe, Na, Mg, Al, Si and Ca (Rausch et al., 2022)(Figure A C.4). Even if there were far less numerous (quantification not available), the same particles could also be detected in the pellet material, indicating the combination of ultrasonication and density separation with NaBr do not allow to isolate the whole range of TWP densities.

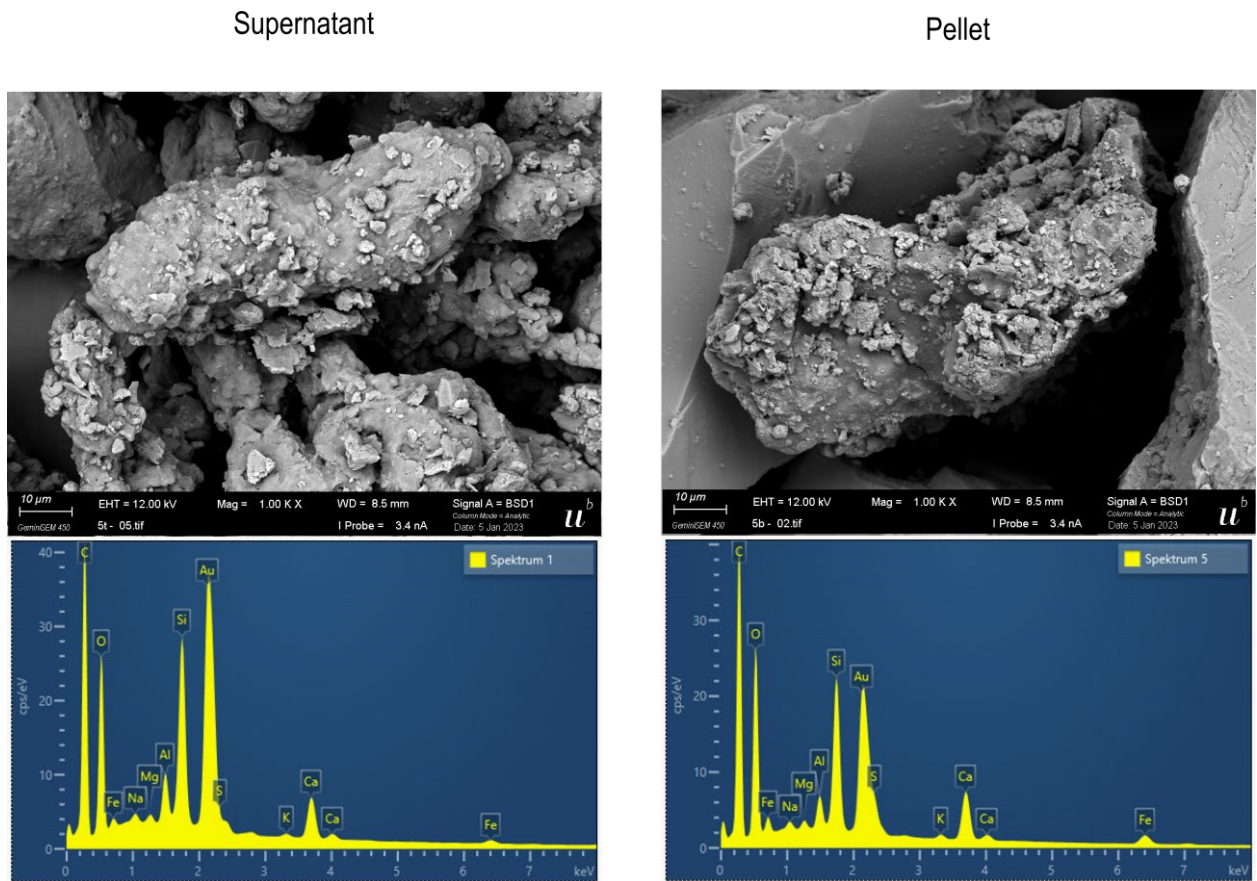


Figure A C.4: Representative example of SEM-EDX analysis of particles found in the supernatant and in the pellet after density separation using sodium bromide (NaBr) salt of a 1.5 g/cm³ density.

C.5. Extrapolation of TRWP concentrations

The concentration of TRWP found in the soil samples were extrapolated to kg^{-1} dry soil to facilitate concentrations comparison. The extrapolated concentrations were calculated as follow:

$$\text{TWP number [kg-1 dry weight]} = \frac{\text{number of TRWP found}}{\text{sample dry weight [g]}} * 1000 \quad (1)$$

The mean and standard deviation of the TRWP number [kg^{-1} dry weight] were then calculated for each distance. Raw data and results are presented in Table A C-2.

Table A C-2: Number of particles found in the environmental samples and their extrapolation to kg^{-1} dry soil.

Distance	Number TRWP found	Sample dry weight [g]	TRWP number [kg^{-1} dry weight]	Mean TRWP number [kg^{-1} dry weight]	Standard deviation TRWP number [kg^{-1} dry weight]
MAT1	48	5.015	9571.286	8080.427	1059.822
	38	5.088	7468.553		
	36	4.999	7201.44		
MAT2	69	5.070	13609.47	9106.606	3234.823
	38	5.030	7554.672		
	31	5.036	6155.679		
MAT5	25	5.035	4965.243	4091.15	623.8617
	19	5.056	3757.911		
	18	5.070	3550.296		
MAT10	19	5.059	3755.683	2562.835	1160.34
	15	5.098	2942.33		
	5	5.048	990.4913		

C.6. Estimation TWP mass content in soil samples

The total TWP mass each highway adjacent soil samples was calculated using the model previously developed by (Tanoiri et al., 2021):

$$\text{Estimated TWP mass} = \frac{4}{3} \left(\frac{\text{Feret}}{2} \right) \left(\frac{\text{MinFeret}}{2} \right) \left(\frac{0.372 * \text{MinFeret}}{2} \right) \pi \rho \quad (2)$$

Where Feret and MinFeret correspond to the longest and shortest dimensions of an ellipse fitted on the particle and $\rho = 1.2 \text{ g/cm}^3$ is the estimated density of tire wear (Degaffe and Turner, 2011). The calculated mass concentration of the highway soil samples had a similar variation pattern as the one observed for particles number, where the concentration was higher closer to the road (Figure A C.5)

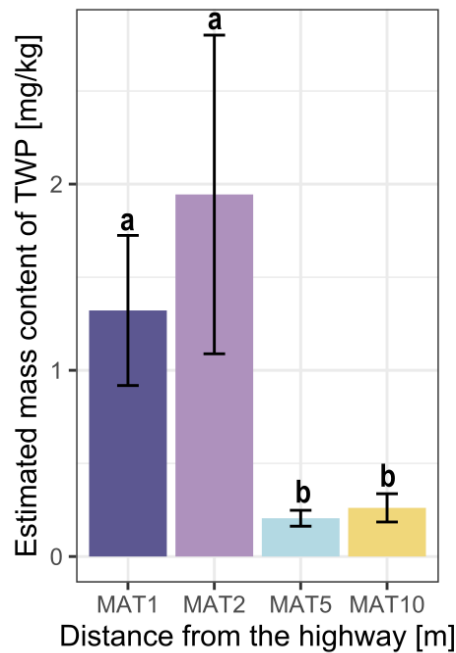


Figure A C.5: Mean TWP mass $\text{mg} \cdot \text{kg}^{-1}$ with standard error. Different letters indicate significant differences between mean mass content for each distance to the road (Dunn test, p -value < 0.05)

C.7. Correlation of particle size and circularity

The Figure A C.6 shows the size of the TRWP identified in the environmental samples in relation with their circularity. A circularity value of 1 indicates a perfect sphere, while a value of 0 indicate an elongated shape, such as a fibre. Here, no correlation could be observed, indicating that TRWP have all kind of shapes and they are not related to their size.

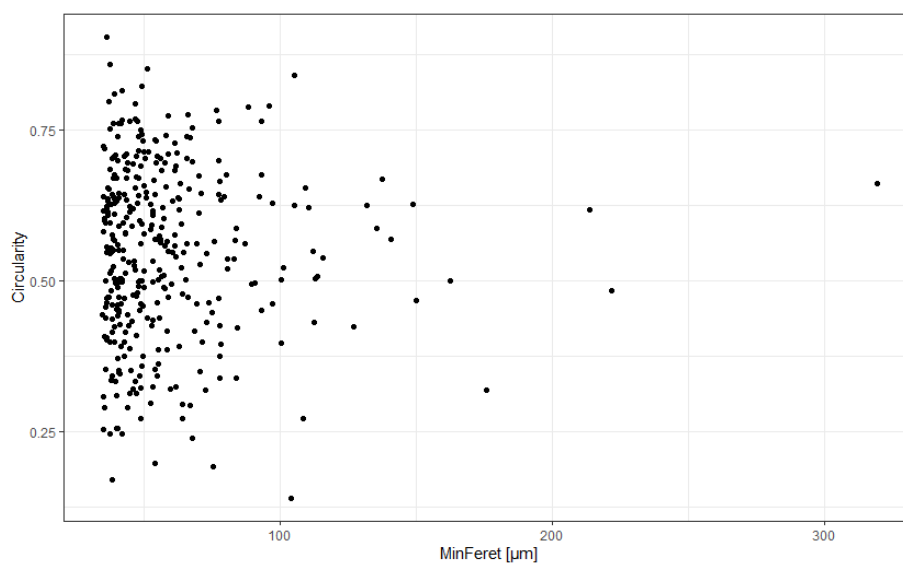


Figure A C.6: TRWP particles size (MinFeret) according to their circularity.

C.8. List of the equipment used for the extraction and identification processes

The following reagents and equipment were used to perform the extraction and identification of TRWP at the University of Bern.

Reagents

- Iron(II) sulfate heptahydrate ($\text{Fe}_2\text{SO}_4 \cdot 7\text{H}_2\text{O}$), $\geq 99\%$ p.a. ACS, Roth P015.2
- Hydrochloric acid 37 % (HCl), NORMAPUR Reag. Ph. Eur., VWR 20.252.420
- Hydrogen peroxide 30% (H_2O_2), Sigma-Aldrich 95321-500 mL
- Sodium bromide (NaBr), 99+% water <1%, Alfa Aesar A10552.01
- Sulfuric acid 95-97% (H_2SO_4), EMSURE Iso for analysis, Merck 1.007.312.511
- MiliQ, Merck ZIQ7000T0
- NaOH >99% (Carl Roth, Art.Nr. 9356.1)
- Urea, Sigma Aldrich, Germany, $\geq 98\%$
- Thiourea, Merck, Germany, $\geq 98\%$

Material and instruments

- Drying oven
- Mortar
- 5 and 2 mm sieves
- Aluminium containers for dried samples
- Vacuum filtration apparatus for 47 mm membranes
- Vacuum filtration apparatus for 13 mm membranes
- Membranes 0.8 μm , polycarbonate Whatman Nuclepore, 47 mm, Track-Etched Membranes, Sigma-Aldrich WHA111109
- 10 μm stainless steel filter (Rolf Körner GmbH, Werkstoff 1.4401, MW 10 μm , K. 71 μm , S. 41 μm , 200x1400 Mesh)
- Anodisc 25, 0.2 μm , 25 mm, 6809–6022, Whatman membranes, Sigma-Aldrich WHA68096022
- 50ml Centrifuge Tubes (medical grade PolyPropylene) 2*number of sample or glass centrifuge tubes (PYREX(R) CLS9950250-72EA)
- Sonication bath
- Orbital shaker
- Centrifuge
- Decanting-aid
- Pasteur pipette
- Metallic spatula
- Heating blocs
- thermometer
- pH meter
- glass bottles to store solutions
- ice bath
- heating bath
- aluminium foil
- Petri dishes
- Beaker
- Magnetic stirrer and stirring/heating plate
- Laboratory forceps
- Clean hood
- Fume hood
- Microscope
- 32RAM computer
- Fiji free software
- Automatic picture stitching software

Appendix D. Chapter 3

D.1. Preparation of nanomaterial

When possible, polymer pellets were pre-grounded with a Pulverisette 11 (Fritsch, Germany). The resulting powders were successively sieved to obtain size fractions <500, <250, <100 and <63 μm . The smaller size fractions of each polymer were used to fill up a third of the MM400 grinding jar volume. In Table A D-1, the size fraction used correspond to the highest size fraction added to the jars. When a pre grinding step with Pulveristte 11 was not possible, pellets were used as received for cryo-grinding.

Table A D-1: Detail of grinding processes for each polymer

	Pulveristte pregrinding	Size fraction used [μm]	Stainless steel beads [mm]	MM400 cryogrinding time [min]
PP	no	Pellets	3	195
PEHD	yes	<250	3	195
PELD	no	Pellets	15	195
PA	yes	<250	3	210
PMMA	yes	<63	No cryogrinding	No cryogrinding
PC	yes	<250	3	190
PVC	no	<500	15	133

The method of nanoparticle preparation depends strongly on the initial polymer properties, the amount of plastic in the smaller fractions, the cryo-grinding efficiency and the volume of ethanol used to suspend the final powder, the concentration and size distribution of NP in suspension vary depending on the polymer.

NP powders were either suspended in ethanol (pure solutions) or used as powder for the spiking experiment (except for PET (Appendix 0)). As suspensions were freshly prepared before each sample deposition to ensure no NP alteration, the concentration and size distribution of the solutions used in this study are unknown. Spiked samples were amended with a high quantity of polymer powders to maximize the presence of nanoparticles in the final soil extract.

D.2. Detailed protocol for PET nanoparticle production

Small pieces cut from a PET bottle were dissolved in 10 mL 90% tetrafluoroacetic acid (TFA) and precipitated by lowering the TFA concentration down to 20%. The solution was then centrifuged at 2500 g for 30 minutes and the supernatant discarded. Instead of suspending the resulting pellet into an 0.5% sodium dodecyl sulphate (SDS) solution, as described in the original procedure, the pellet was suspended in 100 mL of 100% ethanol. The solution was allowed to settle for 1 h in a 100 mL cylinder and the upper 50 mL collected.

D.3. TOC reduction indices by the hydrogen peroxide treatment

Figure A D.1 shows the effect of a 5% H_2O_2 which without (a) and with (b) sequential additions of H_2O_2 .

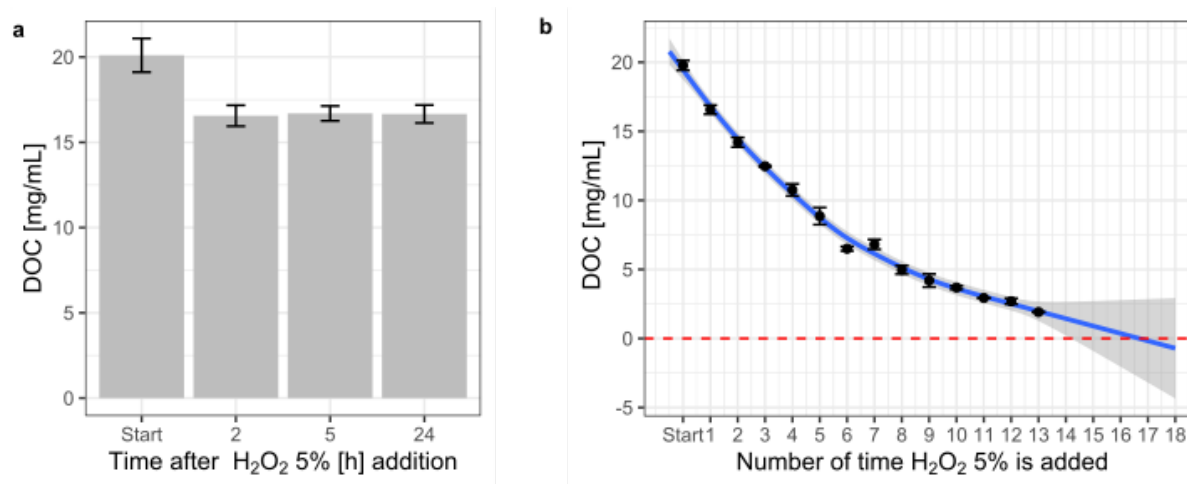


Figure A D.1: : Effect of the H_2O_2 treatment on the dissolved organic carbon fraction (DOC) in the samples. a) if the H_2O_2 concentration is set once to 5% the DOC decreases within the first 2h but stay constant after up to 24h, b) if H_2O_2 is adjusted every 2 h to 5% the DOC concentration decrease further. The general additive model of the data is represented in with a blue line with a 95% confidence interval in grey. The measurements were acquired on triplicates; the error bars show the standard deviation.

D.4. Radiation damage

We observed that, in the case of PET and PA, the electron beam of the SEM induced strong radiation damages to the particle chemical structure when high magnification pictures were acquired (Figure A D.2). For PET, damage included loss of all peaks except at 285.2 eV. In the case of PA, there was a loss of the main peak at 288.2 eV and two new peaks appeared at 285 and 286.7 eV. The changes in NEXAFS spectra observed here are similar, but of a higher intensity, than the modifications observed in another study where PET and PA films were exposed to 2700 and 1400 eV/nm³ of soft X-ray radiation, respectively (Coffey et al., 2002). Since radiation damage depends on the dose (Egerton et al., 2004), these results show that the dose required to capture images of 20-60x10³ x magnification with SEM is too high and induces molecular structure changes in the polymer that later prevents the NEXAFS identification of the polymer. Other polymers have also been shown to be affected by electron beam radiation (Egerton et al., 2004; Leijten et al., 2017). Therefore, we strongly recommend not to use SEM/TEM prior to STXM analyses. On the other hand, it is possible to perform imaging and spectral analysis by STXM and then analyze the sample afterwards by SEM if a high-resolution image and more precise size measurements are needed.

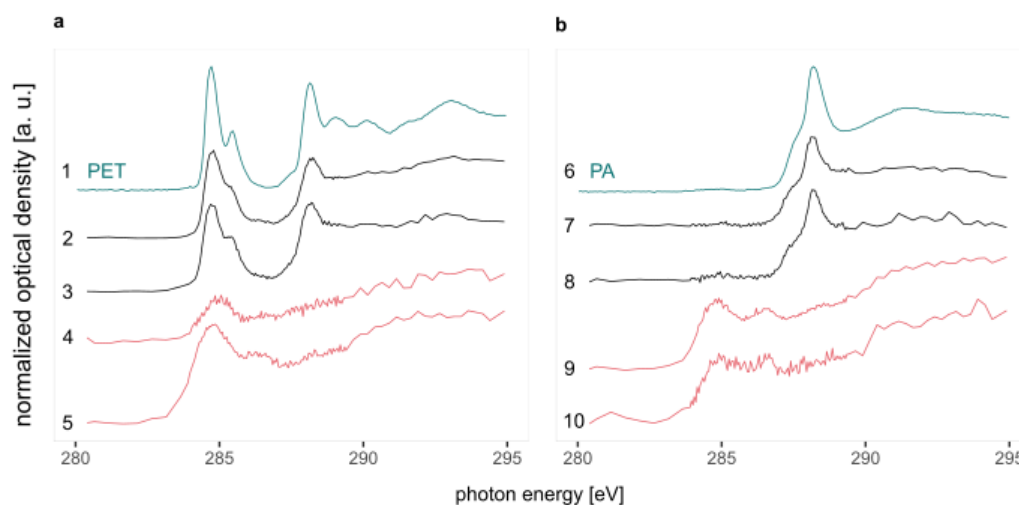


Figure A D.2: Illustration of the effect of SEM beam radiation on the NEXAFS of PET (a) and PA (b) nanoparticles. The reference spectra (Dhez et al., 2003) of PET and PA are the blue lines at the top of each subsection. The black spectra in position 2-3 for PET and 7-8 for PA correspond to particles for which no high magnification picture was acquired with SEM. The red spectra in position 4-5 for PET and 9-10 for PA correspond to particles for which we acquired a high magnification picture with SEM-

D.5. Particle high resolution picture and measurement

When a particle is found with STXM, its position is recorded to allow to finding it again with SEM and take a high quality picture. This picture is opened with ImageJ, the free hand selection tool is used to draw a line around the particle and the size is then measured with the “analyze particle” tool. The area, standard deviation, perimeter, circularity, Feret diameter and minimum Feret diameter are recorded for each particle (Figure A D.3).

When a SEM picture was not available, the size measurement was performed directly on the STXM picture.

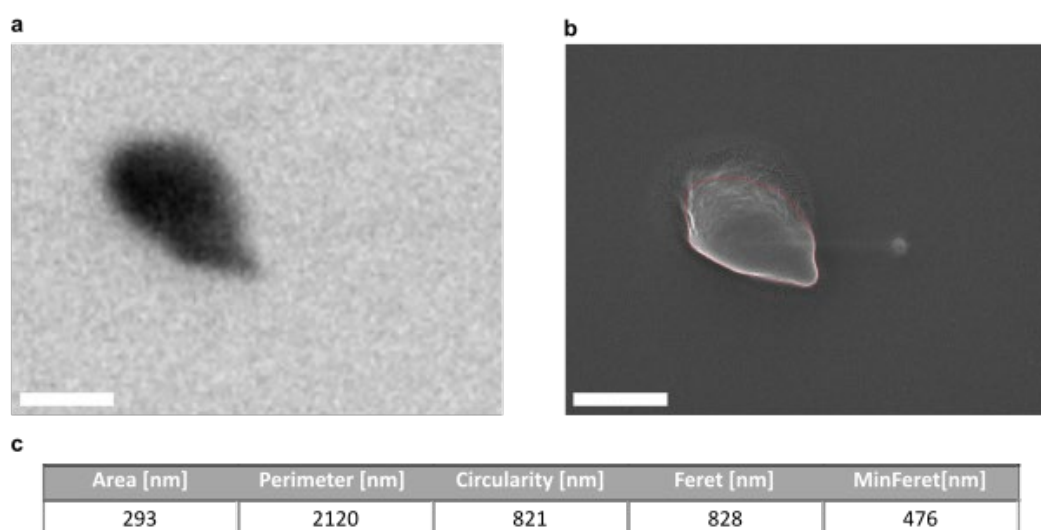


Figure A D.3: Example of a particle size measurement with ImageJ. (a) STXM picture of a particle. (b) SEM picture of the same particle as in a. (c) Results of the size measurement of the particle with ImageJ. The scale bar represents 250 nm.

D.6. Polymers attenuation length

Table A D-2: Polymer properties used to compute attenuation length of the different polymers at 320 eV. The data were collected from https://henke.lbl.gov/optical_constants/atten2.html

Polymer	Chemical formula	Density [g/cm ³]	Attenuation length [nm]
Polypropylene	C ₃ H ₆	0.90	328
Polyethylene	C ₂ H ₄	0.95	309
Polyvinyl chloride	C ₂ H ₃ Cl	1.38	192
Polyethylene Terephthalate	C ₁₀ H ₈ O ₄	1.38	276
Polystyrene	C ₈ H ₈	1.05	259
Polyamide	C ₁₂ H ₂₂ N ₂ O ₂	1.14	334
Polycarbonate	C ₁₆ H ₁₄ O ₃	1.20	272
Polymethylmetacrylate	C ₅ H ₈ O ₂	1.19	336

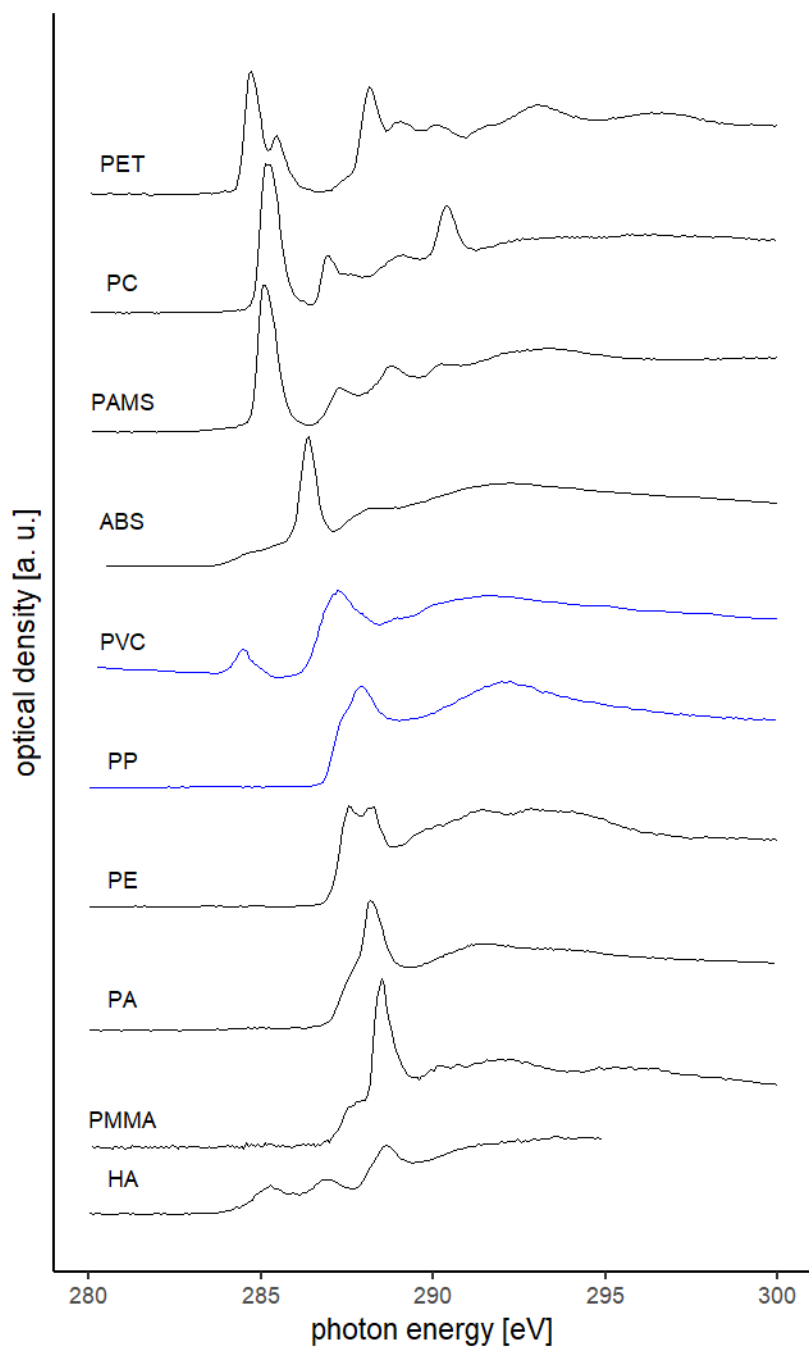
D.7. Polymers NEXAFS reference spectra

Figure A D.4: NEXAFS spectra of the most common polymers used as reference in this study and humic acid as an example for natural organic substances in the environment. Except for ABS and PVC (blue lines) that were acquired for this study, all spectra come from the literature (Christl and Kretzschmar, 2007; Dhez et al., 2003). Spectra were normalized for them to all fit the same scale.

D.8. Instrumental limitations

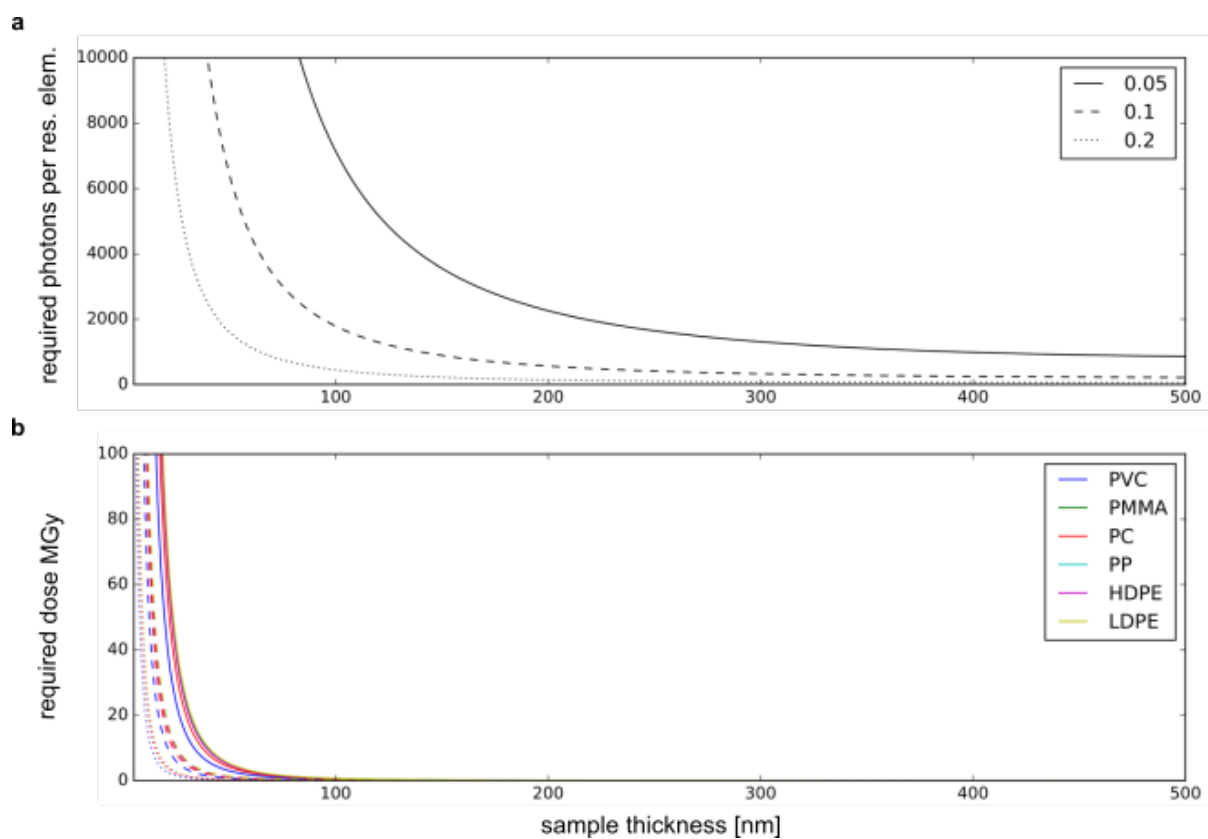


Figure A D.5: Theoretical limitations of STXM for nanoplastic identification. (a) Required photons per resolution element for a given spectral quality (noise fraction) as a function of the sample thickness. (b) Required dose to be applied to a given polymer as a function of the sample thickness.

D.9. Estimated radiation dose

Table A D-3: STX scan parameters and the corresponding radiation dose estimates.

Fig	scan file name	line mode	spot (nm)	step (nm)	stability [X,Y] (nm)	effective size [X,Y] (nm)	over-lap	dwell (ms)	material	dose (eV/nm ³)	dose (MGy)
1	Sample_Stack_2020-11-27_047.hdf5	analog	40.8	100.0	[69.7,11.4]	[100.0,42.4]	-	20	PMMA	3674	495
1	Sample_Stack_2020-11-27_047.hdf5	analog	40.8	100.0	[69.7,11.4]	[100.0,42.4]	-	20	PC	4539	606
2	Sample_Line_2020-07-01_114.hdf5	analog	40.2	20.0	[15.5,8.9]	[43.0,41.1]	-	50	PP	38761	6900
2	Sample_Line_2020-07-01_083.hdf5	analog	40.2	20.0	[15.0,7.3]	[42.9,40.8]	-	20	PP	20407	3633
2	Sample_Line_2020-07-01_092.hdf5	analog	40.2	25.0	[18.4,8.3]	[44.2,41.0]	-	30	PP	35485	6317
2	Sample_Line_2020-07-01_238.hdf5	analog	40.2	30.0	[21.2,7.8]	[45.4,40.9]	-	50	PE	27559	4648
2	Sample_Line_2020-06-29_299.hdf5	analog	40.2	20.0	[15.8,7.2]	[43.2,40.8]	-	20	PE	18598	3137
2	Sample_Line_2020-06-29_320.hdf5	analog	40.2	10.0	[10.5,7.2]	[41.5,40.8]	-	20	PE	26901	4537
Ref	Sample_Line_2019-03-20_086.hdf5	analog	72.1	200.0	[137.2,7.5]	[200.0,72.5]	-	20	PVC	76955	8935
2	Sample_Line_2020-07-02_001.hdf5	analog	40.2	37.5	[26.7,7.6]	[48.2,40.9]	-	50	PVC	59375	6893
2	Sample_Line_2020-07-02_019.hdf5	analog	40.2	30.0	[21.9,8.1]	[45.8,41.0]	-	50	PVC	61613	7153
2	Sample_Line_2020-07-02_015.hdf5	analog	40.2	20.0	[15.5,8.0]	[43.1,41.0]	-	50	PVC	94640	10988
2	Sample_Line_2020-07-01_009.hdf5	analog	40.2	25.0	[18.3,7.1]	[44.1,40.8]	-	20	PET	17871	2075

2	Sample_Line_2020-07-01_008.hdf5	analog	40.2	20.0	[15.1,7.1]	[42.9,40.8]	-	20	PET	20620	2394
2	Sample_Line_2020-07-01_006.hdf5	analog	40.2	12.5	[10.7,7.3]	[41.6,40.8]	-	20	PET	21336	2477
2	Sample_Line_2019-04-13_106.hdf5	analog	41.0	37.5	[26.8,8.5]	[49.0,44.6]	-	20	PS	60443	9223
2	Sample_Line_2019-04-13_136.hdf5	analog	41.0	12.5	[11.8,9.6]	[42.7,44.8]	-	20	PS	101457	15481
2	Sample_Line_2020-07-02_093.hdf5	point	40.2	7.5	[9.1,9.8]	[41.2,41.4]	5.36	50	PS	274740	41922
2	Sample_Line_2020-07-02_195.hdf5	point	40.2	50.0	[49.1,7.5]	[63.5,40.9]	-	50	PA	24586	3455
2	Sample_Line_2020-07-03_023.hdf5	point	40.2	30.0	[29.5,7.5]	[49.8,40.9]	1.34	50	PA	35729	5021
2	Sample_Line_2020-07-03_003.hdf5	point	40.2	20.0	[20.6,7.4]	[45.1,40.8]	2.01	50	PA	69315	9742
2	Sample_Line_2020-02-19_135.hdf5	analog	40.2	13.0	[13.8,9.5]	[42.5,41.3]	-	20	PC	38338	5119
2	Sample_Line_2020-07-02_154.hdf5	point	40.2	20.0	[15.9,10.7]	[43.2,41.6]	2.01	100	PC	127992	17089
2	Sample_Line_2020-07-02_156.hdf5	point	40.2	15.0	[15.6,9.6]	[43.1,41.3]	2.68	50	PC	102931	13743
2	Sample_Line_2020-07-03_073.hdf5	point	40.2	30.0	[30.5,9.1]	[50.4,41.2]	1.34	50	PMMA	68529	9227
2	Sample_Line_2020-07-03_089.hdf5	point	40.2	50.0	[35.2,9.7]	[53.4,41.3]	-	80	PMMA	66251	8920
2	Sample_Line_2020-07-03_076.hdf5	point	40.2	20.0	[21.2,8.6]	[45.4,41.1]	2.01	50	PMMA	137021	18448
2	Sample_Stack_2020-12-01_020.hdf5	analog	40.8	100.0	[68.9,9.7]	[100.0,41.9]	-	20	tea	2609	351
2	Sample_Stack_2020-11-30_078.hdf5	analog	40.8	100.0	[69.4,11.0]	[100.0,42.3]	-	20	tea	3027	408

Appendix

2	Sample_Stack_2020-12-01_013.hdf5	analog	40.8	100.0	[69.5,9.9]	[100.0,42.0]	-	20	tea	4843	652
2	Sample_Stack_2020-09-03_040.hdf5	analog	57.1	75.0	[51.7,6.2]	[77.0,57.5]	-	20	soil	2779	374
2	Sample_Line_2020-09-04_184.hdf5	analog	56.2	10.0	[9.9,6.7]	[57.1,56.6]	-	20	soil	10400	1400
2	Sample_Stack_2020-09-02_027.hdf5	analog	57.1	133.3	[243.9,59.3]	[250.5,82.3]	-	20	soil	557	75
3	Sample_Stack_2020-11-27_056.hdf5	analog	40.8	100.0	[68.6,10.8]	[100.0,42.2]	-	20	PMMA	3357	452
3	Sample_Stack_2020-11-27_097.hdf5	analog	40.8	100.0	[68.8,11.7]	[100.0,42.5]	-	80	PC	15816	2112
3	Sample_Stack_2020-11-27_054.hdf5	analog	40.8	100.0	[68.6,11.9]	[100.0,42.5]	-	20	PET	5182	602
3	Sample_Stack_2020-11-30_030.hdf5	analog	40.8	100.0	[68.5,12.5]	[100.0,42.7]	-	80	PA	15952	2242
3	Sample_Stack_2020-09-03_023.hdf5	analog	57.1	133.3	[156.7,23.0]	[166.8,61.6]	-	20	PA	1601	225
3	Sample_Line_2019-06-27_185.hdf5	analog	44.7	4.0	[8.1,10.6]	[45.4,45.9]	-	20	PS	135190	20628
3	Sample_Line_2019-06-27_185.hdf5	analog	44.7	4.0	[8.1,10.6]	[45.4,45.9]	-	20	PA	104833	14733
4	Sample_Line_2020-09-05_009.hdf5	analog	56.2	8.0	[8.8,6.2]	[56.9,56.6]	-	20	PS	7417	1132
4	Sample_Line_2019-09-01_188.hdf5	analog	40.2	50.0	[34.9,11.8]	[53.2,44.4]	-	20	PS	42980	6558
4	Sample_Stack_2020-09-05_027.hdf5	analog	57.1	100.0	[69.4,6.4]	[100.0,57.5]	-	20	PP	1428	254
4	Sample_Stack_2020-09-04_099.hdf5	analog	57.1	66.7	[45.9,6.3]	[73.3,57.5]	-	20	PP	2484	442
4	Sample_Stack_2020-09-04_003.hdf5	analog	57.1	100.0	[68.5,5.8]	[100.0,57.4]	-	20	PA	2594	365

4	Sample_Line_2019-03-21_056.hdf5	analog	44.7	30.0	[21.8,7.6]	[49.7,45.3]	-	20	PA	130726	18373
4	Sample_Line_2020-09-04_210.hdf5	analog	56.2	12.0	[10.7,6.2]	[57.2,56.6]	-	20	PVC	19083	2216

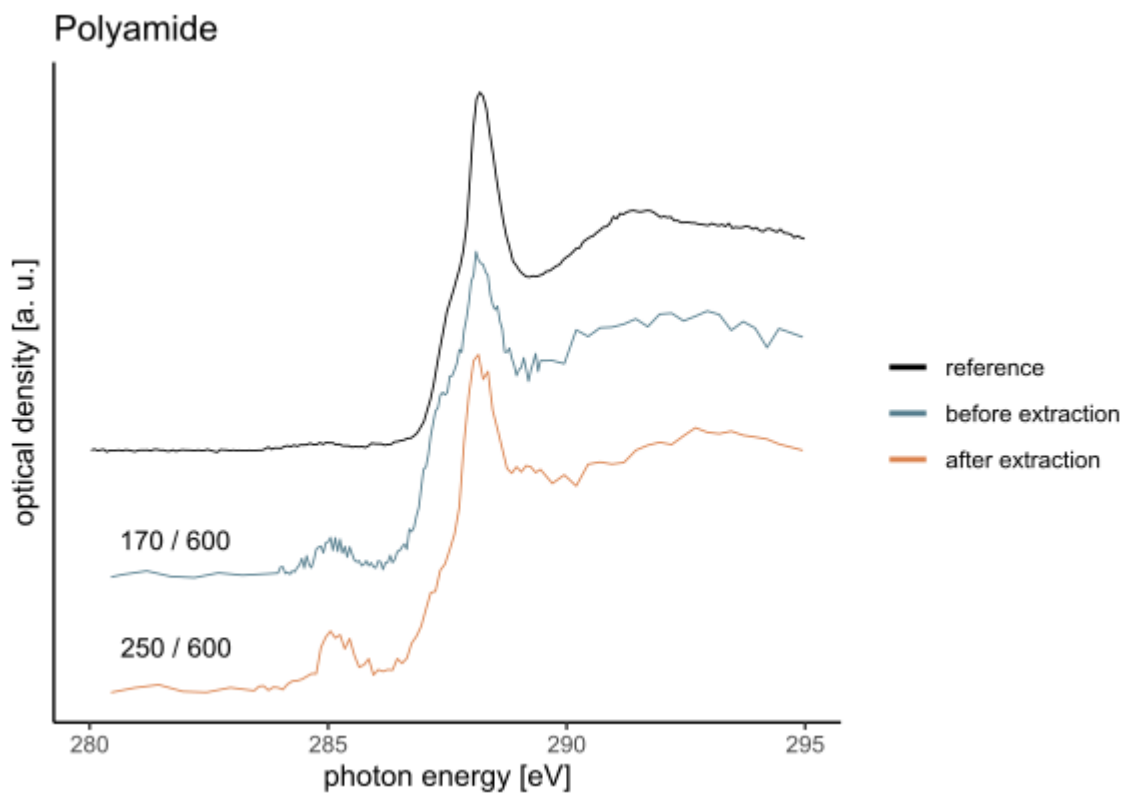
D.10. Effect of the extraction on polymer NEXAFS

Figure A D.6: Spectrum quality assessment. PA reference spectrum (Dhez et al., 2003) (black line). Spectrum of a particle of PA suspended in 100% ethanol and centrifuged down a Si_2N_4 substrate (blue line). Spectrum of a particle after extraction process (orange line). All spectra were normalized to fit the same scale. The thickness [nm]/ Feret diameter [nm] is given on the left side of the 2 measurements.

Appendix E. Chapter 4

E.1. Calculation of UV exposure equivalent in days

The calculation is done according to (Gewert et al., 2018), the same reference value was used for the average European UV irradiance: 60 kWh/(m² x year).

The conversion can be obtained with the following formula:

Total irradiance exposed / mean European UV irradiance x 365 = simulated days

(D1)

The Suntest Xenon lamp has an intensity of 65 W/m² → 65 x 160h = 10.4 KWh/m²

(D2)

→(10.4/60) x 365 = 63.2 days

E.2. Water holding capacity

The following method for determining the maximum water holding capacity (WHC) of the soil has been found to be appropriate. It is described in Annex C of the ISO DIS 11268-2 (Soil Quality - Effects of pollutants on earthworms (*Eisenia fetida*). Part 2: Determination of effects on reproduction (3)).

Collect a defined quantity (e.g. 5 g) of the test soil substrate using a suitable sampling device (auger tube etc.). Cover the bottom of the tube with a wet piece of filter paper and then place it on a rack in a water bath. The tube should be gradually submerged until the water level is above the top of the soil. It should then be left in the water for about three hours. Since not all water absorbed by the soil capillaries can be retained, the soil sample should be allowed to drain for a period of two hours by placing the tube onto a bed of very wet finely ground quartz sand contained within a covered vessel (to prevent drying). The sample should then be weighed and dried to a constant mass at 105 °C. The water holding capacity (WHC) must be calculated as follows:

$$\text{WHC (in\% of dry mass)} = (S - T - D)/D \times 100 \quad (\text{D3})$$

Where:

S = water-saturated substrate + mass of tube + mass of filter paper

T = tare (mass of tube + mass of filter paper)

D = dry mass of substrate

E.3. Measurements estimated energy dose

Table A E-1: STXM scan parameters and the corresponding radiation dose estimates

Name	fragment	Line mode	Spot [nm]	Step [nm]	Stability [nm]	Effective size [nm]	Dwell [ms]	Polymer	Dose [eV/nm ³]	Dose [MGy]
Sample_Stack_2022-05-02_172.hdf5	ES_10	analog	2704.8	15.4	[11.3,7.8]	[15.4,100.0]	60	PP	1316.8	234.4
Sample_Stack_2022-05-02_191.hdf5	ES_10	analog	2704.8	15.4	[11.4,7.6]	[15.4,100.0]	60	PP	1197	213.1
Sample_Stack_2022-05-02_220.hdf5	ES_10	analog	2704.8	15.4	[11.3,7.6]	[15.4,100.0]	60	PP	1257.3	223.8
Sample_Stack_2022-05-03_018.hdf5	ES_15	analog	2704.8	15.4	[11.6,6.8]	[15.4,100.0]	60	PS	1440.7	219.8
Sample_Stack_2022-05-03_029.hdf5	ES_15	analog	2704.8	15.4	[11.4,6.5]	[15.4,100.0]	60	PS	1584.7	241.8
Sample_Stack_2022-05-03_037.hdf5	ES_15	analog	2704.8	15.4	[11.4,6.9]	[15.4,100.0]	60	PS	1547.8	236.2
Sample_Stack_2022-05-03_045.hdf5	ES_15	analog	2704.8	15.4	[11.4,7.2]	[15.4,100.0]	60	PS	1504.6	229.6
Sample_Stack_2022-04-30_076.hdf5	ES_2	analog	2704.8	15.4	[11.4,5.5]	[15.4,100.0]	60	PET	1348.9	156.6
Sample_Stack_2022-04-30_077.hdf5	ES_2	analog	2704.8	15.4	[11.4,5.6]	[15.4,100.0]	60	PET	1319.9	153.2
Sample_Stack_2022-05-01_006.hdf5	ES_2	analog	2704.8	15.4	[11.4,5.6]	[15.4,100.0]	60	PET	1370.1	159.1
Sample_Stack_2022-05-01_026.hdf5	ES_2	analog	2704.8	100	[4.3,11.9]	[100.0,15.4]	60	PET	1720.6	199.8
Sample_Stack_2022-05-01_033.hdf5	ES_2	analog	2704.8	15.4	[11.3,6.3]	[15.4,100.0]	60	PET	1595.4	185.2
Sample_Stack_2022-05-01_162.hdf5	ES_6	analog	2704.8	15.4	[11.3,5.8]	[15.4,100.0]	60	PS	1798.4	274.4
Sample_Stack_2022-05-01_174.hdf5	ES_6	analog	2704.8	15.4	[11.3,6.5]	[15.4,100.0]	60	PS	1788.7	272.9
Sample_Stack_2022-05-02_009.hdf5	ES_6	analog	2704.8	15.4	[11.5,7.2]	[15.4,100.0]	60	PS	1672.9	255.3
Sample_Stack_2022-05-02_087.hdf5	ES_9	analog	2704.8	15.4	[11.5,8.9]	[15.4,100.0]	60	PS	1403.3	214.1

Sample_Stack_2022-05-02_089.hdf5	ES_9	analog	2704.8	100	[4.7,13.4]	[100.0,15.4]	60	PS	1881.7	287.1
Sample_Stack_2022-05-02_101.hdf5	ES_9	analog	2704.8	15.4	[11.5,9.8]	[15.4,100.0]	60	PS	1333.8	203.5
Sample_Stack_2022-05-02_126.hdf5	ES_9	analog	2704.8	100	[5.0,13.2]	[100.0,15.4]	60	PS	1612.3	246
Sample_Stack_2021-03-10_053.hdf5	GUR3									
Sample_Stack_2021-03-10_059.hdf5	GUR3	analog	40.8	100	[67.9,4.9]	[100.0,14.3]	20	PS	99.2	15.1
Sample_Stack_2021-10-25_039.hdf5	GUR3	analog	2704.8	100	[11.8,21.3]	[100.0,15.4]	60	PS	252.2	38.5
Sample_Stack_2021-10-25_041.hdf5	GUR3	analog	2704.8	100	[11.5,20.7]	[100.0,15.4]	60	PS	309.9	47.3
Sample_Stack_2021-10-25_044.hdf5	GUR3	analog	2704.8	100	[10.4,19.3]	[100.0,15.4]	60	PS	227.1	34.7
Sample_Stack_2021-10-25_046.hdf5	GUR3	analog	2704.8	100	[10.9,20.2]	[100.0,15.4]	60	PS	301.5	46
Sample_Stack_2022-08-31_060.hdf5	GUR3	analog	3382.2	100	[8.9,23.8]	[100.0,15.4]	60	PS	120.9	18.4
Sample_Stack_2022-08-31_063.hdf5	GUR3	analog	3382.2	100	[9.2,25.2]	[100.0,15.4]	60	PS	111.7	17
Sample_Stack_2022-08-31_067.hdf5	GUR3	analog	3382.2	100	[9.3,25.0]	[100.0,15.4]	60	PS	56.4	8.6
Sample_Stack_2021-09-06_115.hdf5	GUR3b	analog	40.8	15.4	[12.6,12.6]	[15.4,43.6]	60	PS	1159.6	176.9
Sample_Stack_2021-09-06_123.hdf5	GUR3b	analog	40.8	15.4	[12.5,12.2]	[15.4,43.5]	60	PS	939.4	143.3
Sample_Stack_2021-09-06_133.hdf5	GUR3b	analog	40.8	15.4	[12.5,11.1]	[15.4,43.2]	60	PS	1087.6	166
Sample_Stack_2021-09-06_141.hdf5	GUR3b	analog	40.8	15.4	[12.4,11.8]	[15.4,43.4]	60	PS	1134.5	173.1
Sample_Stack_2021-09-07_015.hdf5	GUR3b	analog	40.8	15.4	[12.4,11.9]	[15.4,43.4]	60	PS	1037.2	158.3
Sample_Stack_2022-08-30_080.hdf5	GUR3b	point	3382.2	15.4	[15.7,20.6]	[15.4,100.0]	60	PS	165.1	25.2
Sample_Stack_2022-08-30_092.hdf5	GUR3b	analog	3382.2	15.4	[13.3,12.3]	[15.4,100.0]	60	PS	135.3	20.6

Appendix

Sample_Stack_2022-08-31_011.hdf5	GUR3b	analog	3382.2	15.4	[12.6,12.9]	[15.4,100.0]	60	PS	184.1	28.1
Sample_Stack_2022-08-31_020.hdf5	GUR3b	analog	3382.2	15.4	[12.4,12.0]	[15.4,100.0]	60	PS	160.2	24.4
Sample_Stack_2022-09-01_017.hdf5	GUR3b	analog	3382.2	15.4	[12.8,14.2]	[15.4,100.0]	60	PS	103.6	15.8
Sample_Stack_2022-05-01_098.hdf5	PC_A_ L	analog	2704.8	100	[4.4,12.8]	[100.0,15.4]	60	PC	1951.1	260.5
Sample_Stack_2022-05-01_110.hdf5	PC_A_ L	analog	2704.8	15.4	[11.3,6.0]	[15.4,100.0]	60	PC	1613.2	215.4
Sample_Stack_2022-05-01_111.hdf5	PC_A_ L	analog	2704.8	15.4	[11.3,5.9]	[15.4,100.0]	60	PC	1664.3	222.2
Sample_Stack_2021-06-25_015.hdf5	PC_A_ S	analog	40.8	15.4	[14.0,9.8]	[15.4,42.0]	80	PC	1665.8	222.4
Sample_Stack_2021-06-25_016.hdf5	PC_A_ S	analog	40.8	15.4	[13.9,9.2]	[15.4,41.8]	80	PC	1681.7	224.5
Sample_Stack_2021-06-25_017.hdf5	PC_A_ S	analog	40.8	15.4	[13.8,9.1]	[15.4,41.8]	80	PC	1653.3	220.7
Sample_Stack_2021-06-25_036.hdf5	PC_ctrl	analog	40.8	100	[68.3,8.1]	[100.0,15.4]	60	PC	611.8	81.7
Sample_Stack_2021-06-25_038.hdf5	PC_ctrl	analog	40.8	100	[5.4,13.7]	[100.0,15.4]	60	PC	664.9	88.8
Sample_Stack_2021-06-25_039.hdf5	PC_ctrl	analog	40.8	100	[5.0,13.6]	[100.0,15.4]	60	PC	608.8	81.3
Sample_Stack_2022-05-01_051.hdf5	PC_N_ L	analog	2704.8	15.4	[11.9,5.7]	[15.4,100.0]	60	PC	1519.3	202.8
Sample_Stack_2022-05-01_064.hdf5	PC_N_ L	analog	2704.8	100	[5.3,12.1]	[100.0,15.4]	60	PC	2273.9	303.6
Sample_Stack_2022-05-01_077.hdf5	PC_N_ L	analog	2704.8	15.4	[11.4,6.9]	[15.4,100.0]	60	PC	1592.8	212.7
Sample_Stack_2022-05-01_086.hdf5	PC_N_ L	analog	2704.8	15.4	[11.4,6.3]	[15.4,100.0]	60	PC	1399.8	186.9
Sample_Stack_2022-05-30_207.hdf5	PC3	analog	2704.8	15.4	[25.0,8.4]	[15.4,100.0]	60	PC	2105.9	281.2
Sample_Stack_2022-05-30_239.hdf5	PC3	analog	2704.8	15.4	[16.0,7.5]	[15.4,100.0]	60	PC	2641.8	352.7
Sample_Stack_2022-04-30_049.hdf5	PET_A_ L	analog	2704.8	100	[4.2,11.9]	[100.0,15.4]	60	PET	2529.5	293.7

Sample_Stack_2022-04-30_052.hdf5	PET_A L	analog	2704.8	100	[4.0,11.9]	[100.0,15.4]	60	PET	2121.7	246.3
Sample_Stack_2021-06-24_019.hdf5	PET_A S	analog	40.8	15.4	[14.7,9.9]	[15.4,42.0]	20	PET	617.4	71.7
Sample_Stack_2021-06-24_028.hdf5	PET_A S									
Sample_Stack_2022-09-01_104.hdf5	PET_A S	analog	3382.2	15.4	[16.4,18.0]	[15.4,100.0]	60	PET	64.1	7.4
Sample_Stack_2022-09-01_149.hdf5	PET_A S	analog	3382.2	15.4	[13.7,8.9]	[15.4,100.0]	60	PET	107	12.4
Sample_Stack_2021-06-24_054.hdf5	PET_ctr I	analog	40.8	15.4	[13.6,8.6]	[15.4,41.7]	20	PET	683.6	79.4
Sample_Stack_2021-06-24_061.hdf5	PET_ctr I	analog	40.8	14.3	[12.6,7.5]	[14.3,30.0]	40	PET	1651.5	191.7
Sample_Stack_2021-06-25_001.hdf5	PET_ctr I	analog	40.8	14.3	[12.6,7.6]	[14.3,30.0]	40	PET	1728.8	200.7
Sample_Stack_2021-06-25_002.hdf5	PET_ctr I	analog	40.8	14.3	[12.6,7.5]	[14.3,30.0]	40	PET	1724.5	200.2
Sample_Stack_2022-04-30_032.hdf5	PET_N L	analog	2704.8	15.4	[11.5,5.9]	[15.4,100.0]	60	PET	1342.3	155.8
Sample_Stack_2022-09-01_214.hdf5	PET3	analog	3382.2	15.4	[12.3,9.3]	[15.4,100.0]	60	PET	99.9	11.6
Sample_Stack_2022-09-01_220.hdf5	PET3	analog	3382.2	15.4	[12.2,9.5]	[15.4,100.0]	60	PET	88.9	10.3
Sample_Stack_2022-09-01_227.hdf5	PET3	analog	3382.2	15.4	[11.9,7.9]	[15.4,100.0]	80	PET	129.5	15
Sample_Stack_2022-05-31_042.hdf5	PP3	analog	2704.8	15.4	[13.7,7.4]	[15.4,100.0]	60	PP	2014.9	358.7
Sample_Stack_2022-05-31_053.hdf5	PP3	analog	2704.8	15.4	[14.3,8.7]	[15.4,100.0]	60	PP	1673.8	298
Sample_Stack_2022-09-01_037.hdf5	PP3	analog	3382.2	15.4	[12.6,11.8]	[15.4,100.0]	60	PP	85.2	15.2
Sample_Stack_2021-10-24_090.hdf5	PS_ctrl	analog	2704.8	15.4	[54.7,153.2]	[15.4,100.0]	60	PS	1202	183.4
Sample_Stack_2021-10-24_094.hdf5	PS_ctrl	analog	2704.8	15.4	[50.8,133.9]	[15.4,100.0]	60	PS	1266.3	193.2
Sample_Stack_2021-10-25_002.hdf5	PS_ctrl	analog	2704.8	15.4	[35.3,83.0]	[15.4,100.0]	60	PS	1134.9	173.2

Appendix

Sample_Stack_2022-08-31_108.hdf5	PS2	analog	3382.2	15.4	[12.9,14.3]	[15.4,100.0]	60	PS	97.6	14.9
Sample_Stack_2022-08-31_118.hdf5	PS2	analog	3382.2	15.4	[13.1,13.9]	[15.4,100.0]	60	PS	99.1	15.1
Sample_Stack_2022-08-31_129.hdf5	PS2	analog	3382.2	15.4	[13.2,13.5]	[15.4,100.0]	60	PS	96	14.6
Sample_Stack_2022-05-30_251.hdf5	PS3	analog	2704.8	15.4	[nan,nan]	[15.4,100.0]	60	PS		
Sample_Stack_2022-05-31_023.hdf5	PS3	analog	2704.8	15.4	[15.3,7.7]	[15.4,100.0]	60	PS	2050.9	312.9
Sample_Stack_2022-05-31_025.hdf5	PS3	analog	2704.8	15.4	[13.9,7.5]	[15.4,100.0]	60	PS	1013.8	154.7
Sample_Stack_2021-09-06_046.hdf5	SAN1a	analog	40.8	15.4	[12.4,11.3]	[15.4,43.2]	60	PET	856.7	99.5
Sample_Stack_2021-09-06_081.hdf5	SAN1a	analog	40.8	15.4	[12.7,11.6]	[15.4,43.3]	60	PET	1314.9	152.7
Sample_Stack_2021-09-07_096.hdf5	SAN1a	analog	40.8	15.4	[14.1,12.3]	[15.4,43.5]	60	PET	890.2	103.4
Sample_Stack_2021-09-07_104.hdf5	SAN1a	analog	40.8	15.4	[13.0,12.3]	[15.4,43.5]	60	PET	793	92.1
Sample_Stack_2021-09-05_191.hdf5	SAN2b	analog	40.8	15.4	[40.5,8.8]	[15.4,42.6]	60	PP	449.7	80
Sample_Stack_2021-09-05_192.hdf5	SAN2b	analog	40.8	15.4	[15.4,6.5]	[15.4,42.2]	60	PP	282.4	50.3

E.4. Polymer attenuation length estimations

Table A E-2: Polymer properties used to compute attenuation length of the different polymers at 320 eV. Data were collected from https://henke.lbl.gov/optical_constants/atten2.html.

Polymer	Chemical formula	Density [g/cm ³]	Attenuation length [nm]
Polypropylene	C ₃ H ₆	0.90	328
Polyethylene Terephthalate	C ₁₀ H ₈ O ₄	1.38	276
Polystyrene	C ₈ H ₈	1.05	259
Polycarbonate	C ₁₆ H ₁₄ O ₃	1.20	272

E.5. Polymer surface alteration on naturally-weathered fragments in soil

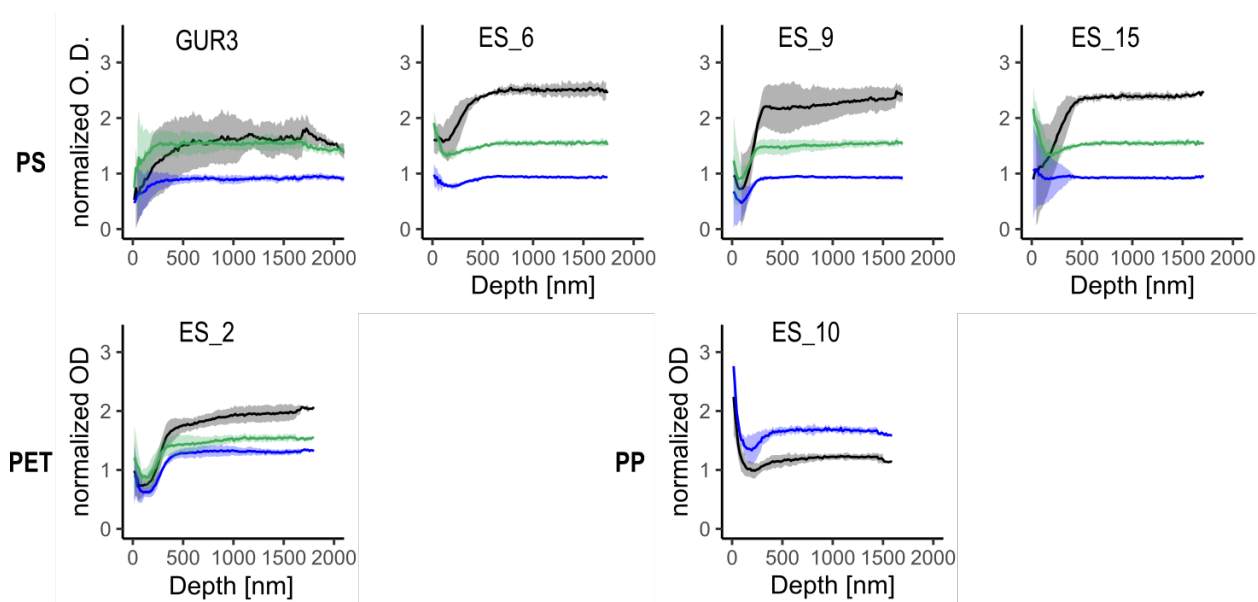


Figure A E.1: STXM-NEXAFS analysis of plastic fragments retrieved from agricultural and road-sided soil. All NEXAFS data were normalized to pre- and post-edge to remove the effect of the sample thickness on the optical density. Average intensity of the peaks highlighted by the arrow in Figure 2A.

Literature cited

- Abbe, E., 1873. Beiträge zur Theorie des Mikroskops und der mikroskopischen Wahrnehmung. *Archiv für Mikroskopische Anatomie* 9, 413–468. <https://doi.org/10.1007/BF02956173>
- Ade, H., Hitchcock, A.P., 2008. NEXAFS microscopy and resonant scattering: Composition and orientation probed in real and reciprocal space. *Polymer* 49, 643–675. <https://doi.org/10.1016/j.polymer.2007.10.030>
- Ade, H., Stoll, H., 2009. Near-edge X-ray absorption fine-structure microscopy of organic and magnetic materials. *Nature Mater* 8, 281–290. <https://doi.org/10.1038/nmat2399>
- Ainali, N.M., Bikiaris, D.N., Lambropoulou, D.A., 2021. Aging effects on low- and high-density polyethylene, polypropylene and polystyrene under UV irradiation: An insight into decomposition mechanism by Py-GC/MS for microplastic analysis. *Journal of Analytical and Applied Pyrolysis* 158, 105207. <https://doi.org/10.1016/j.jaap.2021.105207>
- Alimi, O.S., Claveau-Mallet, D., Kurusu, R.S., Lapointe, M., Bayen, S., Tufenkji, N., 2022. Weathering pathways and protocols for environmentally relevant microplastics and nanoplastics: What are we missing? *Journal of Hazardous Materials* 423, 126955. <https://doi.org/10.1016/j.jhazmat.2021.126955>
- Amaral-Zettler, L.A., Zettler, E.R., Mincer, T.J., 2020. Ecology of the plastisphere. *Nat Rev Microbiol* 18, 139–151. <https://doi.org/10.1038/s41579-019-0308-0>
- Amobonye, A., Bhagwat, P., Singh, S., Pillai, S., 2021. Plastic biodegradation: Frontline microbes and their enzymes. *Science of The Total Environment* 759, 143536. <https://doi.org/10.1016/j.scitotenv.2020.143536>
- An, L., Liu, Q., Deng, Y., Wu, W., Gao, Y., Ling, W., 2020. Sources of Microplastic in the Environment, in: He, D., Luo, Y. (Eds.), *Microplastics in Terrestrial Environments, The Handbook of Environmental Chemistry*. Springer International Publishing, Cham, pp. 143–159. https://doi.org/10.1007/698_2020_449
- Arganda-Carreras, I., Kaynig, V., Rueden, C., Eliceiri, K.W., Schindelin, J., Cardona, A., Sebastian Seung, H., 2017. Trainable Weka Segmentation: a machine learning tool for microscopy pixel classification. *Bioinformatics* 33, 2424–2426. <https://doi.org/10.1093/bioinformatics/btx180>
- Astner, A.F., Hayes, D.G., O'Neill, H., Evans, B.R., Pingali, S.V., Urban, V.S., Young, T.M., 2019. Mechanical formation of micro- and nano-plastic materials for environmental studies in agricultural ecosystems. *Science of The Total Environment* 685, 1097–1106. <https://doi.org/10.1016/j.scitotenv.2019.06.241>
- Awet, T.T., Kohl, Y., Meier, F., Straskraba, S., Grün, A.-L., Ruf, T., Jost, C., Drexel, R., Tunc, E., Emmerling, C., 2018. Effects of polystyrene nanoparticles on the microbiota and functional diversity of enzymes in soil. *Environmental Sciences Europe* 30. <https://doi.org/10.1186/s12302-018-0140-6>
- Baensch-Baltruschat, B., Kocher, B., Kochleus, C., Stock, F., Reifferscheid, G., 2021. Tyre and road wear particles - A calculation of generation, transport and release to water and soil with special regard to German roads. *Science of The Total Environment* 752, 141939. <https://doi.org/10.1016/j.scitotenv.2020.141939>
- Baensch-Baltruschat, B., Kocher, B., Stock, F., Reifferscheid, G., 2020. Tyre and road wear particles (TRWP) - A review of generation, properties, emissions, human health risk, ecotoxicity, and fate in the environment. *Science of The Total Environment* 733, 137823. <https://doi.org/10.1016/j.scitotenv.2020.137823>
- Baudrimont, M., Arini, A., Guégan, C., Venel, Z., Gigault, J., Pedrono, B., Prunier, J., Maurice, L., Ter Halle, A., Feurtet-Mazel, A., 2020. Ecotoxicity of polyethylene nanoplastics from the North Atlantic oceanic gyre on freshwater and marine organisms (microalgae and filter-feeding bivalves). *Environ Sci Pollut Res* 27, 3746–3755. <https://doi.org/10.1007/s11356-019-04668-3>

- Bigalke, M., Fieber, M., Foetisch, A., Reynes, J., Tollan, P., 2022. Microplastics in agricultural drainage water: A link between terrestrial and aquatic microplastic pollution. *Science of The Total Environment* 806, 150709. <https://doi.org/10.1016/j.scitotenv.2021.150709>
- Bläsing, M., Amelung, W., 2018. Plastics in soil: Analytical methods and possible sources. *Science of The Total Environment* 612, 422–435. <https://doi.org/10.1016/j.scitotenv.2017.08.086>
- Boller, K., Haelbich, R.-P., Hogrefe, H., Jark, W., Kunz, C., 1983. Investigation of carbon contamination of mirror surfaces exposed to synchrotron radiation. *Nuclear Instruments and Methods in Physics Research* 208, 273–279. [https://doi.org/10.1016/0167-5087\(83\)91134-1](https://doi.org/10.1016/0167-5087(83)91134-1)
- Boscherini, F., Meneghini, C., Mobilio, S. (Eds.), 2015. *Synchrotron Radiation: Basics, Methods and Applications*, 1st ed. 2015. ed. Springer Berlin Heidelberg : Imprint: Springer, Berlin, Heidelberg. <https://doi.org/10.1007/978-3-642-55315-8>
- Braun, M., Mail, M., Krupp, A.E., Amelung, W., 2023. Microplastic contamination of soil: Are input pathways by compost overridden by littering? *Science of The Total Environment* 855, 158889. <https://doi.org/10.1016/j.scitotenv.2022.158889>
- Brydson, J.A., 1999. *Plastics materials*, 7th ed. ed. Butterworth-Heinemann, Oxford ; Boston.
- Büks, F., Kaupenjohann, M., 2022. What comes after the Sun? On the integration of soil biogeochemical pre-weathering into microplastic experiments. *SOIL* 8, 373–380. <https://doi.org/10.5194/soil-8-373-2022>
- Büks, F., Kaupenjohann, M., 2020. Global concentrations of microplastics in soils – a review. *SOIL* 6, 649–662. <https://doi.org/10.5194/soil-6-649-2020>
- Cadée, G.C., 2002. Seabirds and floating plastic debris. *Marine Pollution Bulletin* 44, 1294–1295. [https://doi.org/10.1016/S0025-326X\(02\)00264-3](https://doi.org/10.1016/S0025-326X(02)00264-3)
- Cai, L., Wang, J., Peng, J., Wu, Z., Tan, X., 2018. Observation of the degradation of three types of plastic pellets exposed to UV irradiation in three different environments. *Science of The Total Environment* 628–629, 740–747. <https://doi.org/10.1016/j.scitotenv.2018.02.079>
- Cao, D., Wang, X., Luo, X., Liu, G., Zheng, H., 2017. Effects of polystyrene microplastics on the fitness of earthworms in an agricultural soil. *IOP Conf. Ser.: Earth Environ. Sci.* 61, 012148. <https://doi.org/10.1088/1755-1315/61/1/012148>
- Cao, G., Wang, W., Zhang, J., Wu, P., Zhao, X., Yang, Z., Hu, D., Cai, Z., 2022. New Evidence of Rubber-Derived Quinones in Water, Air, and Soil. *Environ. Sci. Technol.* 56, 4142–4150. <https://doi.org/10.1021/acs.est.1c07376>
- Carpenter, E.J., Smith, K.L., 1972. Plastics on the Sargasso Sea Surface. *Science* 175, 1240–1241. <https://doi.org/10.1126/science.175.4027.1240>
- Cerasa, M., Teodori, S., Pietrelli, L., 2021. Searching Nanoplastics: From Sampling to Sample Processing. *Polymers* 13, 3658. <https://doi.org/10.3390/polym13213658>
- Chapman, D.V., Du, H., Lee, W.Y., Wiesner, U.B., 2020. Optical super-resolution microscopy in polymer science. *Progress in Polymer Science* 111, 101312. <https://doi.org/10.1016/j.progpolymsci.2020.101312>
- Chen, Z., Zhao, W., Xing, R., Xie, S., Yang, X., Cui, P., Lü, J., Liao, H., Yu, Z., Wang, S., Zhou, S., 2020. Enhanced in situ biodegradation of microplastics in sewage sludge using hyperthermophilic composting technology. *Journal of Hazardous Materials* 384, 121271. <https://doi.org/10.1016/j.jhazmat.2019.121271>
- Christl, I., Kretzschmar, R., 2007. C-1s NEXAFS Spectroscopy Reveals Chemical Fractionation of Humic Acid by Cation-Induced Coagulation. *Environ. Sci. Technol.* 41, 1915–1920. <https://doi.org/10.1021/es062141s>
- Cinque, G., Kelley, C.S., Frogley, M.D., Filik, J., Wehbe, K., Fitzpatrick, A., Donaldson, P.M., 2016. World First for Diamond in Synchrotron-Based IR Photothermal Nanospectroscopy. *Synchrotron Radiation News* 29, 37–39. <https://doi.org/10.1080/08940886.2016.1198675>
- Clark, D.T., Munro, H.S., 1983. Surface aspects of the photo-degradation of bisphenol A polycarbonate, in oxygen and air as a function of relative humidity, as revealed by

- ESCA. Polymer Degradation and Stability 5, 227–236. [https://doi.org/10.1016/0141-3910\(83\)90013-7](https://doi.org/10.1016/0141-3910(83)90013-7)
- Coffey, T., Urquhart, S.G., Ade, H., 2002. Characterization of the effects of soft X-ray irradiation on polymers. *Journal of Electron Spectroscopy and Related Phenomena* 122, 65–78. [https://doi.org/10.1016/S0368-2048\(01\)00342-5](https://doi.org/10.1016/S0368-2048(01)00342-5)
- Cole, M., Lindeque, P., Halsband, C., Galloway, T.S., 2011. Microplastics as contaminants in the marine environment: A review. *Marine Pollution Bulletin* 62, 2588–2597. <https://doi.org/10.1016/j.marpolbul.2011.09.025>
- Colpaert, R., Petit dit Grézériat, L., Louzon, M., de Vaufleury, A., Gimbert, F., 2022. Polyethylene microplastic toxicity to the terrestrial snail *Cantareus aspersus*: size matters. *Environ Sci Pollut Res* 29, 29258–29267. <https://doi.org/10.1007/s11356-021-15824-z>
- Colson, B.C., Michel, A.P.M., 2021. Flow-Through Quantification of Microplastics Using Impedance Spectroscopy. *ACS Sens.* 6, 238–244. <https://doi.org/10.1021/acssensors.0c02223>
- Committee for Risk Assessment (RAC), 2020. Opinion on an Annex XV Dossier Proposing Restrictions on Intentionally added Microplastics. Committee for Socio-economic Analysis S.E.A.C. collab, 2020.
- Corradini, F., Meza, P., Eguiluz, R., Casado, F., Huerta-Lwanga, E., Geissen, V., 2019. Evidence of microplastic accumulation in agricultural soils from sewage sludge disposal. *Science of The Total Environment* 671, 411–420. <https://doi.org/10.1016/j.scitotenv.2019.03.368>
- Cowger, W., Steinmetz, Z., Gray, A., Munno, K., Lynch, J., Hapich, H., Primpke, S., De Frond, H., Rochman, C., Herodotou, O., 2021. Microplastic Spectral Classification Needs an Open Source Community: Open Specy to the Rescue! *Anal. Chem.* 93, 7543–7548. <https://doi.org/10.1021/acs.analchem.1c00123>
- Danso, D., Chow, J., Streit, W.R., 2019. Plastics: Environmental and Biotechnological Perspectives on Microbial Degradation. *Appl Environ Microbiol* 85, e01095-19. <https://doi.org/10.1128/AEM.01095-19>
- Dawson, A.L., Kawaguchi, S., King, C.K., Townsend, K.A., King, R., Huston, W.M., Bengtson Nash, S.M., 2018. Turning microplastics into nanoplastics through digestive fragmentation by Antarctic krill. *Nat Commun* 9, 1001. <https://doi.org/10.1038/s41467-018-03465-9>
- de Ruijter, V.N., Redondo-Hasselerharm, P.E., Gouin, T., Koelmans, A.A., 2020. Quality Criteria for Microplastic Effect Studies in the Context of Risk Assessment: A Critical Review. *Environ. Sci. Technol.* 54, 11692–11705. <https://doi.org/10.1021/acs.est.0c03057>
- de Souza Machado, A.A., Lau, C.W., Kloas, W., Bergmann, J., Bachelier, J.B., Faltin, E., Becker, R., Görlich, A.S., Rillig, M.C., 2019. Microplastics Can Change Soil Properties and Affect Plant Performance. *Environ. Sci. Technol.* 53, 6044–6052. <https://doi.org/10.1021/acs.est.9b01339>
- Degaffe, F.S., Turner, A., 2011. Leaching of zinc from tire wear particles under simulated estuarine conditions. *Chemosphere* 85, 738–743. <https://doi.org/10.1016/j.chemosphere.2011.06.047>
- Demir, E., 2020. *An in vivo* study of nanorod, nanosphere, and nanowire forms of titanium dioxide using *Drosophila melanogaster*: toxicity, cellular uptake, oxidative stress, and DNA damage. *Journal of Toxicology and Environmental Health, Part A* 83, 456–469. <https://doi.org/10.1080/15287394.2020.1777236>
- Deng, H., Su, L., Zheng, Y., Du, F., Liu, Q.-X., Zheng, J., Zhou, Z., Shi, H., 2022. Crack Patterns of Environmental Plastic Fragments. *Environ. Sci. Technol.* acs.est.1c08100. <https://doi.org/10.1021/acs.est.1c08100>
- Dhez, O., Ade, H., Urquhart, S.G., 2003. Calibrated NEXAFS spectra of some common polymers. *Journal of Electron Spectroscopy and Related Phenomena* 128, 85–96. [https://doi.org/10.1016/S0368-2048\(02\)00237-2](https://doi.org/10.1016/S0368-2048(02)00237-2)

- Duan, J., Bolan, N., Li, Y., Ding, S., Atugoda, T., Vithanage, M., Sarkar, B., Tsang, D.C.W., Kirkham, M.B., 2021. Weathering of microplastics and interaction with other coexisting constituents in terrestrial and aquatic environments. *Water Research* 196, 117011. <https://doi.org/10.1016/j.watres.2021.117011>
- Duemichen, E., Eisenraut, P., Celina, M., Braun, U., 2019. Automated thermal extraction-desorption gas chromatography mass spectrometry: A multifunctional tool for comprehensive characterization of polymers and their degradation products. *Journal of Chromatography A* 1592, 133–142. <https://doi.org/10.1016/j.chroma.2019.01.033>
- Egerton, R.F., 2009. Electron energy-loss spectroscopy in the TEM. *Reports on Progress in Physics* 72, 016502. <https://doi.org/10.1088/0034-4885/72/1/016502>
- Egerton, R.F., Li, P., Malac, M., 2004. Radiation damage in the TEM and SEM. *Micron* 35, 399–409. <https://doi.org/10.1016/j.micron.2004.02.003>
- Elzhov, T.V., Mullen, K.M., Spiess, A.-N., Bolker, B., 2022. minpack.lm: R Interface to the Levenberg-Marquardt Nonlinear Least-Squares Algorithm Found in MINPACK, Plus Support for Bounds.
- Enders, K., Lenz, R., Stedmon, C.A., Nielsen, T.G., 2015. Abundance, size and polymer composition of marine microplastics $\geq 10 \mu\text{m}$ in the Atlantic Ocean and their modelled vertical distribution. *Marine Pollution Bulletin* 100, 70–81. <https://doi.org/10.1016/j.marpolbul.2015.09.027>
- Fausser, P., Tjell, J.C., Mosbaek, H., Pilegaard, K., 2002. TIRE-TREAD AND BITUMEN PARTICLE CONCENTRATIONS IN AEROSOL AND SOIL SAMPLES. *Petroleum Science and Technology* 20, 127–141. <https://doi.org/10.1081/LFT-120002092>
- Favre, H.A., Powell, W.H., 2014. Nomenclature of Organic Chemistry: IUPAC Recommendations and Preferred Names 2013. The Royal Society of Chemistry. <https://doi.org/10.1039/9781849733069>
- Fechine, G.J.M., Rabello, M.S., Souto-Maior, R.M., 2002. The effect of ultraviolet stabilizers on the photodegradation of poly(ethylene terephthalate). *Polymer Degradation and Stability* 75, 153–159. [https://doi.org/10.1016/S0141-3910\(01\)00214-2](https://doi.org/10.1016/S0141-3910(01)00214-2)
- Fernández-González, V., Andrade-Garda, J.M., López-Mahía, P., Muniategui-Lorenzo, S., 2021. Impact of weathering on the chemical identification of microplastics from usual packaging polymers in the marine environment. *Analytica Chimica Acta* 1142, 179–188. <https://doi.org/10.1016/j.aca.2020.11.002>
- Fischer, B., Smith, M., Pau, G., 2020. rhdf5: R Interface to HDF5.
- Foetisch, A., Filella, M., Watts, B., Vinot, L.-H., Bigalke, M., 2022. Identification and characterisation of individual nanoplastics by scanning transmission X-ray microscopy (STXM). *Journal of Hazardous Materials* 426, 127804. <https://doi.org/10.1016/j.jhazmat.2021.127804>
- Fok, L., Cheung, P.K., Tang, G., Li, W.C., 2017. Size distribution of stranded small plastic debris on the coast of Guangdong, South China. *Environmental Pollution* 220, 407–412. <https://doi.org/10.1016/j.envpol.2016.09.079>
- Folkesson, L., Bækken, T., Brenčić, M., Dawson, A., Frančoiš, D., Kuřimská, P., Leitão, T., Ličbinský, R., Vojtěšek, M., 2009. Sources and Fate of Water Contaminants in Roads, in: Dawson, A. (Ed.), *Water in Road Structures, Geotechnical, Geological and Earthquake Engineering*. Springer Netherlands, Dordrecht, pp. 107–146. https://doi.org/10.1007/978-1-4020-8562-8_6
- FronD, H.D., Wong, D.C., Coffin, D.S., 2022. Standard Operating Procedures for Extraction and Measurement by Infrared Spectroscopy of Microplastic Particles in Drinking Water 35.
- Gewert, B., Plassmann, M., Sandblom, O., MacLeod, M., 2018. Identification of Chain Scission Products Released to Water by Plastic Exposed to Ultraviolet Light. *Environ. Sci. Technol. Lett.* 5, 272–276. <https://doi.org/10.1021/acs.estlett.8b00119>
- Gewert, B., Plassmann, M.M., MacLeod, M., 2015. Pathways for degradation of plastic polymers floating in the marine environment. *Environ. Sci.: Processes Impacts* 17, 1513–1521. <https://doi.org/10.1039/C5EM00207A>

- Geyer, R., Jambeck, J.R., Law, K.L., 2017. Production, use, and fate of all plastics ever made. *Science Advances* 3, e1700782. <https://doi.org/10.1126/sciadv.1700782>
- Gigault, J., Halle, A. ter, Baudrimont, M., Pascal, P.-Y., Gauffre, F., Phi, T.-L., El Hadri, H., Grassl, B., Reynaud, S., 2018. Current opinion: What is a nanoplastic? *Environmental Pollution* 235, 1030–1034. <https://doi.org/10.1016/j.envpol.2018.01.024>
- Gilbert, B., Andres, R., Perfetti, P., Margaritondo, G., Rempfer, G., De Stasio, G., 2000. Charging phenomena in PEEM imaging and spectroscopy. *Ultramicroscopy* 83, 129–139. [https://doi.org/10.1016/S0304-3991\(99\)00196-5](https://doi.org/10.1016/S0304-3991(99)00196-5)
- Gillibert, R., Balakrishnan, G., Deshoules, Q., Tardivel, M., Magazzù, A., Donato, M.G., Maragò, O.M., Lamy de La Chapelle, M., Colas, F., Lagarde, F., Gucciardi, P.G., 2019. Raman Tweezers for Small Microplastics and Nanoplastics Identification in Seawater. *Environ. Sci. Technol.* 53, 9003–9013. <https://doi.org/10.1021/acs.est.9b03105>
- Glover, P., Mansfield, S.P., 2002. Limits to magnetic resonance microscopy. *Rep. Prog. Phys.* 65, 1489–1511. <https://doi.org/10.1088/0034-4885/65/10/203>
- Goßmann, I., Halbach, M., Scholz-Böttcher, B.M., 2021. Car and truck tire wear particles in complex environmental samples – A quantitative comparison with “traditional” microplastic polymer mass loads. *Science of The Total Environment* 773, 145667. <https://doi.org/10.1016/j.scitotenv.2021.145667>
- Grbic, J., Nguyen, B., Guo, E., You, J.B., Sinton, D., Rochman, C.M., 2019. Magnetic Extraction of Microplastics from Environmental Samples. *Environmental Science & Technology Letters* 6, 68–72. <https://doi.org/10.1021/acs.estlett.8b00671>
- Gunawardana, C., Goonetilleke, A., Egodawatta, P., Dawes, L., Kokot, S., 2012. Source characterisation of road dust based on chemical and mineralogical composition. *Chemosphere* 87, 163–170. <https://doi.org/10.1016/j.chemosphere.2011.12.012>
- Gustafsson, M., Blomqvist, G., Gudmundsson, A., Dahl, A., Swietlicki, E., Bohgard, M., Lindbom, J., Ljungman, A., 2008. Properties and toxicological effects of particles from the interaction between tyres, road pavement and winter traction material. *Science of The Total Environment* 393, 226–240. <https://doi.org/10.1016/j.scitotenv.2007.12.030>
- Hartmann, N.B., Hüffer, T., Thompson, R.C., Hassellöv, M., Verschoor, A., Daugaard, A.E., Rist, S., Karlsson, T., Brennholt, N., Cole, M., Herrling, M.P., Hess, M.C., Ivleva, N.P., Lusher, A.L., Wagner, M., 2019. Are We Speaking the Same Language? Recommendations for a Definition and Categorization Framework for Plastic Debris. *Environ. Sci. Technol.* 53, 1039–1047. <https://doi.org/10.1021/acs.est.8b05297>
- Hashimoto, K., Badarla, V.R., Kawai, A., Ideguchi, T., 2019. Complementary vibrational spectroscopy. *Nat Commun* 10, 4411. <https://doi.org/10.1038/s41467-019-12442-9>
- He, D., Luo, Y., Lu, S., Liu, M., Song, Y., Lei, L., 2018. Microplastics in soils: Analytical methods, pollution characteristics and ecological risks. *TrAC Trends in Analytical Chemistry* 109, 163–172. <https://doi.org/10.1016/j.trac.2018.10.006>
- He, D., Zhang, X., Hu, J., 2020. Methods for separating microplastics from complex solid matrices: Comparative analysis. *Journal of Hazardous Materials* 124640. <https://doi.org/10.1016/j.jhazmat.2020.124640>
- Helmberger, M.S., Tiemann, L.K., Grieshop, M.J., 2020. Towards an ecology of soil microplastics. *Funct Ecol* 34, 550–560. <https://doi.org/10.1111/1365-2435.13495>
- Hernandez, L.M., Xu, E.G., Larsson, H.C.E., Tahara, R., Maisuria, V.B., Tufenkji, N., 2019. Plastic Teabags Release Billions of Microparticles and Nanoparticles into Tea. *Environmental Science & Technology* 53, 12300–12310. <https://doi.org/10.1021/acs.est.9b02540>
- Hidalgo-Ruz, V., Gutow, L., Thompson, R.C., Thiel, M., 2012. Microplastics in the Marine Environment: A Review of the Methods Used for Identification and Quantification. *Environmental Science & Technology* 46, 3060–3075. <https://doi.org/10.1021/es2031505>
- Hitchcock, A.P., Dynes, J.J., Johansson, G., Wang, J., Botton, G., 2008. Comparison of NEXAFS microscopy and TEM-EELS for studies of soft matter. *Micron* 39, 311–319. <https://doi.org/10.1016/j.micron.2007.09.008>

- Horton, A.A., Cross, R.K., Read, D.S., Jürgens, M.D., Ball, H.L., Svendsen, C., Vollertsen, J., Johnson, A.C., 2021. Semi-automated analysis of microplastics in complex wastewater samples. *Environmental Pollution* 268, 115841. <https://doi.org/10.1016/j.envpol.2020.115841>
<https://lightsources.org>, n.d.
<https://wayforlight.eu>, n.d.
<http://unicorn.mcmaster.ca/aXis2000.html>, n.d.
- Hu, H., Larson, R.G., 2002. Evaporation of a Sessile Droplet on a Substrate. *The Journal of Physical Chemistry B* 106, 1334–1344. <https://doi.org/10.1021/jp0118322>
- Huang, J., Chen, H., Zheng, Y., Yang, Y., Zhang, Y., Gao, B., 2021. Microplastic pollution in soils and groundwater: Characteristics, analytical methods and impacts. *Chemical Engineering Journal* 425, 131870. <https://doi.org/10.1016/j.cej.2021.131870>
- Huang, Y., Liu, Q., Jia, W., Yan, C., Wang, J., 2020. Agricultural plastic mulching as a source of microplastics in the terrestrial environment. *Environmental Pollution* 260, 114096. <https://doi.org/10.1016/j.envpol.2020.114096>
- Hurley, R.R., Lusher, A.L., Olsen, M., Nizzetto, L., 2018. Validation of a Method for Extracting Microplastics from Complex, Organic-Rich, Environmental Matrices. *Environmental Science & Technology* 52, 7409–7417. <https://doi.org/10.1021/acs.est.8b01517>
- Hurley, R.R., Nizzetto, L., 2018. Fate and occurrence of micro(nano)plastics in soils: Knowledge gaps and possible risks. *Current Opinion in Environmental Science & Health* 1, 6–11. <https://doi.org/10.1016/j.coesh.2017.10.006>
- Imhof, H.K., Schmid, J., Niessner, R., Ivleva, N.P., Laforsch, C., 2012. A novel, highly efficient method for the separation and quantification of plastic particles in sediments of aquatic environments: Novel plastic particle separation method. *Limnol. Oceanogr. Methods* 10, 524–537. <https://doi.org/10.4319/lom.2012.10.524>
- Jacobsen, C., 2019. X-ray Microscopy, *Advances in Microscopy and Microanalysis*. Cambridge University Press, Cambridge. <https://doi.org/10.1017/9781139924542>
- Jiang, B., Kauffman, A.E., Li, L., McFee, W., Cai, B., Weinstein, J., Lead, J.R., Chatterjee, S., Scott, G.I., Xiao, S., 2020. Health impacts of environmental contamination of micro- and nanoplastics: a review. *Environ Health Prev Med* 25, 29. <https://doi.org/10.1186/s12199-020-00870-9>
- Juergen Bertling, Hamann, L., Bertling, R., 2018. *Kunststoffe in der Umwelt*. <https://doi.org/10.24406/UMSICHT-N-497117>
- Julienne, F., Lagarde, F., Delorme, N., 2019. Influence of the crystalline structure on the fragmentation of weathered polyolefines. *Polymer Degradation and Stability* 170, 109012. <https://doi.org/10.1016/j.polymdegradstab.2019.109012>
- Junhao, C., Xining, Z., Xiaodong, G., Li, Z., Qi, H., Siddique, K.H.M., 2021. Extraction and identification methods of microplastics and nanoplastics in agricultural soil: A review. *Journal of Environmental Management* 294, 112997. <https://doi.org/10.1016/j.jenvman.2021.112997>
- Kamweru, P.K., Ndiritu, F.G., Kinyanjui, T.K., Muthui, Z.W., Ngumbu, R.G., Odhiambo, P.M., 2011. Study of Temperature and UV Wavelength Range Effects on Degradation of Photo-Irradiated Polyethylene Films Using DMA. *Journal of Macromolecular Science, Part B* 50, 1338–1349. <https://doi.org/10.1080/00222348.2010.516172>
- Käppler, A., Fischer, D., Oberbeckmann, S., Schernewski, G., Labrenz, M., Eichhorn, K.-J., Voit, B., 2016. Analysis of environmental microplastics by vibrational microspectroscopy: FTIR, Raman or both? *Anal Bioanal Chem* 408, 8377–8391. <https://doi.org/10.1007/s00216-016-9956-3>
- Katsumi, N., Kusube, T., Nagao, S., Okochi, H., 2020. The role of coated fertilizer used in paddy fields as a source of microplastics in the marine environment. *Marine Pollution Bulletin* 161, 111727. <https://doi.org/10.1016/j.marpolbul.2020.111727>
- Kayhanian, M., McKenzie, E.R., Leatherbarrow, J.E., Young, T.M., 2012. Characteristics of road sediment fractionated particles captured from paved surfaces, surface run-off and detention basins. *Science of The Total Environment* 439, 172–186. <https://doi.org/10.1016/j.scitotenv.2012.08.077>

- Kernchen, S., Löder, M.G.J., Fischer, F., Fischer, D., Moses, S.R., Georgi, C., Nölscher, A.C., Held, A., Laforsch, C., 2022. Airborne microplastic concentrations and deposition across the Weser River catchment. *Science of The Total Environment* 818, 151812. <https://doi.org/10.1016/j.scitotenv.2021.151812>
- Khalid, N., Aqeel, M., Noman, A., Fatima Rizvi, Z., 2022. Impact of plastic mulching as a major source of microplastics in agroecosystems. *Journal of Hazardous Materials* 130455. <https://doi.org/10.1016/j.jhazmat.2022.130455>
- Kim, L., Lee, T.-Y., Kim, H., An, Y.-J., 2022. Toxicity assessment of tire particles released from personal mobilities (bicycles, cars, and electric scooters) on soil organisms. *Journal of Hazardous Materials* 437, 129362. <https://doi.org/10.1016/j.jhazmat.2022.129362>
- Kim, S.W., Leifheit, E.F., Maaß, S., Rillig, M.C., 2021. Time-Dependent Toxicity of Tire Particles on Soil Nematodes. *Front. Environ. Sci.* 9, 744668. <https://doi.org/10.3389/fenvs.2021.744668>
- Klein, R.J., Fischer, D.A., Lenhart, J.L., 2008. Systematic Oxidation of Polystyrene by Ultraviolet-Ozone, Characterized by Near-Edge X-ray Absorption Fine Structure and Contact Angle. *Langmuir* 24, 8187–8197. <https://doi.org/10.1021/la800134u>
- Klößner, P., Reemtsma, T., Eisentraut, P., Braun, U., Ruhl, A.S., Wagner, S., 2019. Tire and road wear particles in road environment – Quantification and assessment of particle dynamics by Zn determination after density separation. *Chemosphere* 222, 714–721. <https://doi.org/10.1016/j.chemosphere.2019.01.176>
- Klößner, P., Seiwert, B., Wagner, S., Reemtsma, T., 2021a. Organic Markers of Tire and Road Wear Particles in Sediments and Soils: Transformation Products of Major Antiozonants as Promising Candidates. *Environ. Sci. Technol.* 55, 11723–11732. <https://doi.org/10.1021/acs.est.1c02723>
- Klößner, P., Seiwert, B., Weyrauch, S., Escher, B.I., Reemtsma, T., Wagner, S., 2021b. Comprehensive characterization of tire and road wear particles in highway tunnel road dust by use of size and density fractionation. *Chemosphere* 279, 130530. <https://doi.org/10.1016/j.chemosphere.2021.130530>
- Knight, L.J., Parker-Jurd, F.N.F., Al-Sid-Cheikh, M., Thompson, R.C., 2020. Tyre wear particles: an abundant yet widely unreported microplastic? *Environ Sci Pollut Res* 27, 18345–18354. <https://doi.org/10.1007/s11356-020-08187-4>
- Kole, P.J., Löhr, A.J., Van Belleghem, F., Ragas, A., 2017. Wear and Tear of Tyres: A Stealthy Source of Microplastics in the Environment. *IJERPH* 14, 1265. <https://doi.org/10.3390/ijerph14101265>
- Kotar, S., McNeish, R., Murphy-Hagan, C., Renick, V., Lee, C.-F.T., Steele, C., Lusher, A., Moore, C., Minor, E., Schroeder, J., Helm, P., Rickabaugh, K., De Frond, H., Gesulga, K., Lao, W., Munno, K., Thornton Hampton, L.M., Weisberg, S.B., Wong, C.S., Amarpuri, G., Andrews, R.C., Barnett, S.M., Christiansen, S., Cowger, W., Crampond, K., Du, F., Gray, A.B., Hankett, J., Ho, K., Jaeger, J., Lilley, C., Mai, L., Mina, O., Lee, E., Primpke, S., Singh, S., Skovly, J., Slifko, T., Sukumaran, S., van Bavel, B., Van Brocklin, J., Vollnhals, F., Wu, C., Rochman, C.M., 2022. Quantitative assessment of visual microscopy as a tool for microplastic research: Recommendations for improving methods and reporting. *Chemosphere* 308, 136449. <https://doi.org/10.1016/j.chemosphere.2022.136449>
- Kovochich, M., Liong, M., Parker, J.A., Oh, S.C., Lee, J.P., Xi, L., Kreider, M.L., Unice, K.M., 2021. Chemical mapping of tire and road wear particles for single particle analysis. *Science of The Total Environment* 757, 144085. <https://doi.org/10.1016/j.scitotenv.2020.144085>
- Kreider, M.L., Panko, J.M., McAtee, B.L., Sweet, L.I., Finley, B.L., 2010. Physical and chemical characterization of tire-related particles: Comparison of particles generated using different methodologies. *Science of The Total Environment* 408, 652–659. <https://doi.org/10.1016/j.scitotenv.2009.10.016>
- Krueger, M.C., Harms, H., Schlosser, D., 2015. Prospects for microbiological solutions to environmental pollution with plastics. *Appl Microbiol Biotechnol* 99, 8857–8874. <https://doi.org/10.1007/s00253-015-6879-4>

- Kwak, J.I., An, Y.-J., 2021. Microplastic digestion generates fragmented nanoplastics in soils and damages earthworm spermatogenesis and coelomocyte viability. *Journal of Hazardous Materials* 402, 124034. <https://doi.org/10.1016/j.jhazmat.2020.124034>
- Lambert, S., Wagner, M., 2016. Characterisation of nanoplastics during the degradation of polystyrene. *Chemosphere* 145, 265–268. <https://doi.org/10.1016/j.chemosphere.2015.11.078>
- Leads, R.R., Weinstein, J.E., 2019. Occurrence of tire wear particles and other microplastics within the tributaries of the Charleston Harbor Estuary, South Carolina, USA. *Marine Pollution Bulletin* 145, 569–582. <https://doi.org/10.1016/j.marpolbul.2019.06.061>
- Ledieu, L., Tramoy, R., Ricordel, S., Astrie, D., Tassin, B., Gasperi, J., 2022. Amount, composition and sources of macrolitter from a highly frequented roadway. *Environmental Pollution* 303, 119145. <https://doi.org/10.1016/j.envpol.2022.119145>
- Lehmann, A., Fitschen, K., Rillig, M., 2019. Abiotic and Biotic Factors Influencing the Effect of Microplastic on Soil Aggregation. *Soil Syst.* 3, 21. <https://doi.org/10.3390/soilsystems3010021>
- Leijten, Z.J.W.A., Keizer, A.D.A., de With, G., Friedrich, H., 2017. Quantitative Analysis of Electron Beam Damage in Organic Thin Films. *The Journal of Physical Chemistry C* 121, 10552–10561. <https://doi.org/10.1021/acs.jpcc.7b01749>
- Leontowich, A.F.G., Hitchcock, A.P., 2012. Secondary electron deposition mechanism of carbon contamination. *Journal of Vacuum Science & Technology B, Nanotechnology and Microelectronics: Materials, Processing, Measurement, and Phenomena* 30, 030601. <https://doi.org/10.1116/1.3698602>
- Li, L., Luo, Y., Li, R., Zhou, Q., Peijnenburg, W.J.G.M., Yin, N., Yang, J., Tu, C., Zhang, Y., 2020. Effective uptake of submicrometre plastics by crop plants via a crack-entry mode. *Nature Sustainability*. <https://doi.org/10.1038/s41893-020-0567-9>
- Liang, C.-K., Eller, M.J., Verkhoturov, S.V., Schweikert, E.A., 2015. Mass Spectrometry of Nanoparticles is Different. *J. Am. Soc. Mass Spectrom.* 26, 1259–1265. <https://doi.org/10.1007/s13361-015-1151-9>
- Liang, Y., Lehmann, A., Ballhausen, M.-B., Muller, L., Rillig, M.C., 2019. Increasing Temperature and Microplastic Fibers Jointly Influence Soil Aggregation by Saprobic Fungi. *Front. Microbiol.* 10, 2018. <https://doi.org/10.3389/fmicb.2019.02018>
- Liu, M., Song, Y., Lu, S., Qiu, R., Hu, J., Li, X., Bigalke, M., Shi, H., He, D., 2019. A method for extracting soil microplastics through circulation of sodium bromide solutions. *Science of The Total Environment* 691, 341–347. <https://doi.org/10.1016/j.scitotenv.2019.07.144>
- Liu, P., Zhan, X., Wu, X., Li, J., Wang, H., Gao, S., 2020. Effect of weathering on environmental behavior of microplastics: Properties, sorption and potential risks. *Chemosphere* 242, 125193. <https://doi.org/10.1016/j.chemosphere.2019.125193>
- Lozano, Y.M., Lehnert, T., Linck, L.T., Lehmann, A., Rillig, M.C., 2021. Microplastic Shape, Polymer Type, and Concentration Affect Soil Properties and Plant Biomass. *Front. Plant Sci.* 12, 616645. <https://doi.org/10.3389/fpls.2021.616645>
- Luo, H., Xiang, Y., Li, Y., Zhao, Y., Pan, X., 2020a. Weathering alters surface characteristic of TiO₂-pigmented microplastics and particle size distribution of TiO₂ released into water. *Science of The Total Environment* 729, 139083. <https://doi.org/10.1016/j.scitotenv.2020.139083>
- Luo, H., Xiang, Y., Zhao, Y., Li, Y., Pan, X., 2020b. Nanoscale infrared, thermal and mechanical properties of aged microplastics revealed by an atomic force microscopy coupled with infrared spectroscopy (AFM-IR) technique. *Science of The Total Environment* 744, 140944. <https://doi.org/10.1016/j.scitotenv.2020.140944>
- Luo, Z., Zhou, X., Su, Y., Wang, H., Yu, R., Zhou, S., Xu, E.G., Xing, B., 2021. Environmental occurrence, fate, impact, and potential solution of tire microplastics: Similarities and differences with tire wear particles. *Science of The Total Environment* 795, 148902. <https://doi.org/10.1016/j.scitotenv.2021.148902>
- Lwanga, E.H., Beriot, N., Corradini, F., Silva, V., Yang, X., Baartman, J., Rezaei, M., van Schaik, L., Riksen, M., Geissen, V., 2022. Review of microplastic sources, transport

- pathways and correlations with other soil stressors: a journey from agricultural sites into the environment. *Chem. Biol. Technol. Agric.* 9, 20. <https://doi.org/10.1186/s40538-021-00278-9>
- Mamin, H.J., Kim, M., Sherwood, M.H., Rettner, C.T., Ohno, K., Awschalom, D.D., Rugar, D., 2013. Nanoscale Nuclear Magnetic Resonance with a Nitrogen-Vacancy Spin Sensor. *Science* 339, 557–560. <https://doi.org/10.1126/science.1231540>
- Mampallil, D., Eral, H.B., 2018. A review on suppression and utilization of the coffee-ring effect. *Advances in Colloid and Interface Science* 252, 38–54. <https://doi.org/10.1016/j.cis.2017.12.008>
- Markelonis, A.R., Wang, J.S., Ullrich, B., Wai, C.M., Brown, G.J., 2015. Nanoparticle film deposition using a simple and fast centrifuge sedimentation method. *Appl Nanosci* 5, 457–468. <https://doi.org/10.1007/s13204-014-0338-x>
- Mattonai, M., Nacci, T., Modugno, F., 2022. Analytical strategies for the quali-quantitation of tire and road wear particles – A critical review. *TrAC Trends in Analytical Chemistry* 154, 116650. <https://doi.org/10.1016/j.trac.2022.116650>
- Meides, N., Mauel, A., Menzel, T., Altstädt, V., Ruckdäschel, H., Senker, J., Strohhriegl, P., 2022. Quantifying the fragmentation of polypropylene upon exposure to accelerated weathering. *Micropl.&Nanopl.* 2, 23. <https://doi.org/10.1186/s43591-022-00042-2>
- Meides, N., Menzel, T., Poetzschner, B., Löder, M.G.J., Mansfeld, U., Strohhriegl, P., Altstaedt, V., Senker, J., 2021. Reconstructing the Environmental Degradation of Polystyrene by Accelerated Weathering. *Environ. Sci. Technol.* 55, 7930–7938. <https://doi.org/10.1021/acs.est.0c07718>
- Mennekes, D., Nowack, B., 2022. Tire wear particle emissions: Measurement data where are you? *Science of The Total Environment* 830, 154655. <https://doi.org/10.1016/j.scitotenv.2022.154655>
- Merkus, H.G., 2009. Particle size measurements: fundamentals, practice, quality, Particle technology series. Springer, New York?
- Mitrano, D.M., Beltzung, A., Frehland, S., Schmiedgruber, M., Cingolani, A., Schmidt, F., 2019. Synthesis of metal-doped nanoplastics and their utility to investigate fate and behaviour in complex environmental systems. *Nature Nanotechnology* 14, 362–368. <https://doi.org/10.1038/s41565-018-0360-3>
- Möller, J.N., Löder, M.G.J., Laforsch, C., 2020. Finding Microplastics in Soils: A Review of Analytical Methods. *Environ. Sci. Technol.* 54, 2078–2090. <https://doi.org/10.1021/acs.est.9b04618>
- Monteiro, S.S., Pinto da Costa, J., 2022. Methods for the extraction of microplastics in complex solid, water and biota samples. *Trends in Environmental Analytical Chemistry* 33, e00151. <https://doi.org/10.1016/j.teac.2021.e00151>
- Mooney, S.D., Tinner, W., 2011. The analysis of charcoal in peat and organic sediments 18.
- Müller, A., Kocher, B., Altmann, K., Braun, U., 2022. Determination of tire wear markers in soil samples and their distribution in a roadside soil. *Chemosphere* 294, 133653. <https://doi.org/10.1016/j.chemosphere.2022.133653>
- Mylläri, V., Ruoko, T.-P., Syrjälä, S., 2015. A comparison of rheology and FTIR in the study of polypropylene and polystyrene photodegradation. *J. Appl. Polym. Sci.* 132, n/a-n/a. <https://doi.org/10.1002/app.42246>
- Nabi, I., Bacha, A.-U.-R., Zhang, L., 2022. A review on microplastics separation techniques from environmental media. *Journal of Cleaner Production* 337, 130458. <https://doi.org/10.1016/j.jclepro.2022.130458>
- Naebe, M., Abolhasani, M.M., Khayyam, H., Amini, A., Fox, B., 2016. Crack Damage in Polymers and Composites: A Review. *Polymer Reviews* 56, 31–69. <https://doi.org/10.1080/15583724.2015.1078352>
- Nan, C., Yue, W., Tao, L., Yang, X., 2021. Fourier transform infrared nano-spectroscopy: Mechanism and applications. *Applied Spectroscopy Reviews* 56, 531–552. <https://doi.org/10.1080/05704928.2020.1830789>

- Nan, C., Yue, W., Tao, L., Yang, X., 2020. Fourier transform infrared nano-spectroscopy: Mechanism and applications. *Applied Spectroscopy Reviews* 0, 1–22. <https://doi.org/10.1080/05704928.2020.1830789>
- Nizzetto, L., Futter, M., Langaas, S., 2016. Are Agricultural Soils Dumps for Microplastics of Urban Origin? *Environ. Sci. Technol.* 50, 10777–10779. <https://doi.org/10.1021/acs.est.6b04140>
- Olsen, L.M.B., Knutsen, H., Mahat, S., Wade, E.J., Arp, H.P.H., 2020. Facilitating microplastic quantification through the introduction of a cellulose dissolution step prior to oxidation: Proof-of-concept and demonstration using diverse samples from the Inner Oslofjord, Norway. *Marine Environmental Research* 161, 105080. <https://doi.org/10.1016/j.marenvres.2020.105080>
- Otake, Y., Kobayashi, T., Asabe, H., Murakami, N., Ono, K., 1995. Biodegradation of low-density polyethylene, polystyrene, polyvinyl chloride, and urea formaldehyde resin buried under soil for over 32 years. *J. Appl. Polym. Sci.* 56, 1789–1796. <https://doi.org/10.1002/app.1995.070561309>
- Panko, J.M., Chu, J.A., Kreider, M.L., McAtee, B.L., Unice, K.M., 2012. Quantification of tire and road wear particles in the environment. Presented at the Urban Transport 2012, A Coruna, Spain, pp. 59–70. <https://doi.org/10.2495/UT120061>
- Penders, J., Pence, I.J., Horgan, C.C., Bergholt, M.S., Wood, C.S., Najer, A., Kauscher, U., Nagelkerke, A., Stevens, M.M., 2018. Single Particle Automated Raman Trapping Analysis. *Nat Commun* 9, 4256. <https://doi.org/10.1038/s41467-018-06397-6>
- Perez, C.N., Carré, F., Hoarau-Belkhir, A., Joris, A., Leonards, P.E.G., Lamoree, M.H., 2022. Innovations in analytical methods to assess the occurrence of microplastics in soil. *Journal of Environmental Chemical Engineering* 10, 107421. <https://doi.org/10.1016/j.jece.2022.107421>
- Pérez-Reverón, R., González-Sálamo, J., Hernández-Sánchez, C., González-Pleiter, M., Hernández-Borges, J., Díaz-Peña, F.J., 2022. Recycled wastewater as a potential source of microplastics in irrigated soils from an arid-insular territory (Fuerteventura, Spain). *Science of The Total Environment* 817, 152830. <https://doi.org/10.1016/j.scitotenv.2021.152830>
- Pielichowski, Njurguna, 2005. Thermal degradation of polymeric materials, iSmithers Rapra. ed. iSmithers Rapra, Shawbury, UK.
- Pietz, O., Augenstein, M., Georgakakos, C.B., Singh, K., McDonald, M., Walter, M.T., 2021. Macroplastic accumulation in roadside ditches of New York State's Finger Lakes region (USA) across land uses and the COVID-19 pandemic. *Journal of Environmental Management* 298, 113524. <https://doi.org/10.1016/j.jenvman.2021.113524>
- Pikula, K., Chaika, V., Zakharenko, A., Markina, Z., Vedyagin, A., Kuznetsov, V., Gusev, A., Park, S., Golokhvast, K., 2020. Comparison of the Level and Mechanisms of Toxicity of Carbon Nanotubes, Carbon Nanofibers, and Silicon Nanotubes in Bioassay with Four Marine Microalgae. *Nanomaterials* 10, 485. <https://doi.org/10.3390/nano10030485>
- PlasticsEurope, 2022. *Plastics - the Facts 2022*. An analyse of European plastic production, demand and waste Data 2022.
- Popczun, N.J., Breuer, L., Wucher, A., Winograd, N., 2017. On the SIMS Ionization Probability of Organic Molecules. *J. Am. Soc. Mass Spectrom.* 28, 1182–1191. <https://doi.org/10.1007/s13361-017-1624-0>
- Primpke, S., Cross, R.K., Mintenig, S.M., Simon, M., Vianello, A., Gerdt, G., Vollertsen, J., 2020. Toward the Systematic Identification of Microplastics in the Environment: Evaluation of a New Independent Software Tool (siMPle) for Spectroscopic Analysis. *Applied Spectroscopy* 74, 1127–1138. <https://doi.org/10.1177/0003702820917760>
- Raabe, J., Tzvetkov, G., Flechsig, U., Böge, M., Jaggi, A., Sarafimov, B., Vernooij, M.G.C., Huthwelker, T., Ade, H., Kilcoyne, D., Tyliszczak, T., Fink, R.H., Quitmann, C., 2008. PolLux: A new facility for soft x-ray spectromicroscopy at the Swiss Light Source. *Review of Scientific Instruments* 79, 113704. <https://doi.org/10.1063/1.3021472>

- Ramani, R., Ranganathaiah, C., 2000. Degradation of acrylonitrile-butadiene-styrene and polycarbonate by UV irradiation. *Polymer Degradation and Stability* 69, 347–354. [https://doi.org/10.1016/S0141-3910\(00\)00081-1](https://doi.org/10.1016/S0141-3910(00)00081-1)
- Rånby, B., 1989. Photodegradation and photo-oxidation of synthetic polymers. *Journal of Analytical and Applied Pyrolysis* 15, 237–247. [https://doi.org/10.1016/0165-2370\(89\)85037-5](https://doi.org/10.1016/0165-2370(89)85037-5)
- Rausch, J., Jaramillo-Vogel, D., Perseguers, S., Schnidrig, N., Grobéty, B., Yajan, P., 2022. Automated identification and quantification of tire wear particles (TWP) in airborne dust: SEM/EDX single particle analysis coupled to a machine learning classifier. *Science of The Total Environment* 803, 149832. <https://doi.org/10.1016/j.scitotenv.2021.149832>
- Re, V., 2019. Shedding light on the invisible: addressing the potential for groundwater contamination by plastic microfibers. *Hydrogeol J* 27, 2719–2727. <https://doi.org/10.1007/s10040-019-01998-x>
- Ren, X., Tang, J., Wang, L., Liu, Q., 2021. Microplastics in soil-plant system: effects of nano/microplastics on plant photosynthesis, rhizosphere microbes and soil properties in soil with different residues. *Plant Soil* 462, 561–576. <https://doi.org/10.1007/s11104-021-04869-1>
- Rillig, M.C., 2012. Microplastic in Terrestrial Ecosystems and the Soil? *Environ. Sci. Technol.* 46, 6453–6454. <https://doi.org/10.1021/es302011r>
- Rødland, E.S., Samanipour, S., Rauert, C., Okoffo, E.D., Reid, M.J., Heier, L.S., Lind, O.C., Thomas, K.V., Meland, S., 2022. A novel method for the quantification of tire and polymer-modified bitumen particles in environmental samples by pyrolysis gas chromatography mass spectroscopy. *Journal of Hazardous Materials* 423, 127092. <https://doi.org/10.1016/j.jhazmat.2021.127092>
- Rodríguez-Hernández, A.G., Muñoz-Tabares, J.A., Aguilar-Guzmán, J.C., Vazquez-Duhalt, R., 2019. A novel and simple method for polyethylene terephthalate (PET) nanoparticle production. *Environmental Science: Nano* 6, 2031–2036. <https://doi.org/10.1039/C9EN00365G>
- Rodriguez-Seijo, A., Lourenço, J., Rocha-Santos, T.A.P., da Costa, J., Duarte, A.C., Vala, H., Pereira, R., 2017. Histopathological and molecular effects of microplastics in *Eisenia andrei* Bouché. *Environmental Pollution* 220, 495–503. <https://doi.org/10.1016/j.envpol.2016.09.092>
- Rogge, W.F., Hildemann, L.M., Mazurek, M.A., Cass, G.R., Simoneit, B.R.T., 1993. Sources of fine organic aerosol. 3. Road dust, tire debris, and organometallic brake lining dust: roads as sources and sinks. *Environ. Sci. Technol.* 27, 1892–1904. <https://doi.org/10.1021/es00046a019>
- RStudio Team, 2020. RStudio: Integrated Deveolpment for R.
- Saito, T., Niki, E., Kamiya, Y., 1981. Ozonization of Organic Compounds. V. Aromatic Compounds. *BCSJ* 54, 253–257. <https://doi.org/10.1246/bcsj.54.253>
- Sander, M., Kohler, H.-P.E., McNeill, K., 2019. Assessing the environmental transformation of nanoplastic through ¹³C-labelled polymers. *Nature Nanotechnology* 14, 301–303. <https://doi.org/10.1038/s41565-019-0424-z>
- Scarascia-Mugnozza, G., Sica, C., Russo, G., 2011. PLASTIC MATERIALS IN EUROPEAN AGRICULTURE: ACTUAL USE AND PERSPECTIVES. *Journal of Agricultural Engineering* 14.
- Scheurer, M., Bigalke, M., 2018. Microplastics in Swiss Floodplain Soils. *Environmental Science & Technology* 52, 3591–3598. <https://doi.org/10.1021/acs.est.7b06003>
- Schindelin, J., Arganda-Carreras, I., Frise, E., Kaynig, V., Longair, M., Pietzsch, T., Preibisch, S., Rueden, C., Saalfeld, S., Schmid, B., Tinevez, J.-Y., White, D.J., Hartenstein, V., Eliceiri, K., Tomancak, P., Cardona, A., 2012. Fiji: an open-source platform for biological-image analysis. *Nat Methods* 9, 676–682. <https://doi.org/10.1038/nmeth.2019>

- Schwaferts, C., Niessner, R., Elsner, M., Ivleva, N.P., 2019. Methods for the analysis of submicrometer- and nanoplastic particles in the environment. *TrAC Trends in Analytical Chemistry* 112, 52–65. <https://doi.org/10.1016/j.trac.2018.12.014>
- Schwertfeger, D.M., Velicogna, J.R., Jesmer, A.H., Saatcioglu, S., McShane, H., Scroggins, R.P., Princz, J.I., 2017. Extracting Metallic Nanoparticles from Soils for Quantitative Analysis: Method Development Using Engineered Silver Nanoparticles and SP-ICP-MS. *Analytical Chemistry* 89, 2505–2513. <https://doi.org/10.1021/acs.analchem.6b04668>
- Selonen, S., Dolar, A., Jemec Kokalj, A., Sackey, L.N.A., Skalar, T., Cruz Fernandes, V., Rede, D., Delerue-Matos, C., Hurley, R., Nizzetto, L., van Gestel, C.A.M., 2021. Exploring the impacts of microplastics and associated chemicals in the terrestrial environment – Exposure of soil invertebrates to tire particles. *Environmental Research* 201, 111495. <https://doi.org/10.1016/j.envres.2021.111495>
- Sheng, Y., Liu, Y., Wang, K., Cizdziel, J.V., Wu, Y., Zhou, Y., 2021. Ecotoxicological effects of micronized car tire wear particles and their heavy metals on the earthworm (*Eisenia fetida*) in soil. *Science of The Total Environment* 793, 148613. <https://doi.org/10.1016/j.scitotenv.2021.148613>
- Sieber, R., Kawecki, D., Nowack, B., 2020. Dynamic probabilistic material flow analysis of rubber release from tires into the environment. *Environmental Pollution* 258, 113573. <https://doi.org/10.1016/j.envpol.2019.113573>
- Siegfried, M., Koelmans, A.A., Besseling, E., Kroeze, C., 2017. Export of microplastics from land to sea. A modelling approach. *Water Research* 127, 249–257. <https://doi.org/10.1016/j.watres.2017.10.011>
- Smith, A.P., Urquhart, S.G., Winesett, D.A., Mitchell, G., Ade, H., 2001. Use of near Edge X-Ray Absorption Fine Structure Spectromicroscopy to Characterize Multicomponent Polymeric Systems. *Appl Spectrosc* 55, 1676–1681. <https://doi.org/10.1366/0003702011954008>
- Sommer, F., Dietze, V., Baum, A., Sauer, J., Gilge, S., Maschowski, C., Gieré, R., 2018. Tire Abrasion as a Major Source of Microplastics in the Environment. *Aerosol Air Qual. Res.* 18, 2014–2028. <https://doi.org/10.4209/aaqr.2018.03.0099>
- Stöhr, J., 1992. NEXAFS Spectroscopy, Springer Series in Surface Sciences. Springer Berlin Heidelberg, Berlin, Heidelberg. <https://doi.org/10.1007/978-3-662-02853-7>
- Sun, X.-D., Yuan, X.-Z., Jia, Y., Feng, L.-J., Zhu, F.-P., Dong, S.-S., Liu, J., Kong, X., Tian, H., Duan, J.-L., Ding, Z., Wang, S.-G., Xing, B., 2020. Differentially charged nanoplastics demonstrate distinct accumulation in *Arabidopsis thaliana*. *Nature Nanotechnology*. <https://doi.org/10.1038/s41565-020-0707-4>
- Tanoiri, H., Nakano, H., Arakawa, H., Hattori, R.S., Yokota, M., 2021. Inclusion of shape parameters increases the accuracy of 3D models for microplastics mass quantification. *Marine Pollution Bulletin* 171, 112749. <https://doi.org/10.1016/j.marpolbul.2021.112749>
- Ter Halle, A., Jeanneau, L., Martignac, M., Jardé, E., Pedrono, B., Brach, L., Gigault, J., 2017. Nanoplastic in the North Atlantic Subtropical Gyre. *Environmental Science & Technology* 51, 13689–13697. <https://doi.org/10.1021/acs.est.7b03667>
- The GIMP Development Team, 2019. GIMP.
- Thomas, J., Cutright, T., Pugh, C., Soucek, M.D., 2023. Quantitative assessment of additive leachates in abiotic weathered tire cryogrinds and its application to tire wear particles in roadside soil samples. *Chemosphere* 311, 137132. <https://doi.org/10.1016/j.chemosphere.2022.137132>
- Thomas, J., Moosavian, S.K., Cutright, T., Pugh, C., Soucek, M.D., 2022. Method Development for Separation and Analysis of Tire and Road Wear Particles from Roadside Soil Samples. *Environ. Sci. Technol.* [acs.est.2c03695](https://doi.org/10.1021/acs.est.2c03695). <https://doi.org/10.1021/acs.est.2c03695>
- Thomas, P.J., Perono, G., Tommasi, F., Pagano, G., Oral, R., Burić, P., Kovačić, I., Toscanesi, M., Trifuoggi, M., Lyons, D.M., 2021. Resolving the effects of environmental micro- and

- nanoplastics exposure in biota: A knowledge gap analysis. *Science of The Total Environment* 780, 146534. <https://doi.org/10.1016/j.scitotenv.2021.146534>
- Tian, Z., Gonzalez, M., Rideout, C.A., Zhao, H.N., Hu, X., Wetzel, J., Mudrock, E., James, C.A., McIntyre, J.K., Kolodziej, E.P., 2022. 6PPD-Quinone: Revised Toxicity Assessment and Quantification with a Commercial Standard. *Environ. Sci. Technol. Lett.* 9, 140–146. <https://doi.org/10.1021/acs.estlett.1c00910>
- Torikai, A., Murata, T., Fueki, K., 1984. Photo-induced reactions of polycarbonate studied by ESR, viscosity and optical absorption measurements. *Polymer Photochemistry* 4, 255–269. [https://doi.org/10.1016/0144-2880\(84\)90047-2](https://doi.org/10.1016/0144-2880(84)90047-2)
- Turton, T.J., White, J.R., 2001. Degradation depth profiles and fracture of UV exposed polycarbonate. *Plastics, Rubber and Composites* 30, 175–182. <https://doi.org/10.1179/146580101101541606>
- UNEP, 2022. End plastic pollution: towards an international legally binding instrument (United Nations Environment Programme). United Nations Environment Programme, Nairobi.
- Unice, K.M., Bare, J.L., Kreider, M.L., Panko, J.M., 2015. Experimental methodology for assessing the environmental fate of organic chemicals in polymer matrices using column leaching studies and OECD 308 water/sediment systems: Application to tire and road wear particles. *Science of The Total Environment* 533, 476–487. <https://doi.org/10.1016/j.scitotenv.2015.06.053>
- Verschoor, A., de Poorter, L., Rianne Dröge, R., Jeroen Kuenen, J., de Valk, E., 2016. Emission of microplastics and potential mitigation measures: abrasive cleaning agents, paints and tyre wear (No. 0026). National Institute for Public Health and the Environment (RIVM), Bilthoven (NL).
- Villarrubia-Gómez, P., Cornell, S.E., Fabres, J., 2018. Marine plastic pollution as a planetary boundary threat – The drifting piece in the sustainability puzzle. *Marine Policy* 96, 213–220. <https://doi.org/10.1016/j.marpol.2017.11.035>
- Wagner, S., Hüffer, T., Klöckner, P., Wehrhahn, M., Hofmann, T., Reemtsma, T., 2018. Tire wear particles in the aquatic environment - A review on generation, analysis, occurrence, fate and effects. *Water Research* 139, 83–100. <https://doi.org/10.1016/j.watres.2018.03.051>
- Wahl, A., Le Juge, C., Davranche, M., El Hadri, H., Grassl, B., Reynaud, S., Gigault, J., 2021. Nanoplastic occurrence in a soil amended with plastic debris. *Chemosphere* 262, 127784. <https://doi.org/10.1016/j.chemosphere.2020.127784>
- Wang, C., Xian, Z., Jin, X., Liang, S., Chen, Z., Pan, B., Wu, B., Ok, Y.S., Gu, C., 2020. Photo-aging of polyvinyl chloride microplastic in the presence of natural organic acids. *Water Research* 183, 116082. <https://doi.org/10.1016/j.watres.2020.116082>
- Wang, F., Feng, X., Liu, Y., Adams, C.A., Sun, Y., Zhang, S., 2022a. Micro(nano)plastics and terrestrial plants: Up-to-date knowledge on uptake, translocation, and phytotoxicity. *Resources, Conservation and Recycling* 185, 106503. <https://doi.org/10.1016/j.resconrec.2022.106503>
- Wang, F., Wang, Q., Adams, C.A., Sun, Y., Zhang, S., 2022b. Effects of microplastics on soil properties: Current knowledge and future perspectives. *Journal of Hazardous Materials* 424, 127531. <https://doi.org/10.1016/j.jhazmat.2021.127531>
- Wang, J., Morin, C., Li, L., Hitchcock, A.P., Scholl, A., Doran, A., 2009. Radiation damage in soft X-ray microscopy. *Journal of Electron Spectroscopy and Related Phenomena* 170, 25–36. <https://doi.org/10.1016/j.elspec.2008.01.002>
- Wang, M., Gao, B., Tang, D., 2016. Review of key factors controlling engineered nanoparticle transport in porous media. *Journal of Hazardous Materials* 67.
- Wang, T., Li, B., Zou, X., Wang, Y., Li, Y., Xu, Y., Mao, L., Zhang, C., Yu, W., 2019. Emission of primary microplastics in mainland China: Invisible but not negligible. *Water Research* 162, 214–224. <https://doi.org/10.1016/j.watres.2019.06.042>
- Wang, Z., Taylor, S.E., Sharma, P., Flury, M., 2018. Poor extraction efficiencies of polystyrene nano- and microplastics from biosolids and soil. *PLOS ONE* 13, e0208009. <https://doi.org/10.1371/journal.pone.0208009>

- Watts, B., Ade, H., 2012. NEXAFS imaging of synthetic organic materials. *Materials Today* 15, 148–157. [https://doi.org/10.1016/S1369-7021\(12\)70068-8](https://doi.org/10.1016/S1369-7021(12)70068-8)
- Watts, B., Pilet, N., Sarafimov, B., Witte, K., Raabe, J., 2018. Controlling optics contamination at the PoLux STXM. *J. Inst.* 13, C04001–C04001. <https://doi.org/10.1088/1748-0221/13/04/C04001>
- Watts, B., Swaraj, S., Nordlund, D., Lüning, J., Ade, H., 2011. Calibrated NEXAFS spectra of common conjugated polymers. *The Journal of Chemical Physics* 134, 024702. <https://doi.org/10.1063/1.3506636>
- Way, C., Hudson, M.D., Williams, I.D., Langley, G.J., 2022. Evidence of underestimation in microplastic research: A meta-analysis of recovery rate studies. *Science of The Total Environment* 805, 150227. <https://doi.org/10.1016/j.scitotenv.2021.150227>
- Weinstein, J.E., Crocker, B.K., Gray, A.D., 2016. From macroplastic to microplastic: Degradation of high-density polyethylene, polypropylene, and polystyrene in a salt marsh habitat: Degradation of plastic in a salt marsh habitat. *Environ Toxicol Chem* 35, 1632–1640. <https://doi.org/10.1002/etc.3432>
- Weithmann, N., Möller, J.N., Löder, M.G.J., Piehl, S., Laforsch, C., Freitag, R., 2018. Organic fertilizer as a vehicle for the entry of microplastic into the environment. *Sci. Adv.* 4, eaap8060. <https://doi.org/10.1126/sciadv.aap8060>
- Wien, K., 1997. TOF-SIMS analysis of polymers. *Nuclear Instruments and Methods in Physics Research Section B: Beam Interactions with Materials and Atoms* 131, 38–54. [https://doi.org/10.1016/S0168-583X\(97\)00147-X](https://doi.org/10.1016/S0168-583X(97)00147-X)
- Wöll, D., Flors, C., 2017. Super-resolution Fluorescence Imaging for Materials Science. *Small Methods* 1, 1700191. <https://doi.org/10.1002/smt.201700191>
- Wright, S.L., Ulke, J., Font, A., Chan, K.L.A., Kelly, F.J., 2020. Atmospheric microplastic deposition in an urban environment and an evaluation of transport. *Environment International* 136, 105411. <https://doi.org/10.1016/j.envint.2019.105411>
- Yu, Y., Flury, M., 2021. How to take representative samples to quantify microplastic particles in soil? *Science of The Total Environment* 784, 147166. <https://doi.org/10.1016/j.scitotenv.2021.147166>
- Zhang, K., Hamidian, A.H., Tubić, A., Zhang, Y., Fang, J.K.H., Wu, C., Lam, P.K.S., 2021. Understanding plastic degradation and microplastic formation in the environment: A review. *Environmental Pollution* 274, 116554. <https://doi.org/10.1016/j.envpol.2021.116554>
- Zhang, S., Wang, J., Liu, X., Qu, F., Wang, Xueshan, Wang, Xinrui, Li, Y., Sun, Y., 2019. Microplastics in the environment: A review of analytical methods, distribution, and biological effects. *TrAC Trends in Analytical Chemistry* 111, 62–72. <https://doi.org/10.1016/j.trac.2018.12.002>
- Zhou, P.H., Kizilkaya, O., Morikawa, E., 2008. Electronic structure of photo-degraded polypropylene ultrathin films. *Chemical Physics Letters* 465, 241–244. <https://doi.org/10.1016/j.cplett.2008.10.006>
- Zhu, B.-K., Fang, Y.-M., Zhu, D., Christie, P., Ke, X., Zhu, Y.-G., 2018. Exposure to nanoplastics disturbs the gut microbiome in the soil oligochaete *Enchytraeus crypticus*. *Environmental Pollution* 239, 408–415. <https://doi.org/10.1016/j.envpol.2018.04.017>
- Zumstein, M.T., Schintlmeister, A., Nelson, T.F., Baumgartner, R., Woebken, D., Wagner, M., Kohler, H.-P.E., McNeill, K., Sander, M., 2018. Biodegradation of synthetic polymers in soils: Tracking carbon into CO₂ and microbial biomass. *Sci. Adv.* 4, eaas9024. <https://doi.org/10.1126/sciadv.aas9024>

Declaration of consent

on the basis of Article 18 of the PromR Phil.-nat. 19

Name/First Name: Foetisch Alexandra

Registration Number: 370.548

Study program: PhD in Geography

Bachelor Master Dissertation

Title of the thesis: Occurrence and fate of micro- and nanoplastics in the terrestrial environment

Supervisor: Prof. Dr. Moritz Bigalke, Prof.Dr. Adrien Mestrot

I declare herewith that this thesis is my own work and that I have not used any sources other than those stated. I have indicated the adoption of quotations as well as thoughts taken from other authors as such in the thesis. I am aware that the Senate pursuant to Article 36 paragraph 1 litera r of the University Act of September 5th, 1996 and Article 69 of the University Statute of June 7th, 2011 is authorized to revoke the doctoral degree awarded on the basis of this thesis.

For the purposes of evaluation and verification of compliance with the declaration of originality and the regulations governing plagiarism, I hereby grant the University of Bern the right to process my personal data and to perform the acts of use this requires, in particular, to reproduce the written thesis and to store it permanently in a database, and to use said database, or to make said database available, to enable comparison with theses submitted by others.

Bern, 30. January 2023

Place/Date

Signature



